

UNDERSTANDING THE ESSENTIAL ROLE OF THE E3 UBIQUITIN LIGASE TRAIP DURING THE EUKARYOTIC CELL CYCLE

by

Shaun Scaramuzza

A thesis submitted to the University of Birmingham for the degree of Doctor of Philosophy

Institute of Cancer and Genomic Sciences

School of Cancer Sciences

College of Medical and Dental Sciences

University of Birmingham

March 2022

UNIVERSITY OF
BIRMINGHAM

University of Birmingham Research Archive

e-theses repository

This unpublished thesis/dissertation is copyright of the author and/or third parties. The intellectual property rights of the author or third parties in respect of this work are as defined by The Copyright Designs and Patents Act 1988 or as modified by any successor legislation.

Any use made of information contained in this thesis/dissertation must be in accordance with that legislation and must be properly acknowledged. Further distribution or reproduction in any format is prohibited without the permission of the copyright holder.

Abstract

The RING-type E3 ubiquitin ligase TRAIP has been widely associated with the promotion of genomic stability throughout the cell cycle. In addition, TRAIP has been linked with several aspects of health and disease; mutations to TRAIP have been reported to lead to primordial dwarfism in patients and TRAIP is differentially expressed across several forms of cancer. However, despite this, the essential role of TRAIP during the otherwise unperturbed cell cycle, responsible for the associated cell lethality and primordial dwarfism phenotypes, remained unclear.

This PhD project aimed to understand further the roles of TRAIP during individual stages of the cell cycle. Through the generation of conditional degron cell lines, we demonstrate that the essential role for TRAIP occurs specifically during S-phase. Further work then identified the likely underlying mechanisim of action: the resolution of damaging DNA replication - transcription conflicts. As a result, without TRAIP, cells accumulate DNA damage throughout S-phase, arrest in G2 due to ATR checkpoint activation, and ultimately exit the cell cycle via senescence.

Following the characterisation of these S-phase mechanisms involving TRAIP, we next

explored any requirements during mitosis. The Gambus lab had previously found TRAIP to accumulate with the terminating replisome, upon inhibition of the S-phase replisome disassembly pathway. Subsequent work then revealed the ability of TRAIP to drive mitotic replisome disassembly in *X. laevis* egg extract. In this project, we demonstrate that the core mechanisms of replisome disassembly, described using *X. laevis* egg extract, *C. elegans*, and *S. cerevisiae*, are likely conserved into human somatic cells. Moreover, we present evidence to suggest that TRAIP can also drive mitotic replisome disassembly in mammalian cell lines. Finally, TRAIP was shown to be important for mitotic timing, independently of any S-phase roles.

Acknowledgements

First I would like to say a massive thank you to my supervisor Aga, for all your help and guidance. For giving me the freedom to explore my ideas and for the support when my experiments failed. I really appreciate all the time and opportunities you have given me over the years, I feel very lucky to have had you as my supervisor. I would also like to thank everyone in the Gambus group past and present - Abi, Becky, Nev, Cyntia, Divya, Zeynep, Sarmi, Angeliki, Alicja, Paolo, and Georgia. The last few years would not have been so enjoyable without you all. Becky, thank you for all your advice and guidance when things got a bit stressful. Abi, Nev, and Paolo, this PhD would not have been the same without you - and all the pub trips that kept me sane!! Thanks also to Marco, Martina, and Jianming for all your advice and collaboration throughout my project. I would like to express my thanks to the JSPS summer fellowship cohort and the Molecular Cell Engineering Lab. In particular, Masato and Toyo for showing me both the sights and culture of Japan, whilst teaching me exciting new lab techniques. Finally, thank you to our collaborators at Astra Zeneca (Mark, Johanna, and Carolyn) for all your advice, and giving me a different insight into the science world.

I would like to thank all my family for their love and support. Niamh, it has honestly been a privilege to have done this crazy PhD journey together. You are an inspiration, and I

could not have done this without your motivational pep talks or spontaneous trips to the zoo. Thank you for being you - and for putting up with all my questions on R scripting ofcourse!! To my mum Diane, dad Michael, and brother Danny, thank you for everything you have done for me over the years, for pushing me to achieve my goals, and for helping me move house many times! Lastly, thanks to my grandparents Christine and John, for always showing an interest in my work, listening to me ramble about it endlessly, and for always being my biggest supporters.

Contents

1 Introduction **23**

1.1 Ubiquitin 23

1.1.1 Different Types of Protein Ubiquitylation 25

1.1.2 The Ubiquitylation Cascade 27

1.1.3 Deubiquitylating Enzymes and Ubiquitin Recycling 33

1.1.4 Ubiquitin-Like Protein Modifiers 34

1.2 The Eukaryotic Cell Cycle 35

1.3 Eukaryotic DNA Replication 39

1.3.1 DNA Replication Initiation 39

1.3.2 Limiting DNA Replication to Once-Per Cell Cycle 44

1.3.3 Replication Elongation 46

1.3.4 Replication Termination 51

1.3.5 Other Mechanisms Associated with DNA Replication 55

1.3.6 The Interplay between DNA Replication and Transcription (Replication-Transcription Conflicts) 57

1.4 Replication Stress and the DNA Damage Response 61

1.4.1 Replication Stress Response: Stalled Helicase or Polymerase 62

1.4.2 The DNA Damage Response 67

1.5 The Association Between DNA Replication Proteins and Primordial Dwarfism . . 68
1.6 Model Systems and Methods Used to Study DNA Replication Termination . . . 70
1.6.1 *Xenopus laevis* Egg Extract . . . 70
1.6.2 Immortalised Human Somatic Cell Lines . . . 71
1.7 Selection of a Candidate Pool . . . 74
1.7.1 Candidate E3 Ubiquitin Ligases . . . 78
1.7.2 Candidate Deubiquitylating Enzmyes . . . 80
1.8 Project Aims and Objectives . . . 82

2 Materials and Methods 85

2.1 Tables . . . 85
2.2 Working With Proteins . . . 96
2.2.1 SDS-PAGE . . . 96
2.2.2 Coomassie Protein Staining . . . 97
2.2.3 Immunoblotting . . . 98
2.2.4 Estimating Protein Concentration Using Bradford's Reagent . . . 99
2.2.5 Estimating Protein Concentration using BSA Gradients . . . 100
2.3 Working With DNA . . . 102
2.3.1 DNA Gel Electrophoresis . . . 102
2.3.2 Polymerase Chain Reaction . . . 102
2.3.3 Molecular Cloning . . . 103
2.3.4 Plasmid Construction for Auxin-Inducible Degron Cell Lines . . . 106
2.4 Working With Bacteria . . . 107
2.4.1 Bacterial Transformation . . . 107

2.4.2 Generating Bacterial Stocks and Growing Bacterial Cultures 108
2.4.3 Protein Expression Testing 108
2.4.4 Protein Solubility Testing 109
2.4.5 Purification of Recombinant Proteins of Interest 110
2.4.6 Purification of USP22 115
2.5 Working With *Xenopus laevis* 115
2.5.1 Preparation of Metaphase II Arrested *X. laevis* Egg Extract 115
2.5.2 Preparation of Demembranated *X. laevis* Sperm Nuclei 117
2.5.3 Measuring DNA Replication through α^{32}-P-dATP Incorporation 119
2.6 Working With Mammalian Cell Lines 120
2.6.1 Cell Growth Conditions 120
2.6.2 Generation of Cell Stocks and Waking up Cells 121
2.6.3 Generation of Conditional Auxin-Inducible Degron Cell Lines 122
2.6.4 Confirmation of bi-allelic gene tagging by Genomic PCR 124
2.6.5 Colony Forming Assays 125
2.6.6 Proliferation Growth Curves 126
2.6.7 Cell Synchronisation 126
2.6.8 Preparation of Whole Cell Extracts 130
2.6.9 BrdU Incorporation Assays 131
2.6.10 Click-IT to Measure Global Replication and Transcription 131
2.6.11 Proximity Ligation Assay 132
2.6.12 CSK Extraction of Soluble Cellular Fractions 134
2.6.13 GFP-TRAP 135

2.6.14 Immunostaining . . . 136
2.6.15 Immunofluorescence . . . 137
2.6.16 Flow Cytometry . . . 137
2.6.17 Cell Senescence Assay . . . 139
2.6.18 Annexin V Apoptosis Assay . . . 140
2.6.19 ChIP-Sequencing . . . 140
2.6.20 Mycoplasma Testing . . . 143
2.7 Data Analysis . . . 144

3 Raising Antibodies Against Recombinant Proteins of Interest 146
3.1 Introduction . . . 146
3.2 Results . . . 147
3.2.1 Protein Expression Testing . . . 148
3.2.2 Protein Solubility Testing . . . 151
3.2.3 Purification of Recombinant Proteins for Raising Antibodies . . . 153
3.2.4 Testing Raised Sera against Candidates of Interest . . . 156
3.2.5 Selection of TRAIP for further study . . . 159
3.3 Discussion . . . 164

4 The Generation and Characterisation of Conditional AID Degrons Against TRAIP and LRR1 175
4.1 Introduction . . . 175
4.2 Results . . . 177
4.2.1 Generation of Conditional Degron Cell Lines against LRR1 . . . 177
4.2.2 LRR1 is Degraded Following IAA Treatment . . . 181

4.2.3 LRR1 is Important for Cell Viability 182
4.2.4 Generation of Conditional Degron Cell Lines against TRAIP 184
4.2.5 TRAIP is Rapidly Degraded Following IAA Treatment 186
4.2.6 TRAIP is Essential for Cell Viability 187
4.2.7 TRAIP is Essential for Cell Proliferation and Cell Cycle Progression 189
4.2.8 Cells without TRAIP accumulate in G2 198
4.2.9 TRAIP-Dependent G2 Cell Cycle Arrest is Dependent on ATR but not ATM 202
4.2.10 Cells without TRAIP Exhibit Increased Cell and Nuclear Size 203
4.2.11 Cells Lacking TRAIP Exit the Cell Cycle in G2/M through Senescence . . 206
4.2.12 TRAIP Degradation does not Induce Apoptosis in HCT116 Cell Lines . . . 209
4.3 Discussion 210

5 TRAIP is Essential during S-Phase for the Resolution of DNA Replication - Transcription Conflicts 218

5.1 Introduction 218
5.2 Results 219
5.2.1 The Loss of TRAIP Results in the Accumulation of DNA Damage 219
5.2.2 TRAIP does not Appear to be Required for Progression through G2/M . 222
5.2.3 TRAIP is Essential for S-Phase 224
5.2.4 TRAIP does not Appear to be Required for DNA Synthesis 228
5.2.5 γ-H2AX ChIP-Sequencing Reveals Links Between TRAIP and Transcription 232
5.2.6 TRAIP Degradation does not Increase Global Transcription 244
5.2.7 TRAIP's Mechanism of Action Requires RNA Polymerase II 245

5.2.8 TRAIP Degradation Leads to Increased DNA Replication - Transcription Collisions . . . 249
5.2.9 TRAIP and ATR Show Possible Interactions in Inducing DNA Damage . . 251
5.3 Discussion . . . 254

6 The Role of TRAIP in Replisome Disassembly 261
6.1 Introduction . . . 261
6.2 Results . . . 262
6.2.1 The Role of p97 in Replisome Disassembly . . . 262
6.2.2 The Role of Cullin-Type Ubiquitin Ligases in Replisome Disassembly . . 273
6.2.3 The Role of TRAIP in Replisome Disassembly . . . 280
6.2.4 TRAIP Degradation Prolongs DNA Replication into G2 . . . 287
6.2.5 TRAIP is Important for Mitotic Progression . . . 289
6.3 Discussion . . . 291

7 Discussion 302
7.1 The Essential Role of TRAIP during S-Phase . . . 303
7.2 Roles of TRAIP During Mitosis . . . 312
7.3 Is TRAIP a Druggable Target? . . . 317
7.4 Conclusion . . . 323

A Plasmid Constructs and Expression Sequences 324
A.1 Plasmid constructs and sequences used for recombinant protein expression and purification . . . 324
A.1.1 USP10 Insert Sequence . . . 325

A.1.2 USP22 Insert Sequence 326
A.1.3 USP34 Insert Sequence 327
A.1.4 USP37 Insert Sequence 328
A.1.5 RFWD3 Insert Sequence 329
A.1.6 TRAIP Insert Sequence 330
A.1.7 TRIP12 Insert Sequence 331
A.2 Plasmid constructs and sequences used in mammalian cell lines 333
A.2.1 LRR1 334
A.2.2 TRAIP 338

Bibliography **342**

List of Figures

Figure 1.1 Structural Confirmation of Ubiquitin 24

Figure 1.2 Different Types of Ubiquitin Modifications 27

Figure 1.3 Mechanism of Action for E1 Activation Enzymes 28

Figure 1.4 Ubiquitin Transfer to E2 Conjugation Enzymes 29

Figure 1.5 Mechanism of HECT-Type E3 Ubiquitin Ligases 30

Figure 1.6 Mechanism of RING-type E3 Ubiquitin Ligases 31

Figure 1.7 Mechanism of Ring-Between-Ring Ubiquitin Ligases 32

Figure 1.8 Structure of Cullin-Ring Type E3 Ubiquitin Ligases 33

Figure 1.9 Overview of the Eukaryotic Cell Cycle 36

Figure 1.10 Summary Schematic of Origin Licensing. 42

Figure 1.11 Summary Schematic of Origin Firing in Budding Yeast. 44

Figure 1.12 A Simplified Schematic of DNA Synthesis 48

Figure 1.13 Schematic Depicting PCNA Loading onto DNA. 49

Figure 1.14 Summary of Okazaki Fragment Maturation. 51

Figure 1.15 The Current Working Model of Replisome Disassembly 55

Figure 1.16 Summary of the Sources of Replication Stress 61

Figure 1.17 Summary of CRISPR-Cas9 Gene Editing and Auxin-Inducible Degradation . 74

Figure 2.1 Example Standard Curve for Bradford's Assay 100

Figure 2.2 Estimation of Protein Concentration Using BSA Gradients 101

Figure 2.3 Lovastatin Mediated G1 Arrest and Release 127

Figure 2.4 RO-3306 Mediated G2 Arrest and Release 129

Figure 2.5 Example FACS Gating Strategy 139

Figure 2.6 Example Mycoplasma Testing DNA Gel 144

Figure 2.7 Example Q-Q Plot 145

Figure 3.1 Protein Purification Workflow 148

Figure 3.2 Example Protein Expression Test 151

Figure 3.3 Example of Solubility Testing 153

Figure 3.4 Panel of Candidate Protein Purifications 156

Figure 3.5 Measuring DNA Synthesis in Egg Extracts 157

Figure 3.6 Immunoblots of *X. laevis* egg extract to detect candidate proteins 159

Figure 3.7 Purification of Recombinant WT and C25A TRAIP 162

Figure 3.8 TRAIP Ubiquitin Ligase Activity Drives Mitotic Replisome Disassembly . . . 163

Figure 4.1 Generation of Conditional LRR1 Degron Cells 180

Figure 4.2 mAC-LRR1 is Degraded Upon IAA Treatment 182

Figure 4.3 LRR1 is Important for Cell Viability 183

Figure 4.4 Generation of Conditional Degron Cells against TRAIP 185

Figure 4.5 TRAIP-mAID and TRAIP-mAC are Rapidly Degraded 187

Figure 4.6 TRAIP is Essential for Cell Viability 189

Figure 4.7 TRAIP is Required for Cell Proliferation 191

Figure 4.8 Degradation of TRAIP leads to G2/M Cell Cycle Accumulation after 24 h of IAA Treatment 193

Figure 4.9 Degradation of TRAIP leads to G2/M Cell Cycle Accumulation after 48 h of IAA Treatment 194

Figure 4.10 Degradation of TRAIP leads to G2/M Cell Cycle Accumulation after 72 h of IAA Treatment 195

Figure 4.11 TRAIP Depletion causes an Accumulation of Cells with < 2N DNA Content 197

Figure 4.12 Cells without TRAIP do not Accumulate in Mitosis 199

Figure 4.13 Cells without TRAIP Accumulate in G2 by a WEE1 Dependent Manner . . 201

Figure 4.14 TRAIP-Dependent G2 Cell Cycle Arrest is Rescued by ATR Inhibition 203

Figure 4.15 Cells without TRAIP Exhibit Increased Cell Size 205

Figure 4.16 Cells without TRAIP Exhibit Increased Nuclear Size 206

Figure 4.17 Cells Lacking TRAIP Exit the Cell Cycle in G2/M *via* Senescence 208

Figure 4.18 TRAIP degradation does not lead to high levels of apoptosis in HCT116 cells 210

Figure 5.1 The Loss of TRAIP Results in Accumulating DNA Damage Foci 221

Figure 5.2 TRAIP does not Appear to be Required for Progression through G2/M . . . 223

Figure 5.3 TRAIP is Important for S-Phase Progression 225

Figure 5.4 TRAIP Function in Mitosis does not Impact on the G2 Cell Cycle Arrest Observed Upon TRAIP Degradation 227

Figure 5.5 TRAIP Degradation does not Change Global DNA Replication Levels: BrdU . 229

Figure 5.6 TRAIP Degradation does not Change Global DNA Replication Levels: EdU . 230

Figure 5.7 TRAIP does not Appear to be Required for Unperturbed Replisome Disassembly 232

Figure 5.8 TRAIP is Important for the Prevention of DNA Damage in Otherwise Unperturbed Cells (I) 234

Figure 5.9 TRAIP is Important for the Prevention of DNA Damage in Otherwise Unperturbed Cells (II) 235

Figure 5.10 Accumulating γ-H2AX was not Associated with Known Replication Features 237

Figure 5.11 TRAIP Dependent γ-H2AX is Associated with Transcription Start Sites . . . 238

Figure 5.12 The Conserved Peaks are Replicated During Early S-Phase 240

Figure 5.13 TRAIP-Dependent γ-H2AX Appeared to Correlate with RNA Polymerase II 241

Figure 5.14 TRAIP-Dependent γ-H2AX Accumulates at the First TSS Possessing Bi-Directional Transcription Encountered by the Replisome 243

Figure 5.15 TRAIP Degradation does not Induce Excessive Transcription Levels 245

Figure 5.16 DNA Damage Induced by TRAIP Degradation Requires RNA Polymerase II on Chromatin 247

Figure 5.17 DNA Damage Induced by TRAIP Degradation is Epistatic with Transcription Inhibition by DRb 248

Figure 5.18 Loss of TRAIP leads to Increased Presence of RNA Polymerase II on Nascent DNA 250

Figure 5.19 TRAIP and ATR Show Possible Interactions in Inducing DNA Damage . . . 253

Figure 6.1 p97 Inhibition Leads to Reductions in the Mitotic Cell Population 264

Figure 6.2 p97 is Important for MCM7 Binding Throughout the Cell Cycle I 266

Figure 6.3 p97 is Required for S-Phase Progression 268

Figure 6.4 WEE1 Inhibition Pushes Cells into Mitosis 270

Figure 6.5 p97 Inhibition Leads to Reductions in the Mitotic Cell Population II 272

Figure 6.6 p97 is Important for MCM7 Binding Throughout the Cell Cycle II 273

Figure 6.7 MLN4924 Treatment Causes G1 Cell Cycle Accumulation 275

Figure 6.8 MLN4924 Treatment Induces MCM7 Retention on Chromatin 276

Figure 6.9 MK-1775 Treatment Overcomes MLN4924-induced G1 Cell Cycle Accumulation 278

Figure 6.10 Mitotic Replisome Disassembly Appears to be Conserved in HCT116 Cells . 279

Figure 6.11 282

Figure 6.11 TRAIP has no Detectable Impact on MCM2-7 Levels by Flow Cytometry . 283

Figure 6.12 The TRAIP Mitotic Replisome Disassembly Pathway Appeared to be Active in Human Somatic Cells 286

Figure 6.13 TRAIP Degradation Prolongs DNA Replication into G2 289

Figure 6.14 TRAIP is Important for Mitotic Progression 291

Figure 7.1 The proposed mechanism of action for TRAIP during DNA replication-transcription conflicts 311

Figure 7.2 Sites of Conserved TRAIP-Dependent DNA Damage have more Copy Number Aberrations in TRAIP-Defective Cancer Models 319

Figure 7.3 A Summary of the Designed High Throughput Screen to Identify Small Molecule Inhibitors of TRAIP 322

Figure A.1 pET28 Plasmid Map 325

Figure A.2 pCA528 Plasmid Map 332

Figure A.3 CRISPR plasmid used to generate LRR1 degron cells 334

Figure A.4 DONOR plasmid used to generate mAID-LRR1 cell lines 335

Figure A.5 DONOR plasmid used to generate mAID-LRR1 cell lines II 336

Figure A.6 DONOR plasmid used to generate mAC-LRR1 cell lines 337

Figure A.7 CRISPR plasmid used to generate TRAIP degron cells 338

Figure A.8 DONOR plasmid used to generate TRAIP-mAID cell lines 339

Figure A.9 DONOR plasmid used to generate TRAIP-mAID cell lines II 340

Figure A.10 DONOR plasmid used to generate TRAIP-mAC cell lines 341

List of Tables

Table 1.1 Summary of *X. laevis* Mass Spectrometry Data. 77

Table 2.1 Buffers Used 85

Table 2.2 Plasmids Used 91

Table 2.3 Compounds Used 92

Table 2.4 Primers Used 93

Table 2.5 Antibodies Used 94

Table 2.6 Mammalian Cell Lines Used 95

Table 2.7 Composition of SDS-PAGE Gels 97

Table 2.9 Summary of Polymerase Chain Reactions Reagents 103

Table 2.10 Summary of Restriction Digestion Reactions 105

Table 2.11 Overview of Candidates to be Purified 111

Table 2.13 Seeding Densities Mammalian Cell Experiments 121

Table 5.1 Summary of the Significant GOTerms Identified from Genes Isolated by γ-H2AX ChIP-sequencing 239

Abbreviations

ACS: ARS consensus sequence

AID: Auxin-inducible degradation

AIM: Auto-inducing media

APC: Anaphase-promoting complex

APL: Apoprotein, Pepstatin, Leuprotein

ARS: Autonomously replicating sequence

ATM: Ataxia-telangiectasia mutated

ATP: Adenosine triphosphate

ATR: Ataxia telangiectasia and Rad3-related

BSA: Bovine serum albumin

BrdU: Bromodeoxyuridine

CDK: Cyclin-dependent kinase

CFS: Common fragile site

ChIP: Chromatin immunoprecipitation

CRL: Cullin ring ubiquitin ligase

CSK: Cytoskeletal

DDT: DNA damage tolerance

DDK: Dbf4-dependent kinase

DNA: Deoxyribonucleic acid

Dox: Doxycycline

DPC: DNA protein crosslink

DRB: 1-β-D-ribofuranosylbenzimidazole

DSB: Double strand break

dsDNA: Double-stranded DNA

DUB: Deubiquitylating enzyme

EdU: 5-ethynyl-2'-deoxyuridine

Eu: 5-ethynyl uridine

FA: Fanconi anaemia

FACS: Fluorescent activated cell sorting

FBS: Fetal bovine serum

FSC: Forward scatter

GINS: go-ichi-ni-san

h/Hrs: Hours

HECT: Homologous to E6AP C-terminus

HR: Homologous recombination

HRP: Horseradish peroxidase

HSS:High speed supernatant

HU: Hydroxyurea

IAA: 3-indoleacetic acid

ICL: Interstrand crosslink

IP: Immunoprecipitation

iPOND: Isolation of proteins on nascent DNA

IPTG: Isopropyl β-d-1-thiogalactopyranoside

LB: Lysogeny broth / Luria-bertani

l: Litre

LSS: Low speed supernatant

mAC: Mini auxin inducible degron mCLOVER

mAID: Mini auxin inducible degron

MCM: Mini chromosome maintenance complex

MW: Molecular weight

NCC: Nascent chromatin capture

NHEJ: Non homologous end joining

NPE: Nucleoplasmic extract

OD: Optical density

PAM: Protospacer adjacent motif

PBS: Phosphate buffered saline

PCNA: Proliferating cell nuclear antigen

PCR: Polymerase chain reaction

PI: Propidium iodide

PLA: Proximity ligation assay

PMSF: Phenylmethylsulfonyl fluoride

Pre-RC: Pre-replicative complex

PRO-Seq: Precision run on sequencing

PT-Junction: Primer template junction

PTM: Post-translational modification

PVDF: Polyvinylidene fluoride

Rb: Retinoblastoma

RBR: Ring between ring

RFC: Replication factor C

RING: Really interesting new gene

RNA: Ribonucleic acid

RPA: Replication protein A

RPC: Replisome protection complex

SDS-PAGE: Sodium dodecyl sulfate-polyacrylamide gel electrophoresis

SSC: Side scatter

ssDNA: Single stranded DNA

TSS: Transcription start site

V: Volts

WT: Wild type

Chapter 1

Introduction

1.1 Ubiquitin

Ubiquitin is a small regulatory protein that acts as the main functional component of the post-translational modification (PTM) ubiquitylation. Protein ubiquitylation can be defined as the covalent attachment of a single ubiquitin monomer, or polyubiquitin chain, to a protein substrate. Whilst the most well described purpose of ubiquitin signalling is to induce protein degradation through the recruitment of the 26S proteasome (Hershko and Ciechanover, 1998); several other processes have also been reported, including cell division, protein activation or inactivation, protein localisation, and apoptosis (Sun and Chen, 2004). The potential implications of this modification are, in fact, so diverse that the use of ubiquitin as a protein modifier is often described as a 'signalling code'.

Ubiquitin is a highly conserved, 76-amino acid protein with an approximate molecular weight of 8.5 kDA. Ubiquitin was first described in 1975 as a polypeptide expressed across all

cell and tissue types capable of inducing T- and B- cell differentiation *in vitro* (Goldstein et al., 1975). Since then, considerable research efforts have gone into, and successfully described, many aspects of ubiquitin structure and function. Figure 1.1 depicts the tertiary protein structure of ubiquitin in two different layouts, either as a 'ribbon' or 3D representation. It is worth noting that only 3 amino acid base changes separate Yeast and Human ubiquitin and all the key residues discussed are well conserved across eukaryotic evolution (Komander and Rape, 2012).

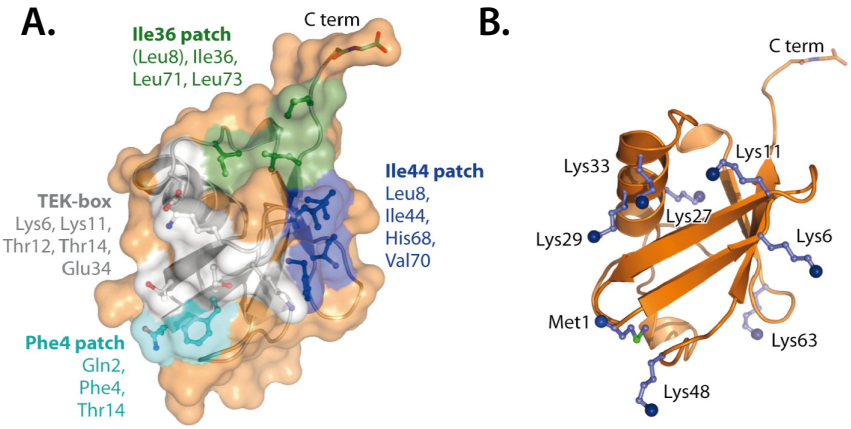


Figure 1.1: **Structural Confirmation of Ubiquitin. A.** 3D visual representation of a single ubiquitin monomer. The five functionally important regions for protein ubiquitylation, and key residues are highlighted, namely the C-terminus, Ile36 patch, Ile44 patch, TEK-box, and Phe4 patch. **B.** Ribbon format of a single ubiquitin monomer. Both β-sheets (arrow) and α-helices (coils) are represented. Shown are the 7 Lysine residues and single Methionine residue known to be important for protein ubiquitylation. Figure adapted by the author, with protein structures and raw images from Komander and Rape (2012).

Structurally, ubiquitin is composed of a compact hydrophobic core made up of mixed β-sheets and α-helices as well as a distinct, flexible, C-terminal tail (Figure 1.1B). Many of the functional roles associated with ubiquitin can be mapped to interactions at specific regions or patches across its tertiary structure (Figure 1.1A). Notably, five key regions have been identified and are required either mechanistically for ubiquitylation (C-terminus, TEK box, and Ile36 patch)

(Hospenthal et al., 2013; Wickliffe et al., 2011), or for interacting with components of the respective downstream signalling pathways associated (Ile44 and Phe4 patches) (Sloper-Mould et al., 2001; Swatek and Komander, 2016).

1.1.1 Different Types of Protein Ubiquitylation

The truly diverse nature of protein ubiquitylation can be appreciated when considering the multiple different forms of ubiquitin chains and chain structures built. The first ubiquitin monomer is attached to a substrate through isopeptide bonds between ubiquitin's C-terminal tail and a single contributing amino acid, usually Lysine, from the substrate (Varshavsky, 2001). Any further ubiquitylation to the same substrate then has one of two possible outcomes: either the attachment of additional ubiquitin monomers to different sites (Figure 1.1B), or the formation of polypeptide ubiquitin chains (Figure 1.1C-F).

Both mono-ubiquitylation and multi mono-ubiquitylation are generally thought to be insufficient to induce protein degradation. Instead, these modifications are thought to act as signals for numerous regulatory pathways (e.g. transcriptional repression or activation and DNA repair) (Nakagawa and Nakayama, 2015). Conversely, poly-ubiquitin chains can trigger protein degradation dependent on the substrate residue modified, or the ubiquitin linkage involved. Typically, ubiquitylation takes place specifically at Lysine residues on both the protein substrate, and in the formation of ubiquitin chains. Ubiquitin itself possesses 7 Lysine residues that act as targets for protein ubiquitylation (K8, K11, K27, K29, K33, K48, and K63) (Akutsu et al., 2016). The structure of poly-ubiquitin chains is influenced by the respective lysine linkage used, and different linkages are recognised by different effector

proteins. Ubiquitin chains utilising K-48, K-6, or K-11 linkages result in a compact structure due to hydrophobic patch interactions. On the other hand, chains utilising K-63 linkages are thought to create more open conformations (Komander and Rape, 2012). K-48 and K-11 linked chains are commonly causative of protein degradation; whilst K-63 linked chains have been shown to be important for the recruitment of repair factors to DNA during the DNA damage response (Komander and Rape, 2012). Moreover, N-terminal ubiquitin-ubiquitin conjugation has also been reported and results in the formation of linear ubiquitin chains (Figure 1.1C) (Walczak et al., 2012). In addition to the homogenous chain structures described, ubiquitin can also form heterogeneous or branched chains (1.1D -F). The structure and function of mixed and branched chains are less well understood. However, it is thought that these chain types may offer a mechanism to increase the complexity of ubiquitin signalling (Akutsu et al., 2016; French et al., 2021).

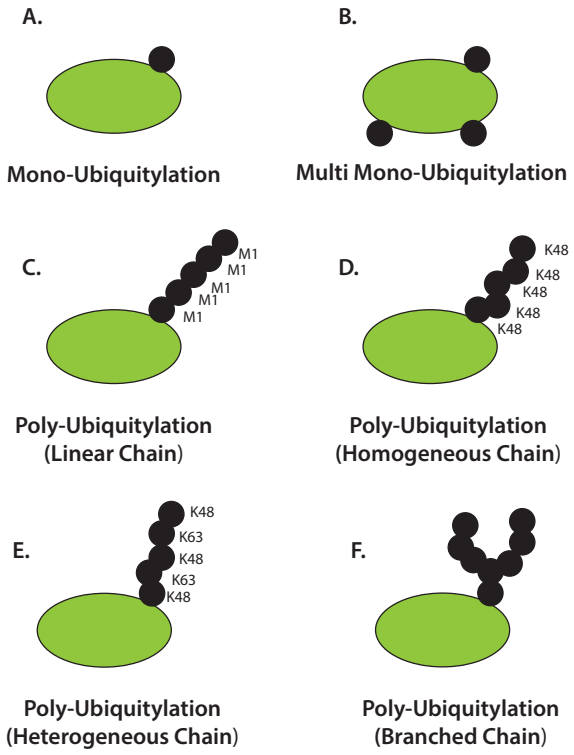


Figure 1.2: **Different Types of Ubiquitin Modifications.** Shown are different forms of ubiquitin modifications (black) on a substrate protein (green). **A.** Protein mono-ubiquitylation. **B.** Multi mono-ubiquitylation. **C.** Linear poly-ubiquitin chains, demonstrated by N-terminal methionine linked ubiquitylation. **D.** Homogeneous polyubiquitin chains, representative example from K-48 linkages. **E.** Heterogeneous polyubiquitin chains, representative example of K-48 and K-63 mixed chains. **F.** Branched poly-ubiquitin chains.

1.1.2 The Ubiquitylation Cascade

The chemical process by which ubiquitin is attached to a protein substrate is a three-step, ATP dependent mechanism henceforth referred to as the ubiquitylation cascade. Three classes of enzymes are required: E1 activating enzymes, E2 conjugation enzymes, and E3 ubiquitin ligases. The available pool of enzymes increases drastically with each step in the cascade, with 2-well established E1 enzymes, 38 E2 enzymes, and > 600 E3 ubiquitin ligases expressed in humans; offering increased substrate specificity and complexity to protein ubiquitylation (George et al., 2018; Schulman and Harper, 2009; Ye and Rape, 2009).

E1 Activating Enzymes

The first step of the ubiquitylation cascade is the activation of free cellular ubiquitin through association with an E1 activating enzyme (Figure 1.3). Ubiquitin monomers are primarily modified with C-terminal acyl-adenylation groups (AMPylation) by the E1 in a reaction requiring ATP. The high energy AMPylation reaction induces conformational changes within the E1 enzyme to enable thioester bond formation, between ubiquitin and an E1 catalytic cysteine residue. Upon binding to the E1 enzyme, the C-terminal acyl-adenylation group then dissociates from ubiquitin to form the active E1-ubiquitin complex required for the next step of the cascade (Hann et al., 2019; Schulman and Harper, 2009).

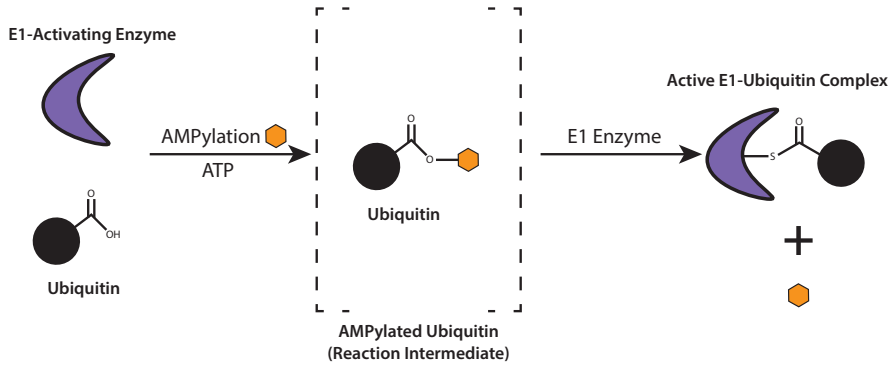


Figure 1.3: **Mechanism of Action for E1 Activation Enzymes.** Shown is a schematic summarising the activation and conjugation of free cellular ubiquitin to E1 activation enzymes. Initially, ubiquitin (black) is activated by the E1 enzyme (purple) through C-terminal AMPylation (orange) in a mechanism catalysed by ATP. This creates an intermediate AMPylated ubiquitin product that can form thioester bonds with a catalytic cysteine residue within the E1 active site.

E2 Conjugation Enzymes

The second step in the cascade is the transfer of activated ubiquitin from the E1 to an E2 conjugation enzyme (Figure 1.4). Elegant work by a number of groups has shown that the conformational change to the E1 during activation reveals otherwise obscured E2 interacting

domains (Huang et al., 2007; Lee and Schindelin, 2008; Olsen and Lima, 2013). Once associated with this domain, ubiquitin can be transferred to a similar catalytic cysteine residue on the E2 enzyme. Interestingly E2 enzymes are not simply 'stepping stones' in the cascade as first thought, and are in-fact, key regulators of ubiquitylation as a whole. It is now known that different E2 enzymes are required to catalyse mono-ubiquitylation or chain elongation, following the addition of the first ubiquitin. Moreover, each E2 enzyme typically facilitates only one or two different Lysine-linked ubiquitin chain types and so different enzymes are required for different signalling purposes (Christensen et al., 2007; Ye and Rape, 2009).

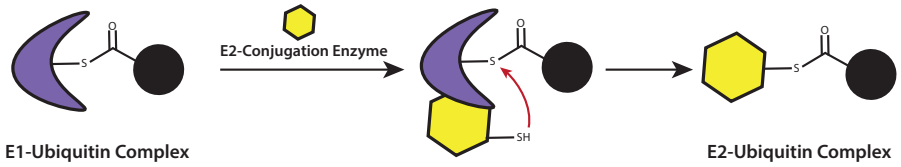


Figure 1.4: **Ubiquitin Transfer to E2 Conjugation Enzymes.** Shown is a simplified mechanism of action for E2-conjugation enzymes. The process of ubiquitin activation induces conformational changes within the structure of the E1 enzyme (purple), allowing E2 binding (yellow). Once associated, ubiquitin (black) is transferred from the E1 to a catalytic cysteine residue within the E2 active site.

E3 Ubiquitin Ligases

The third and final step in the cascade is the transfer of ubiquitin from the E2 enzyme to an appropriate protein substrate. This step is facilitated by a large family of enzymes called E3 ubiquitin ligases. The vast numbers of E3 ubiquitin ligases expressed (>600 in mammalian cells) allows for strict substrate specificity and recognition. The E3 ubiquitin ligases can be further broken down into three major groups, based on their respective mechanisms of action: Homologous to E6AP Carboxyl Terminus (HECT), Really Interesting New Gene (RING), and Ring Between RING (RBR).

Homologous to E6AP Carboxyl Terminus Ubiquitin Ligase

First reported in 1995, the HECT family of enzymes was the first group of E3 ubiquitin ligases to be described (Huibregtse et al., 1995). Since then, a total of 28 individual HECT enzymes have been identified in human cells (Scheffner and Kumar, 2014). All HECT-type ubiquitin ligases share a similar structure, comprising of a catalytically active C-terminal domain connected to a larger N-terminal region by a flexible linker. Protein ubiquitylation takes place in a two-step mechanism (Figure 1.5). The E2-ubiquitin conjugate binds specifically to the N-terminus of a HECT ligase; enabling the thioester transfer of ubiquitin to the catalytic C-terminal domain of the E3 enzyme. Ubiquitin moieties can then be transferred, from the E3, to the substrate through nucleophillic attack by the respective residue to be modified (Lorenz, 2018).

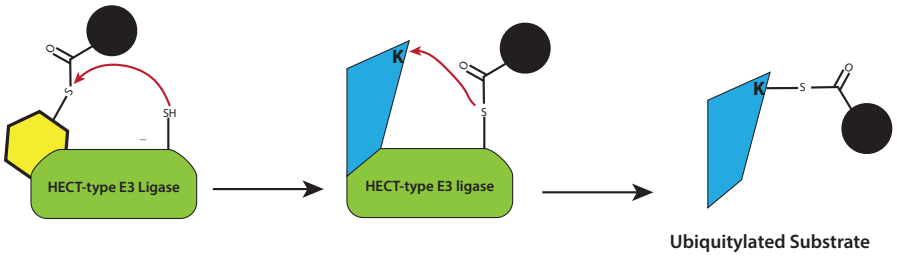


Figure 1.5: **Mechanism of HECT-Type E3 Ubiquitin Ligases.** Shown is a summary of the mechanism of ubiquitylation by HECT E3 ubiquitin ligases. Ubiquitin (black) is first transferred from the E2 enzyme (yellow) to a catalytic cysteine residue on the C-terminus of the E2 conjugation enzyme (Green). Ubiquitin is then transferred in similar fashion from the E2 enzyme to the respective lysine residue on the substrate to be modified.

Really Interesting New Gene Ubiquitin Ligase

RING type E3 ubiquitin ligases are the largest family of E3 enzymes. Unlike the HECT mechanism of action, RING-type ligases do not act as catalytic intermediates for ubiquitin transfer and instead function as scaffold proteins to bring ubiquitin spatially close to its substrate (Figure 1.6) (**?**). Structural studies have shown that E2-ubiquitin conjugates interact with the C-terminus of RING-type ligases to allow for direct hydrophobic interactions, between ubiquitin and the E3

protein surface. This orientates ubiquitin as to achieve optimal nucleophilic attack from suitable substrate lysine residues, on the ubiquitin thioester bond, facilitating the transfer of ubiquitin to the respective substrate (Plechanovova et al., 2012).

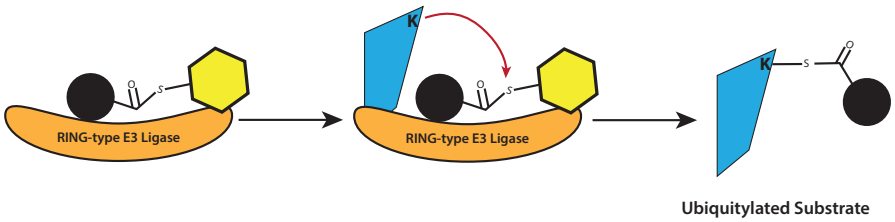


Figure 1.6: **Mechanism of RING-type E3 Ubiquitin Ligases.** Shown is a summary of the mechanism of ubiquitylation by RING-type E3 ubiquitin ligases. The E2 – conjugation enzyme (yellow) associates with the C-terminus of the RING ligase (orange). Ubiquitin (black) is held in place through hydrophobic interactions with the surface of the ligase. This interaction orientates ubiquitin as to provide optimal nucleophilic attack of the thioester bond from a substrate (blue) donor residue. This results in the transfer of ubiquitin directly from the E2, to the substrate.

RING Between RING Ubiquitin Ligases

RBR is the smallest and most recently discovered family of E3 ubiquitin ligases, with only 14 members identified as of 2018 (Walden and Rittinger, 2018). RBR ligases share features with both the RING and HECT-type E3 ubiquitin ligases. Notably, RBR enzymes comprise of two RING domains (RING1/RING2) separated by an In-Between Ring region (IBR). Surprisingly, studies on this family of enzymes also revealed a HECT-like catalytic cysteine residue within RING2 (**?**). Protein ubiquitylation by RBR is achieved through a two-step process (Figure 1.7). First, the E2 enzyme is recruited to RING1. Ubiquitin is then transferred from RING1, to the catalytic cysteine residue on RING2, before being subject to nucleophilic attack from substrate lysine residues (Walden and Rittinger, 2018). Intriguingly, work with arguably the most-studied RBR ligase, Parkin, revealed high levels of autoinhibition in endogenous conformations; raising the question of whether RBR ligases require activation prior to functioning as a ubiquitin ligase (Trempe et al., 2013).

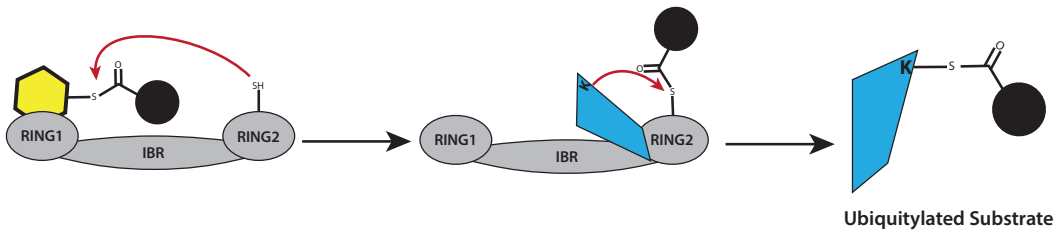


Figure 1.7: **Mechanism of Ring-Between-Ring Ubiquitin Ligases.** Shown is a summary of the mechanism of ubiquitylation by RING-type E3 ubiquitin ligases. The E2 conjugation enzyme (yellow) associates with the RING1 domain of the ligase (grey). Ubiquitin is then transferred from the E2 to a HECT-like catalytic cysteine residue within the RING2 domain. The ubiquitin is finally added onto the appropriate residue of a substrate (blue) from the RING2 domain in a mechanism similar to that seen in HECT-type ubiquitin ligases.

Cullin-Type Ubiquitin Ligases

Whilst not strictly classed as an standalone family of E3 ubiquitin ligases, the Cullin-Ring E3 Ligases (CRL) sub-family are responsible for as much as 20% of all ubiquitin-mediated protein degradation in mammalian cells (Soucy et al., 2009). Notably, Cullin-type ubiquitin ligases are a major regulatory factor in cell cycle progression and DNA replication (Moreno and Gambus, 2015). CRLs are multi subunit enzymes composed of a central Cullin scaffold protein, C-terminal RING-finger domain containing protein, as well as an N-terminal substrate recognition protein and adaptor protein (Figure 1.8). In mammalian cells, seven cullin-type protein scaffolds are expressed and form the core structure of approximately 500 CRL complexes (Cul1, Cul2, Cul3, Cul4A, Cul4B, Cul5, and Cul7) (Zimmerman et al., 2010). The RING-domain protein recruited to the N-terminus of the cullin scaffold contains the catalytic domain required for ubiquitin ligase activity. In mammalian cells, only two RING-type proteins have been identified to form complexes with CRLs (Rbx1 and Rbx2). The final two components, the substrate recognition and adaptor proteins function to recruit protein substrates and facilitate binding of the substrate recognition protein to the cullin scaffold, respectively (Nguyen and Wang, 2017; Zimmerman et al., 2010). The main separating factor of CRLs compared to other types

of ubiquitin ligase is a requirement for pre-activation. Cullin-type ubiquitin ligases are first activated by attachment of the ubiquitin-like protein NEDD8. Interestingly, it is thought that the RING-type proteins RBX1 and RBX2 are able to function as both ubiquitin and NEDD8 E3 ligases, and so effectively facilitate activation of themselves (Nguyen and Wang, 2017; Petroski and Deshaies, 2005). Cullin activation by neddylation serves to induce structural changes to facilitate protein ubiquitylation by bringing the catalytic RING-domain containing protein spatially closer to the respective substrate.

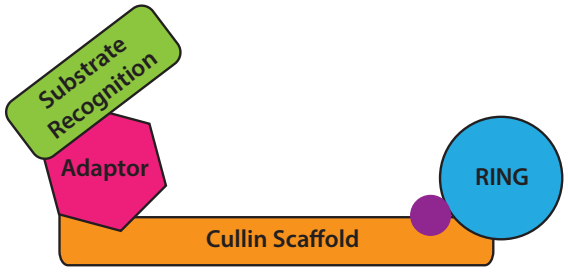


Figure 1.8: **Structure of Cullin-Ring Type E3 Ubiquitin Ligases.** Shown is a representative example of an activated Cullin ubiquitin ligase (CRL). CRLs are composed of a Cullin protein scaffold (orange), C-terminal catalytic RING-domain containing protein (blue), adaptor protein (pink), and substrate recognition complex (green). CRLs require activation prior to carrying out protein ubiquitylation; achieved through C-terminal protein Neddylation (purple).

1.1.3 Deubiquitylating Enzymes and Ubiquitin Recycling

To ensure the constant availability of protein ubiquitylation as a PTM, sufficient quantities of free ubiquitin must be maintained at all times. The pool of ubiquitin available for ubiquitylation within a cell can be sustained through two different mechanisms: recycling of existing ubiquitin bound to substrates by deubiquitylation, of the *de novo* synthesis of new ubiquitin from pre-cursors. In mammalian cells there are four genes responsible for the expression of ubiquitin precursors (UBA52, UBA80, UBB, and UBC). UBA52 and UBA80 encode

for ubiquitin-ribosomal fusion proteins whilst UBB and UBC encode for polymeric ubiquitin chains (Grou et al., 2015). However, in all cases, ubiquitin monomers must be cleaved from their respective bound components by deubiquitylating enzymes.

Deubiquitylating enzymes or DUBs are a family of proteases that specifically target, and cleave, isopeptide bonds between conjoined ubiquitin monomers or ubiquitin–substrate complexes. Seven families of DUBs have been identified to be active in mammalian cells to date: the cysteine proteases USPs, UCHs, OTUs, MJds/Josephins, MINDYs, ZUP1, and the zinc dependent metalloproteinases MPN/JAMMs (Clague et al., 2019). Typically, each individual DUB has preference for binding to the substrate proteins themselves, or specific lysine-linked ubiquitin chains. Once bound, protein deubiquitylation then takes place using either EXO-DUB activity (interacting with the last ubiquitin in the chain), or ENDO-DUB activity (binding within polyubiquitin chains) (Mevissen and Komander, 2017). DUBS are important for a wide range of cellular signalling processes, including maintaining suitable quantities of free ubiquitin. Of particular note is the significance of deubiquitylation in ubiquitin-mediated proteasomal degradation. For any protein targetted for degradation to fit within proteasome channel, ubiquitin chains must first be removed. Several essential DUBs have been identified to interact with the proteasome to fulfil this purpose, including USP14, UCHL5, and PSMD14 (Poot et al., 2017).

1.1.4 Ubiquitin-Like Protein Modifiers

Ubiquitylation is not unique as a post-translational modification involving the attachment of small protein modifiers. Throughout evolution there have been a number of proteins

found to share a ‘ubiquitin-like’ β-fold, including the sulphur carrying bacterial proteins This (thiamine-biosynthesis family) and moaD (molybdenum cofactor biosynthesis) (Rudolph et al., 2001; Wang et al., 2001). In mammalian cells 8 different ubiquitin-like proteins (UBLs) have been identified (NEDD8, FUBI, FAT10, ISG15, Atg8, Atg12, Urm1, and UFM1) (Hochstrasser, 2009). All UBLs are thought to share a similar mechanism of action. They are first activated through adenylation/AMPylation by an E1 activating enzyme before being conjugated first to an E2 enzyme, and then the substrate of interest through association with E3 ligases. Together, ubiquitin-like proteins regulate a wide range of cellular processes, including the DNA damage response, autophagy, and protein trafficking throughout a cell. Interestingly, ubiquitin-like modifiers and ubiquitin itself show some degree of cooperation, exemplified by the regulation of Cullin-type E3 ubiquitin ligases by the small protein modifier NEDD8 (Neddylation) (Taherbhoy et al., 2012).

1.2 The Eukaryotic Cell Cycle

Cell growth, and ultimately cell division, is governed by the cyclic progression through four distinct stages (G1, S-phase, G2, and mitosis; Figure 1.9). G1 and G2 are commonly referred to as ’gap’ or growth stages. During G1 and G2, the cell undergoes limited morphological change but remains biochemically active, growing and synthesising all the required components for DNA replication and cytokinesis; subsequently taking place during S-phase and mitosis, respectively (Schafer, 1998). Transitions between each stage of the cell cycle are mediated by Cyclin Dependent Kinases (CDKs), activated through site-specific phosphorylation and the association to a cell-cycle stage dependent cyclin (Galderisi et al., 2003). Once activated, Cyclin-CDK holoenzymes phosphorylates specific targets to trigger signalling cascades and

cell cycle transition. For example, Cyclin D-CDK4/6 phosphorylates the tumour suppressor Retinoblastome (Rb) during G1 to facilitate the transcription of several genes essential for S-phase entry (Vélez-Cruz and Johnson, 2017). On the other hand, Cyclin-CDK inactivation also plays an important role in cell cycle progression. During mitosis, the inactivation of Cyclin B-CDK1 is required for mitotic exit and G1 entry (Noton and Diffley, 2000). This control of Cyclin-CDK activity throughout the cell cycle is primarily exerted through CDK inhibition and cyclin degradation by the ubiquitin-proteasome pathway. Notably, the Anaphase Promoting Complex (APC) targets Cyclins A and B for degradation during the mitotic-G1 transition, whereas the SKP1-Cullin1-RBX1 (SCF complex) ubiquitylates Cyclins D and E during the G1-S transition (Tu et al., 2012).

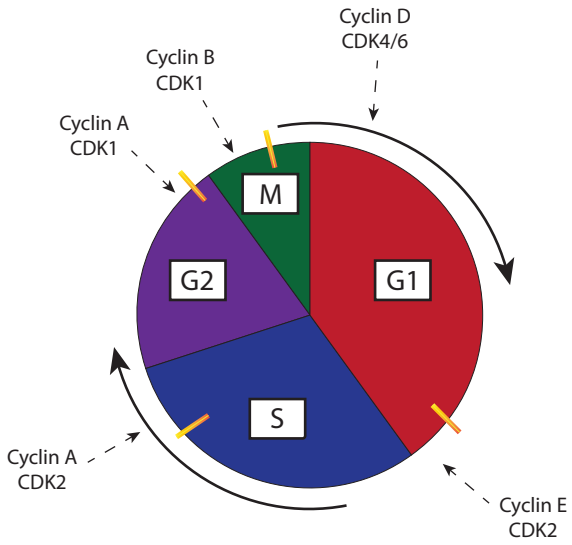


Figure 1.9: **Overview of the Eukaryotic Cell Cycle.** Shown are the four major stages of the cell cycle: G1 (red), S (blue), G2 (purple), and mitosis (green). Arrows indicate directionality through the cell cycle. The transitions between each respective stage is controlled by the activity of Cyclin-CDK holoenzymes, depicted. In addition, four major checkpoints exist to prevent the preservation of potentially damaging mistakes occurring throughout the cell cycle (shown as orange lines): the G1 or restriction checkpoint, intra S-phase checkpoint, G2 or DNA damage checkpoint, and mitotic or spindle assembly checkpoint.

The temporal separation of different cell cycle stages ensures that cellular growth can be halted if any abnormalities are detected. Four major cell cycle checkpoints exist to prevent the

propagation and preservation of damaged cells: G1/S (DNA damage), intra S-phase, G2 (DNA damage), and mitosis (Spindle Assembly Checkpoint). For a cell to progress from G1 stage of the cell cycle into S-phase, a switch from growth-factor dependent to independent signalling occurs. Defined as the G1 restriction point, this is the stage where cells are committed to the proliferative cell cycle. In the presence of proliferation-driving growth factors, increasing Cyclin D-CDK4/6 activity leads to the hyper-phosphorylation of Rb, preventing its inhibitory binding to E2F transcription factors and facilitating the expression of Cyclin E-CDK2 to drive S-phase entry (Moser et al., 2018). Conversely, in anti-proliferative conditions Rb is hypo-phosphorylated to maintain E2F inhibition, preventing cell cycle entry. Alongside this described cell cycle regulation, a second mechanism exists during G1 to prevent S-phase entry in the presence of DNA damage. Described as a two-wave model, the G1/S DNA damage checkpoint occurs in a p53-independent and p53-dependent manner, facilitating both a rapid and sustained response. First, the phosphatase CDC25A is rapidly targetted for ubiquitylation and protein degradation through the activation of ATM/ATR kinases followed by CHK2/CHK1, respectively dependent on DNA damage type (Falck et al., 2001; Mailand et al., 2000). The rapid degradation of CDC25A functions to prevent activation of CDK2 and therefore block S-phase entry (Bartek and Lukas, 2001). Second, the detection of DNA damage leads to the stabilisation of the tumour suppressor p53 through multiple modifications. p53 can then stimulate the transcription of the CDK inhibitor p21, preventing Cyclin E-CDK2 activity and therefore S-phase progression (Bartek and Lukas, 2001).

The intra S-phase checkpoint functions to sustain DNA replication by protecting active replication forks, a response discussed further in Chapter **1.4**. Several processes have been

reported to be controlled by this checkpoint, including origin firing, the replication stress response, and DNA damage repair (Segurado and Tercero, 2009). The G2 or DNA damage checkpoint acts to prevent damaged DNA from being segregated into two daughter cells. Activation of the DNA damage response, primarily by the master kinases ATR and ATM (discussed further in **1.4**), triggers a signalling cascade to arrest cells during G2 and block mitotic entry. Specifically, the detection of DNA damage results in the inactivation of the phosphatase CDC25, as well as WEE1 kinase activation, to inhibit CDK1 activity required for mitosis (Patil et al., 2013). The mitotic checkpoint is a final failsafe to ensure the correct segregation of sister chromatids. Through the recruitment of a Spindle Assembly Complex (composed of MAD1, MAD2, MAD3, BUB1, and BUB3) to unattached kinetochores, APC activity is blocked and mitotic exit inhibited until all kinetochores are stably attached to the spindle (Lara-Gonzalez et al., 2012).

1.3 Eukaryotic DNA Replication

DNA replication constitutes the semi-conservative duplication of all cellular genetic material. In eukaryotes, the entire genome is compacted within the nucleus into complex structure called chromatin; composed of DNA tightly wrapped around histones (the nucleosome), subsequently forming higher order structures. Every cell cycle, the chromatin must be unwound and nucleosomes displaced before the DNA is copied and repackaged into chromatin structures prior to division into two identical daughter cells. To maintain cellular propagation, DNA replication must be executed without error. As such, the respective mechanisms involved are highly conserved across evolution. However, DNA replication does not take place in isolation and stringent regulation is required to ensure co-operation with several other essential processes taking place simultaneously (e.g., DNA repair pathways and transcription). Mistakes during DNA replication are particularly damaging and commonly give rise to genomic instability, a key hallmark of tumour development (Gaillard et al., 2015). In addition, several inheritable genetic disorders have been associated with mutations in genes encoding for key components of DNA replication and repair, further highlighting the essential nature of these processes, including: Meier-Gorlin's Syndrome, Bloom's Syndrome, and Werner's Syndrome (Jackson et al., 2014).

1.3.1 DNA Replication Initiation

The first stage of DNA replication, initiation, is a two-step mechanism spanning several stages of the cell cycle. First, the core of the replicative helicase (MCM2-7 double hexamers) is assembled onto chromatin at origins of replication. The loaded complexes are then activated specifically in S-phase to form a platform for the recruitment of additional replisome components, facilitating

DNA unwinding and de novo DNA synthesis.

Origins of Replication

Replication origins are genomic locations that act as the start sites for DNA replication. The respective numbers of origins present correlates with genome size and complexity, ranging from approximately 400 in yeast, to between 30 000 – 50 000 active origins in mammalian cells (Leonard and Mechali, 2013). First identified in *Saccharomyces cerevisiae*, origins were initially reported as short (100 – 150 bp) sequences promoting plasmid replication irrespective of genome incorporation (Clyne and Kelly, 1995; Stinchcomb et al., 1979). Appropriately named autonomously replicating sequences (ARS), all ARS contain a highly conserved 11 bp ARS consensus sequence (ACS) that is required for origin recognition by DNA replication factors (Bell and Labib, 2016). However, unlike other aspects of DNA replication, origins do not appear to be fully conserved throughout evolution. In budding yeast, replication origins are defined by the ACS sequence. Conversely, studies in higher eukaryotes (e.g. *Xenopus laevis*, *Drosophila melanogaster*, and mammalian cell lines) found no such consensus sequence (Cvetic and Walter, 2005). Despite this, the location of replication origins in higher eukaryotes is not thought to be random. Work from several groups has coupled next generation sequencing with biochemical approaches to capture replication intermediates and gain further insight. These studies revealed a robust replication timing programme, centred around origin activation time (Prioleau and MacAlpine, 2016). Replication origins activated in early S-phase are generally found in euchromatic coding regions, close to G-C rich CpG islands. Whilst those activated in mid-late S-phase typically reside in the more compact heterochromatic regions (Picard et al., 2014). Furthermore, several epigenetic markers have been found to be potentially indicative

of replication origins, conserved over multiple mammalian cell line (Chandra et al., 2012; Ryba et al., 2010; Thurman et al., 2007).

Origin Licensing

During late mitosis and G1 of the cell cycle, the enzymatically inactive core of the replicative helicase (MCM2-7 double hexamers) is loaded onto chromatin (Figure 1.10). The mechanism of origin licensing has been successfully reconstituted *in vitro* using purified proteins: the AAA^+ ATPase family proteins ORC, Cdc6, and MCM2-7, as well as the licensing factor Cdt1 (Evrin et al., 2009; Remus et al., 2009). ORC first binds to replication origins and subsequently recruits Cdc6 (Seki and Diffley, 2000). The resulting ORC-Cdc6 complex then acts as a platform for Cdt1-MCM2-7 recruitment to form the Pre-Replicative Complex (Pre-RC). Pre-RC assembly also requires a series of ATP hydrolysis reactions, enabling the MCM2-7 ring to open and enclose DNA, as well as the dissociation of both Cdt1 from MCM7, and MCM2-7 from ORC-Cdc6 (Randell et al., 2006). Whilst MCM2-7, ORC, and Cdc6 all possess ATPase activity, differential requirements have been demonstrated in different model systems (Bowers et al., 2004; Coster et al., 2014; Fernández-Cid et al., 2013; Randell et al., 2006; Speck et al., 2005).

The origin licensing model detailed in Figure 1.10 describes how a single MCM2-7 hexamer is loaded onto chromatin. However, to allow for bi-directional DNA synthesis, the final product of origin licensing are double MCM2-7 hexamers loaded in a 'head to head' (N-terminus to N-terminus) fashion (Evrin et al., 2009; Gambus et al., 2011; Remus et al., 2009). A recent landmark paper in the field utilised electron microscopy to capture replication intermediates and shed light on this highly debated aspect of origin licensing (Miller et al., 2019). The authors

showed that, following the dissociation of Cdc6 and Cdt1 from the pre-RC, a second ORC complex interacted with the N-terminus of MCM2-7; facilitating the recruitment of a second MCM2-7 hexamer (Miller et al., 2019).

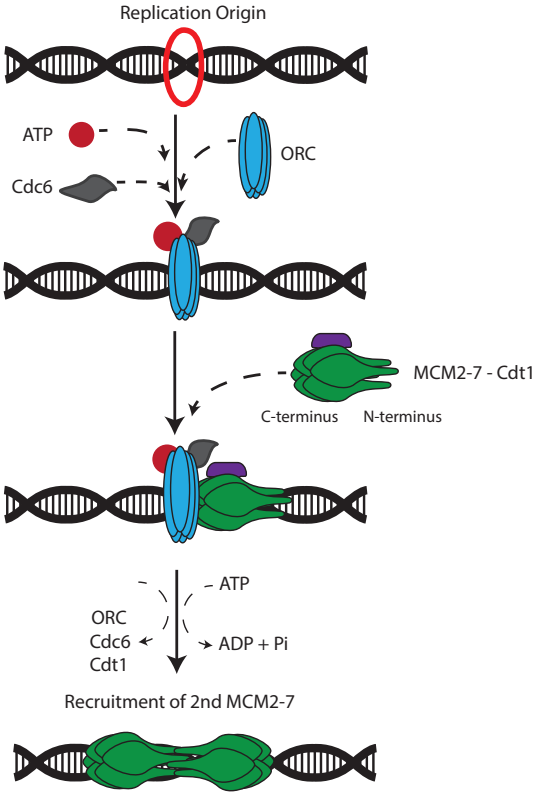


Figure 1.10: **Summary Schematic of Origin Licensing.** The ORC hexameric protein binds to replication origins in an ATP dependent manner, which in turn associates with Cdc6. The ORC-Cdc6 complex can then recruit MCM2-7-Cdt1. ATP hydrolysis results in the opening and closing of the MCM ring around DNA, dissociation of Cdt1 from MCM2-7, and MCM2-7 dissociation from ORC. The final step is to form double MCM2-7 hexamers through replication intermediates not shown.

Origin Firing

The second step of DNA replication initiation is the activation of the loaded MCM2-7 double hexamers, known as origin firing (Figure 1.11). Helicase activation takes place specifically during S-phase and revolves around the recruitment of Cdc45 and GINS (Sld5, Psf1, Psf2, and Psf3) to MCM2-7, forming the active CMG complex (Cdc45-MCM2-7-GINS; Figure 1.3.2) (Aparicio

et al., 2009; Gambus et al., 2006; Ilves et al., 2010; Moyer et al., 2006). Notably, the process of helicase activation also induces a distinctive change to the MCM2-7 binding pattern, from double stranded DNA to single stranded DNA. Similar to origin licensing, much of our current knowledge of origin firing has been derived from biochemical reconstitution using yeast purified proteins, and will therefore be described. The key factors involved are: DDK (Cdc7/Dbf4), Sld3 (Treslin), Sld7 (MTBP), Cdc45, CDK, Dpb11 (TopBP1), Sld2 (RecQ4), Pol ϵ, GINS, and MCM10 (Yeeles et al., 2015). In budding yeast, the DDK Cdc7 phosphorylates MCM2-7 to facilitate interaction with Sld3-Sld7-Cdc45 (Heller et al., 2011). Following this, CDK catalysed phosphorylation of Sld2 and Sld3 triggers the recruitment of a pre-loading complex (Pre-LC) to CDC45-MCM2-7 (Pre-LC: CDC45-MCM2-7, phosphorylated Sld2, Dpb11, Pol ϵ, and GINS) (Masumoto et al., 2002; Tanaka and Araki, 2013). The final component of the active replisome, MCM10, is thought to be recruited alongside GINS in a CDK dependent manner (Gambus et al., 2006; Heller et al., 2011; Yeeles et al., 2017). Whilst not essential for CMG assembly, MCM10 is required for CMG activation and the unwinding of origin DNA (Kanke et al., 2012). Interestingly, MCM10 has also been implicated in Cdc45 recruitment, potentially suggesting additional interactions with the replicative helicase (Sawyer et al., 2004; Wohlschlegel et al., 2002).

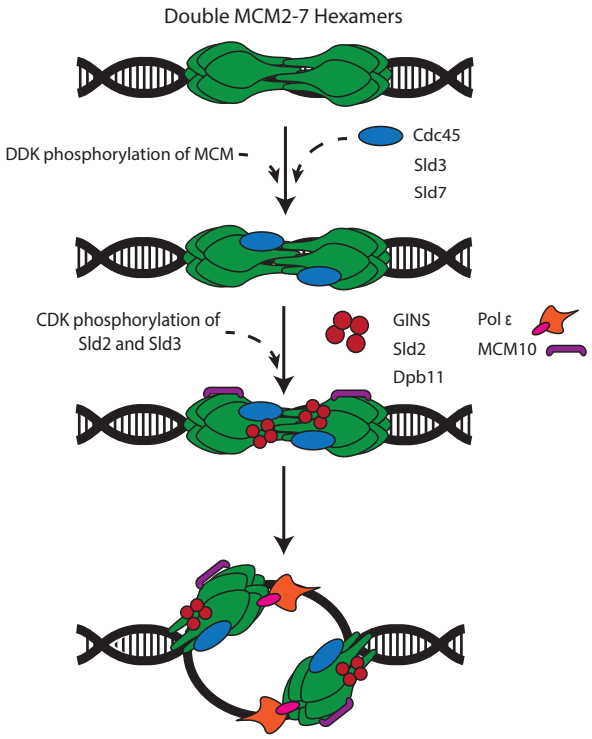


Figure 1.11: **Summary Schematic of Origin Firing in Budding Yeast.** The inactive replicative helicases loaded during origin licensing are activated upon entry into S-phase. First, DDK catalysed phosphorylation of MCM2-7 results in the recruitment of Cdc45, Sld3, and Sld7. Subsequent phosphorylation of Sld2 and Sld3 by CDK's leads to binding of GINS, Sld2, Dpb11, and Pol ϵ to the complex. Exactly when MCM10 is recruited remains an area of discussion, with studies showing recruitment following GINS binding as well as a requirement to for Cdc45 interaction with the pre-RC..

1.3.2 Limiting DNA Replication to Once-Per Cell Cycle

To maintain genomic stability, and ensure proper cell propagation, DNA replication must be restricted to take place exactly once per cell cycle. For this, origin licensing and origin firing are restricted to different cell cycle stages. In addition, a stringent replication timing programme exists to prevent the over-replication of nascent DNA; whilst simultaneously ensuring the establishment of sufficient numbers of MCM2-7 double hexamers for the complete and timely duplication of the entire genome.

Over-replication of the genome, commonly referred to as re-replication, is a highly cytotoxic event that often results in aberrant gene amplification as well as the accumulation of damaging DNA lesions (Truong and Wu, 2011). In eukaryotes, re-replication is primarily prevented through the temporal separation of origin licensing and origin firing. Origin licensing can only take place when CDK activity is low, during late mitosis and G1 stages of the cell cycle. Conversely, origin firing requires CDK activity and therefore must take place during S-phase, when CDK activity is high. The diminished CDK levels allowing for origin licensing is, in part, achieved through APC activity (See **1.2**). Notably, during G1, the APC targets mitotic CDKs, the CDK activating protein Cdc25, and geminin for degradation (Moreno and Gambus, 2015). Geminin, if allowed to accumulate, would block origin licensing through Cdt1 inhibition and so its degradation promotes the incorporation of MCM2-7 to the pre-RC (Tada et al., 2001; Wohlschlegel et al., 2000). In addition, the CDK inhibitors p21 and p27 also block CDK activity in late mitosis and G1 to promote the stability of pre-RC components (Siddiqui et al., 2013). During S-phase, the APC is inactivated and CDK activity increases. Importantly for origin firing, the switch in CDK and APC levels essentially blocks all pre-RC components to prevent any further origin licensing. The loss of APC activity allows geminin to accumulate, blocking Cdt1. Moreover, increased S-phase CDK activity results in Cdt1 and Cdc6 phosphorylation, flagging these proteins for ubiquitylation and subsequent degradation by the proteasome (Moreno and Gambus, 2015). Furthermore, any residual Cdt1 can also be degraded during S-phase in a PCNA-dependent manner (Arias and Walter, 2006).

Due to the strict regulation surrounding origin licensing and origin firing, no more MCM2-7 complexes can be loaded onto chromatin following entry into S-phase. Therefore, sufficient

quantities of MCM2-7 must be loaded during G1 to ensure the complete duplication of the entire genome. In addition, the loaded double hexamers must also function to rescue any potential losses of replicative activity due to fork stalling or damage. For these purposes, MCM2-7 double hexamers are loaded in excess at each replication origin and become distributed across large stretches of DNA surrounding ORC in a phenomenon known as the MCM paradox (Edwards et al., 2002). Whilst the numerous inactive helicases are assembled at every origin, only a subset of these are then activated, with the rest remaining dormant. Moreover, origin firing is heterogeneous and inactive dormant origins can be activated at any point throughout S-phase (Das et al., 2014). In the case of replication fork stalling or DNA damage, which would otherwise result in regions of under-replicated DNA, the stochastic nature of dormant origin activation enables firing of additional double hexamers to ensure the complete duplication of the genome (Alver et al., 2014). Interestingly, the presence of multiple MCM2-7 subunits on DNA does not impair replication fork progression. Studies have shown that loaded MCM2-7 complexes are not fixed in place on chromatin and can be pushed by ongoing replication forks (Douglas et al., 2018; Remus et al., 2009). However, the resulting MCM 'trains' do act as a barrier when two neighbouring replication forks converge. Recent work has shown that together with the active replisome, the ATP-dependent helicase Pif1 can unload inactive MCM2-7 complexes to facilitate CMG convergence and replication termination (Hill et al., 2020).

1.3.3 Replication Elongation

The CMG assembled onto chromatin during replication initiation forms the core replicative helicase, and the binding platform for replisome components. Alongside CMG the key

components of the active replisome include: the replication progression complex (RPC: Mrc1/MRC1, Tof1-Csm3/TIMELESS-TIPIN, FACT, Topoisomerase I, and Ctf4/And-1; Gambus et al. (2006)), PCNA, RPA, Replication Factor C (RFC), Pol α, Pol δ, and Pol ϵ (Yao and O'donnell, 2010). Once fully assembled, the RPC resides on the leading DNA strand, at the tips of replication forks, and is responsible for the unwinding of double stranded DNA in a 3' to 5' direction (Georgescu et al., 2017). Due to the antiparallel nature of DNA, each CMG loaded is situated on opposite DNA strands, and therefore translocates DNA in opposite directions to create the replication forks, or the replication bubble between them. The single stranded DNA resulting from CMG helicase activity is rapidly coated in the DNA binding protein RPA to prevent nuclease activity and DNA hairpin formation (Fanning et al., 2006).

The Role of DNA Polymerases in DNA Synthesis

Three DNA polymerases are required for the *de novo* synthesis of single stranded DNA: Pol α, Pol δ, and Pol ϵ. A simplified schematic of the replication machinery during DNA synthesis is shown in Figure 1.12. Although leading strand synthesis is primarily carried out by Pol ϵ, all three DNA polymerases are required. A particularly elegant study by Yeeles et al. (2017) demonstrated the mechanism of leading strand synthesis *in vitro* using purified recombinant proteins. Following CMG activation, the replisome initially unwinds template DNA at a slow rate. The resulting single stranded regions are bound to by Pol α to generate short DNA-RNA nucleotide priming sequences. The RFC complex then associates with these priming sequences, recruiting PCNA and then Pol δ to the replication fork (Figure 1.13). At this stage, as the rate of DNA unwinding is slower than DNA synthesis, Pol δ will ultimately collide with the replisome where it is displaced by the more efficient Pol ϵ (Yeeles et al., 2017). Interactions between Pol

ϵ and CMG, through a Dpb2 subunit of Pol ϵ (Sengupta et al., 2013), increases the speed of DNA unwinding to facilitate continuous leading strand synthesis (Yeeles et al., 2017). Lagging strand synthesis, on the other hand, is carried out discontinuously in the opposite direction to replication fork progression. Similar to leading strand synthesis, Pol α is required for putting down the primer, stimulating PCNA and DNA polymerase recruitment to facilitate elongation; which, in the case of lagging strand synthesis, is carried out entirely by Pol δ (Kunkel and Burgers, 2008; Pellegrini and Costa, 2016). However, unlike leading strand synthesis, and due to the discontinuous nature of lagging strand synthesis, there is a constant requirement for DNA priming. Consequently Pol α is coupled to GINS (Sld5) through a trimeric Ctf4 complex to generate the short DNA-RNA priming sequences needed as the replisome progresses through chromatin (Simon et al., 2014).

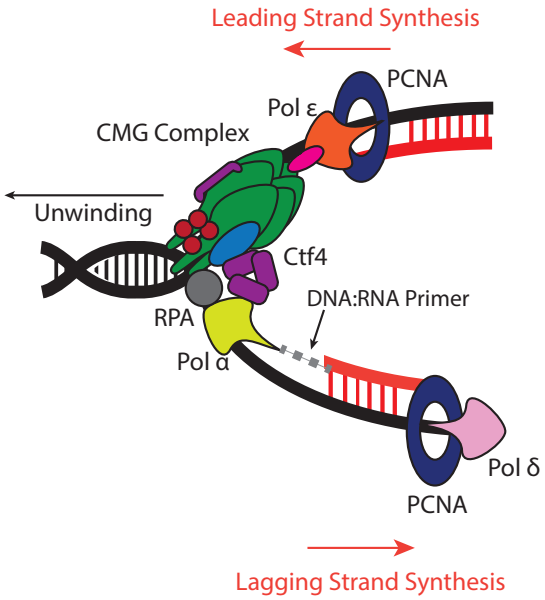


Figure 1.12: **A Simplified Schematic of DNA Synthesis.** The CMG complex is situated on the leading strand at the tip of replication forks and unwinds double stranded DNA in a 3' to 5' manner. DNA replication of the leading strand is carried out by Pol ϵ, coupled to the CMG complex through DPB2. Lagging strand synthesis is carried out discontinuously by Pol α priming activity followed by Pol δ mediated elongation.

The DNA Clamp PCNA is Essential for Replication Elongation

The proliferating cellular nuclear antigen (PCNA) is a homotrimer essential for DNA replication. During replication elongation, PCNA is loaded onto single stranded DNA to anchor the polymerases to the respective strand being synthesised. In addition, the recruitment of PCNA has been shown to increase the enzymatic processivity of DNA polymerases to comparable final levels; by 100-fold and 6-fold for Pol δ and Pol ϵ, respectively (Boehm et al., 2016). The henteropentameric complex RFC is responsible for loading PCNA onto ssDNA (Figure 1.13) at the 3' end of the primer template generated by Pol α (PT junction). ATP hydrolysis is required for the PCNA ring to encircle DNA, as well as for the dissociation of RFC from PCNA, and to induce conformational changes reducing the PCNA-DNA binding affinity; essential for translocation and DNA synthesis (Hedglin et al., 2013).

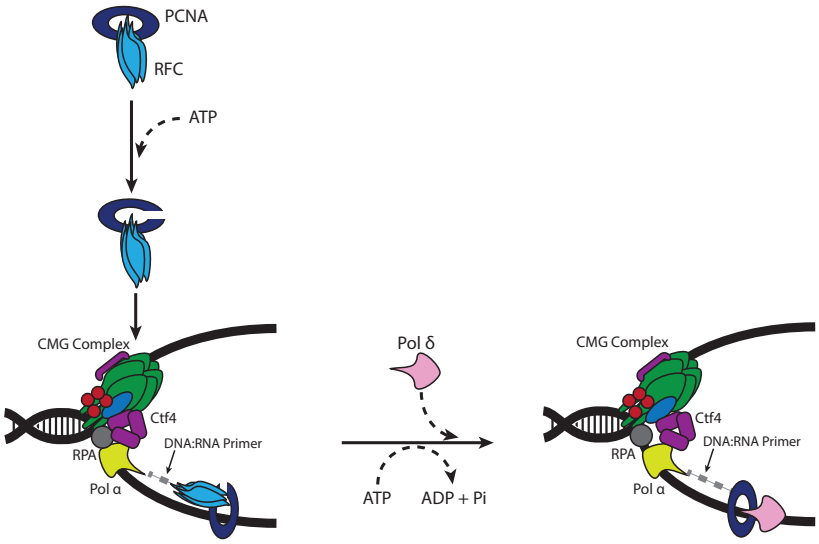


Figure 1.13: **Schematic Depicting PCNA Loading onto DNA.** The RFC associates with PCNA and ATP to induce a conformational change and PCNA ring opening. PCNA is then loaded onto chromatin at PT junctions. Subsequent ATP hydrolysis leads to RFC dissociation and ring clamping around DNA.

Okazaki Fragment Maturation

Lagging strand synthesis requires the regular placement of RNA-DNA primers, subsequently extended by Pol δ. As a result, newly synthesised double stranded DNA is flanked by DNA-RNA primers (Okazaki fragment) at each PT junction. Okazaki fragment maturation describes the pathways responsible for the removal of RNA primer sequences generated by Pol α, and the ligation of discontinuous nascent DNA into a single strand. Two different mechanisms for Okazaki fragment maturation have been identified and will be described: the short flap or long flap pathways (Figure 1.14). Upon encountering an RNA-DNA primer during lagging strand synthesis, Pol δ will advance short distances to displace the RNA from template DNA, creating a flap. If the generated RNA flaps are short enough in length (approximately 1-2 nucleotides), then the 5' – 3' endonuclease FEN1 can bind and cleave RNA (short-flap pathway). This mechanism continues in an iterative fashion, alternating between flap displacement and cleavage, until the RNA primer has been removed (Burgers, 2009; Liu et al., 2004; Zheng and Shen, 2011). However, if the RNA flaps displaced by Pol δ remain unprocessed, RPA will bind and block FEN1 activity. In this scenario, the nuclease DNA2 is required to remove RPA and the associated RNA. Any residual RNA remaining is then processed by the short-flap pathway. Finally, the 5' endonuclease activity of FEN1 combined with the 3' exonuclease activity of Pol δ generates nicks within the newly synthesised DNA strand that are ligated together by DNA Ligase (Burgers, 2009).

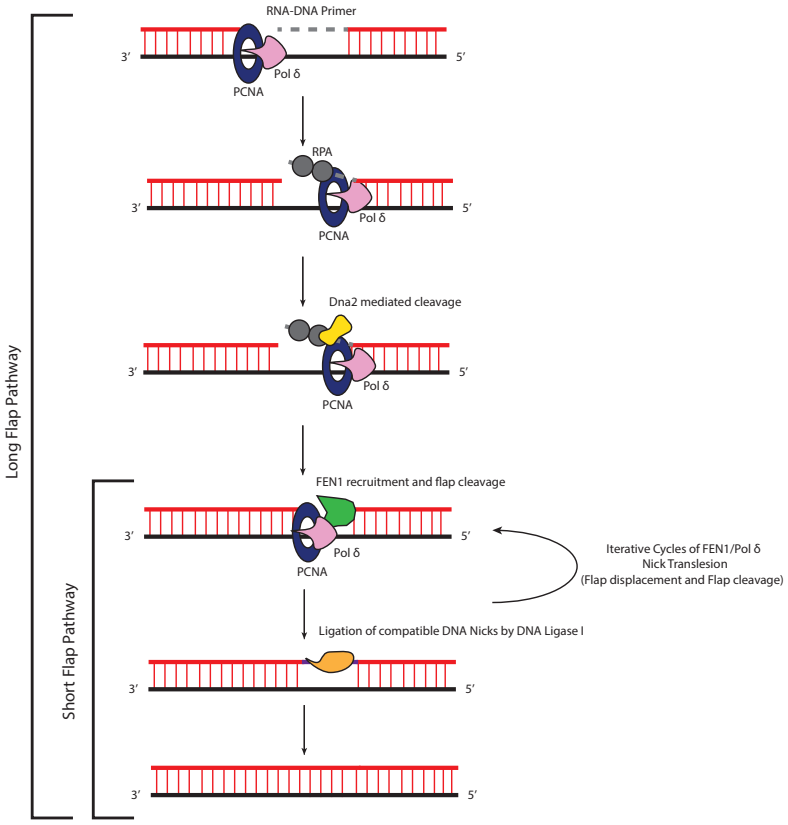


Figure 1.14: **Summary of Okazaki Fragment Maturation.** Both the long and short flap pathway are shown. In the Long flap pathway, the RNA – DNA primer displaced by Pol δ over 1-2 nucleotides in length is rapidly coated in RPA. DNA2 nuclease removes RPA and cleaves the flap to leave a shortened residual flap. This shortened flap is then processed by the Short Flap Pathway. FEN1 associates with PCNA and cleaves short RNA-DNA primers. Iterative cycles of FEN1 cleavage and Pol δ displacement removes all RNA and generates suitable DNA nicks for ligation. The final step is ligation by DNA Ligase I to create a continuous strand.

1.3.4 Replication Termination

Replication termination describes the events surrounding the completion of DNA synthesis in every replicon. As origin firing is not a synchronised mechanism, DNA replication termination takes place throughout the entirety of S-phase, whenever two replisomes from neighbouring origins converge. The process of termination encompasses multiple events, including the resolution of torsional stress and catenane's as well as replisome disassembly. This PhD project has partly focused on uncovering the respective mechanistic and regulatory aspects of mitotic

replisome disassembly.

Resolution of Torsional Stress and Catenane Formation

As the double helical structure of DNA is unwound by CMG, torsional stress accumulates in front of the replication fork due to overwound helical structures. The CMG complex has no intrinsic mechanism to overcome this overwound DNA. Ultimately, if not resolved, the torsional stress generated will block replication fork progression and convergence (Dewar et al., 2015). The majority of supercoiled DNA is relaxed through the direct action of type I and type II topoisomerases. Topoisomerase I is part of the RPC and is therefore responsible for the resolution of positive supercoiling ahead of the replication fork (Gambus et al., 2006). Mechanistically, Topoisomerase I nicks a single strand of DNA to enable rotation of the nicked strand around the intact one. There are cases, however, where topoisomerase I action is blocked (e.g., during replisome convergence). In this scenario, the replication fork itself can rotate in a clockwise direction allowing to effectively 'unravel' the supercoiled DNA. But fork rotation itself does not resolve the accumulating torsional stress, and instead transfers it to behind the replication fork to form catenane's. Catenane structures are regions of intertwined sister DNA strands resolved through Topoisomerase II action (Keszthelyi et al., 2016; Postow et al., 2001). Topoisomerase II cuts both DNA strands, with the cleavage sites separated by approximately 4 nucleotides. The staggered cutting sites allow for the relaxation of torsional stress by rotation of double stranded DNA, through the gap created; subsequently re-ligated by Topoisomerase II (Pommier et al., 2016).

Replisome Convergence and Eukaryotic Replisome Disassembly

As two replication forks from neighbouring origins begin to converge, the section of un-replicated DNA between shortens and Topoisomerase I will be sterically inhibited (Keszthelyi et al., 2016). Thus, if left unsolved, the replication forks will stall. In prokaryotic systems, fork rotation alone is sufficient to resolve the formed torsional stress and support replisome convergence. However during eukaryotic replication, using a yeast *in vitro* reconstitution system, converging replisomes were found to stall immediately prior to termination, suggesting that additional factors were required. Subsequent work showed that the DNA helicases Rrm3 and Pif1 (unwinding DNA in the opposite direction to CMG) were sufficient in this system to support full replisome convergence, independently of Topoisomerase II action (Deegan et al., 2019). Due to the anti-parallel nature of DNA, encroaching replisomes are always situated on opposite DNA strands. Therefore, upon convergence, the two complexes pass each other and translocate onto the double stranded DNA of the last Okazaki fragment (Dewar et al., 2015). This mechanism facilitates the completion of DNA synthesis through ligation of the leading strand, to downstream lagging strands (Dewar et al., 2015). Furthermore, recent studies from several groups have demonstrated that the change in DNA binding during convergence, and loss of the excluded lagging strand from CMG, acts as the cellular signal for replisome disassembly (Deegan et al., 2020; Jenkyn-Bedford et al., 2021; Zhou et al., 2021).

The final stage of DNA replication termination is then the removal of the replication machinery from chromatin, summarised in Figure 1.15. Following replisome convergence and the progression of CMG onto double stranded DNA, MCM7 is targetted for ubiquitylation. Specifically, Cullin2^{LRR1} (SCF^{Dia2} in budding yeast) ubiquitylates MCM7 with Lysine-48 linked

ubiquitin chains (Maric et al., 2014; Moreno et al., 2014; Sonneville et al., 2017). The respective ubiquitin chains formed are then recognised by the p97-UFD1-NPL4 segregase complex through the co-factors Faf1 (UBXN3) and UBXN7, reducing the ubiquitin threshold required for p97 recruitment to CMG and resulting in efficient unloading of the replisome from chromatin. Notably, UBXN7 appears to be important for substrate specificity as it can interact with Cullin2^{LRR1} (Fujisawa and Labib, 2022; Tarcan et al., 2021). Following the initial discovery of the mechanisms surrounding replisome disassembly, our group was particularly interested in the potential consequences of a non-functioning unloading pathway. Surprisingly when MCM7 ubiquitylation was blocked during S-phase, the terminating replisomes were retained on chromatin into mitosis where they were then disassembled. The removal of replisomes during mitosis, like the S-phase pathway, was dependent on CMG ubiquitylation. Although the respective ubiquitin ligase responsible was unclear. Moreover, in *C. elegans*, the p97 segregase was also required alongside its co-factor UBXN-3 to remove any replisomes found on chromatin in mitosis (Sonneville et al., 2017).

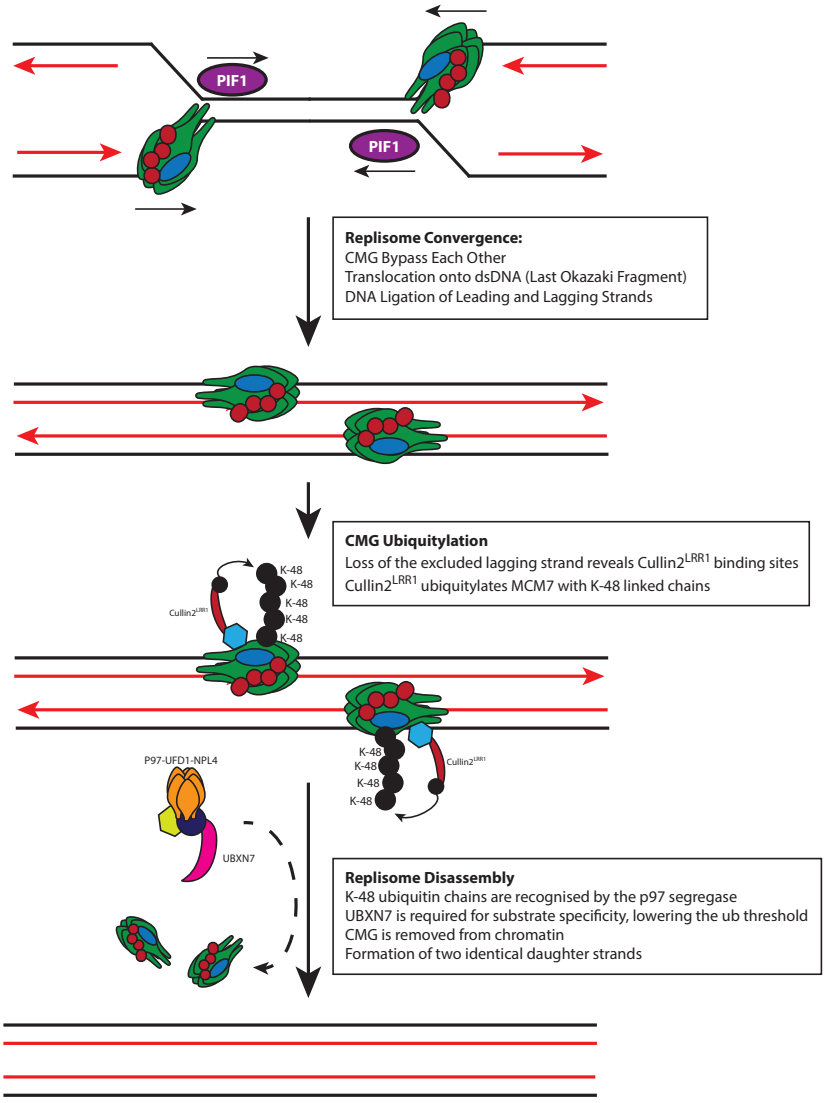


Figure 1.15: **The Current Working Model of Replisome Disassembly.** Replisomes originating from neighbouring origins converge and translocate past each other onto double stranded DNA of the last okazaki fragment. The loss of the excluded lagging strand from CMG reveals Cullin2^{LRR} binding sites, facilitating MCM7 ubiquitylation with K-48 linked chains. Upon reaching a suitable ubiquitin threshold (approximately 5 monomers), p97 can associate with CMG due to interactions between UBXN7 and CMG bound Cullin2^{LRR}; facilitating the removal of the replication machinery from chromatin.

1.3.5 Other Mechanisms Associated with DNA Replication

To maintain genomic stability and support cell propagation DNA replication must be co-ordinated with several other mechanisms taking place on chromatin simultaneously; including nucleosome packaging and the establishment of epigenetic marks, sister chromatid

cohesion, transcription, and the response to replication stress or DNA damage (See **1.4**). If not properly regulated, defects to any of these processes have potentially disastrous consequences for cell viability and are commonly causative of genetic disease-associated phenotypes.

Nucleosome Packaging and the Establishment of Epigenetic Marks

The nucleosome is the most basic packing unit of chromatin, functioning to condense lengths of DNA into a highly ordered state. Structurally each nucleosome is composed of approximately 147 base pairs of DNA tightly wrapped around a histone octamer, formed from two copies of each Histone: H2A, H2B, H3, and H4 (Luger et al., 1997). Furthermore, DNA methylation and histone post-translational modifications (acetylation, methylation, and phosphorylation) are thought to regulate chromatin structure and gene expression levels. During replication, parental nucleosomes must be unwound ahead of the replication fork and then both daughter strands repackaged. In addition, any epigenetic marks present must also be maintained. To allow for this, parental histones are recycled following their disruption by replication fork progression and combined with nascent histones, before being deposited onto DNA to form nucleosomes (Zhang et al., 2020). Daughter nucleosomes are assembled behind the replisome through the action of the histone chaperones FACT, CAF1, and ASF1 (MacAlpine and Almouzni, 2013). Interestingly, it is also thought that the replisome itself is pivotal in nucleosome formation. CAF1 is recruited specifically to replication forks through interaction with the sliding DNA clamp PCNA (MacAlpine and Almouzni, 2013). In addition, it is thought that MCM2-Polα -AND-1 can reposition parental histones onto the lagging strand, allowing for inheritance of the epigenetic marks (Gan et al., 2018). Furthermore, MCM2 has also been shown to be important for nucleosome formation *in vivo*, interacting with Histone H3 and H4 along with

the chaperones FACT and ASF1 (Zhang et al., 2020).

Sister Chromatid Cohesion

Following DNA synthesis, the resulting sister chromatids are held together for the remainder of S-phase and into mitosis by a multi-subunit protein ring called Cohesin. The physical tethering of the two identical DNA strands as a single chromosome is essential during mitosis, orientating the chromatids for symmetrical segregation and preventing aneuploidy in the resulting daughter cells (Peters and Nishiyama, 2012). Structurally, cohesin is composed of two Structural Maintentenance of Chromatin proteins (Smc1 and Smc3) to encircle DNA, bridged by Scc1 forming a 45 nm closed ring. During G1 and S-phase, it is thought that cohesin is loaded onto chromatin where it associates with Pds5 and Wapl (Sherwood et al., 2010). Evidence also exists for the direct association of the cohesin complex with the replisome, with Smc1 and Smc3 found to form a complex with MCM2-7 (Guillou et al., 2010). The widely accepted model of sister chromatid cohesion describes first the entrapment of leading strand dsDNA along with lagging strand ssDNA; subsequently replicated to fully establish sister chromatids (Henrikus and Costa, 2021).

1.3.6 The Interplay between DNA Replication and Transcription (Replication-Transcription Conflicts)

Transcription is the mechanism used to convert template DNA into RNA, subsequently used to exert a functional cellular output. Three different RNA Polymerases transcribe mammalian DNA throughout the cell cycle, with different enzymes possessing different transcript specificities: RNA Polymerase I (ribosomal RNA; rRNA), RNA Polymerase II (messenger RNA;

mRNA, and most small RNA products), and RNA Polymerase III (transfer RNA; tRNA) (Saponaro, 2022). RNA Polymerase II acts as part of large multi-protein complexes responsible for driving gene expression alongside numerous accessory proteins. Mechanistically, RNA Polymerase II mediated transcription takes place within spatial entities termed transcription factories or condensates, occupying large proportions of the genome throughout the cell cycle (Rieder et al., 2012), required for the timely expression of several key cell cycle regulators (Liu et al., 2017). The stringent regulation of transcription is important on both a global population level for the processing of identical genomes to generate hundreds of cell types and maintain homeostasis; but also on a molecular level to facilitate the navigation of crowded chromatic regions and overcome insults to DNA.

Research over the last few decades has highlighted transcription as a key source of genomic instability. The first evidence for transcription driving mutagenesis originated from bacterial models, where the rate of sustained mutation after treatment with the Acridine mutagen ICR-191, or UV irradiation, was enhanced within highly transcribed operons (Savić and Kanazir, 1972; Herman and Dworkin, 1971). Transcription was also shown to underpin the spontaneous reversion of frame shift mutations, subsequently incorporated into the genome if the strand was then replicated (Datta and Jinks-Robertson, 1995). Further work revealed transcription to be capable of driving gene recombination. Interesting, several of the mechanisms by which transcription threatens genome stability can be tracked to specific cell cycle stages. Specifically, transcription-associated gene recombination is thought to primarily take place during S-phase, in a mechanism dependent on DNA Replication (Gottipati et al., 2008).

During S-phase, RNA Polymerase II must compete for unimpeded access to chromatin with several other processes utilising template DNA. As both DNA replication and transcription can traverse chromatin in two directions (5' to 3' or 3' to 5'), encounters between the two respective processes are unavoidable and form a major source of genomic instability. Three overarching hypotheses exist for how DNA Replication-Transcription conflicts threaten genome stability. First: the unwinding of template DNA ahead of either process generates torsional stress, potentially acting as barriers to transcription bubble progression (Bermejo et al., 2012; Champoux, 2001). Second: direct collisions between the progressing replisome and RNA Polymerase II. Such conflicts can occur in either a co-directional (travelling in the same direction) or head-to-head (travelling in opposite directions) arrangement. Head-to-head conflicts are reportedly more deleterious than co-directional encounters and form barriers to both processes (Saponaro, 2022). Third: the formation of RNA:DNA hybrid structures commonly referred to as R-loops, where the nascent RNA strand base pairs with template DNA to displace the non-template strand (Bermejo et al., 2012). Once formed, R-loop structures are particularly stable and may form barriers to both DNA replication and transcription. Several proteins have been implicated in the resolution of R-loops, including RNA processing factors, topoisomerases, endonucleases (notably RNase HI and RNase HII), accessory helicases, or DNA repair proteins (Schauer et al., 2020; Petermann et al., 2022).

Given the essential nature of both DNA replication and transcription, the resolution of conflicts between the two processes is pivotal for genome stability; particularly to limit the highly toxic head-to-head collisions. One potential mechanism for the avoidance of such events would be the temporal separation of replication and transcription, as cells are

committed to proliferation and no longer reliant on the expression of growth factors following progression past the G1 restriction point (Bertoli et al., 2013). However transcription is active continuously throughout the cell cycle, with the possible exception being late mitosis where it has been reported that chromosome condensation may exclude transcription factories from chromatin (Liang et al., 2015). Notably, RNA polymerase II activity is obligatory during S-phase for the expression of several key replication factors (van der Meijden et al., 2002). Furthermore, it has been shown that the overall transcriptional activity in human cells is not radically altered throughout S-phase (Wang et al., 2021). Alternatively, DNA replication and transcription could be spatially separated on chromatin. In bacterial systems, there is general genome organisation ensuring that essential or highly transcribed genes are situated on the leading strand, facilitating shared directionality on chromatin to limit head-to-head encounters (Srivatsan et al., 2010). Despite this, as the respective speeds of traversal differ between the helicase and polymerase, co-directional conflicts remain inevitable. Conversely, no such organisation has been reported to exist in human cells. Furthermore, the processes of DNA replication and transcription overlap during S-phase, although actively replicating genes do exhibit slightly reduced levels of transcriptional activity (Wang et al., 2021).

Direct encounters between DNA replication and transcription can, theoretically, occur anywhere throughout the genome stochastically during S-phase. Interestingly, however, several features have been identified to confer an increased frequency of collisions. These identified 'hotspots' have been reported to exist at particularly crowded chromatin locations containing either several protein complexes associated with DNA (e.g., the progressing replisome), or sequences susceptible to secondary structure formation (Germain et al.,

2021). As such, transcription start sites have emerged as preferential locations for DNA replication-transcription conflicts. Recent work has described transcription start sites as difficult to replicate regions during S-phase, underpinned by the presence of stalled RNA Polymerase II around the proximal pause site, that are instead duplicated upon entry into G2 and mitosis (Wang et al., 2021). Although, overall, conflicts between replication and transcription remain poorly understood and much is still to be discovered about how the eukaryotic replisome overcomes the transcription machinery, or bulky adducts, on chromatin.

1.4 Replication Stress and the DNA Damage Response

Replication stress can be broadly defined as any situation in which the replication fork or associated machinery is impaired, often upon encountering aberrant structures or DNA lesions on chromatin (Zeman and Cimprich, 2014). Many different types, both from exogenous and endogenous sources, of replication stress have been reported (Figure 1.16). The impact of transcription on replication stress and overall genomic stability has been discussed previously (See **1.3**).

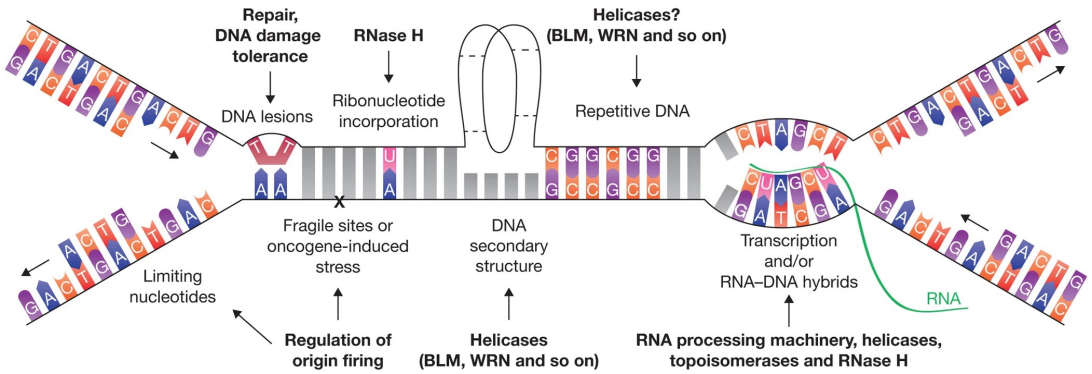


Figure 1.16: **Summary of the Sources of Replication Stress.** Shown is a schematic detailing the variety of replication stress within a cell. Detailed are the respective sources of the stress (normal text) as well as the associated mechanism in place to overcome each obstacle (shown in bold). Figure taken from Zeman and Cimprich (2014)

.

1.4.1 Replication Stress Response: Stalled Helicase or Polymerase

The immediate consequence of the replisome encountering an obstacle on chromatin is replication fork stalling. Dependent on the type of stress present, either the progression of the replicative helicase or DNA polymerase will be blocked. Changes to nucleotide availability or damaged DNA bases have limited impact on CMG progression as these sites are able to pass through the central MCM2-7 channel. However, such forms of stress impede replisome-associated DNA polymerases, and thus often result in leading-strand polymerase stalling. Lagging strand DNA changes do not act as major impediments to the replication fork due to the discontinuous nature of synthesis (Lambert and Carr, 2013). Conversely, DNA lesions on the leading strand often result in the uncoupling of DNA unwinding and DNA synthesis; the replicative helicase will continue to unwind DNA whilst DNA polymerase will halt. The resulting single-stranded DNA generated by this process is rapidly coated with RPA, which, alongside the primer-template junction, acts as the binding platform for the recruitment of repair proteins (Byun et al., 2005). Specifically, the ssDNA generated triggers activation of the essential ATR kinase and the ATR interacting protein (ATRIP). ATR-ATRIP primarily functions to phosphorylate Histone H2AX, RPA1, and CHK1 to stabilise the replication fork until the damage can be repaired, as well as suppressing nearby late-firing origins (Nam and Cortez, 2011). Typically, if the replication stress is local (limited to small numbers of replication forks) then the damage is rapidly resolved and replication continues. Conversely, if the stress is experienced on a more global scale, then ATR phosphorylation of CHK1 activates the G2 cell cycle checkpoint to prevent cell proliferation (Zeman and Cimprich, 2014).

The primary aim of the response to replication stress is to enable the continuation of

DNA replication in a timely manner. For this, the first step is often to facilitate replication fork bypass through DNA Damage Tolerance mechanisms (DDT). Translesion synthesis associated DNA polymerases (e.g., Pol η or Pol κ) possess the ability to insert nucleotides opposite non-canonical sequences. Therefore, these polymerases allow replication through damaged DNA bases (Sale, 2013). Different polymerases have been demonstrated to be required to resolve different types of replication stress. Moreover, work has shown that in several cases, two polymerases are needed sequentially; one to insert bases opposite the sites of damage, and a second to extend past the mismatched sequence created (Shachar et al., 2009). However, translesion synthesis polymerases are highly mutagenic and the sites inserted likely require correction through additional mechanisms, such as Base Excision Repair (Sale, 2013). Alternatively, as CMG can translocate several DNA lesions, it is also possible that the DNA synthesis can be re-primed downstream of the damage site to continue replication (Berti and Vindigni, 2016). Several factors are thought to be required for DNA re-priming, including polymerase recycling or exchange, as well as an appropriate primase (e.g., Prim-Pol in the case of UV-induced DNA damage) (Mourón et al., 2013). Fork re-priming does, however, result in a single-stranded DNA gap that requires processing by translesion synthesis or the ATM-mediated homology directed repair.

Conversely, the replication fork may encounter larger, bulkier, blockages on chromatin that prevent DNA unwinding. In this situation, the entire replication fork, including CMG, will stall. Notable forms of stress inducing helicase stalling are protein-DNA crosslinks (DPC) or conflicts with the transcription machinery, inter-strand DNA crosslinks (ICL), and complex tertiary DNA structures. The progression of the replisome past complex DNA structures, such

as G-quadruplexes or R-loops, is thought to be facilitated by the association of accessory helicases (e.g., PIF1, BLM, RTEL1) that are both capable of unwinding DNA through the respective obstacle, and protecting against DNA breakage (Lerner and Sale, 2019). Work in *X. laevis* egg extract has highlighted the mechanisms required for the replisome to overcome protein blockages on chromatin. The current DPC repair model includes degradation of the protein blockage ahead of the replication fork by the ubiquitin-proteasome system, resulting in a peptide-DNA adduct bypassed by CMG (Duxin et al., 2014). DNA synthesis can then continue until DNA polymerase encounters the adduct where it will stall and trigger uncoupling, likely resolved as previously described (Duxin et al., 2014; Sparks et al., 2019). On the other hand, replication fork progression past ICLs is more complex. In eukaryotes, the Fanconi Anaemia pathway is primarily responsible for replication-coupled ICL repair. Briefly, phosphorylated FANCM associates with the ICL to recruit a 10-protein complex possessing ubiquitin ligase activity (FA complex). Once assembled, the FA complex associates with structure specific DNA nucleases to cleave DNA either side of the ICL; allowing 'unhooking' of the crosslink from DNA and formation of a single-stranded gap (Li et al., 2021). Interestingly, it has been reported that ICL repair during S-phase may require two converging replication forks, with ICL repair found to be blocked when a single replication fork encountered ICLs (Zhang et al., 2015). The same study also highlighted that the observed defect to ICL repair was rescued upon the arrival of a second replication fork; suggesting CMG disassembly may be required (Zhang et al., 2015). Subsequent work then demonstrated that upon two replisomes converging at an ICL, one was unloaded to allow fork reversal of the second CMG and ICL repair (Amunugama et al., 2018). In addition to the described FA pathway of ICL repair, the glycosylase NEIL3, an important component of Base Excision Repair, has also been shown to facilitate ICL unhooking. However the respective

mechanisms underpinning pathway choice is not yet clear (Nejad et al., 2020). Intriguingly, single molecule work has also revealed the ability of CMG to traverse ICLs, suggesting that, in certain situations, ICLs are not complete blocks to replisome progression (Huang et al., 2013).

Replication fork reversal is thought to be another DTT mechanism important for preserving genomic stability through remodelling of replication forks. First, the replication fork encountering the respective source of stress traverses backwards allowing for re-annealing of template DNA. The previously synthesised daughter strands anneal and extrude from the reversed fork to form a 4-pronged structure (Qiu et al., 2021). Moreover, in this structure, it is thought that annealed daughter strands resemble a double-strand break and therefore must be protected from end-resection and cleavage by nucleases. Several proteins have been reported to be important for this, including BRCA1, BRCA2, RAD52 (Qiu et al., 2021). Fork reversal provides time for upstream replication stress to be resolved, where-upon the replication fork is then re-started. The mechanisms underpinning replication fork restart remain contested, with numerous DNA helicases, nucleases, and repair proteins implicated (e.g., SMARCAL1, BLM, WRN, PARP1, MRE11, XRCC3, and RAD51). Furthermore, current models also suggest a requirement for double-strand breaks during fork re-start (Petermann and Helleday, 2010). Aside from DDT or repair of damage, the excess MCM2-7 double hexamers loaded during G1 also play an important role during the replication stress response. Whilst the activation of ATR prevents the firing of replication origins in new replicons, it stimulates the activation of otherwise dormant MCM2-7 double hexamers in the replicon experiencing replication stress.

If replication stress cannot be resolved, or replication forks remain stalled for prolonged

periods of time, it is likely that the replication fork structure will collapse resulting in double-stranded break formation. Notably, it is thought that the replisome is disassembled or displaced from collapsed replication forks, although the precise regulation of CMG at these sites is not known (Berti and Vindigni, 2016). Any unresolved sites of replication stress commonly results in the preservation of under-replicated regions of DNA, as well as DNA damage, into mitosis; commonly characterised by impaired chromosome condensation and the presence of DNA bridges between segregating chromosomes (Anaphase or Ultra-fine bridges) (Gelot et al., 2015). Interestingly, even though replication stress can occur anywhere in the genome, specific regions have been identified as hotspots for DNA breakage during mitosis upon the induction of replication stress (Common Fragile Sites). Despite being an area of intense research, the underlying reasons surrounding the increased preference for damage at common fragile sites are still unclear. Several hypotheses exist, including potentially increased A-T DNA content, DNA Replication – Transcription collisions, or being located within long genes with limited replication origins (Ma et al., 2012). Furthermore, the classical consequences of replication stress may also be characteristic of broader replication problems throughout multiple stages of the cell cycle. Recently, research is emerging that changes the perspective suggesting that the entire genome is duplicated solely in S-phase. Upon extensive replication fork stalling, it is likely that DNA replication can be sustained during different cell cycle stages. This is exemplified by the finding that anaphase bridges and 53BP1 bodies during G1 stage of the cell cycle provide a mechanism for the resolution of under-replicated regions (Moreno et al., 2016). In addition, the replication of classically difficult to replicate sites (e.g., transcription start sites) has also been reported to take place late in the cell cycle during G2 and mitosis (Wang et al., 2021).

1.4.2 The DNA Damage Response

Alongside the replication stress response, the DNA damage response also acts as an important protector against genomic instability. DNA Damage Repair is an extremely wide field of research covering numerous different mechanisms, including Mismatch Repair, Base Excision Repair, Nucleotide Excision, Homologous Recombination, and Non-Homologous End Joining. However, for the purposes of this PhD, only the two major pathways of double-strand break (DSB) repair will be summarised. Overall, the DNA damage response is driven by the action of three master kinases: ATR, ATM, or DNA-PK. ATR acts in response to replication stress, as discussed previously, whilst ATM and DNA-PK primarily mediate the repair of double-strand breaks by Homologous Recombination (HR) and Non-Homologous End Joining (NHEJ), respectively (Jackson and Bartek, 2009). The cellular mechanisms sensing double strand breaks begins with the binding of MRE11-RAD50-Nbs1, which, in turn, brings ATM to sites of damage. ATM then phosphorylates multiple targets, including H2AX, CHK2, and p53 to facilitate the recruitment of further DNA damage repair proteins. Notably, positive feedback loops formed by MDC1-ATM interactions spread sites of phosphorylation to neighbouring histones, amplifying the cellular signal. Finally, RNF8/168 recruits RAP80-BRCA1 and 53BP1 to double strand breaks. Importantly, the association of either BRCA1 or 53BP1 is thought to determine repair pathway choice. The presence of 53BP1 antagonises HR, promoting repair by NHEJ. Conversely BRCA1 is an E3 ubiquitin ligase pivotal for HR (Maréchal and Zou, 2013; Panier and Boulton, 2013).

NHEJ functions throughout the entirety of the cell cycle. Mechanistically each side of the double-strand break is bound to by Ku70 and Ku80. Ku70/Ku80 then act as a scaffold

for the recruitment of the NHEJ repair proteins (including DNA-PK, XRCC4, DNA Ligase IV, and APLF). Each end of the double-strand break is then resected by DNA processing enzymes (Artemis and APLF) to generate compatible ends, subsequently ligated together by DNA Ligase IV (Chang et al., 2017; Davis and Chen, 2013). HR, on the other hand, functioning during S-phase and G2, has important roles in promoting the stability and recovery of replication forks. First, each end of the break is resected to generate 3' over-hangs by exonucleases likely associated with the MRE11-RAD50-XRS2 complex (e.g., EXO1). The resulting single stranded DNA created is then coated in RPA, subsequently targetted for strand invasion and RAD51 filament formation by BRCA2 action. RAD51 filaments mediate location of a homologous DNA sequence to be used for repair. The strand invasion step results in a 'D-loop' intermediate, aligning the single stranded DNA with a complimentary template so that DNA synthesis can ensue. Finally, the products are annealed together by RAD52 and processed by helicases (e.g., BLM-TOPOII) and endonucleases (Li and Heyer, 2008).

1.5 The Association Between DNA Replication Proteins and Primordial Dwarfism

As the process responsible for genome duplication, underpinning cell propagation, it is not surprising that errors during DNA replication have severe and widespread implications for human health and disease. Notably, mutations in replication proteins have been extensively linked with a group of single-gene disorders termed primordial dwarfism; including: Seckel Syndrome, Meier-Gorlin Syndrome, and microcephalic osteodysplastic primordial dwarfism (Klingseisen and Jackson, 2011). To date, several mutations to genes encoding

replication-associated proteins have been reported in patients presenting with primordial dwarfism conditions, including: DNA2 (Tarnauskaitė et al., 2019), DNA Polymerase ε (Logan et al., 2018), PRIM1 (Parry et al., 2020), CDC45 (Fenwick et al., 2016), DONSON (Reynolds et al., 2017), ORC1 (Bicknell et al., 2011a,b), DNA Polymerase α (Van Esch et al., 2019), ORC4 (Bicknell et al., 2011a; Guernsey et al., 2011), CDT1 (Bicknell et al., 2011a), CDC6 (Bicknell et al., 2011a), and the MCM2-7 components MCM3 and MCM7 (Knapp et al., 2021).

Interestingly, despite the variety of distinctive genetic disorders reported, and the wide-ranging mechanisms likely affected by the different mutations highlighted, patients often present with clinically similar features. Specifically, primordial dwarfism conditions are defined by a short stature, possible increased cancer predisposition, and microcephaly likely caused by reduced brain size (Jackson et al., 2014; Klingseisen and Jackson, 2011). In most cases, these clinical characteristics were associated with homozygous missense mutations to the described replication proteins, discovered using whole exome sequencing. The primary consequence of the reported mutations appeared to be overall reductions in protein activity, either through reduced catalytic activity, impaired DNA binding or protein interaction capabilities, and protein de-stabilisation. However, intronic variants impacting alternative splicing have also been discovered within the DNA2 gene, also leading to increased protein destabilisation (Tarnauskaitė et al., 2019). Alongside shared clinical features, subsequent characterisation of these mutations in human cell models revealed shared phenotypic characteristics. In particular a number of studies have highlighted slower overall cell doubling times due to slowed S-phase progression and impaired replication fork progression (Logan et al., 2018; Parry et al., 2020; Reynolds et al., 2017; Bicknell et al., 2011b; Van Esch et al., 2019; Knapp et al.,

2021). It is believed that cell size and cell volume are key factors determining organism size (Conlon and Raff, 1999). Slowed cell proliferation arising from mutations to genes associated with DNA replication will therefore likely influence the overall size of an organism, relating the functional cellular mechanism affected by mutations to DNA replication proteins, to observed clinical features (Klingseisen and Jackson, 2011).

1.6 Model Systems and Methods Used to Study DNA Replication Termination

Several model systems have been used over the years to study the process of DNA replication termination, including *Saccharomyces cerevisiae*, *Caenorhabditis elegans*, *Xenopus laevis* egg extracts, and reconstituted *in vitro* systems. Notably, studies by our group and others exploiting *X. laevis* egg extracts and reconstituted *in vitro* systems have significantly advanced to our knowledge of replisome disassembly. This PhD project aimed to build upon this work using the egg extract system, as well as immortalised human somatic cell lines. Therefore, only these models will be discussed further.

1.6.1 *Xenopus laevis* Egg Extract

X. laevis egg extracts are highly concentrated, cell free model systems commonly used to study both DNA replication and the DNA damage response. Three different types of egg extract exist: Low Speed Supernatent (LSS), High Speed Supernatent (HSS), and Nucleoplasmic Extract (NPE). Work in this PhD project utilised LSS only. Low Speed Supernatent extracts, prepared through the centrifugation of *X. laevis* eggs naturally arrested in metaphase of meiosis

II, possess all the required components to facilitate one complete round of the cell cycle. Any DNA added into LSS (demembranated *X. laevis* sperm nuclei) is readily packaged into chromatin before the pre-replicative complex (Pre-RC) is loaded rapidly onto replicative origins; followed by nuclear envelope formation and a single round of DNA replication (Gillespie et al., 2012a). Furthermore, LSS egg extracts can be supplemented with mitotic cyclins to facilitate chromosomal segregation. Notably, use of the egg extract is especially advantageous when it comes to studying DNA replication, being a synchronised system lacking transcription. In addition, the methodology involved in working with *X. laevis* egg extracts allows for the rapid screening of candidate proteins. Extracts are able to accurately recapitulate the majority of biological functions observed in oocytes, including complete rounds of the cell cycle (Gillespie et al., 2012a). The system is also particularly useful when it comes to biochemical manipulation. As an *in vitro*, cell free model, the extract can be supplemented with recombinant proteins or respective drug treatments without several of the potential issues arising in alternative systems (e.g., rejection of exogenous material, transient expression levels, and inability of small molecules to cross membranes). Moreover, endogenous proteins within the egg extract can also be easily isolated or removed through conjugation to antibodies (immunodepletion and immunoprecipitation).

1.6.2 Immortalised Human Somatic Cell Lines

To translate any observations made in the egg extract to a more physiologically relevant setting, we aimed to also carry out experiments using immortalised human cell lines. Common cell types used for the study of DNA replication or the DNA damage response includes HeLa, U2OS, HCT116, HEK293, and RPE1. To select suitable models for this PhD project, we considered

the respective characteristics of each cell line. One frequent feature of cancer cell lines is abnormal chromosome numbers. This is particularly problematic when considering gene modification, potentially increasing the number of allele's to be modified. Due to this, we aimed to select diploid cell models (23 chromosome pairs). U2OS, HeLa, and HEK293 were not selected due to inherent aneuploidy. In addition, HeLa cells possess variable p53 expression and likely associated checkpoint defects, caused by HPV infection (Hoppe-Seyler and Butz, 1993). Therefore, we elected to use the near diploid HCT116 (cancerous) and Tert-immortalised (over-expression of the telomerase reverse transcriptase) RPE1 (non-cancerous) models.

One key consideration when working with mammalian cell lines is how the respective protein of interest can be both isolated, and removed. Protein depletions are often achieved through CRISPR-Cas9 gene knockouts or treatment of the cells with siRNA and shRNA; forming the RNA-induced silencing complex (RISC) to block translation (Carthew and Sontheimer, 2009). However, over recent years, the increased use of degron technologies has surfaced, offering efficient ways to both isolate, and degrade proteins of interest in mammalian cells (e.g., AID, SMASh, HaLo, TRIM) (Roth et al., 2019). Specifically, we were interested in using the Auxin-Inducible degradation, developed by Prof. M. Kanemaki's group.

The AID system (Figure 1.17), developed from existing plant technologies, allows for the rapid and inducible degradation of proteins of interest from mammalian cell lines. Moreover, with a reported half-life of 20 minutes, the direct consequences of protein depletion can be observed without any additional secondary effects arising (Natsume et al., 2016; Yesbolatova et al., 2019). To generate AID cells, suitable cell lines are modified by CRISPR-Cas9 to insert

both the auxin-responsive F-box protein *Oryza sativa* Tir1 (OsTIR1), and an appropriate degron tag. The Cas9 enzyme is targetted to specific sites of the genome by complementary guide RNA sequences. Enzymatic activity is then activated through protospacer adjacent motif (PAM) site recognition to cleave DNA 3-5 base pairs upstream (Figure 1.17A). The insertion of a donor plasmid, containing the appropriate tag, can then be utilised to repair the resulting double-strand break using homology directed repair (HDR) (Jiang and Doudna, 2017; Ran et al., 2013). Several tags have been developed for both N- and C-terminal attachment, including the core mAID degron component along with additional modifications for protein identification (e.g., FLAG, mCLOVER, and mCHERRY; Yesbolatova et al. (2019)). Once incorporated, OsTIR1 forms a stable E3 ubiquitin ligase complex with Cullin1-RBX1-SKP1. Protein degradation can then be induced through the addition of the plant hormone auxin (Indole-3 acetic acid, IAA); associating with the respective degron tag to facilitate protein ubiquitylation and degradation by the OsTIR1-Cullin1 ligase complex (Natsume et al., 2016).

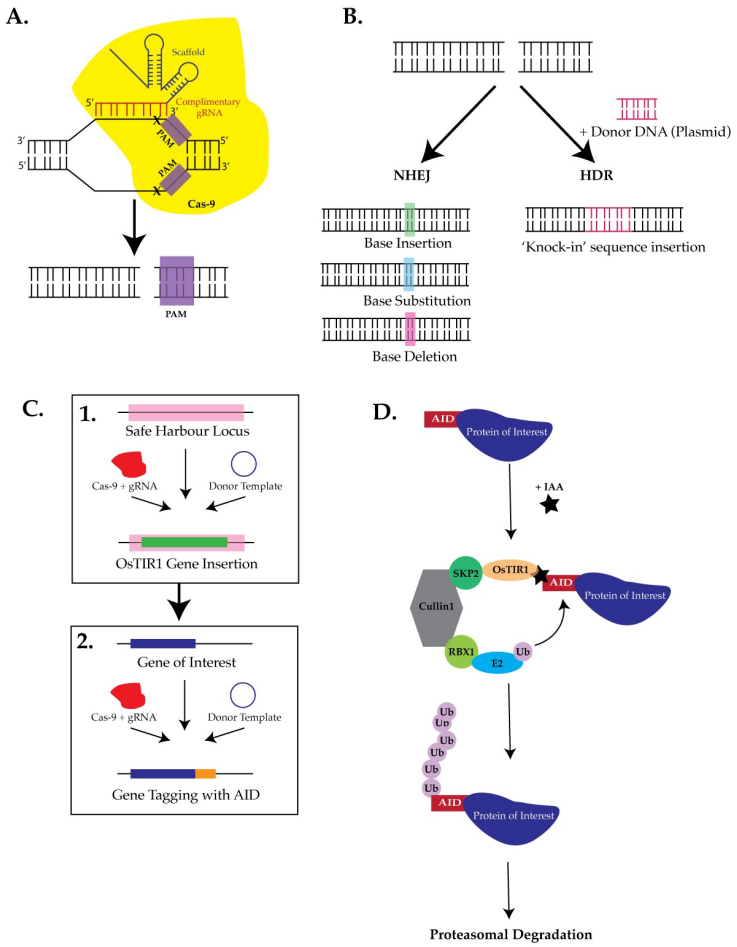


Figure 1.17: **Summary of CRISPR-Cas9 Gene Editing and Auxin-Inducible Degradation.** **A.** CRISPR-Cas9 gene targeting. Cas9 forms a stable complex with gRNA scaffolds, recruited to the genome through complementary sequence association. Cas9 is then activated through PAM site recognition and cleaves DNA 3-5 bases upstream to result in double stranded breaks. **B.** Summary of methods used to repair Cas9-mediated DSB in cells. NHEJ takes place in the absence of template DNA; often resulting in the inclusion of several modifications, shown. HDR takes place when template DNA is provided and can facilitate tag insertion into the gene of interest. **C.** Summary of modifications in AID cell lines. The OsTIR1 gene is inserted into a safe harbour locus. Cells are then further modified through tagging of genes of interest with AID tags. **D.** Overview of AID-mediated degradation. IAA binds to the AID tag, which subsequently interacts with the OsTIR1-Cullin1 ligase complex. This leads to protein polyubiquitylation and degradation through the proteasome system. Figures **A** and **B** were adapted from Jiang and Doudna (2017). Figures **C** and **D** were adapted from Natsume et al. (2016).

1.7 Selection of a Candidate Pool

To understand the regulation surrounding eukaryotic replisome disassembly, our group utilised mass spectrometry to analyse the composition of the post-termination replisome. Three experiments were carried out: LRR1 immunoprecipitation (LRR1 IP), MCM3

immunoprecipitation (MCM3 IP), and Cullin2 CHROMASS (Cul2 CHROMASS). For the LRR1 IP, *Xenopus laevis* egg extracts were treated with the small molecule inhibitor MLN4924. Use of this inhibitor prevented activation of Cullin-type ubiquitin ligases via the inhibition of the NEDD8 E1 activating enzyme (Brownell et al., 2010). Thus, in our replication reactions, inactive $Cullin2^{LRR1}$ was able to bind to but not ubiquitylate terminated CMG. Immunoprecipitation using antibodies against LRR1 then isolated the $Cullin2^{LRR1}$ complex interacting with the replisomes. The MCM3 IP was carried out in *X. laevis* egg extracts supplemented in excess with a catalytically inactive mutant of the p97 segregase, along with optional MLN4924 treatments. By adding recombinant mutant p97, we were able to out-compete the endogenous protein and prevent the disassembly of terminating replisomes. In addition, the inclusion of MLN4924 treatment allowed for comparison between ubiquitylated and non-ubiquitylated terminating replisomes. Finally, we conducted CHROMASS analysis of Cullin2 depleted *X. laevis* egg extracts. CHROMASS is a method established to identify proteins present on bulk chromatin (Raschle et al., 2015). Cullin2 was removed from the egg extract (immunodepletion) before chromatin was isolated from two timepoints (mid/late S-phase) and analysed using mass spectrometry. A summary of the novel candidate pool selected for this PhD project is shown in Table 1.1. We identified TRAIP and TRIP12 to accumulate specifically with the terminating replisome. In addition, TRIP12 and USP10 were found to also accumulate on chromatin during late S-phase. Furthermore, the ubiquitin ligase RFWD3 was suggested to us for study by a collaborating research group (Prof. S. Prasanth, School of Molecular and Cellular Biology, University of Illinois).

To further expand our candidate pool, published iPOND and NCC data sets were studied

to identify potentially novel E3 ubiquitin ligases or deubiquitylating enzymes involved in DNA Replication. First, a study by Dungrawala et al. (2015) utilised the Isolation of Proteins on Nascent DNA (iPOND), from human cells, to identify novel interactors of the replication fork. Briefly, newly synthesised DNA was labelled using the thymidine analogue EdU and cross-linkers added to conjugate protein complexes to DNA. Subsequent incorporation of biotin, to the EdU, through copper catalysed click chemistry allowed for the simple purification of nascent DNA and any associated proteins. Using this technique, Dungrawala et al. (2015) explored the replisome-associated proteome across 32 different conditions. TRIP12, USP22, and USP37 were found to be enriched on nascent DNA. In addition, USP22, USP34, and USP37 also accumulated specifically with the replication fork. TRAIP was detected at stalled replication forks only (Dungrawala et al., 2015). Second, Alabert et al. (2014) used Nascent Chromatin Capture (NCC) to investigate the replication fork proteome. NCC is similar to iPOND in that it involves the isolation of nascent DNA and associated complexes through the incorporation of thymidine analogues into replicating chromatin. Conversely, NCC was developed specifically for large-scale proteomic approaches and therefore incorporates stronger cross-linking, nuclei isolation, and the direct introduction of conjugated Biotin-dUTPs not included with iPOND. Despite these differences RFWD3, TRIP12, USP22, USP34, and USP37 were all detected to be enriched on nascent chromatin by NCC (Alabert et al., 2014).

In addition to the data described, used to select the candidate proteins, several additional screens have also attempted to identify novel proteins associated with the replication fork Lossaint et al. (2013); Aranda et al. (2014); Lopez-Contreras et al. (2013); Sirbu et al. (2013); Lecona et al. (2016); Wessel et al. (2019). All the candidate proteins were shown to be enriched

on nascent DNA in a second iPOND screen by the Cortez group, building on the data from Dungrawala et al. (2015). Notably, although detected, TRIP12, USP10, and USP22 did not meet statistical significance thresholds (Wessel et al., 2019). TRIP12 has also been identified in a third iPOND screen investigating novel DUBs interacting with the replication fork (Lecona et al., 2016). However, one of the major drawbacks of large-scale proteomics screening is sensitivity. The respective experimental set-up, or instrumentation used, will not be able to detect every protein involved. Often, low copy number or weakly bound proteins will fall outside detection limits. Therefore, although the majority of replisome components were detected in the detailed studies, there were several differences in the protein panels presented and the candidates selected were not identified in all screens (Lopez-Contreras et al., 2013; Lossaint et al., 2013; Sirbu et al., 2013). Despite this, our chosen proteins have appeared across multiple studies (Lecona et al., 2016; Alabert et al., 2014; Wessel et al., 2019; Dungrawala et al., 2015), strengthening the argument for their involvement during DNA Replication.

Table 1.1: **Summary of *X. laevis* Mass Spectrometry Data.** Shown are the resulting peptide data from experiments aiming to identify novel interactors of the terminating replisome. The number of peptides identified between control and 'test' experiments are detailed in the three *X. laevis* experiments carried out by members of the Gambus group (LRR1 IP, MCM3 IP, and Cul2 CHROMASS). Information shown from iPOND and NCC was taken from published data sets, and therefore only the location of protein enrichment is shown; either on nascent chromatin or stalled replication forks (Alabert et al., 2014; Dungrawala et al., 2015).

Candidate	**LRR1 IP** (Mock / MLN4924)	**MCM3 IP** (Mock / + p97 / + p97 + MLN4924	**Cul2 CHROMASS** (Mock / - Cul2)	**iPOND**	**NCC**
TRAIP	3 / 22	0 / 22 / 34	Mid S-phase: 2 / 42 Late S-phase: 0 / 11	Stalled	N/A
TRIP12	0 / 8	N/A	Mid S-phase: 0 / 0 Late S-phase: 14 / 13	Nascent	Nascent
RFWD3	N/A	N/A	N/A	N/A	Nascent
USP10	N/A	N/A	Mid S-phase: 0 / 0 Late S-phase: 9 / 11	N/A	N/A
USP22	N/A	N/A	N/A	Nascent	Nascent
USP34	N/A	N/A	N/A	Nascent	Nascent
USP37	N/A	N/A	N/A	Nascent	Nascent

1.7.1 Candidate E3 Ubiquitin Ligases

Three E3 ubiquitin ligases were selected for this PhD project: TRAIP, TRIP12, and RFWD3. Importantly, at the commencement of this project, none of the candidate proteins chosen had defined roles during unperturbed DNA Replication. The state of knowledge surrounding each candidate protein, with respect to DNA Replication and the DNA damage response, at the start of this PhD project will be summarised. Any recent developments since candidate selection is detailed in the appropriate results Chapters. Ring Finger and WD Repeat Domain 3 (RFWD3) was first identified as an ATR substrate from large scale proteomics screens after inducing DNA damage in mammalian cell lines (Matsuoka et al., 2007; Mu et al., 2007). Since its discovery, RFWD3 has been found to interact and ubiquitylate RPA on single-stranded DNA following the induction of DNA damage; facilitating the recruitment of DNA damage repair proteins (Elia et al., 2015; Gong and Chen, 2011; Liu et al., 2011). Analogous to this role, RFWD3 has also been implicated in regulating p53 and CHK1 as part of the checkpoint response to DNA damage (Fu et al., 2010; Gong and Chen, 2011).

Thyroid Hormone Receptor Interactor 12 (TRIP12) is a HECT type E3 ubiquitin ligase thought to be important for cell proliferation, and essential for mouse embryogenesis (Kajiro et al., 2011). Similar to RFWD3, TRIP12 has also been linked to DNA damage repair. It is thought that TRIP12 acts to regulate USP7 protein level, a key deubiquitylating enzyme stabilising p53 upon the detection of DNA damage (Liu et al., 2016). Moreover, TRIP12 has also been shown to function with a second HECT type ubiquitin ligase, UBR5, to control RNF168 accumulation at DNA lesions, preventing excess spreading of histone ubiquitylation and the hyper-recruitment of DNA damage proteins (53BP1, CHK1, BRCA1) (Gudjonsson et al., 2012).

The final ubiquitin ligase selected is the TRAF-interacting protein or TRAIP (also known as TRIP and RNF206). TRAIP was originally identified as a novel interacting partner of the CD30-TRAF complex and the tumour suppressor CYLD, functioning to inhibit NF-χB activation (Lee et al., 1997; Regamey et al., 2003). The most well studied of all the selected candidates, TRAIP is an essential protein for both mouse and *Drosophila* embyrogenesis, as well as in immortalised mammalian cell lines (Hart et al., 2015; Park et al., 2007; Merkle et al., 2009). Interestingly, mutations to TRAIP have been associated with the reduced cell proliferation observed in Seckel Syndrome (primordial dwarfism). Specifically, two homozygous mutations have been identified in patients to date: Cytosine 553 to Thymine (found in 2 individuals; nonsense mutation) and Cytosine 52 to Thymine (found in 1 individual; missense mutation) (Harley et al., 2016). In both situations it was reported that TRAIP mutations were hypomorphic; leading to reduced ubiquitin ligase activity through protein de-stabilisation and lower overall protein levels (Harley et al., 2016).

TRAIP is expressed ubiquitously throughout the entire cell cycle, peaking during G2/M (Chapard et al., 2015) where it has been shown to regulate mitotic and meiotic progression, likely through roles in the spindle assembly checkpoint (Chapard et al., 2014a; Park et al., 2015; Yuan et al., 2016). However, TRAIP has also been highlighted to be important during S-phase. Found to reside predominantly in the nucleolus due to sumoylation (Park et al., 2016), TRAIP re-localises to sites of DNA damage through interactions with a C-terminal PCNA interacting domain (PIP box), where it is required for efficient γ-H2AX and RPA2 phosphorylation (Harley et al., 2016; Hoffmann et al., 2016). Furthermore, TRAIP is thought to be necessary for the

translocation of RAP80 to DNA lesions through N-terminal interactions (Soo Lee et al., 2016).

1.7.2 Candidate Deubiquitylating Enzmyes

Four deubiquitylating enzymes were selected for study during this PhD project: USP10, USP22, USP34, and USP37. USP10 has been shown to be a key regulator of translesion synthesis (TLS), cleaving mono-ubiquitin moieties from ISGylated PCNA after damage bypass; to release DNA Polymerase η and allow replicative polymerases to re-associate (Park et al., 2014). In addition, USP10 is thought to deubiquitylate the mismatch repair protein MutS Homologue 2 (MSH2) to promote protein stability and DNA repair pathways (Zhang et al., 2016). Alongside these roles in translesion synthesis and mismatch repair, USP10 is also phosphorylated by ATM in response to DNA damage, subsequently deubiquitylating the major p53 regulator Mdm2. Ubiquitylated Mdm2 is thought to signal for p53 nuclear export. Therefore, by removing these chains, USP10 promotes the tumour suppressive role of p53 in response to DNA damage (Yuan et al., 2010). Finally, USP10 has been highlighted as an important regulator of topoisomerase II α (Topo II). TOPOII is essential for maintaining genomic stability as well as facilitating chromosome condensation during mitosis. Whilst RNF168 polyubiquitylates Topo II to promote its activity; USP10 does the opposite, removing conjugated ubiquitin chains to restrict Topo II chromatin binding (Guturi et al., 2016).

USP22 is a known subunit of the SAGA complex (Spt-Ada-Gcn5), where it is thought to deubiquitylate histone H2B to contribute to transcriptional regulation. Moreover, the recruitment of USP22 to several genes is thought to be controlled through association with the Myc oncoprotein (Zhang et al., 2008). Similar to this, a second study identified mono-ubiquitin

moieties on Lysine 20 of Histone H2B as sites specific for USP22 activity (Melo-Cardenas et al., 2016). In addition, USP22 has also been implicated in cell proliferation, particularly as USP22 dysregulation in cancerous cells results in a hyper-proliferative state (McCann et al., 2020). This includes a role in promoting the G1/S cell cycle transition through the upregulation of the transcription factor FOXM1, likely by controlling β-catenin localisation (Ning et al., 2014). Moreover, USP22 has been reported to cleave Lysine-63 linked ubiquitin chains from the transcriptional regulator FBP1 at the cyclin dependent kinase inhibitor p21 gene to increase the stable association of FBP1, to gene loci (Atanassov and Dent, 2011).

USP34 has been implicated in double strand break repair through the deubiquitylation of RNF168 at sites of DNA damage. It is known that in unchallenged conditions, RNF168 is rapidly degraded by the ubiquitin-proteasome system. Upon the induction of double strand breaks, USP34 has been shown to stabilise RNF168 specifically at sites of DNA damage to prevent its degradation and promote recruitment of the canonical DNA damage repair proteins to chromatin (Sy et al., 2013).

The final deubiquitylating enzyme included in the candidate pool, USP37, has been shown to be important for cell cycle progression, USP37 is thought to be expressed predominantly during G1 and S-phase, where it is activated by CDK2 phosphorylation. Active USP37 deubiquitylates cyclin A, preventing its degradation and promoting the G1 – S cell cycle transition (Huang et al., 2011). Further work has shown that USP37 is then degraded during G2 by the ubiquitin ligase $SCF^{\beta TrCP}$ to facilitate mitotic entry (Burrows et al., 2012). Conversely, the same study also reported that USP37 is required for sister chromatid alignment and cohesin release

from chromatin through interactions with cohesin and WAPL, respectively (Burrows et al., 2012). Alongside roles in cell cycle progression, USP37 has also emerged to be a key regulator of homologous recombination. USP37 is thought to be important to prevent aberrant spreading of ubiquitylation across chromatin. Specifically, USP37 has been shown to be partly responsible (alongside USP26) for removing ubiquitin chains built around double strand breaks by RNF8/RNF168; thus limiting the general association of BRCA1 to ubiquitin chains, whilst promoting complex formation specifically at resected damage sites between BRCA1–PALB2–BRCA2–RAD51, required for homologous recombination (Typas et al., 2015).

1.8 Project Aims and Objectives

Protein ubiquitylation and deubiquitylation are fundamental regulatory processes underpinning genomic stability and DNA repair. Many of these pathways have been extensively studied and are well understood. However, much less is known about the mechanisms and regulation of unperturbed DNA replication. Recent years shown that polyubiquitylation is required for replisome disassembly upon replication fork convergence. However, at the start of this PhD project, it was not known whether the replisome disassembly pathways identified *X. laevis* and *C. elegans* were conserved into mammalian cell models. In addition, the respective consequences of impaired replisome disassembly were unclear. Therefore, the overarching aim of this PhD project was to identify and characterise novel ubiquitin ligases or deubiquitylating enzymes potentially involved in DNA replication and repair. For this, four main research questions were established.

1. Are there Additional Factors Required for DNA Replication Termination?

Previous work by members of the Gambus group had conducted mass spectrometry analysis of the terminating replisome in both unperturbed and perturbed conditions. This work, alongside published screens exploring components of active replication forks, identified 7 E3 ubiquitin ligases and deubiquitylating enzymes found to accumulate with CMG. Using Xenopus laevis egg extract we aimed to screen each of the candidate proteins for any interactions with the replication fork, and for any roles during DNA replication and replisome disassembly. It was thought that this data would then be used to refine our candidate pool, selecting one protein to take forward for the remainder of the PhD.

2. What is the Essential Function of the Selected Candidate?

Following selection of my protein of interest I next aimed to identify its primary mechanism of action first in *Xenopus* system, and then in human cells. I also planned to use human immortalised cells to understand the respective consequences of the loss of this protein, during the eukaryotic cell cycle. To do this, we established a collaboration with Prof. Kanemaki (National Institute of Genetics, Japan) to generate several conditional degron cell lines (against LRR1 and the candidate protein selected) in both cancerous (HCT116) and non-cancerous (RPE1) cell lines.

3. Is the Eukaryotic Replisome Disassembly Pathway Conserved in Human Cells?

To date, limited work has been carried out exploring mammalian replisome disassembly. Using the generated AID degron cell lines against LRR1, alongside varying inhibitor treatments, I aimed to first validate that our existing knowledge of replisome disassembly was conserved in immortalised human cell lines. In addition, any involvement of the selected candidate protein

during replisome disassembly, if not previously characterised during aim 2, will be explored.

4. Is the Identified Candidate a Druggable Target?

Finally, working with industrial collaborators (High Throughput Screening, Astra Zeneca), I wanted to explore any differential gene expression of the candidate protein in a panel of cancerous cell lines. If differences were identified, we aimed to investigate whether, by reducing candidate enzymatic activity, we could sensitise cells to existing treatment regimes. For this, a high throughput small inhibitor screen would be conducted; and any validated hits tested in the models established during this PhD project.

Chapter 2

Materials and Methods

2.1 Tables

Table 2.1: **Buffers Used.**Shown is a summary of the buffers used throughout this PhD project. Detailed is the respective composition and storage temperatures for each solution.

Buffer	Composition	Storage Conditions
Tris-Glycine Running Buffer	25 mM Tris-HCl pH 7.4 250 mM Glycine 0.1% SDS	Room temperature
Coomassie Blue Stain	0.1% Coomassie Blue 20% methanol 10% acetic acid H2O	Room temperature
Destaining Buffer	10% acetic acid 50% methanol H2O	Room temperature
Transfer Buffer	25 mM Tris-HCL pH 7.4 190 mM Glycine 20% methanol	Room temperature
TBST	20 mM Tris-HCL pH 7.4 150 mM NaCl 0.1% Tween-20	Room temperature

Table 2.1 continued from previous page

Buffer	Composition	Storage Conditions
TRAIP Lysis	50 mM NaH2PO4 500 mM NaCl 2mM MgCl2 0.05% Brij 10% Glycerol 10 mM Imidazole 1 µg/ml APL 0.1 mM PMSF 1 mg/ml Lysozyme pH 9.0	Prepared Fresh for Use
RFWD3 Lysis	50 mM TRIS-HCL 500 mM NaCl 2 mM MgCl2 0.05% Triton-X 10 mM Imidazole 1 µg/ml APL 0.1 mM PMSF 1 mg/ml Lysozyme pH 8.0	Prepared Fresh for Use
TRIP12 Lysis	50 mM NaH2PO4 500 mM NaCl 2 mM MgCl2 1 mM DTT 1 µg/ml APL 0.1 mM PMSF 1 mg/ml Lysozyme pH 8.7	Prepared Fresh for Use
USP10 Lysis	50 mM NaH2PO4 500 mM NaCl 2 mM MgCl2 0.05% Triton-X 1 mM DTT 1 µg/ml APL 0.1 mM PMSF 1 mg/ml Lysozyme pH 8.7	Prepared Fresh for Use

Table 2.1 continued from previous page

Buffer	Composition	Storage Conditions
USP34 Lysis	50 mM NaH2PO4 500 mM NaCl 2 mM MgCl2 0.05% Triton-X 1 mM DTT 1 µg/ml APL 0.1 mM PMSF 1 mg/ml Lysozyme pH 8.7	Prepared Fresh for Use
USP37 Lysis	50 mM NaH2PO4 500 mM NaCl 2 mM MgCl2 0.05% Triton-X 10 mM Imidazole 1 µg/ml APL 0.1 mM PMSF 1 mg/ml Lysozyme pH 8.0	Prepared Fresh for Use
10X MMR	1M NaCl 20 mM KCl 50 mM HEPES 10 mM MgCl2 20 mM CaCl2 1mM EDTA pH 7.8 (NaOH)	Room temperature
Cysteine Solution	2.2% Cysteine 5 mM EGTA pH 7.6 (KOH)	Prepared Fresh for Use
UEB	50 mM KCl 50 mM HEPES 5 mM MgCl2 5 mM EDTA pH 7.6 (KOH)	4 °C,

Table 2.1 continued from previous page

Buffer	Composition	Storage Conditions
EB	50 mM KCL 5 mM MgCl2 2 mM β-mercaptoethanol 50 mM HEPES (pH 7.6 with KOH)	Prepared Fresh for Use
Stop-C	0.5% (w:v) SDS 5 mM EGTA 20 mM TRIS (pH 7.5 with HCL)	Prepared Fresh for Use
ER	1 M Phosphocreatine K Salt 600 µg/ml Creatine Phosphokinase	-20 °C
LFB1/50	10% Sucrose 50 mM KCL 40 mM HEPES (pH 8.0) 20 mM K Phosphate (pH 8.0) 2 mM MgCl2 1 mM EGTA 2 mM DTT 1 µg/ml APL	Prepared Fresh for Use
LFB1/100	10% Sucrose 100 mM KCL 40 mM HEPES (pH 8.0) 20 mM K Phosphate (pH 8.0) 2 mM MgCl2 1 mM EGTA 2 mM DTT 1 µg/ml APL	Prepared Fresh for Use
SuNaSp	0.25 M Sucrose 75 mM NaCl 0.5 mM Spermidine 0.15 mM Spermine 15 mM HEPES (pH 7.6 with KOH)	Prepared Fresh for Use
Stop-C Buffer	0.5% (w:v) SDS 5 mM EGTA 20 mM TRIS (pH 7.5 with HCL)	Prepared Fresh for Use
10% TCA	10% (w:v) TCA 2% (w:v) Na4P2O7.10H2O	4 °C
UTB Extraction Buffer	8M Urea 50 mM Tris-HCL pH 8.0 150 mM b-mercaptoethanol	Prepared Fresh for Use

Table 2.1 continued from previous page

Buffer	Composition	Storage Conditions
CSK Extraction Buffer	25 mM HEPES pH 7.4 50 mM NaCl 3 mM MgCl2 300 mM Sucrose 0.5% TritonX-1000 1X cOmplete Protease Inhibitor	-20 °C
Methylene Blue Stain	2 % (w/v) methylene blue 50% ethanol in H2O	Room temperature
IF Washing Buffer	5% (w/v) BSA 0.1% Tween 20 PBS	4 °C
LRR1 GFP-TRAP	10 mM TRIS-HCL pH 7.5 150 mM NaCl 0.5 mM EDTA 0.5% NP-40	Prepared Fresh for Use
ChIP Cell Lysis	5 mM HEPES pH 8.0 85 mM KCL 0.5% NP-40 1% cOmplete protease inhibitor	Prepared Fresh for Use
ChIP Nuclear Lysis	50 mM Tris-HCL pH 8.0 10 mM EDTA pH 8.0 1% SDS 1% cOmplete protease inhibitor	Prepared Fresh for Use
ChIP Dilution	16.7 mM Tris-HCL pH 8.0 1.2 mM EDTA pH 8.0 0.01% SDS 1.1% Triton X-100 167 mM NaCl 1% Protease Inhibitor	Prepared Fresh for Use
ChIP Low Salt	20 mM Tris-HCL pH 8.0 2 mM EDTA pH 8.0 0.1% SDS 1% Triton X-100 150 mM NaCl	Prepared Fresh for Use

Table 2.1 continued from previous page

Buffer	Composition	Storage Conditions
ChIP High Salt	20 mM Tris-HCL pH 8.0 2 mM EDTA pH 8.0 0.1% SDS 1% Triton X-100 500 mM NaCl	Prepared Fresh for Use
ChIP LiCl	10 mM Tris-HCL pH 8.0 1 mM EDTA pH 8.0 1% NP-40 1% Deoxycholic acid 250 mM LiCl	Prepared Fresh for Use
ChIP Elution Buffer	50 mM Tris-HCL pH 8.0 10 mM EDTA pH 8.0 1% SDS	Prepared Fresh for Use

Table 2.2: **Plasmids Used.** Shown is a summary of the plasmids utilised for work in both *X. leavis* egg extract and mammalian cell lines

Plasmid	Backbone	Insert	Source
Work in X. laevis			
His-TRAIP	pET28	WT TRAIP	Dundee Cell Products
WT His-SUMO-TRAIP	pCA528	WT TRAIP	Generated in this PhD
C25A His-SUMO-TRAIP	pCA528	C25A TRAIP Mutant	Generated in this PhD
His-RFWD3	pET28	WT RFWD3	Dundee Cell Products
His-TRIP12	pET28	C-Terminal TRIP12 Fragment	Dundee Cell Products
His-USP10	pET28	N-Terminal USP10 Fragment	Dundee Cell Products
His-USP22	pET28	WT USP22	Dundee Cell Products
His-USP34	pET28	N-Terminal USP34 Fragment	Dundee Cell Products
His-USP37	pET28	N-Terminal USP37 Fragment	Dundee Cell Products
Work in mammalian cell lines			
pX330-U6-Chimeric_BB-CBh-hSpCas9	N/A	N/A	(Cong et al., 2013)
C-Terminal mAID	pBluescript	N/A	(Natsume et al., 2016)
C-Terminal mAID-mCLOVER	pBluescript	N/A	(Natsume et al., 2016)
N-Terminal mAID	pBluescript	N/A	(Natsume et al., 2016)
N-Terminal mCLOVER-mAID	pBluescript	N/A	(Natsume et al., 2016)
pBS-TRAIP	pBluescript	TRAIP homology arm	This PhD Project
pBS-LRR1	pBluescript	LRR1 homology arm	This PhD Project
TRAIP-CRISPR	PX330	TRAIP gRNA	This PhD Project
TRAIP-DONOR (Hygro)	pBluescript	TRAIP homology arm	This PhD Project
TRAIP-DONOR (Neo)	pBluescript	TRAIP homology arm	This PhD Project
LRR1-Donor (hygro)	pBluescript	LRR1 homology arm	This PhD Project
LRR1-DONOR (Neo)	pBluescript	LRR1 homology arm	This PhD Project
LRR1-CRISPR	PX330	LRR1 gRNA	This PhD Project
PMXX-FLAG-AID	pBluescript	N/A	This PhD Project

Table 2.3: **Compounds Used.** Shown is a summary of the compounds used throughout this PhD project. Detailed is the compound, source, stock concentrations, and working concentration.

Compound	Source	Stocks (Storage)	Working Concentration
IAA	Sigma (I2886)	500 mM in DMSO (- 20 °C)	100 µM in cell media
Hygromycin	InvivoGen (hg-1)	1 mg/ml in H2O(- 20 °C)	100 mg/ml in cell media
Propidium Iodide	ThermoFisher (P1304)	1 mg/ml from source (4 °C)	50 µg/ml in PBS
Hoechst 33582	Merck (861405)	10 mM in DMSO (- 20 °C)	5 µM in PBS
MK-1775	Stratech (ORB419538-BOR)	10 mM in DMSO (- 20 °C)	5 µM in cell media
ATR Inhibitor	Stratech (AZD6738)	10 mM in DMSO (- 20 °C)	4 µM in cell media
ATM Inhibitor	Stratech (KU-55933)	10 mM in DMSO (- 20 °C)	10 mM in cell media
Hydroxyurea	Sigma (H8627)	Prepared fresh	5 µM in cell media
Triptolide	Sigma-Aldrich (T3652)	100 mM in DMSO (- 20 °C)	100 nM in cell media
DRB	Sigma-Aldrich (D1916)	500 mM in DMSO (- 20 °C)	100 µM in cell media
Aphidicolin	Sigma (A0781)	10 mM in DMSO (- 20 °C)	0.4 µM in cell media
CB5083	Cayman Chemical (19311)	10 mM in DMSO (- 20 °C)	5 mM in cell media
MLN4924	Active Biochem (A01139)	20 mM in DMSO (- 20 °C)	5 µM in cell media
Lovastatin	Acros Organics (A0398529)	20 mM in DMSO (- 20 °C)	20 µM in cell media
Mevalonic Acid	Sigma (BCBX4250)	50 mM in DMSO (- 20 °C)	2 mM in cell media
RO-3306	Selleck Chemical (S7747)	45 mM (- 20 °C)	9 µM in cell media
BrdU	Merck (B5002)	10 mM in DMSO (- 20 °C)	10 µM in cell media
EdU	Thermofisher (A10044)	10 mM in DMSO (- 20 °C)	10 µM in cell media

Table 2.4: **Primers Used.** Shown is a summary of the primers used throughout this PhD project. Primers used for both PCR purposes, as well as cloning, are detailed.

Primer	Sequence
PCR Primers	
TRAIP-AID C-Terminal Forward (1727)	AGATGTGGTGAGTGTGGCTTC
TRAIP-AID C-Terminal Reverse (1728)	GCTGCAGTGATCTCATTCTTTCT
mAID C-term Tag Primer (811)	AAGAACGTGATGGTTTCCTG
mAID N-term Tag Primer (1354)	ATCTTTAGGACAAGCACTCTTCTCC
AID-LRR1 N-Terminal Forward (1719)	AGGAATTGCCAAGTCAAATACAG
AID-LRR1 N-Terminal Reverse (1720)	AGGGAGAATATTGTGGGAGAAAG
AAVS1 Locus Check (926)	CACTTTGAGCTCTACTGGCTTCTGC
CMV Promoter Check (925)	CGGTCAGCCAGGCGGGCCATTTACC
Tet Promoter Check (998)	CGCTCTTGACGATTTTGACCTTGAC
Actin ChIP Check Forward	CATGTACGTTGCTATCCAGGC
Actin ChIP Check Reverse	CTCCTTAATGTCACGCACGAT
Cloning Primers	
X. laevis His-TRAIP to SUMO-His-TRAIP Forward	GATTTGCTCGGACTTCTTCGACAATAC
X. laevis His-TRAIP to SUMO-His-TRAIP Reverse	GTAGCGTAGGCGCGTATGGGCAG
X. laevis WT SUMO-His-TRAIP to C25A SUMO-His-TRAIP Forward	CACGTTCCATCAGGAGTGTTTGTTACAGTG
X. laevis WT SUMO-His-TRAIP to C25A SUMO-His-TRAIP Reverse	TGCCCACGGGTAATCGCGGCCACATC

Table 2.5: **Antibodies Used for this PhD Project.** Shown are a summary of the antibodies utilised for this project. Highlighted is the antibody, species, source, and dilution/usage.

Antibody (Species)	Source	Use
Primary Antibodies		
X. laevis α-SUMO-His-TRAIP (Rabbit)	This PhD Project	Immunoblotting 1:1000 crude sera
X. laevis α-His-TRIP12 (Rabbit 76)	This PhD Project	Immunoblotting 1:1000 crude sera
X. laevis α-His-TRIP12 (Rabbit 77)	This PhD Project	Immunoblotting 1:1000 crude sera
X. laevis α-His-USP10 (Sheep)	This PhD Project	Immunoblotting 1:1000 crude sera
X. laevis α-His-USP34 (Sheep)	This PhD Project	Immunoblotting 1:1000 crude sera
X. laevis α-His-RFWD3 (Rabbit 59)	This PhD Project	Immunoblotting 1:1000 crude sera
X. laevis α-His-RFWD3 (Rabbit 106)	This PhD Project	Immunoblotting 1:1000 crude sera
X. laevis α-His-USP37 (Rabbit 60)	This PhD Project	Immunoblotting 1:1000 crude sera
X. laevis α-His-USP37 (Rabbit 61)	This PhD Project	Immunoblotting 1:1000 crude sera
α-His (Mouse)	Sigma (H1029)	Immunoblotting 1:1000 crude sera
α-γH2AX S139 (Mouse)	Sigma (JBW301)	Immunofluorescence 1:1000
α-γH2AX S139 (Rabbit)	Abcam (29893)	ChIP 1 mg
α-H2AX (Rabbit)	Merck Millipore (07627)	ChIP 1 mg
α-GFP (Rabbit)	Chromotek (PABG1)	Immunoblotting 1:1000
α-TRAIP (Sheep)	Prof. N. Mailand (Hoffmann et al., 2016)	Immunoblotting 1:300
α-Actin	Santa Cruz (C4 HRP)	Immunoblotting 1:5000
α -S10PH3 (Rabbit)	Cell Signalling (ab183626)	Immunoblotting 1:1000 Immunofluorescence 1:500 FACS 1:500
α-CENPF (Rabbit)	Abcam (AC5)	Immunofluorescence 1:1000
α-Mitosin (Mouse)	BD Biosciences (610768)	Immunofluorescence 1:1000
α-53BP1 (Mouse)	NB antibodies (904)	Immunofluorescence 1:1000
α-Biotin (Rabbit)	Bethyl Laboratories (A150-109A)	Proximity Ligation Assay 1:500
α-RNA Polymerase II (Ser5 CTD) (Mouse)	Cell Signalling (2629)	Proximity Ligation Assay 1:250
α-S9.6 (Rabbit)	Crick Institute	Immunofluorescence 1:200
α-BLM (Rabbit)	Crick Institute	Immunofluorescence 1:200
α-MCM7 (Mouse)	Santa Cruz (9966)	Immunofluorescence 1:1000 FACS 1:500
α-CDC45 (Rabbit)	Cell Signalling (D76G)	Immunofluorescence 1:100
α-BrdU (Mouse)	BD Biosciences (B44)	FACS 1:50
Secondary Antibodies		
α-HRP-IgG (Sheep)	Sigma (A34151ML)	Immunoblotting 1: 10000
α-HRP-IgG (Rabbit)	Sigma (A05451ML)	Immunoblotting 1: 25000
α-HRP-IgG (Mouse)	Sigma (52781ML)	Immunoblotting 1: 5000
α-AF488-IgG (Rabbit)	Invitrogen (A32731)	Immunofluorescence 1:1000 FACS 1:1000
α-AF488-IgG (Mouse)	Invitrogen (A32723)	Immunofluorescence 1:1000 FACS 1:1000
α-AF555-IgG (Rabbit)	Invitrogen (A32732)	Immunofluorescence 1:1000 FACS 1:1000
α-AF647-IgG (Mouse)	Invitrogen (A32728)	Immunofluorescence 1:1000 FACS 1:1000
α-Atto 647N-IgG (Rabbit)	Sigma (40839)	Immunofluorescence 1:1000 FACS 1:1000

Table 2.6: **Mammalian Cell Lines Used.** Shown is a summary of all the mammalian cell lines utilised throughout this PhD project. Highlighted are the background/parental cell line, the modifications/genomic alterations, clone identified, and resistance markers.

Background	Genomic Alterations	Clone	Resistance
HCT116	CMV-OsTIR1	N/A	Puromycin
HCT116	CMV-OsTIR1 TRAIP-mAID	C2	Puromycin, Hygromycin
HCT116	CMV-OsTIR1 TRAIP-mAID	D5	Puromycin, Hygromycin
HCT116	CMV-OsTIR1 TRAIP-mAID	F2	Puromycin, Hygromycin
HCT116	CMV-OsTIR1 TRAIP-mAC	C5	Puromycin, Hygromycin
HCT116	CMV-OsTIR1 TRAIP-mAC	G4	Puromycin, Hygromycin
HCT116	CMV-OsTIR1 TRAIP-mAC	F2	Puromycin, Hygromycin
HCT116	CMV-OsTIR1 mAID-LRR1	D2	Puromycin, Hygromycin
HCT116	CMV-OsTIR1 mAID-LRR1	F3	Puromycin, Hygromycin
HCT116	CMV-OsTIR1 mAID-LRR1	C6	Puromycin, Hygromycin
HCT116	Tet-OsTIR1	N/A	Puromycin
HCT116	Tet-OsTIR1 mAC-LRR1	B4	Puromycin, Hygromycin
HCT116	Tet-OsTIR1 mAC-LRR1	G4	Puromycin, Hygromycin
HCT116	F74G CMV-OsTIR1	N/A	N/A
HCT116	F74G CMV-OsTIR1 mAID-LRR1	G2	Hygromycin
HCT116	F74G CMV-OsTIR1 mAID-LRR1	F4	Hygromycin
HCT116	F74G CMV-OsTIR1 mAID-LRR1	D6	Hygromycin
HCT116	F74G CMV-OsTIR1 mAID-LRR1	B10	Hygromycin
HCT116	F74G CMV-OsTIR1 mAID-LRR1	B11	Hygromycin
HCT116	F74G CMV-OsTIR1 mAID-LRR1	A12	Hygromycin
HCT116	F74G CMV-OsTIR1 mAID-LRR1	H11	Hygromycin
HCT116	CMV-OsTIR1 TRAIP-mAID + Tet TRAIP-SFB	C2	Puromycin, Hygromycin, Blasticidin
HCT116	CMV-OsTIR1 TRAIP-mAID + Tet TRAIP-SFB	C4	Puromycin, Hygromycin, Blasticidin
HCT116	CMV-OsTIR1 TRAIP-mAID + Tet C7A TRAIP-SFB	C2	Puromycin, Hygromycin, Blasticidin
HCT116	CMV-OsTIR1 TRAIP-mAID + Tet C7A TRAIP-SFB	C4	Puromycin, Hygromycin, Blasticidin
hTERT-RPE1	N/A	N/A	N/A
hTERT-RPE1	Tet-OsTIR1	N/A	Puromycin
hTERT-RPE1	Tet-OsTIR1 TRAIP-mAID	N/A	Puromycin, G418

2.2 Working With Proteins

2.2.1 SDS-PAGE

Sodium dodecyl sulphate-polyacrylamide gel electrophoresis (SDS-PAGE) is a commonly used method of separating proteins based on their respective molecular weights, by differential migration patterns through a gel matrix. For the purposes of this PhD project, two types of acrylamide gels were used: either pre-cast gels composed of 4-12% acrylamide gradients (Invitrogen NuPAGE), or single-concentration acyrylamide gels prepared immediately prior to use (See Table 2.7). Before sample loading, protein extracts were mixed with detergent-containing loading buffer (NuPAGE SDS Sample Buffer 4X, Novex by Life Technologies) to a final concentration of 1X and boiled at 95°C for 5 minutes. Between 5 - 50 µg of total protein was loaded per well. Protein separation was achieved through application of electrical currents to the gel; with detergent coated peptides migrating towards the positive cathode. SDS-PAGE using pre-cast gels was conducted using MOPS running buffer (20X stock diluted in H_2O; Novex by Life Technologies) at 160 V for 75 minutes. Single concentration acrylamide gels were run using TRIS-Glycine running buffer (Table 2.1) at 100 V for 10 minutes to initially allow migration of peptides through the stacking gel; followed by 120 V for 60 minutes for protein separation through the resolving gel. All samples were run alongside a reference marker of known molecular weight (PageRuler Prestained Plus Protein Ladder, Thermofisher Scientific).

Table 2.7: **Composition of Single Concentration SDS-PAGE gels.** Detailed are the respective components, and volumes required, for preparing SDS-PAGE gels. Both the stacking buffer and resolving buffer (for 6%, 8%, 10%, and 12%) are shown.

	Resolving Gel				Stacking Gel
Component	6%	8%	10%	12%	5%
H2O	2.6 ml	2.3 ml	1.9 ml	1.6 ml	3.4 ml
30% Acrylamide	1.0 ml	1.3 ml	1.7 ml	2.0 ml	0.83 ml
1.5 M Tris (pH 8.8)	1.3 ml	1.3 ml	1.3 ml	1.3 ml	0.63 ml
10% SDS	0.05 ml	0.05 ml	0.05 ml	0.05 ml	0.05 ml
10% ammonium persulfate	0.05 ml	0.05 ml	0.05 ml	0.05 ml	0.05 ml
TEMED	0.004 ml	0.003 ml	0.002 ml	0.002 ml	0.005 ml

2.2.2 Coomassie Protein Staining

Protein samples separated using SDS-PAGE were visualised within the gel matrix using Coomassie Blue Protein Stain (Table 2.1). Coomassie brilliant blue is a triphenylmethane dye that reversibly binds to charged amino acid residues. For staining, SDS-PAGE gels were submerged in Coomassie Blue protein stain for 20 minutes at room temperature, rocking. Any unbound dye was removed through immersion in destaining buffer (Table 2.1) at room temperature, rocking. Typically, the destaining buffer was replaced every 30 minutes until sufficient destaining was observed (approximately 60 - 120 minutes). Destaining buffer contained high methanol concentrations, resulting in gel dehydration and shrinkage. Therefore, following destaining, gels were rehydrated through submersion in distilled H_2O (5-15 minutes at room temperature). Gels were stored in air-tight plastic pouches and images acquired using a standard computer scanner.

2.2.3 Immunoblotting

Whilst Coomassie staining allows the visualisation of all proteins present in a gel matrix, it does not facilitate the detection or identification of specific proteins within a mixed sample. For this, immunoblotting (Western Blotting) was used. Following SDS-PAGE, gels were first equilibrated in transfer buffer (Table 2.1) for 10-15 minutes at room temperature. Gel equilibration functioned to remove excess salt and detergent that may impair protein transfer to a membrane. Two types of membranes were used during this PhD project: Nitrocellulose (VWR), or Polyvinylidene fluoride (PVDF, Merck Millipore). Nitrocellulose membranes were primarily used for samples generated using mammalian cells, whilst PVDF was used for experiments utilising *Xenopus laevis* egg extracts. PVDF membranes possess higher overall binding capacity than nitrocellulose membranes, which is particularly advantageous for the detection of low/high molecular weight proteins. Conversely, this increased binding capacity commonly results in higher background signal, potentially preventing detection of low-copy number proteins. PVDF membranes are also extremely hydrophobic, and required pre-activation in methanol for 5 seconds at room temperature immediately before use.

Following the gel equilibration step, separated proteins were transferred through the application of an electric current. Completed SDS-PAGE gels were placed within a transfer 'sandwich' (Whatmann filter paper, membrane, gel, Whatmann filter paper) and submerged in cold transfer buffer. Transfers were carried out at either 100 V for 60 minutes, 80 V for 90 minutes, or 60 V for 16 Hrs. Transferred membranes were placed immediately in 5% Milk (Marvel, made up in TBST) for 60 minutes at room temperature, rocking, to block the membrane. Blocking acted to coat the transferred membranes with varying additional

proteins present within the milk solution, preventing non-specific antibody binding. Blocked membranes were washed briefly in TBST (Table 2.1), treated with the required primary antibody solution in 5% BSA in PBS (Table 2.5), and incubated for either 4 hours at room temperature, or overnight at 4°C. Membranes were then washed in TBST (3X 10 minutes, rocking) before submersion in a solution containing the appropriate Horseradish Peroxidase (HRP) conjugated secondary antibody in 5% BSA in PBS (Table 2.5). Samples were incubated in secondary antibody for 2 hours at room temperature, rolling. Following antibody staining, membranes were washed as described previously, and the immunoblot signal developed through the application of ECL detection spray (Advansta WesternBright ECL HRP Substrate Spray). The ECL spray contains HRP substrates that associate with the secondary antibodies to generate a detectable chemiluminescent signal, detectable on X-ray films.

2.2.4 Estimating Protein Concentration Using Bradford's Reagent

Bradford's protein assay is a colorimetric method used to quickly determine the total protein concentration of whole cell extracts or protein elutions. The red/brown reagent is rapidly converted to a blue substrate upon protein binding, the respective increase of which is detectable at 595 nm. Protein standards were prepared using Bovine Serum Albumin (BSA; Pierce Standards, ThermoFisher Scientific) and used to generate a standard curve, depicting the linear range of absorbance over a known concentration (Figure 2.1). Typically, protein standards were prepared to final concentrations of 0, 250, 500, 750, and 900 ng/µl, to a final volume of 20 µl; composed of the appropriate amount of 1 mg/ml BSA, 2 µl of the respective extraction buffer (to account for any components interfering with the emissions spectra), and double distilled H_2O. The test protein samples were also diluted 1:10 in H_2O to

a final volume of 20 µl. Sample dilution ensured that the measured absorbance fell within the linear range of the standard curve. If the measured absorbance fell outside this range, then the protocol was repeated using higher dilution factors. To conduct the assay itself, samples were mixed with 1 ml of Bradford's reagent and incubated for 5 minutes at room temperature in the dark. Following this, the absorbance was measured at 595 nm using a standard benchtop spectrophotometer. Values were compared to the standard curve to calculate protein concentration.

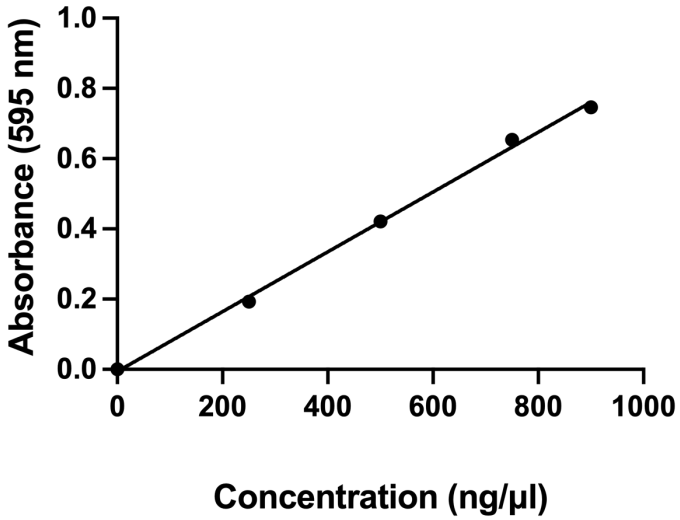


Figure 2.1: **Example Standard Curve for Bradford's Protein Assay.** Shown are the absorbances measured at 595 nm for protein standards at the following concentrations: 0, 250, 500, 750, and 900 ng/µl. Linear regression analysis was used to estimate a trendline, fitted as shown. The resulting equation for the trendline was then used to calculate protein concentration of diluted unknowns, measured at 595 nm.

2.2.5 Estimating Protein Concentration using BSA Gradients

The Bradford's assay described in section *2.2.4* offered a simple method to calculate total protein concentration. However, it does not provide insight into the concentration of individual proteins within a mixed sample. Therefore, if the concentrations of specific proteins were

required (e.g. after protein purification), alternative methods were required. In this case, protein concentrations were calculated through comparison to known protein gradients run on SDS-PAGE gels (Figure 2.2). It is important to note, any approximations made with this method were solely dependent on visual observation, and so were only suitable when precise concentrations were not needed. BSA standards of varying concentrations were prepared through dilution of a 1 mg/ml stock using 2X SDS-PAGE loading buffer. The protein unknown was similarly serially diluted if appropriate. A total of 10 µl of each sample was loaded and run on SDS-PAGE gels before being stained with coomassie protein stain. Through visual observation between the proteins of interest, and known BSA concentrations, estimations as to the total amount of protein present within each band could be determined.

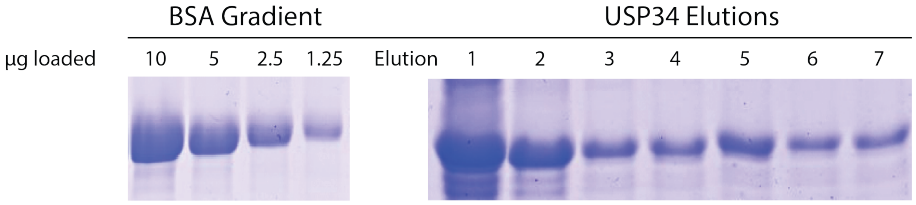


Figure 2.2: **Estimation of Protein Concentration Using BSA Gradients.** Shown are serially diluted BSA gradients (left; 10, 5, 2.5, 1.25 µg of protein loaded) and different elution fractions from His-USP34 protein purification (right). Samples were run using SDS-PAGE with pre-cast 4-12 % gradient gels, subsequently stained with Coomassie Blue Protein Staining. Protein concentration of each respective elution was then approximated through visual comparison to the BSA gradient.

2.3 Working With DNA

2.3.1 DNA Gel Electrophoresis

Agarose gel electrophoresis allows the separation of DNA samples through a gel matrix. The phosphate backbone of DNA is naturally negatively charged, and therefore by applying a current to the gel, the size-dependent migration of DNA towards the positive cathode can be achieved. Agarose gels were prepared by dissolving (through heating) between 0.8-2.0% agarose (w/v; Sigma Aldrich) in TBE buffer (Table 2.1). The heated agarose suspension was allowed to cool slightly, supplemented with 1:1000 dilution of SYBRsafe DNA dye (Thermofisher Scientific), and poured into a gel mould to set. SYBRsafe is a commonly used alternative to ethidium bromide that stains nucleic acids through intercalation and groove binding. Following interactions with DNA, the stain is excited under UV light to emit a detectable signal. To run the gel, DNA samples were mixed with 6X DNA loading dye (New England Biolabs) to a final concentration of 1X. Between 2-10 µl of each sample was loaded onto the prepared agarose gel. Samples were run in TBE buffer at 100 V, or 200 V for 45 minutes, dependent on tank size. All samples were run alongside a molecular size marker (New England Biolabs).

2.3.2 Polymerase Chain Reaction

Polymerase chain reaction (PCR) amplification of DNA sequences of interest was carried out for several reasons throughout this PhD project (e.g. molecular cloning, confirmation of gene tagging, or mycoplasma testing). Two different reaction kits were used, dependent on the respective experimental requirements. Q5 high fidelity PCR reagents (New England Biolabs) were utilised for molecular cloning purposes. GoTaq HotStart Green Master Mix (Promega)

was used for exploring genome tagging or mycoplasma testing, wherever higher throughput was required. Primer oligonucleotides (Table 2.4) were designed to flank specific regions of interest, optionally inserting amino acid modifications or restriction binding sites as desired. All reaction compositions and thermocycling conditions used are depicted in Table 2.9. PCR reactions were prepared using nuclease free H_2O, and any resulting reaction products stored at 4°C until use.

Table 2.9: **Summary of Polymerase Chain Reaction Reagents.** Depicted is the standard composition of PCR reactions used throughout this PhD. Two reaction kits are shown, either the Q5 High Fidelity PCR, or GoTaq HotStart Green Master Mix. Alongside each kit and reaction compositions, the thermocycling programme and cycles are shown. Thermocyclying stages indicated with '-' were included in the cycling stage.

Type	Reaction Composition (per reaction)	Thermocycling	Cycles
Q5 High Fidelity PCR	1X Reaction Buffer 200 µM dNTPs 0.5 µM Forward Primer 0.5 µM Reverse Primer 0.02 Units/µl Q5 High fidelity DNA Polymerase 1-10 ng template DNA Made up to the desired reaction volume with nuclease free H2O	Denaturation: 98 °C for 30 s - Denaturation: 98 °C, 5-10 s - Annealing: 65-72 °C, 10-30 s - Extension: 72 °C, 30 s per kB Extension: 72 °C, 2-5 mins	25-30
GoTaq HotStart Green Master Mix	1X GoTaq HotStart Green Master Mix 0.5 µM Forward Primer 0.5 µM Reverse Primer <250 ng template DNA Made up to the desired reaction volume with nuclease free H2O	Denaturation: 95 °C for 2 min - Denaturation: 95 °C, 30 s – 1 min - Annealing: 5 °C below primer TM - Extension: 72-74 °C, 1 min per kB Extension: 72 °C, 2-5 min	25-40

2.3.3 Molecular Cloning

Molecular cloning techniques were employed for plasmid construction or modification. For this, a standard workflow was followed: PCR amplification of regions of interest, DNA purification, restriction digestion, gel electrophoresis, gel extraction, and ligation. Each individual step is summarised briefly below.

Amplification of Regions of Interest

The DNA template of interest was first amplified using PCR (See **2.3.2**). Primers were designed as previously described.

DNA Purification from PCR Products

The resultant PCR products generated were subsequently purified to isolate the amplified DNA. Sample purification was carried out using the QIAquick PCR purification kit (Qiagen), as per manufacturers instruction. Briefly, the PCR reaction was first mixed with a high salt solution and passed through a silica column. Any DNA fragments between approximately 100 - 10 000 bp bound to the resin. Any small DNA fragments (e.g. unbound oligonucleotides) or other impurities were then removed through a series of centrifugation - wash steps. Finally, the bound DNA was eluted from the column using a low salt buffer (EB buffer).

Restriction Digestion

Varying restriction digestion enzymes were used to induce breaks at defined sites within the amplified, purified DNA fragments. Specifically, restriction digestion was used to generate identical sticky ends in both the donor plasmid backbone and insert fragments to facilitate their ligation. Restriction digestion reactions were prepared as detailed in Table 2.10 and incubated at 37°C for 2 hours. Several restriction enzymes were used during this PhD project, including EcoR1, SacI, SacII, BamH1, Nco1, and Xba1; individual combinations used are detailed alongside the respective results section or in Table 2.4. Plasmid self-ligation was prevented through treatment of digested products with alkaline phosphatase, removing 5' phosphate groups from the formed sticky ends. Following sample digestion, 5 units of Antarctic Phosphatase

(New England Biolabs) was added to the restriction digestion mix alongside 1X concentration of 10X alkaline phosphatase buffer (New England Biolabs). The reaction was incubated for a further 30 minutes at 37°C, and heat inactivated at 80°C for 2 minutes.

Table 2.10: **Summary of Restriction Digestion Reactions.** Shown are the amounts of each respective component required for the restriction digestion of donor and insert fragments. The amounts summarised were used for all molecular cloning experiments.

Component	'Insert' Reaction	'Donor' Reaction
Plasmid	20 µg	10 µg
Restriction Enzyme 1	∼20 – 40 Units (2 µl)	∼20 – 40 Units (2 µl)
Restriction Enzyme 2	∼20 – 40 Units (2 µl)	∼20 – 40 Units (2 µl)
CutSmart Buffer (New England BioLabs)	5 µl	5 µl
Nuclease free H2O	Make up to 50 µl	Make up to 50 µl

Gel Electrophoresis and Band Excision

The respective products yielding from restriction digestion were run on 0.8% agarose gels as previously described (See **2.2.1**). The corresponding donor and insert bands were excised from the gel using a clean surgical scalpel, and placed into 1.5 ml Eppendorf tubes. DNA contained within the gel matrix was extracted using QIAquick gel extraction kits (Qiagen), as per manufacturer's instruction. The gel fragments were first dissolved using a guanidinium thiocyanate containing solubilisation buffer, before the DNA was purified using a similar silica column binding method as detailed in previously.

Ligation

Purified template DNA insert and donor fragments, with compatible sticky ends generated through restriction digestion, were ligated together using the T4 DNA Ligase kit (New England

BioLabs). Briefly, the ligation reactions were set up as follows: 8 µl insert, 2 µl donor, 1 µl T4 DNA Ligase, 2 µl 10X T4 DNA Ligase Reaction Buffer, and 7 µl nuclease free H_2O. All ligation reactions were carried out at 16℃ for 16-18 hours. The resulting plasmid DNA was validated through agarose gel electrophoresis and DNA sequencing (SourceBioscience), before being transformed into a suitable vector for expression.

2.3.4 Plasmid Construction for Auxin-Inducible Degron Cell Lines

Several plasmids, required for the generation of Auxin-Inducible Degron (AID) cell lines were kindly generated and provided for use during this PhD project by Prof. Masato Kanemaki at the Department of Molecular Cell Engineering, National Institute of Genetics, Japan (Table 2.2). Full details of all the plasmids generated are shown in Appendix A1. The Cas9 endonuclease was expressed through the pX330-U6-Chimeric_BB-CBh-hSpCas9 plasmid backbone (Addgene 42230) and targetted to within 30 bp of either the start or stop codon by complimentary sequences (guideRNA). The gRNA sequences used were as follows: LRR1 - 5' TGTAGCTTCATCTCGCCCAA 3'; TRAIP - 5'-CTCACTGTTCTCACGACCAC-3'. DONOR plasmids were generated from pBluescript KS plasmid backbones (Yesbolatova et al., 2019). Homology arms included in DONOR plasmids, approximately 500 bp upstream and downstream of the desired tag position, directed insertion of the degron tag into the breaks created by Cas9. For LRR1, the coverage of designed targetting homology arms was as follows, upstream homology arm: GRCh38:14:49,598,567-49,599,117:1 in refseq CM000676; downstream homology arm: GRCh38:14:49,599,021-49,599,563:1 in refseq CM000676. For TRAIP, the coverage of the designed targetting homology arms was as follows, upstream homology arm: GRCh38:3:49,828,700-49,828,123:2 in refseq CM000665; downstream homology arm;

GRCh38:3:49,828,133-49,828,697:2 in refseq CM000665. To produce plasmids suitable for transfection into RPE1 cell lines, the respective resistance markers within the donor plasmids detailed were exchanged using standard molecular cloning (Hygromycin B Gold to Neomycin G418). All plasmid construction and primer design was carried out using Snapgene.

2.4 Working With Bacteria

Several bacterial strains were generated and utilised throughout this PhD project. Three parental *Escherichia coli* (*E. coli*)) strains were used: XL10-Gold, BL21(DE3), and Rossetta BL21(DE3)pLys. XL10-Gold possess a high transformation efficiency phenotype and were utilised for the amplification and purification of exogenous plasmid DNA. The other two bacterial strains used both expressed T7 RNA polymerase, and were therefore able to transcribe recombinant proteins expressed from plasmids containing suitable T7 promoter sites. In addition, Rossetta additionally expresses a T7 lysozyme as well as additional codons not found in prokaryotic organisms; enhancing the expression of eukaryotic proteins.

2.4.1 Bacterial Transformation

Bacterial transformation describes the process by which exogenous plasmids can be incorporated into ultracompetent bacterial strains. The transformation protocol followed was the same regardless of the bacterial strain used, with the exception of XL10-Gold; which were pre-activated with β-mercaptoethanol for 10 minutes on ice immediately prior to transformation. Bacterial transformation was carried out as follows: 1-2 µl of plasmid DNA was added to 10-50 µl aliquots of ultracompetent bacterial cells and mixed with gentle pippetting. Samples were incubated on ice for 30 minutes, heat shocked at 42°C for 30-45 seconds, and

placed back on ice for a further 5 minutes. Transformed bacterial cells were resuspended in 250 µl of Super Optimal Broth (SOC Media) and incubated for 60 minutes at 37°C. Recovered bacterial cultures were spread onto agar plates, supplemented with the required selection drug. Plates were incubated at either 37°C overnight, or at room temperature for 3 days.

2.4.2 Generating Bacterial Stocks and Growing Bacterial Cultures

All bacterial cultures were grown in either Luria-Bertani Medium (LB Media, Merck) or Auto-Inducing Media (AIM Media; Merck), sterilised through autoclavation and supplemented with the appropriate selection drug prior to use. Single bacterial colonies from transformed cultures were used to inoculate 10 ml of LB broth for 16-18 hours at 37°C, shaking. The resultant bacterial culture was then used for either generating long-term stocks, or growing 'starter cultures' for experimental procedures. Long-term storage was achieved through creating glycerol stocks. Briefly, 500 µl of confluent bacterial culture was supplemented with sterile glycerol to a final concentration of 25 % (v/v) and stored at -80°C. For the generation of subsequent cultures, the frozen glycerol stocks were used to inoculate small volume-cultures as previously described. The resulting starter stocks were in turn used to innoculate larger cultures at approximately 1:500 dilutions.

2.4.3 Protein Expression Testing

The respective expression levels of recombinant proteins, from plasmids transformed into BL21(DE3) or Rossetta bacterial strains, were initially tested in small-scale experiments before protein purification. Plasmids were generated for this PhD project using PET18 plasmid backbones by Dundee Biosciences (Table 2.2). Each respective plasmid contained a T7

promoter, and the peptide of interest fused to a poly-histidine tag positioned within a lac operon. Starter cultures from the appropriate bacterial strain were generated as detailed in **2.4.2**. Individual 10 ml test cultures were then created using the starter cultures as inoculants, and grown at 37°C for 2-3 hours. If LB media was used, the OD_{600} was regularly monitored, and protein expression induced upon reaching OD_{600}: 0.5-0.6 through the addition of 1 mM Isopropyl β-d-1-thiogalactopyranoside (IPTG). IPTG is an allolactose mimic that binds to the lac repressor, activating the lac operon and therefore the transcription of any gene encoded within. Alternatively, if AIM media was used, no IPTG was required. AIM media contained limited glucose, which becomes increasingly depleted as bacterial cultures grow. Once the glucose levels within the media are depleted, the bacterial cultures switch to instead metabolise lactose; producing allolactose and activating transcription through the binding of allolactose to the lac repressor. Immediately prior to sample induction, 1 ml of the bacterial culture was collected (Uninduced Sample), centrifuged (6000 g, 10 minutes, 4°C), and the pellet resuspended in 2X SDS-PAGE sample buffer. The remaining cultures were treated to induce protein expression and incubated for 16-18 hours at 18°C, shaking. Following the overnight incubation, bacterial cultures were collected and centrifuged as described previously. The supernatent was discarded, and the pellet resuspended in 2X SDS-PAGE sample buffer. All samples were boiled at 95°C for 5 minutes and run on SDS-PAGE gels, followed by Coomassie protein staining or immunoblotting.

2.4.4 Protein Solubility Testing

Once the optimal growth conditions for protein expression had been determined, the relative solubility of the expressed recombinant protein was explored. Bacterial cultures (10 ml) were

grown, and protein expression induced as previously described. The resultant cultures were flash frozen and then centrifuged (6000 g, 10 minutes, 4°C), the supernatant discarded, and the pellet resuspended in 200 µl of the respective lysis buffer to be tested. Immediately before use, all lysis buffers were supplemented with 0.1 mM phenylmethylsulfonyl fluoride (PMSF), 1 mg/ml Lysozyme, as well as 0.1 µg/ul Apoprotein, Pepstatin, and Leuprotein. Resuspended cell suspensions were supplemented with 25 units/ml of Bitnuclease or similar (BASEMUNCH, Benzonase) to digest nucleic acids. Samples were incubated at room temperature for 20 minutes, rotating, to lyse the bacterial cells. Following lysis, samples were separated into two equal aliquots, one of which was optionally sonicated (3X, 10 seconds, 20-25 W power, on ice). All samples then were centrifuged (5 minutes, 16 900 G, 4°C) to separate insoluble and soluble fractions; each of which were collected and mixed with 2X SDS-PAGE loading buffer. The solubility of the respective recombinant protein expressed was then assessed using SDS-PAGE followed by Coomassie protein staining and immunoblotting.

2.4.5 Purification of Recombinant Proteins of Interest

Recombinant proteins were expressed from PET28 vectors transformed into suitable bacterial strains. Each respective protein was tagged with a poly-histidine tag, or variant thereof. To maximise protein solubility, the TRAIP sequence was cloned into a His-SUMO vector. Histidine residues readily bind to heavy metal ions, such as Nickel or Cobalt. The inclusion of a poly-histidine tag, therefore facilitated protein purification through peptide binding to Nickel beads. It was possible however, that non-specific peptides containing histidine clusters may also bind to the beads with varying strengths. To account for this, several wash steps were included to remove weakly bound components. Table 2.11 depicts a summary of the conditions

selected, and used, to purify each of the candidates. Individual lysis buffers are detailed in each respective section, and in Table 2.1.

Table 2.11: **Overview of Candidates to be Purified.** Shown are each of the 7 E3 ubiquitin ligases and deubiquitylating enzymes selected for study during this PhD project. Plasmids were generated to express each candidate in the detailed bacterial strain and tag. Also highlighted is further information as to whether a whole or fragment was expressed, the kDa size, as well as the respective bacterial strain and media used to express the candidate.

Candidate	Expressed	Size (kDa)	Tag	Strain	Media
TRAIP	Whole Protein	65	His-SUMO	Rossetta	AIM
RFWD3	N-Terminal Fragment	50	His	BL21(DE3)	LB
TRIP12	C-Terminal Fragment	47	His	BL21(DE3)	AIM
USP10	N-Terminal Fragment	25	His	BL21(DE3)	AIM
USP22	Whole Protein	61	His	BL21(DE3)	Insoluble
USP34	N-Terminal Fragment	27	His	BL21(DE3)	AIM
USP37	N-Terminus	27	His	BL21(DE3)	LB

Purification of WT and Mutant His-SUMO-TRAIP

Plasmids expressing either wild-type recombinant His-SUMO-TRAIP, or a C25A catalytically inactive point mutant (Table 2.2), were transformed into Rossetta pLys cells. Transformed bacterial cultures were grown as previously detailed to innoculate 4 l of AIM media supplemented with 50 µg/ml kanamycin. Cultures were grown at 37°C, shaking, until reaching an approximate OD_{600} of 0.5-0.6. Upon reaching the desired OD, the cultures were rapidly cooled through submersion of the flasks in ice baths, before all samples were incubated for a further 16 hours at 18°C, shaking, to allow recombinant protein expression and folding. Following the overnight incubation, the bacteria were pelleted by centrifugation (6000 g, 10 minutes, 4°C and the supernatent discarded. The resulting bacterial pellets were flash frozen at

-80°C to aid cell lysis. Frozen pellets were allowed to thaw on ice and then resuspended in 30 ml of TRAIP Lysis buffer (Table 2.1), rotated at room temperature for 5 minutes, supplemented with 25 units/ml Benzonase, and rotated for a further 20 minutes at room temperature. The bacterial lysate then sonicated (6X, 20-25 W, 30 seconds, on ice) and the soluble fraction isolated through centrifugation (31 000 g, 30 minutes, 4°C). During the spin, super Ni NTA affinity resin beads (SUPER-NINA100, Generon) were prepared as follows: 5 ml of bead resin was washed with 30 ml double distilled H_2O once followed by two washes using lysis buffer. For each wash, beads were incubated at room temperature for 5 minutes, rolling, in the respective wash buffer, centrifuged (190 g, 5 minutes, 4°C), and the supernatent discarded. The soluble bacterial fraction was added to the prepared beads and incubated for 16-18 hours at 4°C to allow binding of any expressed recombinant protein to the beads. Incubated beads were washed 5 times as previously detailed using TRAIP lysis buffer with the following modifications: Wash 1 - 100 mM NaCl, no Imidazole; Wash 2 - 100 mM NaCl, 20 mM imidazole; Wash 3 - 250 mM NaCl, no imidazole; Wash 4 and 5 - 500 mM NaCl, 20 mM imidazole. At wash 4, the beads were resuspended in wash buffer and loaded onto a column (5 ml Polypropylene column, Qiagen). Wash 5 was applied directly to the column. Purified recombinant TRAIP was eluted using 1 ml fractions of TRAIP lysis buffer supplemented with 400 mM imidazole. Imidazole acts as a competitive inhibitor, binding to His-beads with a high affinity. Thus, the addition of imidazole acts to dissociate bound protein from the beads and allow elution.

Purification of His-RFWD3

Plasmids encoding His-RFWD3 was transformed into Bl21(De3) as previously detailed. Recombinant RFWD3 was purified following the protocol detailed in **Purification of WT and**

Mutant His-SUMO-TRAIP, with the following alterations: bacterial cultures were grown using LB broth, and protein expression induced through the addition of 1 mM IPTG at OD_{600}: 0.5-0.6. Induced cultures were incubated at 20°C for 18 hours shaking. Bacterial pellets were resuspended in RFWD3 lysis buffer (Table 2.1), and all wash steps were carried out using unmodified lysis buffer. Recombinant His-RFWD3 was eluted from the beads in 1 ml fractions as follows; elution 1-4 - lysis buffer supplemented with 250 mM imidazole, elution 5-6 - lysis buffer supplemented with 500 mM imidazole.

Purification of His-TRIP12

Plasmid expressing His-TRIP12 C-terminal fragments was transformed into BL21(DE3) competent bacteria. Cultures were grown, and protein expression induced, as detailed in **Purification of WT and Mutant His-SUMO-TRAIP**. However, protein solubility tests determined that the detergent Sarcosyl was required to generate sufficient quantities of soluble protein for purification. Sarcosyl is a strong anionic detergent commonly used to solubilise recombinant proteins. Importantly, unlike the use of similar strength detergents, Sarcosyl does not precipitate at low temperatures nor does it necessarily induce protein denaturation. To solubilise recombinant TRIP12, the bacterial pellet following centrifugation was resuspended in TRIP12 lysis buffer supplemented with 1% Sarcosyl and sonicated (3X, 20-25 W, 30 seconds, on ice). Resuspended cell pellets were centrifuged (31000 g, 30 minutes, 4°C) and the resulting supernatant mixed at a 1:10 ratio in TRIP12 lysis buffer to dilute out the sarcosyl (impairs protien binding to beads at high concentrations). Diluted lysates were added to Ni NTA beads and incubated at room temperature for 150 minutes. Following the binding of recombinant proteins to His-beads, washes were carried out as previously detailed using the following buffer

compositions: Wash 1 - TRIP12 lysis supplemented with 0.3% sarcosyl, Wash 2 - TRIP12 lysis supplemented with 0.2% sarcosyl, Wash 3 - TRIP12 lysis buffer supplemented with 0.1% sarcosyl, Washes 4-5 - unmodified TRIP12 lysis buffer. Purified recombinant His-TRIP12 was eluted in 1 ml fractions as follows: Elution 1-5 - TRIP12 lysis buffer supplemented with 500 mM imidazole, Elution 6-10 - TRIP12 lysis buffer supplemented with 500 mM imidazole and 1% sarcosyl.

Purification of His-USP10

Plasmid encoding His-USP10 N-terminal fragments was transformed into BL21(DE3) competent *E.coli*. Recombinant protein was purified using the sarcosyl protein purification method detailed in **Purification of His-TRIP12**, using USP10 lysis buffer. All wash and elution steps were carried out as detailed.

Purification of His-USP34

Plasmid expressing His-USP34 N-terminal fragments was transformed into BL21(DE3) cells. Recombinant protein was purified using the sarcosyl protein purification method detailed in **Purification of His-TRIP12**, using USP34 lysis buffer. All wash and elution steps were carried out as detailed.

Purification of His-USP37

Plasmid expressing recombinant His-USP37 N-terminal fragments was transformed into BL21(DE3) ultracompetent cells. Large volume cultures (2 l) were prepared as previously detailed using LB media, and protein expression induced through the addition of 1 mM IPTG to the growth media upon reacing an OD_{600}: 0.5-0.6. Recombinant USP37 was then purified

using the methods previously detailed **Purification of WT and Mutant His-SUMO-TRAIP** using USP37 lysis buffer. All wash and elution steps were carried out as detailed.

2.4.6 Purification of USP22

Despite extensive solubility testing, no suitable conditions were identified for the lysis of cells transformed with plasmid encoding recombinant USP22. In all trials, USP22 was found to reside within the insoluble pellet fractions. Furthermore, attempts to solubilise USP22 using denaturing conditions also did not yield sufficient soluble protein to purify.

2.5 Working With *Xenopus laevis*

Our lab uses *Xenopus laevis* egg extracts as an cell free model. Three different types of egg extract are currently used in the field for studying DNA replication: Low Speed Supernatant (LSS), High Speed Supernatant (HSS), and Nucleoplasmic Extract (NPE). However, this PhD project will only use LSS, therefore all protocols described are optimised for the use of this extract.

2.5.1 Preparation of Metaphase II Arrested *X. laevis* Egg Extract

The preparation and use of metaphase II arrested *Xenopus laevis* egg extract has been well documented, and this protocol is adapted from previously published work (See Gillespie et al. (2012b)). High quality eggs are essential for the production of working egg extract. Thus the care of *Xenopus laevis* individuals is crucial; University of Birmingham follows the internationally accepted 'best practice' guidelines as well as the ASPA scientific procedures act

of 1986.

Female *X.laevis* (10 individuals per extract preparation) were primed with 150 units of Folligon (Pregnant Mare Serum Gonadotrophin, Intervet) 2-7 days prior to egg collection to increase the production of stage 6 oocytes (metaphase II). Approximately 17-20 hours prior to egg collection, 500 units of Chorulon (Serum Gonadotrophin, Intervet) was administered to stimulate laying. Following the second injection, individuals were placed into individual laying tanks containing 2.5 l of 1X MMR buffer (Table 2.1). Laying *X. laevis* individuals were kept at 22-23 ℃ overnight. The next morning, eggs were collected into. Any apoptotic eggs, characterised by a white enlarged appearance, were immediately discarded.

Collected eggs were allowed to settle in the beaker, and the laying buffer (1X MMR) poured off. Eggs were washed using fresh 1X MMR, any apoptotic eggs removed, and the wash buffer poured off. Washed eggs were then de-jellied using cysteine solution; added to the eggs and gently rotated. The entire process of de-jellying eggs takes a maximum of 10 minutes, involving typically three cysteine buffer changes. Characteristic signs of de-jellying included reductions in total volume, and egg flattening. De-jellied eggs were washed again as previously described. It is pivotal that any apoptotic eggs are removed throughout, as any remaining will burst and release apoptotic enzymes, inducing apoptosis in the surrounding eggs. Following this, two types of UEB buffer was prepared: UEB supplemented with 2 mM DTT, and UEB supplemented with 2 mM DTT as well as 10 µg/ml APL. UEB + DTT was first added to the eggs whilst the UEB + DTT/APL was aliquoted in 1 ml fractions to 95 mm centrifuge tubes (Beckman Coulter 344060), and Cytochalasin D added (50 µg/ml; Sigma C8273). Eggs were poured into

each of the centrifuge tubes and packed (JS13.1 rotor, 1 minute, 1400 g, 18°C). Excess buffer, and the layer of apoptotic eggs (on top of packed eggs) was removed.

Packed eggs were next crushed through centrifugation (JS13.1 rotor, 16 000 g, 10 minute, 18°C). Crushing functions to separate the eggs into a number of layers, including an insoluble pellet (grey), cytoplasm (yellow/brown), and a lipid layer (bright yellow/white). The cytoplasmic layer was collected using a 20 Gauge needle, piercing the side of the centrifuge tube to avoid disturbing the other fractions. All extracts were kept on ice and supplemented with 10 µg/ml APL, 10 µg/ml Cytochalasin D, and 15% LFB1/50 buffer. Supplemented egg extract was transferred to SW55 ultracentrifuge rotor tubes and spun using an ultracentrifuge (84 000 g, 20 minutes, 4°C) to clarify the egg extract into fractions. The remains of the lipid layer was removed, and the cytoplasmic layer collected. It was essential at this stage that the mitochondrial layer (between cytoplasm and solid pellet) remained undisturbed. The collected egg extract was supplemented with 1% glycerol and flash frozen into single use 20 µl drops by adding the extract dropwise into liquid nitrogen (using cut p200 pippette tips). Extracts were stored in cryovials at -80°C until use.

2.5.2 Preparation of Demembranated *X. laevis* Sperm Nuclei

The preparation of demembranated *Xenopis laevis* sperm nuclei has been described previously (See Gillespie et al. (2012a)). Demembranated sperm nuclei was prepared by all members of the lab using 10-15 *Xenopus laevis* males. In order to increase sperm yield, males were first primed with 150 units of Chorulon (Intervet) between 5-9 days before the experimental protocol. Primed male frogs were euthanised using standard Schedule 1 methods by approved

individuals. Following the confirmation of death, the testes were removed using a sterile scalpel and placed in ice-cold EB buffer. Excised testes were trimmed to remove blood vessels or extra tissue before being washed using approximately 20 ml EB buffer in a standard 9 cm petri dish. Washed testes were transferred to a clean petri-dish containing a small amount of EB buffer and chopped using a razor blade to release the sperm; subsequently filtered using a 25 µM nylon mesh filter .

Filtered material was transferred to 15 ml falcon tubes and centrifuged (2000 g, 5 minutes, 4°C), the supernatant removed, and the pellet spun a second time using the same conditions. Each pellet was examined for erythrocyte contamination (red fractions), and any such fraction removed. Sperm demembranation was achieved by resuspending the pellet in 500 µl SuNaSp per testis, supplemented with 25 µl Lysolecithin, and incubated for 5 minutes at room temperature. Sample demembranation was checked by mixing 1 µl of sperm with equal volumes of Hoechst 33258. The variant of Hoechst used was less membrane permeable, and thus only demembranated sperm contained stained DNA. The remaining demembranated sperm was cetrifuged (2000 g, 5 minutes, 4°C), the supernatent removed, and the pellet resuspended in 500 µl SuNaSp + 3% BSA (per testis) to quench lysolecithin activity. Samples were centrifuged again as previously described and washed in 500 µl EB buffer. Following washing, the pellet was resuspended in 100 µl EB buffer supplemented with 30% glycerol per testis. Demembranated sperm stocks were then diluted to a final concentration of 1000 ng/µl and stored at -80°C. It is assumed that each individual sperm contained a total of 3 pg DNA content. Therefore, by counting the total numbers of demembranated sperm using a haemocytometer, the total concentration of the preparation can be calculated.

2.5.3 Measuring DNA Replication through α^{32}-P-dATP Incorporation

Activated *X. laevis* egg extracts will undergo a single round of synchronous DNA replication upon the addition of sperm DNA. We are able to track DNA replication in the extract through the introduction of radio-labelled nucleotides, readily incorporated into replicating chromatin. To first activate metaphase arrested egg extracts, 40 µl of extract was supplemented with 0.3 mM $CaCl_2$ (stimulates the 'fertilisation Ca^{2+} and promotes interphase entry), 1/40 dilution of ER buffer (Table 2.1), and 250 µg/l of cyclohexamide (inhibits protein synthesis to block cyclin production and cell cycle progression). Activated extract was incubated for 15 minutes, at which point, radiolabelled nucleotides were added (16.5 nM α^{32}-P-dATP; Perkin Elmer) alongside 10-15 ng/µl sperm DNA. The reaction was mixed well and aliquotted into 5 µl fractions. Samples undergoing DNA replication were incubated at 23°C, and the reaction stopped at 30, 45, 60, 75, 90, and 120 minutes. To halt the reaction, and stop DNA replication in the egg extract, 160 µl of Stop-C buffer supplemented with 0.2 mg/ml Proteinase K was added, and the samples incubated at 37°C for a minimum of 30 minutes. Following completion of all timepoints, DNA was precipitated using 4 ml 10 % TCA Buffer (Table 2.1). Controls were prepared for the total radiolabel signal present within each respective sample by spotting 40 µl of sample onto Whatmann filter paper disks. The remaining samples were then filtered through 40 µl glass filters (Fisherbrand 11512083) using a vacuum attached to a manifold (Millipore). Glass filters were washed twice with 8 ml 5% TCA buffer (prepared from 10% stock solution) and then once with 100% EtOH. Each individual glass filter was placed into a scintillation counter tube alongside 0.5 µl Optiscint scintillation cocktail (scintillant Ultima Gold-F; Perkin Elmer 6013179). Filters were prevented from drying out and counted on a standard scintillation counter. The relative amounts of DNA synthesis were then calculated by multiplying the total incorporated

radiolabelled nucleotide (glass filter signal/whattman spot control) by 0.654. The value of 0.654 takes into account the molecular weight of dNTPs (327 Da), assuming equal incorporation of all 4 bases into the genome (Gillespie et al., 2012a).

2.6 Working With Mammalian Cell Lines

To investigate the role of select ubiquitin ligases and deubiquitylating enzymes throughout the cell cycle, with particular focus on DNA replication, we employed the use of several conditional degron cell lines. A summary of all cell lines used is shown in Table 2.6.

2.6.1 Cell Growth Conditions

HCT116 cells were grown in McCoys 5A medium (HyClone), supplemented with 10% Fetal Bovine Serum (Sigma-Aldrich), 2 mM L-Glutamine (Sigma-Aldrich), 100 U/ml Penicillin, and 100 µg/ml Streptomycin. All cells were maintained in 5.0% carbon dioxide within a 37°C incubator. Cells were kept in passage for a maximum of 2 months before being discarded. All cells were passaged as follows; cells were washed once with PBS (ThermoFisher Scientific) and incubated with 1/10 volume Trypsin-EDTA for 3-5 minutes at 37°C. De-adhered cells were resuspended in growth media and counted using a Countess cell counter before being seeded to the desired dish and concentration. A summary of all seeding densities for experimental procedures and media volumes used is shown on Table 2.13. For maintaining culture, cells were seeded at either a 1/5 dilution (passaged 2 days later) or 1/10 dilution (passaged 3 days later).

Table 2.13: **Seeding Densities Mammalian Cell Experiments.** Detailed are the final seeding densities used for each size of tissue culture dish. Typically, the cells were harvested, counted, and diluted to $2X10^5$ cells/ml. This cell suspension was then used to seed cells, using the total volumes shown unless stated otherwise in the respective methods section.

Tissue Culture Plate Size	Seeding Density (total cells plated)	Media Volume (ml)
20 cm	$4X10^6$ Cells	20
10 cm	$2X10^6$ Cells	10
60 mm	$8X10^5$ Cells	4
6-well	$4X10^5$ Cells	2
12-well	$2X10^5$ Cells	1
24-well	$1X10^5$ Cells	0.5
96-well	$2X10^4$ Cells	0.1

2.6.2 Generation of Cell Stocks and Waking up Cells

Two types of cell stocks were used for this PhD project, temporary and long-term. Temporary cell stocks were generated from confluent 96-well plates containing degron clones requiring genotyping. Briefly, cells were harvested and resuspended in 50 µl of growth media. Cell suspensions were transferred to a fresh 96-well plate, where 50 µl of Bambanker direct freezing medium (Nippon Genetics) was added. Cell suspensions were mixed well, the plate sealed with an aluminium seal, and stored at -80°C until use. For making long-term cell stocks, cells were seeded as detailed in Table 2.13 to 20 cm dishes and grown until approximately 80% confluent. Upon reaching the desired confluency, cells were harvested and transferred to 50 ml falcon tubes. The cell suspension was then centrifuged (400 g, 5 minutes, 4°C) and the supernatant removed. The resulting pellet was washed once in PBS, centrifuged as detailed previously, and resuspended in Bambanker Cell Freezing medium (Nippon Genetics, 5 ml per 20 cm plate). Stocks were aliquoted to cryovials in 1 ml fractions; stored at -80°C for 2-7 days

before being transferred to liquid nitrogen for long term storage.

To wake up fresh cells, frozen cell stocks were defrosted rapidly using a 37°C water bath and added to fresh, warm, cell media pre-added to 15 ml falcon tubes (temporary stocks: 1 ml, long-term stocks: 10 ml). The cell suspension was centrifuged (400 g, 3 minutes, 4°C) and the supernatant removed. The resulting cell pellet was resuspended in fresh, pre-warmed, cell media (temporary stocks: 500 µl, long-term stocks: 10 ml) and the entire cell suspension added to the appropriate sized tissue culture dish (temporary stocks: 24-well plates, long-term stocks: 10 cm dishes). Cells were incubated at 37°C for 2-3 days, or until confluent, when they were passaged as described previously.

2.6.3 Generation of Conditional Auxin-Inducible Degron Cell Lines

All conditional degron cell lines generated during this PhD project are shown in Table 2.6. The respective plasmids utilised for the creation of these cell lines are detailed in Table 2.4. Auxin-Inducible Degron cell lines were made with the assistance of the Kanemaki lab (Yesbolatova et al., 2019; Natsume et al., 2016).

For the generation of conditional degrons in HCT116 cells, parental cell lines (CMV-OsTIR1 Only, F74G CMV-OsTIR1 Only, or Tet-OsTIR1 only; Table 2.6) were grown in a standard 10 cm tissue culture dish until approximately 80% confluent. Cells were then harvested and diluted to a final working concentration of $1X10^5$ cells/ml. A total of 2 ml of the working cell suspension was added to each well of a 6-well plate (Day 0). Day 2: transfection mixtures were prepared as follows, per reaction: 4 µl of 200 ng/µl CRISPR plasmid (Table 2.2), 5 µl of 200 ng/µl

Donor plasmid (Table 2.2), 91 µl OPTI-MEM reduced serum media (ThermoFisher)), and 8 µl FUGENE HD transfection reagents (Promega). The transfection mixture was incubated for 15 minutes at room temperature before 80 µl was added to the appropriate well of a 6-well plate dropwise. No-CRISPR controls were also prepared as described, but using TE buffer instead of the CRISPR plasmid. Day 3: transfected cells were harvested and seeded to standard 10 cm tissue culture dishes in the following dilutions (v/v): 1:100, 1:200, 1:400, and 1:800. Day 4: the appropriate selection drug was added to the cells (Hygromycin B Gold; Table 2.3). Once introduced, the selection drug was maintained continuously until colony isolation. Selection media was exchanged every 3-4 days until sufficient colonies were formed, approximately 11-13 days following plating. Once colonies were observed, 48-96 individual clones were picked using a p200 pippette tip and standard benchtop light microscope. Each of the single colonies selected were seeded to individual wells of a 96-well plate, containing 100 µl of pre-warmed growth media, and incubated at 37°C for 3-7 days. Once confluent, the 96-well plate was duplicated; one for genomic DNA extractions and PCR, the other for making temporary cell stocks.

RPE1 parental cell lines (Tet-OsTIR1 Only, Table 2.6) were grown, transfected, and selected for as detailed above with the following protocol modifications. Cells were initially grown on 20 cm tissue culture plates until approximately 70% confluent, and transfected using a Neon Transfection Electroporation system (ThermoFisher). Briefly, sub-confluent cell cultures were harvested and diluted to a final concentration of $1X10^6$ cells/ml. Diluted cell suspensions were centrifuged (1500 g, 1 minute, 4°), the supernatent removed, and the cell pellet resuspended in 40 µl Buffer R per reaction (Neon transfection kit, Thermofisher). The reaction mix was then

aliquoted into individual reactions, and 0.75 µg CRISPR/Donor plasmid DNA added. From this, 10 µl was taken, electroporated (1350 V, 20 ms, 2 pulses, 3 cycles), and added to individual wells of a 6-well plate containing pre-warmed growth media. Antibiotic selection drugs (Table 2.3) were added 2-3 days following transfection and removed 2 days prior to colony isolation.

2.6.4 Confirmation of bi-allelic gene tagging by Genomic PCR

Bi-allelic gene tagging with conditional degron tags was confirmed through genomic DNA extraction and PCR. Cell genotyping was initially carried out using a high-throughput method before being repeated for individual clone confirmation. For high throughput genotyping, cell genomic DNA was extracted directly from confluent cells grown on 96-well tissue culture plates. The cell media was removed and the cells washed twice with PBS. Cells were then lysed, and the genomic DNA extracted, through the addition of 75 µl Direct PCR Working Solution to each well: 0.5x DirectPCR Lysis Reagent (Viagen) diluted in distilled H_2O and supplemented with 20 mg/ml Proteinase K. Cell lysates were incubated overnight at 55°C, rocking. Following the overnight incubation, plates were placed in a humid chamber and incubated for 90 minutes at 85°C to inactivate the Proteinase K. Extracted genomic DNA was stored at -20°C until use. Regions of interest were amplified by standard PCR (See *Polymerase Chain Reaction*) and analysed using either a Shimadzu Microchip Electrophoresis system (Multi-NA), or DNA gel electrophoresis.

Positive clones identified through the high-throughput methods were grown up using consequential plate sizes (24-well, 6-well, 10 cm), and bi-allelic gene tagging confirmed. Cells were grown on 10 cm tissue culture dishes until reaching approximately 70-80% confluency. At

this point, the cells were harvested, washed twice with PBS, and centrifuged (400 g, 5 minutes, 4°C). Genomic DNA was extracted using the GenElute Mammalian Genomic DNA Miniprep Kit (Sigma Aldrich), following manufacturers instruction. Briefly, cells were lysed in a Proteinase K lysis buffer and incubated at 70°C for 10 minutes. DNA was then precipitated using ethanol and added to a silica binding column. Impurities were removed through a number of wash steps before the DNA was eluted. Extracted genomic DNA was amplified by PCR, as detailed previously, and the resulting gel bands visualised using DNA gel electrophoresis.

2.6.5 Colony Forming Assays

Overall cell viability was explored using colony forming assays. Briefly, cells were harvested and serially diluted to $1X10^4$ cells/ml. Cells were then plated using the diluted cell suspension, to individual wells of 6-well plates at the following seeding densities: 250 cells, 500 cells, 750 cells, 1000 cells. The cells were first incubated for 24 hours before any respective drug treatments added (e.g. auxin for protein degradation, Doxycycline for inducible protein expression), and then further incubated until sufficient colonies were observed (7-11 days). Following the incubation period, the cell growth media was removed and cells stained with methylene blue staining buffer. To stain, approximately 1 ml of staining buffer was added to each well of the 6-well plates and incubated at room temperature for 5-10 minutes. The stain was washed off with H_2O and any resulting colonies counted manually. To compare effects on cell viability, the percentage colony forming ability of the cells was then calculated based on the total number of cells plated.

2.6.6 Proliferation Growth Curves

To explore the effects of protein degradation or drug treatments on cell proliferation, growth curves were used. Cells grown to approximately 80% confluency on 10 cm dishes were harvested and diluted to a seeding concentration of 2X10 ^{4} cells/ml. A total of 4 ml of this diluted cell suspension was plated per sample to 60-mm tissue culture dishes. The cells were incubated for 24 hours at 37°C before the appropriate treatment was added. Following treatment cells were grown for 72 hours, with timepoints being taken every 24 hours. Per each timepoint, cells were harvested and the total numbers of cells counted using a Countess cell counter (Thermofisher Scientific). To count, 10 µl of cell suspension was mixed with 10 µl of Tryptan Blue (ThermoFisher Scientific), added to a cell counting slide (ThermoFisher Countess) . The remaining cells harvested were centrifuged (700 g, 3 minutes, 4°C), washed in PBS, and resuspended in 70% ethanol to fix the cells (16 hours, -20°C). Fixed cells were washed twice in PBS and resuspended in FACS staining buffer (50 µg/ml Propidium Iodids, 50 µg/ml RNase A, PBS) for analysis of cell cycle profiles.

2.6.7 Cell Synchronisation

Inducing G1 Cell Cycle Arrest with Lovastatin

To arrest cells in G1 stage of the cell cycle, we selected to use Lovastatin (Acros Organics), a hydroxymethyl glutaryl (HMG)-CoA reductase inhibitor. Cell cycle release from Lovastatin-arrested cells was subsequently achieved through the addition of Mevalonic Acid (Sigma Aldrich). Cells were seeded for the respective experiment at the concentrations detailed in Table 2.13, and incubated at 37°C for 24 hours. To induce G1 cell cycle arrest, Lovastatin was added dropwise to the cell media to a final working concentration of 20 µM and mixed through

gentle rocking. Approximately 24 hours after treatment, cells were arrested in G1 and became visually rounded. To release cells from the cell cycle arrest, the cell media was removed and the cells washed 3 times with pre-warmed growth media. The appropriate amount of fresh growth media (See 2.13), supplemented with 2 mM Mevalonic acid was then added to cells and the tissue culture dishes returned to the 37°C incubator. Approximate timings associated with G1 cell cycle release are as follows (shown Figure 2.3): 12-13 hours post release - early to mid S phase; 15-16 hours post release - mid to late S phase; 20 hours post release - G2/M; 24 hours post release - G1 stage.

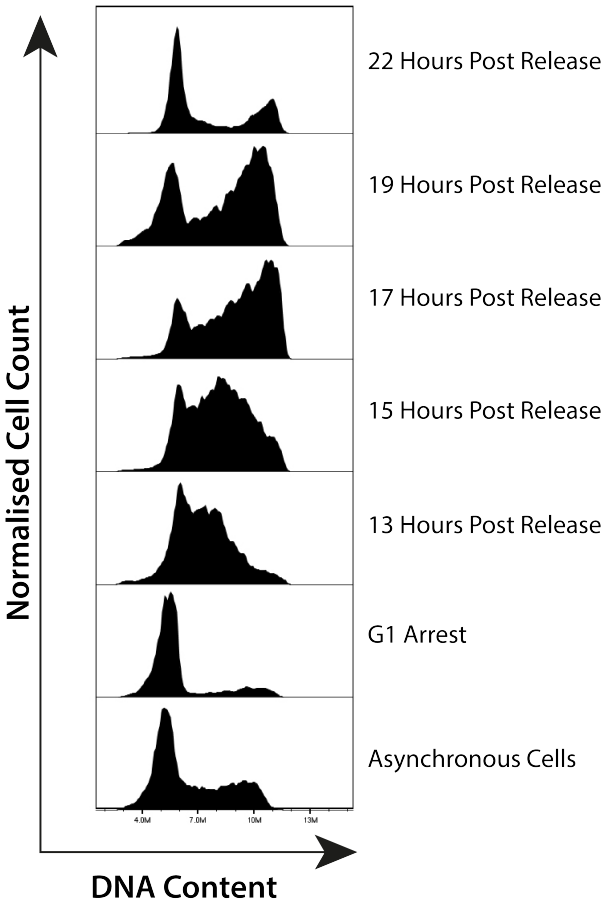


Figure 2.3: **Lovastatin Mediated G1 Arrest and Release.** Cells were plated onto 60-mm dishes as detailed in Table 2.13. Approximately 24 hours after plating, 20 µM Lovastatin (final working concentration) was added and the cells incubated for 24 hours at 37 °C (G1 arrest). Cells were washed three times in warm media and resuspended in media supplemented with 2 mM Mevalonic Acid to release from cell cycle arrest. Timepoints were taken at 13, 15, 17, 19, and 22 hours post-release to track progress through the cell cycle.

Inducing G2 Cell Cycle Arrest with RO-3306

To arrest cells in G2 stage of the cell cycle, we used the potent CDK1 inhibitor RO-3306 (Merck Life Sciences). Cells were seeded for the respective experiment at the concentrations detailed in Table 2.13, and incubated at 37°C for 24 hours. RO-3306 was added to cells at a final working concentration of 9 µM. Cells treated with RO-3306 were arrested in G2 approximately 16 hours post treatment. To release cells from the G2 arrest, the cell media was removed, and the cells washed 3 times with pre-warmed growth media. Fresh media without RO-3306 (for amounts see Table 2.13), and the tissue culture dishes incubated at 37°C. Released cells enter mitosis approximately 30-60 minutes post release (Figure 2.4).

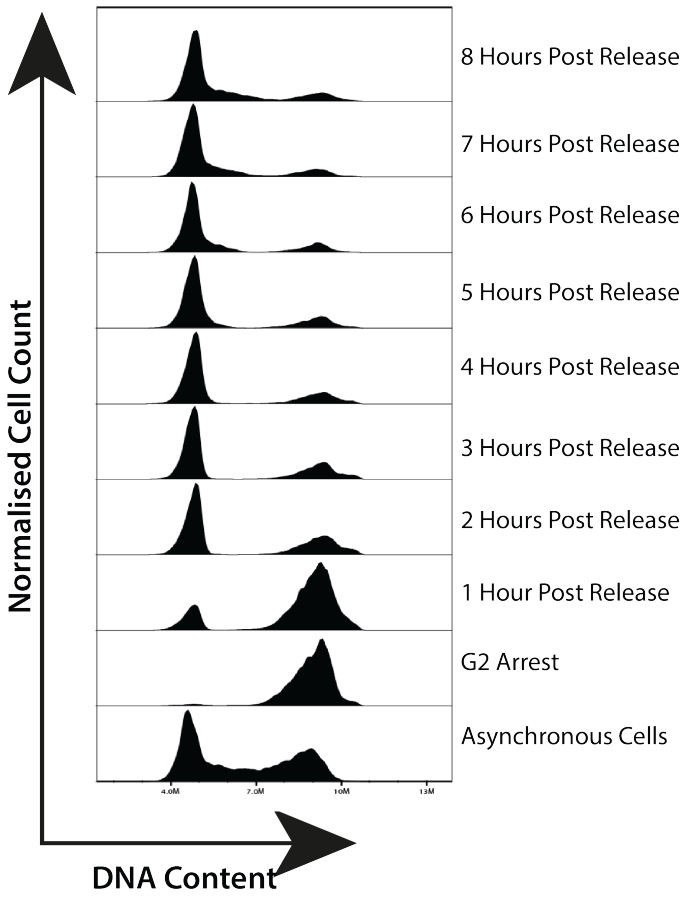


Figure 2.4: **RO-3306 Mediated G2 Arrest and Release.** Cells were plated onto 60-mm dishes as detailed in Table 2.13. Approximately 24 hours after plating, 9 µM RO-3306 (final working concentration) was added and the cells incubated for 16 hours at 37 °C (G2 arrest). Cells were washed three times in media and fresh, pre-warmed media added to the dish. Timepoints were taken between 1 and 8 hours post release to track progress through the cell cycle

.

Sequential G1 and G2 Cell Cycle Arrest

The two previously detailed methods for cell cycle arrest were also combined to induce a controlled, step-wise, progression of cells through the cell cycle. Cells were first arrested in G1 using Lovastatin, and released from the G1 arrest as detailed previously. Approximately 7-8 hours after release from the G1 arrest, RO-3306 was added at a final working concentration of 9 µM for 16 hours. The treated cells were then arrested in G2 stage of the cell cycle upon

completion of S-phase. To allow the G2 arrested cells to progress into mitosis, cells were released as detailed previously.

2.6.8 Preparation of Whole Cell Extracts

Whole cell extracts from mammalian cells were prepared with the purposes of using SDS-PAGE and immunoblotting to investigate specific protein levels within the cells (e.g. protein depletion after AID-mediated degradation). The cell media was collected as mitotic cells de-adhere from the cell dish during division and so were likely present in this fraction. The remaining adhered cells were washed twice with PBS (also collected), and harvested as previously detailed. All collected fractions were pooled and centrifuged (750 g, 5 minutes, 4°C). The resulting supernatent was removed and the cell pellet resuspended in equal volumes of UTB buffer (Table 2.1). UTB buffer is denaturing due to high urea concentrations and so will likely destroy all enzymatic activity within the lysate; as well as enabling the resuspension of both soluble and insoluble protein fractions. Cells incubated in UTB buffer for 10 minutes followed by sonication (Diaganode Bioruptor, 5 minutes, high power, 30 second cycles). Sonicated samples were centrifuged (10 800 g, 20 minutes, 4°C) and the supernatent, containing extracted proteins, transferred to a fresh Eppendorf tube. From this, 2 µl was taken for determining protein concentration (Bradford's Assay), whilst the remaining sample was mixed with 4X loading buffer to a final concentration of 1X and boiled for 5 minutes at 95°C. Between 30-50 µg of total protein was used per SDS-PAGE gel.

2.6.9 BrdU Incorporation Assays

Global DNA replication levels were tracked through the incorporation of the thymidine analogue BrdU into replicating chromatin. Cells were plated onto 60 mm dishes as detailed in Table 2.13, and incubated at 37°for at least 24 hours; optionally treated with varying inhibitors or auxin to induce protein degradation, dependent on the respective experimental requirements. To track replication levels, a working concentration of 10 µM of BrdU was added to the cell media for 30-60 minutes. Cells were then harvested and washed twice in PBS. Harvested cells were fixed through resuspension in ice-cold, 70% EtOH for a minimum of 16 hours at - 20°C. Fixed cells were washed twice in PBS supplemented with 0.1% Tween-20. Each wash consisted of resuspending the cell pellet in 500 µl of the wash buffer followed by centrifugation (700 g, 3 minutes, 4°C) and supernatant removal. Prior to staining, cells were resuspended in 2 M HCl supplemented with 100 µg/ml Pepsin to denature DNA and enable antibody access to incorporated nucleotides. Next, cells were washed twice in PBST and resuspended in primary antibody (Table 2.5 in 5% BSA, 0.1% Tween-20, PBS) for 1 hour at room temperature. Cells were washed once more and resuspended in fluorescently labelled secondary antibody (Table 2.5 in 5% BSA, 0.1% Tween-20, PBS) for 1 hour at room temperature, in the dark. Stained cells were then washed, resuspended in FACS staining buffer, and incubated at 37°C until analysis. All BrdU assays were analysed using Flow Cytometry.

2.6.10 Click-IT to Measure Global Replication and Transcription

Click iT assays were used to track global DNA Replication (through the thymidine analogue EdU - Click-iT EdU Cell Proliferation kit Alexa Fluor 647, Invitrogen) or transcription (through the Uridine analogue EU - Click-iT RNA Alexa Fluor 488). The Click-iT reaction utilises a

copper-catalysed reaction to conjugate an alkyne (the respective analogue) with azide (the fluorophore). Cells were grown on 6-well plates containing sterilised 22 mm X 22 mm microscopy cover slips as detailed in Table 2.13, and treated with IAA to induce protein degradation as required. Exactly 1 hour prior to cell collection, the respective analogue was added into cells to be incorporated (10 mM EdU or 1 mM EU). Following incubation with the alkyl analogue, the growth media was removed and cells fixed using 1 ml 4% PFA in PBS per well (10 minutes, room temperature). After fixation, cells were permeabilised with 1 ml 0.5% Triton-X in PBS per well (5 minutes, room temperature), and washed 2X in fresh PBS. To detect the respective analogue incorporated, cells were treated with 500 µl of Click-IT reaction buffer (Invitrogen) at room temperature for 30 minutes. Finally, cover slips were mounted onto microscope slides using DAPI mounting media (Fluoroshield) and analysed using immunofluorescence.

2.6.11 Proximity Ligation Assay

Proximity ligation assays (PLA) were used to detect interactions between two different components on chromatin; in this case, between nascent DNA and elongating RNA Polymerase II. To detect interactions, each component is targetted by antibodies with conjugated complimentary oligonucleotides. If two oligonucleotides are close enough spatially, they are then amplified by DNA polymerase in a rolling circle assay. Finally, detection oligonucleotides, fused to fluorophores, are able to recognise the products of this rolling circle assay and produce a detectable signal. For this assay, we used the DuoLink PLA Kit, including Duolink anti-rabbit Plus and Duolink anti-mouse Minus probes. The assay was modified from manufacturer instruction for use in 1.5 ml eppendorf tubes.

For the PLA reaction, cells were plated as per Table 2.13 to 60-mm tissue culture dishes, and treated with the required drugs. Exactly 20 minutes before cells were to be collected, 10 mM EdU was added to label nascent DNA. Following this incubation the cells were harvested, and extracted with CSK buffer (See *2.6.12*). Permeabilised cells were treated to label incorporated EdU using the Click-iT reaction detailed previously (volumes were scaled down, and cell pellets resuspended in 50 µl of reaction buffer). The cells were then washed 2X in Washing buffer and the resulting pellet resuspended in 50 µl of primary antibody solution (1:250 anti-mouse Serine 5 CTD, 1:500 anti-rabbit Biotin) overnight at 4°C. After primary antibody staining, cells were washed 3X in PLA Wash Buffer A (DuoLink) and in 30 µl of PLA probe-conjugated secondary antibodies (per reaction: 6 µl '+', 6 µl '-', 18 µl 3% FBS). Cells were incubated in this solution for 100 minutes at 37°C. Next, cells were washed 3X in PLA wash buffer A, resuspended in 30 µl Ligation Buffer (per sample: 6 µl 5X ligation buffer, 0.75 µl DNA ligase, 23.25 µl distilled H_2O), and incubated for 60 minutes at 37°C. Cells were subsequently washed again 3X using PLA wash buffer A, and any ligated PLA probes amplified using a rolling circle assay. For amplification, the cell pellet was resuspended in 30 µl amplification buffer (6 µl 5X amplification buffer, 0.75 µl DNA Polymerase, 23.25 µl H_2O) for 100 minutes at 37°C. Finally, cells were washed 2X in Wash Buffer B (DuoLink), resuspended in 0.01X Wash Buffer B (diluted in H_2O). Finally, diluted cell suspensions were pippetted onto pre-sterilised 20 mm glass coverslips and centrifuged (400 g, 5 mins). Once adhered, cover slips were mounted using DuoLink DAPI Mounting Media.

2.6.12 CSK Extraction of Soluble Cellular Fractions

The isolation of cellular chromatin fractions, and any associated proteins, was primarily analysed using Flow Cytometry or Immunofluorescence. This method has previously been well described (Forment and Jackson, 2015), but has been modified for the specific requirements of this PhD project. Briefly, cells were harvested upon reaching approximately 60-80% confluency; treated as per the requirements of the respective experiment, washed 2X in ice cold PBS in pre-cooled 1.5 ml eppendorf tubes, and the supernatant removed. Cell pellets were resuspended in 400 µl of ice cold CSK buffer (Table 2.1), incubated on ice for 5 minutes to extract all soluble proteins. Following extraction, 800 µl of 1 mg/ml BSA in PBS was added to the suspension and nuclei pelleted by centrifugation (800 g, 3 minutes, 4 °C). The inclusion of BSA acted to limit cell loss through preventing cell adherence to the Eppendorf tube. Nuclei were next resuspended in 200 µl 4% Paraformaldehyde in PBA and incubated at room temperature for 10 minutes. Fixed, extracted, nuclei were washed once in Washing Buffer (Table 2.1), resuspended in FACS staining buffer (either 50 µg/ml Propidium Iodide, 50 µg/ml RNase A in PBS or 5 µg/ml Hoechst in PBS), and kept at 4°C until immunostaining. Due to the un-adherent nature of HCT116 cell lines after CSK-extraction, for immunofluorescence, cell extractions were carried out as detailed and the cells then spun onto 22 mm X 22 mm glass microscopy slides. For this, instead of resuspending the fixed nuclei pellet in storage buffer, they were instead resuspended in 50 µl of PBS, and added on top of microscope slides placed into wells of a 6-well plate. The plates were then centrifuged (400 g, 5 minutes) to spin cells onto the microscopy slides and stored in PBS, at 4°C, until immunostaining.

2.6.13 GFP-TRAP

To detect mCLOVER tagged proteins a GFP-TRAP assay to pull down TRAIP-mAC or mAC-LRR1 from cells. Cells were plated as detailed in Table 2.13 and treated as per the respective experimental requirements. Two 20-cm plates were prepared per condition. Upon reaching the desired timepoint, cells were harvested, pooled, and washed 2X in PBS. Chromatin was isolated from harvested cells using CSK buffer, as detailed in *2.6.12*. Extracted nuclei were then resuspended in 300 µl GFP-TRAP lysis buffer (Table 2.1). Lysates were incubated on ice for 30 minutes, before being sonicated (BioRuptor, 5 minutes, High, 30 second cycles). The resulting lysate was centrifuged (16 900 g, 10 minutes, 4°C). The supernatent, containing soluble proteins, was moved to a fresh eppendorf and supplemented with 200 µl dilution buffer. During the spin, beads were prepared. GFP-TRAP beads (50 µl per sapmle, Chromotek) were added to 500 µl dilution buffer and washed 2X using the same volumes of fresh dilution buffer. To wash, ependorf tubes containing the beads were vortexed, placed on a magnetic rack, and the supernatant carefully removed. The diluted cell lysates (500 µl) were then added to the washed beads and incubated for 1 hour at 4°C to allow binding of GFP-tagged proteins to beads. Following bead-binding, the beads were washed 2X in GFP-TRAP washing buffer; during the second wash step, the salt concentration was increased to 500 mM. Finally, beads were resuspended in 2X SDS-PAGE sample buffer. Any bead-bound proteins were released into the sample buffer through sample boiling (5 minutes, 95°C), and the beads removed through magnetic separation as detailed previously. Samples were run on SDS-PAGE gels for immunoblotting alongside input control samples (taken prior to adding the lysate to the beads).

2.6.14 Immunostaining

Protein immunostaining was used to detect specific targets of interest using either Flow Cytometry or Immunofluorescence. Both CSK-extracted, and unextracted cells were stained using the methods detailed. Un-extracted cells were first permeabilised through the addition of 1 ml Permeabilisation buffer (0.5% Triton X-100 in PBS) to each well of the 6-well plate, incubated at room temperature for 5 minutes. Cells were then washed twice in washing buffer. For FACS experiments, washes were carried out as follows: cells pellets were resuspended 500 µl of buffer, centrifuged (400 g, 3 minutes, 4°C), and the supernatant removed. For immunofluorescence experiments, 1 ml of wash buffer was added to each well of the 6-well plates and incubated for 5 minutes at room temperature, rocking, before the wash buffer was removed. Following washing, the primary antibody (Table 2.5 in 5% BSA, 0.1% Tween 20, PBS) was added to the cells for 1 hour at room temperature (FACS: cell pellet resuspended in 100 µl antibody dilution. Immunofluorescence: 100 µl antibody dilution pipetted dropwise directly onto cover slips). Cells were then washed again 2X in washing buffer, and the appropriate fluorescently labelled secondary antibody added. All secondary antibody staining was carried out in the dark; FACS samples were incubated for 1 hour, whilst immunofluorescence samples were incubated for 2 hours. Following antibody staining, cells were again washed 2X in washing buffer. FACS cells were then resuspended in either 500 µl 50 µg/ml Propidium Iodide, 50 µg/ml RNase A in PBS, or PBS supplemented with 5 µg/µl Hoechst 33582, dependent on the experimental requirements and analysed immediately. Cells on cover slips were mounted onto microscope slides using DAPI mounting media (Fluoroshield with DAPI; abcam), and stored at 4°C until use.

2.6.15 Immunofluorescence

For immunofluorescence experiments using un-extracted cells, cover slips were first sterilised (submersion in ethanol) and placed into wells of 6-well plates. Cells were then plated directly onto the cover slips. All microscopy throughout this PhD project was carried out on a Leica DM6000 wide-field fluorescent microscope, using 40X and 60X objectives with 1 - 1.6X magnification. Control samples were used to set the channel settings, which were then kept constant throughout the imaging process. A total of 7-10 images were taken per sample, aiming to collect data from approximately 500-1000 cells for each experimental condition. Data was exported as raw TIF files. Image analysis was either conducted manually, using ImageJ (FIJI) (Schindelin et al., 2012), or in an automated fashion using CellProfiler (Carpenter et al., 2006; Kamentsky et al., 2011; McQuin et al., 2018). For ImageJ analysis, any data adjustments (e.g. colour levels) were carried out on control image sets, applied to the entire data set for counting. For Cell Profiler, pipelines were established to first isolate the nuclei and then the appropriate measurement taken within this region; again kept constant over all image sets within each experimental repeat.

2.6.16 Flow Cytometry

All Flow Cytometry was conducted using a Beckman CytoFlex instrument. A summary of the primary gating strategy applied for all analyses is shown in Figure 2.5. Additional gates applied for specific quantifications are then detailed in the appropriate results figures. Briefly, the primary population of cells was isolated by plotting the forward scatter area (FSC-A; marker of overall cell size) vs side scatter area (SSC-A; marker of cell granularity). Within this cell population, any doublets were excluded using FSC-A vs FSC-height (FSC-h). Cells were assigned

to cell cycle stages using the appropriate emmissions channel associated with the DNA stain used (Hoechst and Vybrant Violet: PB-450, Propidium Iodide: Cy5.5). As a standard in all analyses, cells were defined into individual stages of the cell cycle (G1: 2 N DNA content, G2/M: 4 N DNA content, S-phase: 2N < DNA Content > 4N). Cells lying outside this range were also captured. Cells with lower than 2N DNA content are often undergoing cell death mechanisms. Containing over 4N DNA content is a typical marker of DNA re-replication (over-replication). All the described gating was carried out using untreated control cells, and the established gates then applied to all treated samples. A minimum of 10,000 cells were measured within the overall cell cycle gate applied for quantification and subsequent statistical analyses, ensuring a flow rate of approximately 500-1000 cells / second. All data was exported as .FCS files and analysed using FlowJo (Version 10). Quantitative data from this analysis was exported into R Studio for statistical analysis and plot preparation.

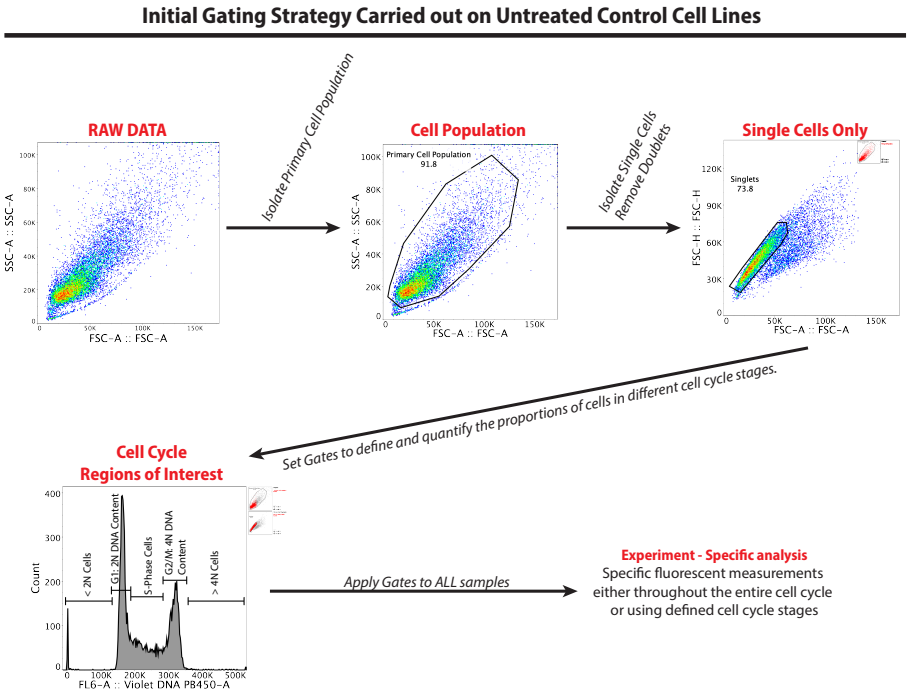


Figure 2.5: **Example FACS Gating Strategy.** Summarised is the standardised gating strategy applied to all FACS samples before experiment-specific measurements. Untreated controls were first gated to isolate the primary cell population (FSC-A vs SSC-A). Single cells (Singlets) were then isolated within this population (FSC-A vs FSC-H). Finally, cells were assigned to specific cell cycle stages using the overall DNA content. The established gates were then applied universally to all samples within the respective experiment; to ensure standardisation of quantification.

2.6.17 Cell Senescence Assay

Cellular senescence was detected using a cleavable fluorescent substrate of β-galactosidase (Cell Meter Cellular Senescence Activity Assay Kit, AAT Bioquest). β- gal is a glycoside hydrolase that is overexpressed in senescent cells. Briefly, cells were plated for proliferation growth curves as detailed in *2.6.11.* At each respective timepoint, cells were harvested and washed with PBS. The resulting cell pellet was resuspended in 100 µl Xite β-D-galactopyranoside solution (AAT Bioquest) and incubated for 45 minutes at 37°C. Following the incubation, cells were washed with Washing buffer and resuspended in 500 µl Assay Buffer (AAT Bioquest). Stained cells were analysed using a Flow Cytometer, utilising the FITC channel to detect β-gal activity.

2.6.18 Annexin V Apoptosis Assay

The presence of apoptotic cells was explored using Annexin V staining, as per manufacturers instruction (eBioscience Annexin V Apoptosis Detection Kit FITC, Invitrogen). Annexin V is a phospholipid binding protein that is shuttled to the exterior of plasma membranes upon the induction of apoptosis for macrophage recognition. Cells were grown on a 60 mm dish for proliferation growth curves, as detailed in *2.6.11.* At each respective timepoint cells were harvested and washed once in PBS, followed by once in 1X Binding Buffer (10X stock diluted in H_2O ThermoFisher Scientific). The cell pellet was then resuspended in 100 µl 1X binding buffer supplemented with 5 µl of fluorochrome coated (Alexa Fluor 488) Annexin V. Samples were incubated for 15 minutes at room temperature in the dark before being washed in 1X binding buffer. Stained cells were resuspended in 200 µl 1X binding buffer supplemented with 50 µg/ml of Propidium Iodide DNA stain (Thermofisher Scientific). Cells were analysed immediately using flow cytometry, using the FITC channel to detect Annexin V.

2.6.19 ChIP-Sequencing

Chromatin immunoprecipitation was used to gain potential insights into the mechanisms of TRAIP. For this project, the ChIP-Seq was carried out using H2AX and γH2AX antibodies, detailed in Table 2.5. ChIP-sequencing protocols were carried out with the assistance of Dr. Marco Saponaro's group.

Sample Preparation

Cells were grown on 20 cm dishes (2X per condition), as per Table 2.13, and harvested at approximately 80% confluency. For this experiment in particular, S-phase cells were obtained

through the use of Lovastatin to arrest cells in G1 stage of the cell cycle. The entirety of the sample preparation was carried out on ice, unless stated otherwise. Cells were harvested as detailed previously and the resulting cell suspension transferred to a 50 ml falcon tube. Formaldehyde, at a working concentration of 1%, was added to the cell suspension to fix and cross-link the cells (10 minutes, room temperature, rotating; subsequently followed by formaldehyde quenching through supplementing the cell suspension with 125 mM Glycine. Fixed cells were centrifuged (400 g, 3 minutes, 4°C), the supernatant removed, and the cell pellet washed twice with ice cold PBS. The resulting cell pellet was then resuspended in 2 ml of ChIP cell lysis buffer (Table 2.1) for 15 minutes. ChIP cell lysis buffer is a hypotonic buffer that burst cell membranes, but left nuclei intact. Nuclei were pelleted by centrifugation (3500 g, 5 minutes, 4°C), and the pellet resuspended in 1.5 ml ChIP nuclear lysis buffer for 10-30 minutes. The nuclear lysis buffer contained high detergent concentrations required to burst the nuclear membrane. Cell lysates could be stored at -80 °C here. Each nuclear lysate was then divided into 200 µl aliquots and sonicated to shear DNA (30 amplitude, 15 seconds on/25 seconds off, 6-16 cycles). Control samples taken throughout and checked for optimal DNA fragments (300-500 bp). The sonicated chromatin was then cleared by centrifugation (20 000 g, 10 minutes, 4°), and the supernatent collected. Sheared chromatin could be stored here at -80°C until use.

Protein A Dynabeads (ThermoFisher) were prepared as follows: 15 µl of Protein A Dynabeads were washed twice, through magnetic separation, using 500 µl of 5% BSA in PBS. Washed beads were resuspended in 200 µl of 5% BSA in PBS and supplemented with approximately 1 µg of the appropriate antibody (anti-rabbit S139 γH2AX 29839 and anti-rabbit H2AX); incubated

for 1 hour at 4°C. To immunoprecipitate targets of interest, alongside any cross-linked sections of chromatin, 150 µl of sonicated cell lysis was first diluted 1:5 in ChIP dilution buffer before being added to Protein A Dynabeads pre-conjugated to antibodies against the protein of interest. The IP samples were incubated overnight at 4°C, rotating. Following the overnight incubation, the beads were washed 2X with each of the following buffers, using magnetic separation as desribed previously: ChIP Low Salt, ChIP High Salt, ChIP LiCl, TE (Table 2.1). Washed beads were centrifuged (3 minutes, 1700 g), and the supernatant removed. Beads were resuspended in 40 µl elution buffer and incubated at 65°C for 10 minutes to reverse the crosslinking and free bound components from the beads. Finally the sample was centrifuged (12 500 g, 1 minute) and the supernatant collected. Samples were supplemented with 1 µg RNAse A and incubated for 1 hour at 40-50°C; immediately followed by the addition of 20 µg/ml Proteinase K, incubated for 2 hours at 55°. DNA was then purified using a similar silica-based column approach as described previously (qiagen PCR MiniElute kit), per manufacturers instruction.

Quantitative PCR

Quantitative PCR was used to validate the ChIP prior to sequencing. Purified DNA (10 µl) was taken per sample and diluted in nuclease free H_2O to give a final volume of 50 µl. This DNA was then used for preparation of the reaction. For the qPCR, the reaction mix was prepared using: 10 µl SYBR Green Master Mix (Meridian Bioscience), 7.6 µl nuclease free H_2O, 2 µL DNA, and 0.4 µl of each 10 µM forward and reverse primers (Table 2.4). Thermocycling was carried out as follows: Denaturation (95°C, 3 minutes), PCR amplification (95°C, 10 seconds; 58°C, 40 seconds; 44 cycles), Melting Curve (95°C, 10 seconds; 60°C, 5 seconds; temperature then increased to

95°C, taking measurements every 1 second).

Library Preparation and Sequencing

Library preparation was carried out by members of Dr. Marco Saponaro's group using the NEBNext® Ultra™ II DNA Library Prep Kit (NewEngland Biolabs) for Illumina NEB, as per manufacturers instruction. Prepared libraries were then sequenced using single-end sequencing with a High-75 kit (Illumina) using an Illumina NextSeq instrument.

2.6.20 Mycoplasma Testing

Mycoplasma infections are a major hindrance in mammalian tissue culture as they are antibiotic resistant and extremely difficult to detect under standard light microscopes. Moreover, mycoplasma contamination may result in chromosomal aberrations, potentially extremely problematic when studying DNA replication. All cell lines were tested for mycoplasma contamination using the EZ-PCR Mycoplasma detection kit (Biological Industries). Briefly, resuspended cell cultures were pelleted by centrifugation (3 minutes, 250 g, 4°C), and the supernatant moved to a fresh Eppendorf; subsequently centrifuged a second time (15 000 g, 10 minutes, 4°C) to pellet any contaminating mycoplasma. The resulting supernatant was discarded and any remaining pellet resuspended in the provided buffer solution. Samples were boiled at 95°C for 3 minutes, and PCR conducted as per manufacturers specifications to detect mycoplasma-specific DNA sequences. In addition, internal controls were included to confirm DNA amplification. Resulting PCR products were run on 2% agarose gels (Figure 2.6).

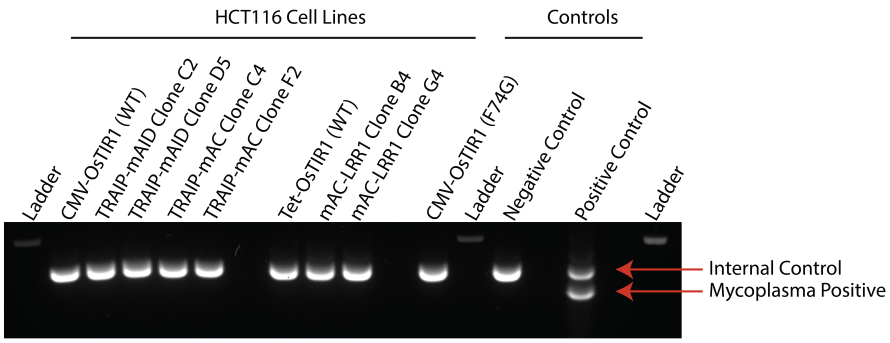


Figure 2.6: **Example Mycoplasma Testing DNA Gel** Cell lines were tested for mycoplasma using the EZ-PCR Mycoplasma detection kit, as per manufacturers instruction (detailed in *2.5.18*. Resulting PCR products were run on an 2% agarose gel alongside negative and positive controls).

2.7 Data Analysis

All data collected throughout this PhD project were analysed and processed as detailed. All figures were prepared using Adobe Photoshop and Adobe Illustrator. Numerical data were saved as csv files and imported into RStudio for data extraction, plot generation, and statistical analysis. All statistical analysis was conducted between experiments, using data collected from three independent experimental repeats unless stated otherwise. For statistical analysis, data normality was first assessed, to direct further statistical analysis, using Q-Q plots (Figure 2.7) and the Shapiro Wilks Test. Following this, the appropriate hypothesis testing was then conducted to determine any statistical differences existing between data sets. Statistical significance was displayed on the plots using the following - *: $p < 0.05$; **: $p < 0.01$; ***: $p < 0.001$. ChIP-sequencing analysis was carried out by Dr. M. Saponaro.

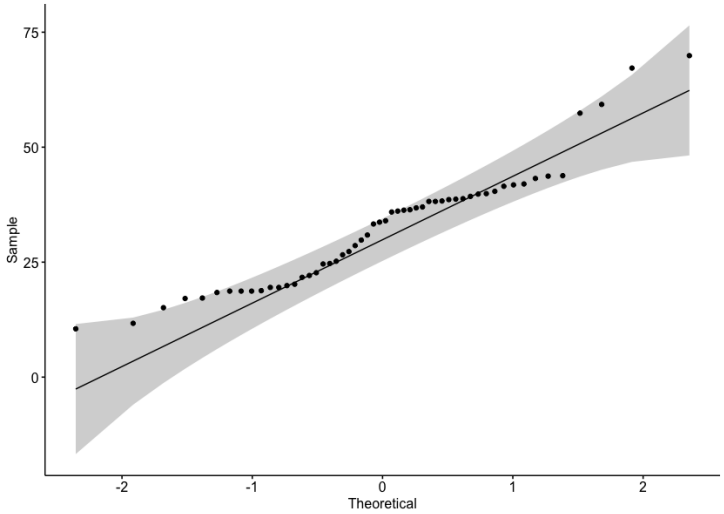


Figure 2.7: **Example Q-Q Plot.** Shown is an example Q-Q plot for assessing data normality. Probability distributions were generated based on the respective interquartile ranges. Reference lines were also added to the plot, with 95 % confidence intervals (grey). Each respective data set were compared to the reference. If the majority of data points resided within the confidence intervals, the data was considered normally distributed and parametric analysis was used. Conversely, if not, non-parametric analysis was used.

Chapter 3

Raising Antibodies Against Recombinant Proteins of Interest

3.1 Introduction

Over the last decade, several papers published by the Gambus group and others provided significant mechanistic insight into the process of eukaryotic replisome disassembly. Altogether, these studies further highlighted the essential role of protein ubiquitylation during DNA replication, particularly in driving replisome disassembly. However, whilst the core mechanisms of replication termination have become apparent, there is still much to be discovered about its regulation. To gain further insight, the Gambus group carried out several experiments investigating the consequences of non-functioning replisome disassembly pathway, and identified several novel E3 ubiquitin ligases or deubiquitylating enzymes to interact with the replisome. The initial work of my PhD project aimed to utilise *X. laevis* egg extracts to understand any roles of the selected candidates during DNA replication or DNA

damage repair.

3.2 Results

The candidate pool generated for this PhD project was made up of E3 ubiquitin ligases and deubiquitylating enzymes (TRAIP, RFWD3, TRIP12, USP10, USP22, USP34, and USP37). Importantly, at the start of this PhD project, none of the candidate proteins had been previously implicated in replisome disassembly, and little was known about their roles during DNA replication. The initial objective of this PhD project was to screen each of the candidate proteins for interactions with either the active or terminating replisome. For this, the use of *Xenopus laevis* egg extract offered several advantages when compared to alternative model systems. Notably, the highly synchronised nature of the egg extract negated requirements for drug-induced cell cycle synchronisation. In addition, its cell free nature allowed for relatively simplistic biochemical manipulation. However, highly specific and tightly binding antibodies were required. Without such, several experiments essential for the functional analysis of selected candidate proteins (e.g. protein immunodepletion and immunoprecipitation) would not be possible. Due to the novel nature of the generated candidate pool, no adequate antibodies were commercially available. Therefore, we first set out to raise antibodies against proteins of interest. Each of the candidate proteins were expressed and purified using bacterial expression systems, and a one-step purification protocol. Figure 3.1 summarises the work conducted, and key steps will be expanded upon throughout this chapter.

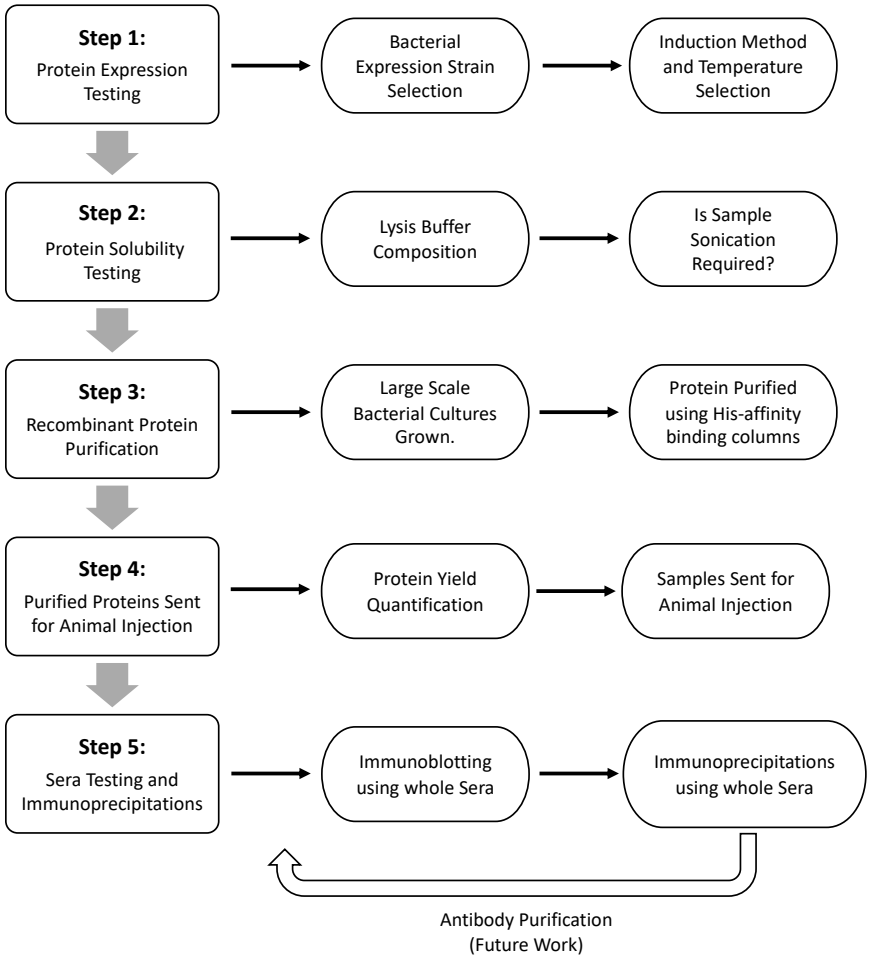


Figure 3.1: **Protein Purification Workflow.** The schematic used to first optimise, and then purify recombinant proteins of interest with the purpose of raising antibodies. First, protein expression testing aimed to determine the optimal bacterial strain, induction method, and temperature for protein expression and folding. Solubility testing then assessed the relative solubility of expressed recombinant protein to determine the optimal lysis buffer composition. Following these steps, each candidate was purified using a one-step approach through binding of His-tagged peptides to Nickel beads. The resulting yields of eluted recombinant protein was quantified, and sufficient amounts sent for injection to raise antibodies. The ability of raised sera to recognise the its target in *X. laevis* egg extract was then characterised briefly through immunoblotting.

3.2.1 Protein Expression Testing

Bacterial expression plasmids, encoding either whole or partial candidate protein sequences, were created prior to the start of this PhD project (See Table 2.2 and Appendix A1). TRAIP and USP22 were cloned as whole protein sequences, whilst the larger RFWD3, TRIP12, USP10,

USP34, and USP37 were prepared as partial peptide sequences. For each plasmid, the respective protein of interest was tagged with a poly-histidine tag (or variant thereof) and cloned into pET28 backbones. The pET28 plasmid backbone contained promoter sites for the bacteriophage T7 polymerase, allowing for recombinant protein expression, flanked by diverging lac repressors to control induction timing.

Protein expression testing was carried out to determine the optimal conditions, resulting in the largest yield of expressed recombinant protein. For this, multiple induction methods and bacterial strains were trialled. Plasmids were transformed into two bacterial expression strains: BL21(DE3) pLys and ROSSETTA BL21(DE3) pLys. Whilst both strains contained the T7 polymerase required to express recombinant proteins, under the control of a lac repressor. ROSSETTA BL21(DE3) pLys additionally contained codons not found in prokaryotic organisms to enhance the transcription and translation of exogenous proteins. In transformed, un-induced, bacterial cultures, the lac repressors prevented both transcription of the T7 polymerase from the bacterial genome and binding of the polymerase to the plasmid promoter. Expression of recombinant protein was induced in the cells through removal of the inhibitory lac repressor. Two different methods of induction were tested: addition of IPTG (allolactose mimic) directly to cells cultured in LB broth, or through an automated method involving a bacterial metabolic switch to digest lactose within the AIM media.

All proteins underwent the same expression testing to determine the optimal growth conditions. For the majority of the candidates, suitable conditions were identified during the expression testing described. The anomaly was TRAIP, which was found to be expressed in all

the conditions tested, but the resulting yields were either too low, or the protein remained insoluble. To resolve this the TRAIP sequence was cloned into a different plasmid backbone, containing a His-SUMO protein tag. Transformed bacterial strains were cultured until reaching approximately mid-log phase growth, where protein expression was induced. Figure 3.2 shows an example Coomassie stained SDS-PAGE gel following a protein expression trial. In the given example USP10, USP22, USP34, USP37, and TRIP12 plasmids were transformed into Bl21(DE3) pLys cells, cultured in LB media, and protein expression induced through IPTG addition. Each sample was run alongside a reference un-induced control. Bands of the appropriate size were observed for TRIP12, USP37, USP34, and USP22. No clear expression was found when exploring the yields of USP10. The final conditions selected for each candidate, following protein expression testing, is shown in Table 2.1.

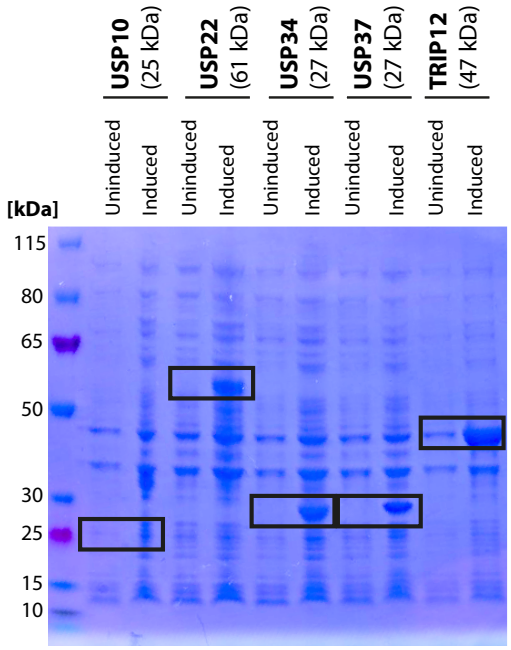


Figure 3.2: **Example Protein Expression Test.** Shown is a Coomassie stained SDS-PAGE gel for expression tests carried out on USP10, USP22, USP34, USP37, and TRIP12. Plasmids were transfected into BL21(DE3) *E. coli* expression strains. Cultures were grown in LB media until reaching an approximate OD of 0.5-0.6 before protein expression was induced using IPTG. Samples were incubated for a further 2 hours before the bacteria were pelleted, mixed with SDS-PAGE loading buffer, and boiled. Samples were run on a 4-12% gradient precast SDS-PAGE gel and stained with Coomassie protein stain. The bands corresponding to expressed protein are highlighted with black boxes. Uninduced samples were run as a reference.

3.2.2 Protein Solubility Testing

Following selection of the optimal bacterial strain and induction methods, I next explored the solubility of expressed recombinant protein. It was important that the respective protein of interest was soluble in the desired lysis buffer to allow purification under natively folded conditions. To test this, each of the selected candidates were expressed using the optimised conditions before the resulting bacterial cultures were pelleted and resuspended in a variety of lysis buffers. Centrifugation was then used to separate the soluble and insoluble fractions.

The lysis buffers trialled all contained the same core components: a pH mediator/buffering

component (maintains pH, stabilising protein structures), salt (ionic strength), Mg^{2+} (required for Benzonase activation), detergent (cell lysis), glycerol (increased protein solubility and stability), lysozyme (cell lysis), and protease inhibitors (prevent protein degradation). Initially, a 'standard' lysis buffer was tested across all candidates, and then modifications were made based on the results observed. The lysis buffers were primarily adjusted by increasing or decreasing the salt and detergent concentrations to alter the strength, or harshness of the buffer. In addition the pH of the lysis buffers were also considered, and buffers ranging between pH 7-9 were used dependent on the protein pKA. One problem when overexpressing exogenous proteins in bacterial systems is their aggregation into highly insoluble inclusion bodies. Two methods were employed to prevent this, if candidates were found to be particularly insoluble. The first was through the addition of osmolytes (Trehalose and Glycine Betaine) or polylols (Mannitol) to the growth media. The selected compounds were discovered during a screen of compounds existing *in vivo* that may enhance protein solubility during purification (Leibly et al., 2012). Unfortunately, none of the tested compounds increased the respective yield of the expressed candidate proteins. Therefore, as an alternative, the mild detergent Sarcosyl was added to lysis buffers. Sarcosyl is particularly useful for the purification of recombinant proteins as it is a non-denaturing detergent that does not precipitate at low temperatures (Chisnall et al., 2014).

A summary of the compositions of chosen buffers for each protein is included in Table 2.1. Figure 3.3 shows examples of the typical result obtained from solubility testing. Bacterial pellets expressing recombinant TRIP12 were resuspended in lysis buffer with or without Sarcosyl. It was clear that, in the lysis buffer without Sarcosyl, TRIP12 C-terminal fragments

were highly insoluble and resided within the pellet fraction. However, the addition of Sarcosyl was sufficient to solubilise recombinant TRIP12, demonstrated by the band shift from the pellet, to the supernatant fraction. The inclusion of sample sonication did not appear to have any impact on the overall solubility of expressed TRIP12. Coomassie staining of SDS-PAGE gels was used to quickly observe whether or not the expressed protein was soluble in the tested lysis buffer. Subsequent immunoblotting using α- Histidine tag antibodies confirmed that the observed bands contained the protein of interest.

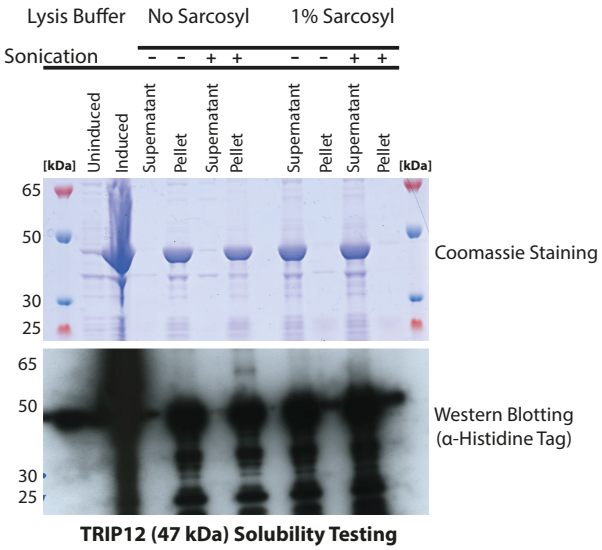


Figure 3.3: **Example of Solubility Testing**. The expressed fragment of TRIP12 was solubilised following Sarcosyl addition. Bacteria expressing TRIP12 protein fragments were pelleted by centrifugation, the pellet resuspended in the appropriate lysis buffer, and optionally sonicated. Soluble and insoluble fractions were then separated by centrifugation. Each collected fraction was then mixed with equal volumes 2X SDS-PAGE loading buffer and run on SDS-PAGE gels. Coomassie protein staining or immunoblotting was used to determine protein solubility.

3.2.3 Purification of Recombinant Proteins for Raising Antibodies

The candidate proteins were expressed and purified under the optimised conditions. A summary of the respective tag, bacterial strain, induction method, and lysis buffer used is shown in Table 2.11. All candidates were expressed with a poly-histidine tag, with the exception

of TRAIP that was cloned into a His-SUMO tag to enhance protein solubility. Purification of each respective candidate was then achieved using a one-step approach involving binding of Histidine tags to nickel ions conjugated to sepharose beads. Briefly, bacterial cells were lysed with the selected buffer and separated into soluble and insoluble fractions. The soluble fraction was then collected and added to the beads for isolation of His-tagged peptides; subsequently eluted from the column through competition for nickel binding by imidazole.

A summary of the protein purifications conducted is shown in Figure 3.4. His-RFWD3 N-terminal fragment, His-SUMO-TRAIP, His-TRIP12 C-terminal fragment, His-USP10 N-terminal fragment, His-USP34 N-terminal fragment, and His-USP37 N-terminal fragment were successfully purified. Unfortunately, His-USP22 N-terminal fragment was not purified as sufficient quantities of soluble protein could not be obtained. Due to time constraints associated with the project, further attempts to purify USP22 were not conducted. Therefore, USP22 was removed from the candidate pool. Interestingly, purified USP10 N-terminal fragment was found to run at approximately 40 kDa on the SDS-PAGE gels, higher than the expected size of 24 kDa. Immunoblotting revealed that the bands observed at 40 kDa were recognised by antibodies specific for the poly-histidine tag (data not shown), suggesting the presence of USP10. It was possible that the expressed USP10 fragment may contain an unusual amino acid sequence or be post-translationally modified following expression, resulting in the unexpected behaviour during electrophoresis observed. Alternatively, it was also possible that the stop codon was mutated during transformation, or skipped during expression; this could be confirmed through the sequencing of plasmids isolated from the expression strain, or mass spectrometry of the purified recombinant protein. However, as the purified protein

did contain the 6X His tag, we decided to use this for antibody preparation as it was likely to contain the USP10 sequence.

The approximate amounts of each protein purified was estimated through comparison to a gradient of known quantities of BSA on SDS-PAGE gels. Elutions were pooled if required, and samples containing either 2 mg or 6 mg of total each respective candidate were sent for raising antibodies in rabbit and sheep, respectively (Dundee Biosciences). USP34, RFWD3, TRIP12, and TRAIP antibodies were raised in Rabbits, whilst USP10 and USP34 antibodies were raised in Sheep.

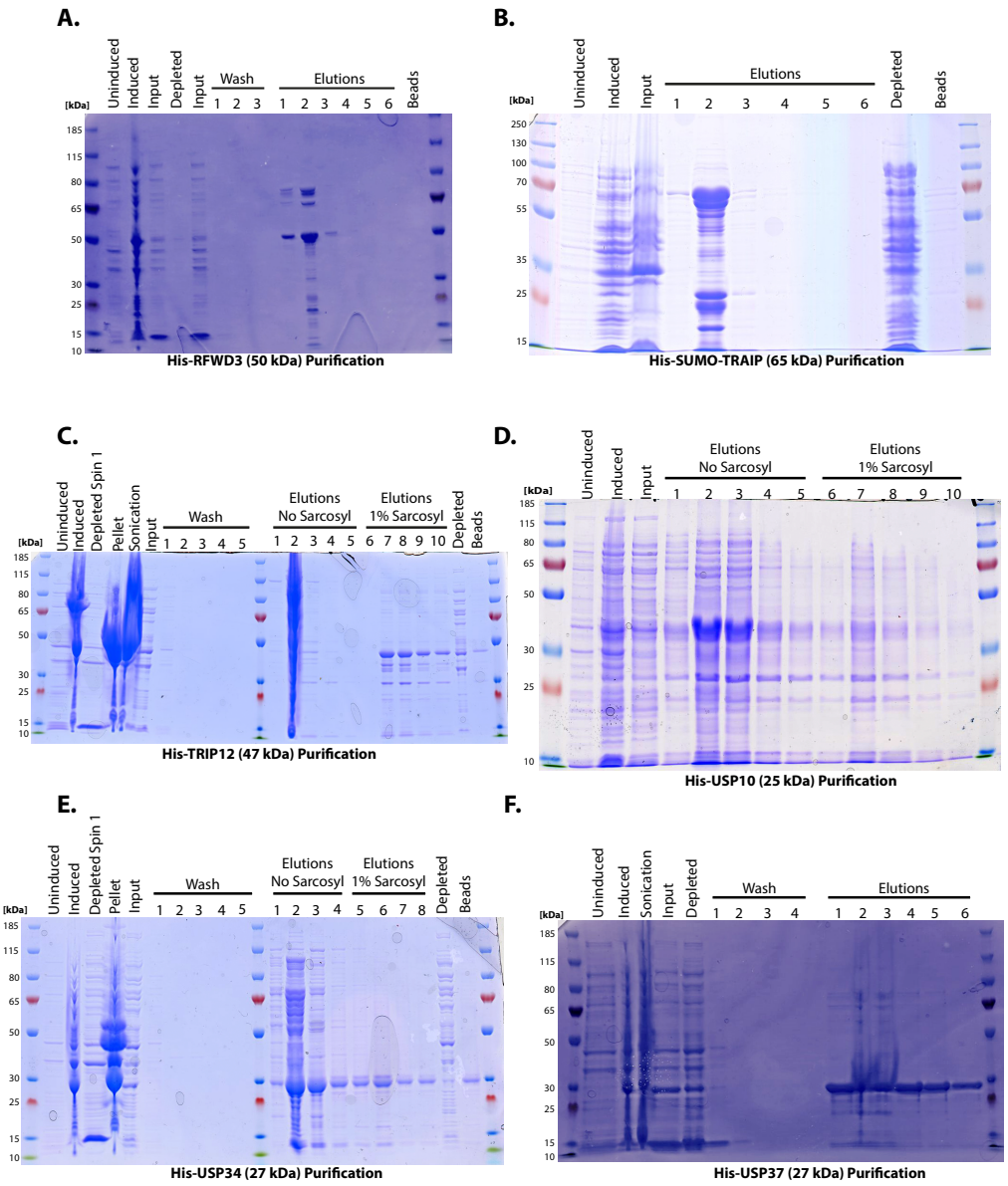


Figure 3.4: **Panel of Candidate Protein Purifications**. Shown are the SDS-PAGE gels resulting from purifications of either whole protein, or fragments, of each respective candidate. All purifications were carried out as detailed in the materials and methods. **A.** Purification of His-RFWD3. **B.** Purification of His-SUMO-TRAIP. **C.** Purification of His-TRIP12 C-terminal fragment. **D.** Purification of His-USP10 N-terminal fragment. **E.** Purification of His-USP34 N-terminal fragment. **F.** Purification of His-USP37 N-terminal fragment.

3.2.4 Testing Raised Sera against Candidates of Interest

The testing and characterisation of antibodies raised against the candidate proteins was carried out through immunoblotting of *Xenopus* egg extract, using the crude sera as the primary

antibody.

Confirming Activity of Generated Egg Extract

LSS *Xenopus laevis* egg extracts were prepared as detailed in the materials and methods. Before testing whether the raised sera were able to recognise their respective targets, I first validated that the egg extract was able to replicate DNA through the incorporation of radiolabelled nucleotides into the newly synthesised DNA. Extracts were first activated to complete meiosis and enter interphase by stimulating the calcium fertilisation wave, and then radiolabelled nucleotide was added. Samples were taken throughout S-phase to determine the relative amounts of replication undertaken. Figure 3.5 shows an example curve from this assay. Extracts were found to begin replication approximately 45 minutes following activation. The completion of DNA replication was found to occur 75-90 minutes after activation, represented by a decrease in radioactive nucleotide incorporation and the plateau of the replication curve.

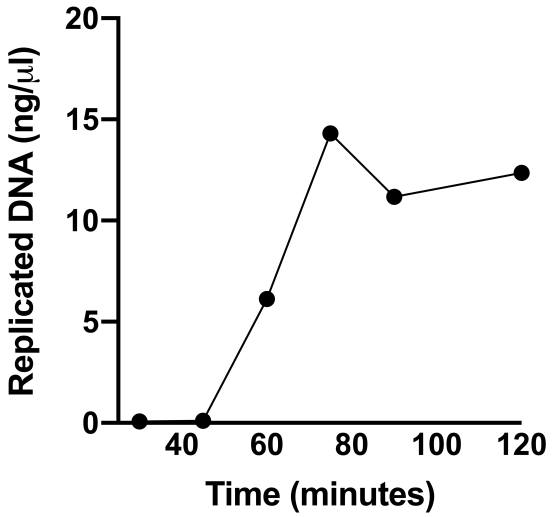


Figure 3.5: **Measuring DNA Synthesis in Egg Extracts.** LSS egg extracts were activated through stimulation of the calcium fertilisation wave, and radiolabelled nucleotides added. Samples were taken at 30, 45, 60, 75, and 120 minutes post activation. The respective amount of DNA synthesis was calculated through the proportion of radiolabelled nucleotides incorporated into replicating chromatin; calculated as described previously with respect to a reference sample. Data was analysed using RStudio.

Sera Immunoblotting

The egg extract was then used to characterise the raised sera. First, I explored whether the sera was able to recognise each respective candidate of interest in the extract system. Small amounts of egg extracts were run on SDS-PAGE gels and used for immunoblotting with the crude sera, diluted as detailed in Table 2.5. To ensure any results obtained were not immunoblotting artifacts, each test was done in duplicate.

The results of the crude sera immunoblotting are shown in Figure 3.6. In each experiment, numerous non-specific bands were observed spanning the entirety of the membranes. This was likely due to a combination of the extremely concentrated nature of the egg extract and the use of crude sera instead of purified antibodies. Despite this, bands were observed at approximately the expected molecular weights for USP37, RFWD3, TRIP12, and USP10; suggesting that raised sera were able to recognise the respective target. Conversely either no, or extremely faint, bands were observed for the sera raised against TRAIP. Ongoing experiments from other members of the lab have demonstrated that endogenous TRAIP is present at low levels in the egg extract and is difficult to detect in whole egg extract. It was, however, observable in immunoblotting experiments from isolated chromatin using antibodies purified from the raised sera (data not shown). USP34 is an extremely large protein (400 kDa). The molecular weight markers used as a reference sample were standard broad range protein markers and only extended to 250 kDa. Therefore, I was unable to determine exactly where a protein of USP34's size would reside on the gel. Initial trials of USP34 sera using standard 4-12% gradient acrylamide gradient gels did not show any clear evidence of USP34 recognition (Figure 3.6F). To attempt to better resolve USP34, the sera test was repeated using a lower

5% concentration gel. Doing so revealed a single, clear band at the top of the gel potentially corresponding to USP34, but further validation is required.

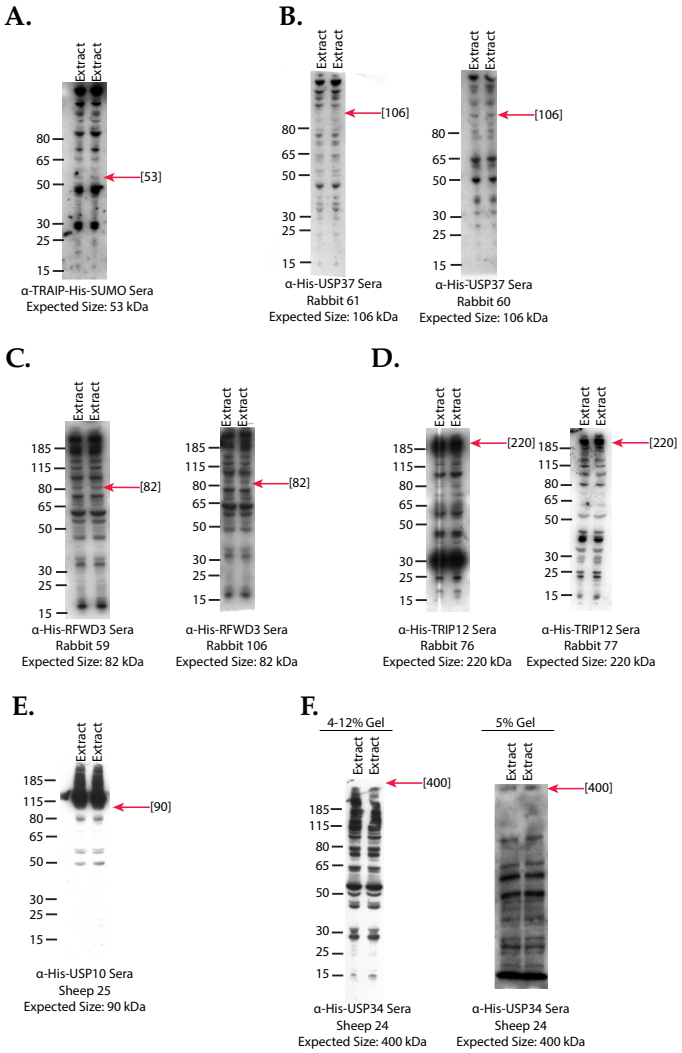


Figure 3.6: **Immunoblots of *X. laevis* egg extract to detect candidate proteins.** Crude sera raised using purified recombinant protein were used as the primary antibody for immunoblotting experiments. Extracts were run in duplicate and immunoblotted using crude sera as primary antibody. Shown are each of the candidate proteins: **A.** TRAIP-His-SUMO Serum. **B.** His-USP37 Sera. **C.** His-RFWD3 Sera. **D.** His-TRIP12 Sera. **E.** His-USP10 Serum. **F.** His-USP34 Serum. For each protein, the expected molecular band size is indicated.

3.2.5 Selection of TRAIP for further study

The primary objective at the start of this PhD project was to raise antibodies against each of the candidate proteins, before then screening for roles in DNA replication using *Xenopus laevis*

egg extract. However, whilst conducting the process of raising antibodies, TRAIP emerged as a protein of interest with several potential roles during DNA replication. Work done by members of our lab and others showed that, upon blocking replisome unloading during S-phase, replisomes were removed from chromatin through a secondary pathway acting in mitosis. Further work revealed that the mitotic unloading mechanism was also driven by MCM7 ubiquitylation. To attempt to identify the ubiquitin ligase responsible, mass spectrometry was carried out to identify novel interactors of post-terminated replisomes, retained on mitotic chromatin due to inhibition of the S-phase unloading mechanism. TRAIP was found to be one of two ubiquitin ligases interacting with such a replisome. Therefore, it was likely that TRAIP was responsible for the ubiquitylation and subsequent unloading of CMG during mitosis. As a result, I aimed to assist with the elucidation of TRAIPs role in mitotic replisome disassembly.

Purification of Wild-Type and Catalytically Inactive TRAIP

To explore whether TRAIP was the ubiquitin ligase responsible for mitotic replisome unloading, we aimed to inhibit mitotic replisome disassembly by outcompeting the endogenous TRAIP with catalytically inactive recombinant TRAIP. For this, sufficient quantities of natively folded wild-type, and mutant (C25A), TRAIP were required. Recombinant TRAIP, expressed using the bacterial systems described, was highly insoluble in all of the initial lysis buffers tested. To overcome this, a number of different approaches were used to increase the yield of soluble protein: testing different pH ranges, altering the salt concentration of the lysis buffer, using different salts or pH mediators, trialling alternative detergents (Triton-X, Brij, Sarcosyl), and supplementing the lysis buffers with compounds known to aid protein solubility (Trehalose, Glycine Betaine, Mannitol). The majority of buffers tested did not aid TRAIP solubility. On the

other hand, supplementing the lysis buffers with strong detergents (Sarcosyl or Triton-X) did increase the soluble protein yield. However, these were avoided due to the risk of protein denaturation associated with the use of strong detergents. Use of the weaker detergent Brij also slightly increased solubility, but not to the extent required for purification. Therefore alternative approaches were needed. To this end, I selected to clone the TRAIP sequence, from the pET28 His-tagged plasmid backbone to a pCA528 His-SUMO-tagged plasmid vector, known to increase protein solubility. Subsequent testing of expressed His-SUMO-TRAIP, using lysis buffers supplemented with Brij, revealed sufficient quantities of soluble protein (data not shown).

The generated plasmid expressing WT His-SUMO-TRAIP was modified using standard molecular cloning techniques to introduce the single point mutation of Cysteine 25 to Alanine, confirmed through plasmid sequencing. The C25A mutation was selected as it has previously been shown to inhibit TRAIP catalytic activity during mitosis (Chapard et al., 2014b). Using the optimised conditions detailed, both wild-type and C25A TRAIP were purified (Figure 3.7). The eluted recombinant protein (lanes 2 and 3) from each respective purification were pooled and dialysed overnight into LFB1/100. Dialysis was carried out for two reasons: first, the lysis buffer used contained high salt and detergent concentrations, both of which were unsuitable for use in *X. laevis* egg extract. Secondly, protein dialysis was conducted using a 35 kDa molecular weight cut-off column, allowing the removal of several contaminating proteins co-eluted with TRAIP. The approximate concentration of dialysed, recombinant WT or C25A TRAIP were then calculated, and the protein flash frozen into single-use aliquots.

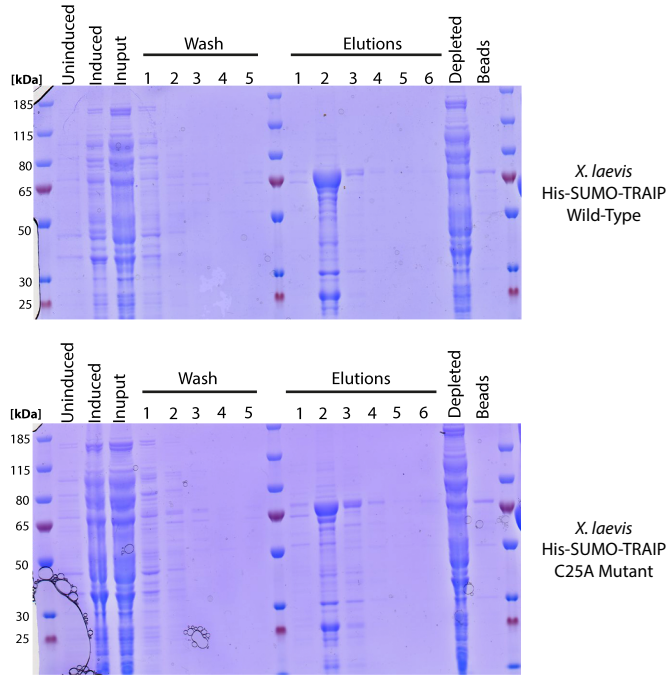


Figure 3.7: **Purification of Recombinant WT and C25A TRAIP.** Recombinant His-SUMO-TRAIP (65 kDa) was expressed using pCA528 and purified as previously described. Elution fractions, as well as various control samples were run on SDS-PAGE gels and stained with Coomassie Protein Staining.

TRAIP is Required for Mitotic Replisome Disassembly

The purified recombinant TRAIP was passed onto other members of the lab for use in the egg extract system. Full details are shown in Moreno et al. (2019), a summary of the key experiment is depicted in Figure 3.8. Briefly, egg extracts were allowed to progress through S-phase in the presence of the NEDD8 activating enzyme (NAE) inhibitor MLN4924. Protein nedddylation (attachment of the ubiquitin-like NEDD8) is required for cullin activation. Therefore, by inhibiting NAE, we were able to robustly block S-phase replisome disassembly through preventing Cullin2^{LRR1} activation. Perturbed extracts were then pushed into mitosis through addition of the mitotic cyclin (Cyclin A1), and high concentrations of recombinant WT and C25A TRAIP was added. Any replisome retained following MLN4924 treatment was found to be disassembled upon entry into mitosis in the control extracts, or those supplemented with

WT His-SUMO-TRAIP (See Psf2, Cdc45 blots in Figure 3.8). Conversely, replisome disassembly was blocked in extracts containing C25A His-SUMO-TRAIP, or through treatment with the p97 inhibitor NMS873. Moreover, increased retention of ubiquitylated MCM7 was also observed after adding recombinant mutant TRAIP to the reaction, further indicative of a loss of replisome disassembly. Overall this data revealed the mechanism of mitotic replisome disassembly. MCM7 is ubiquitylated by TRAIP; the formed ubiquitin chains can then be recognised by the p97 segregase to facilitate CMG removal from chromatin (Moreno et al., 2019).

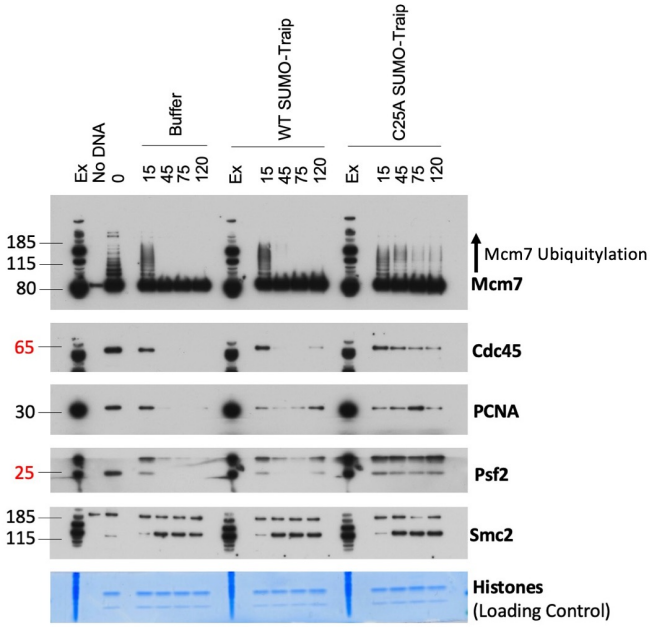


Figure 3.8: **TRAIP Ubiquitin Ligase Activity Drives Mitotic Replisome Disassembly.** Summary of the role of TRAIP during Mitotic replisome disassembly, reproduced from Moreno et al. (2019). *Xenopus laevis* egg extracts were replicated in the presence of MLN4924 to inhibit S-phase replisome disassembly. Following the completion of S-phase, extracts were pushed into mitosis using the mitotic Cyclin A1 where high concentrations of either WT or C25A TRAIP were added. Any defects to replisome disassembly were assessed through chromatin isolation over the timecourse of incubation in mitotic extract and immunoblotting. WT TRAIP was found to act similar to the buffer controls. Conversely, C25A TRAIP addition resulted in the retention of key replisome components (CDC45, PCNA, Psf2, and ubiquitylated MCM7). The experimental work for this figure was carried out by Dr. R. Jones (Moreno et al., 2019). Figure reproduced with permission from the authors.

3.3 Discussion

The first objective of the PhD project was to raise antibodies against each of the 7 selected E3 ubiquitin ligases and deubiquitylating enzymes. Whilst undertaking this work, it became quickly apparent that protein solubility was the major bottleneck of the established workflow. Many of the expressed recombinant proteins were found to be insoluble during the preliminary solubility testing experiments, and further optimisation was needed. The respective solubility of an expressed protein can be influenced by both physiochemical properties of the protein itself (e.g., amino acid sequence and overall net charge, molecular weight, or structural conformations), as well as environmental factors within the experimental procedure (e.g., buffer pH, anionic strength, temperature, and detergent concentration). In addition, it was also important to consider factors specific to the bacterial expression system used. The expression of recombinant proteins in bacterial systems is simple and can produce high yields. However, some eukaryotic proteins require post-translational modifications for proper folding, which cannot be supported in bacteria. Moreover, high levels of natively formed proteins expressed in bacteria can aggregate into highly insoluble structures called inclusion bodies (Martínez-Alonso et al., 2009). These structures, commonly located in the cytoplasm, can be isolated from cell lysates using centrifugation, and purified through protein denaturation and re-folding (Palmer and Wingfield, 2012). Antibodies raised against soluble antigen have a better chance to recognise natively folded protein, and work effficiently in assays such as immunoprecipitation and immunodepletion. However, denaturing conditions could be used to purify respective proteins of interest if the resulting antibodies were required just for immunoblotting purposes, as proteins resolved using SDS-PAGE are denatured.

To resolve any solubility issues not fixed by trialling different lysis buffer conditions, a number of different compounds reported to improve protein solubility were added to the growth media. A study by Leibly et al. (2012) aimed to screen several small compounds reported to aid protein stability *in vivo*, for any ability to improve the solubility of insoluble proteins expressed recombinantly in bacterial systems (Leibly et al., 2012). The three top-performing compounds from the screen were selected for testing with the candidate proteins: Trehalose, Glycine Betaine, and Mannitol. Trehalose and Glycine Betaine are osmolytic compounds required in lower eukaryotes to stabilise proteins, preventing their degradation upon exposure to environmental stress (Jain and Roy, 2009; Auton et al., 2011). The third additive, Mannitol, is a polylol shown to aid protein solubility through by thermal stabilisation (Leibly et al., 2012). In the work carried out, use of these compounds did improve the total yield of soluble protein. However, the majority of expressed recombinant candidates remained insoluble. Therefore, it was concluded that protein aggregation due to over-expression was the likely cause. To extract insoluble protein aggregates, we selected to supplement the lysis buffers with the non-denaturing detergent Sarcosyl (Frankel et al., 1991; Tao et al., 2010; Schlager et al., 2012). Sarcosyl was chosen over similar alternative detergents, such as SDS, due to the fact it does not precipitate at cold temperatures. Sarcosyl also possesed a reduced risk of inducing protein denaturation during the experimental procedures. Any minor changes to the native protein structure caused by the use of sarcosyl would likely not affect the ability of the raised antibodies to recognise their targets, as we raised polyclonal antibodies recognising multiple antigens across the entire surface of the purified protein.

Whilst the use of Sarcosyl effectively solubilised recombinant protein for raising antibodies,

additional considerations were needed when purifying TRAIP for use in egg extract. In order to understand any roles for TRAIP during mitotic replisome disassembly, active recombinant protein was required. It was not known whether the use of Sarcosyl would result in changes to the native tertiary structure of recombinant TRAIP. Thus, in this case, Sarcosyl was ommitted from the lysis buffers. His-tag tagged TRAIP was found to be highly insoluble in all lysis buffers tested. Due to this, alternative approaches were taken to enhance the relative solubility of recombinant TRAIP. The inclusion of SUMO tags have been previously reported to aid protein solubility, allowing for the purification of natively folded, active proteins (Marblestone et al., 2006). Cloning the TRAIP sequence into a His-SUMO- plasmid successfully resulted in the purification of both WT and C25A His-SUMO-TRAIP.

The deubiquitylating enzyme USP22 could not be purified. Expressed USP22 remained insoluble in all conditions tested, including supplementation of the lysis buffer with the described detergents and small compounds, as well as under denaturing conditions. It was possible that changing the purification tag to His-SUMO would lead to the expression of soluble protein. However, due to the emergence of TRAIP as an interesting candidate, the priorities of my PhD project were altered and this was not carried out. During the purification of USP10, the eluted protein was found to run at a larger size than expected on SDS-PAGE gels. Immunoblotting revealed that this band of increased size was recognised by Histidine tag specific antibodies, suggesting that the observed protein band contained His-USP10. We therefore wondered whether any errors were introduced to the DNA sequence during molecular cloning, potentially causative of the band shift (e.g. reading frame shift or missing stop codon).

The sera raised against candidate proteins of interest appeared able to detect bands potentially corresponding to their respective targets. The only exception was TRAIP. Immunoblotting of egg extracts with commercial antibodies against human TRAIP, used by members of the Gambus group, suggested that TRAIP is not very abundant in whole egg extract, and was difficult to detect. TRAIP can be however, accumulated on replicating chromatin upon the inhibition of replisome disassembly and detected by both the commercial antibodies, and antibodies raised in this project. Moreover, to improve the immunoblotting signal, the antibodies from the TRAIP sera raised were purified by members of the Gambus lab. Purified antibodies were able to both recognise endogenous TRAIP, and immunodeplete this from the egg extract. Thus, it is likely that antibodies purified from the remaining sera raised during this PhD project will similarly be able to recognise, immunoprecipitate, or immunodeplete the respective protein of interest within *X. laevis* egg extract.

Overall, during this chapter of work, I have purified and raised antibodies against several interesting candidates with potential roles in DNA replication. This will allow for further projects, for future members of the lab, exploring the respective roles of each candidate protein. Prior to this, however, the raised antibodies will require validation to confirm interactions with the respective proteins of interest. First, the crude sera should be utilised for immunoblotting and immunoprecipitation experiments to ensure recognition of bands at the approximate size. *X. laevis* egg extract is highly concentrated and is is expected that immunoblotting using crude sera will result in the detection of several non-specific bands. Given the chromatin binding ability of DNA replication or DNA repair proteins, therefore, these

experiments should also be trialled using isolated chromatin; acting as a purification step to provide more specific signal. This may be combined with approaches designed to introduce recombinant protein of different sizes (incorporating tags or the use of truncation mutants) to further confirm antibody specificity by band shifts. If, in the described experiments, specific bands representing a protein of interest are observed, then antibodies should be purified using affinity columns containing purified antigen. Once purified, it is expected that the antibodies will still result in the specific band signal, but with reduced non-specific binding capability. Finally, the purified antibodies ability to bind to the protein of interest will be confirmed through immunoprecipitation in both whole egg extract and from isolated chromatin; subsequently sent for mass spectrometry analysis to confirm specific protein enrichment.

Following antibody validation, the purified antibodies raised during this project could then be used to explore any interaction of the candidate proteins with the replisome (both unperturbed and perturbed conditions). This will primarily involve immunodepletion experiments to remove the protein of interest from egg extract and observe any resulting phenotypes. If the initial screen revealed any such interaction, further characterisation would be required; initially through immunodepletion and 'add back' experiments of wild-type or mutant proteins purified using the methods optimised in this chapter.

Since the start of this PhD project, further data has emerged involving the selected candidate proteins. These studies were carefully considered alongside existing Gambus lab data to determine the most interesting candidate to take forward. The deubiquitylating enzymes

USP10, USP22, USP34, and USP37 were initially highlighted as potentially novel interactors of the replisome. Much of the research surrounding the deubiquitylating enzymes selected has focused on differential expression levels in varying types of cancer, often resulting in poorer phenotypes. However, for the purposes of this project, only work involving DNA Replication, Cell Cycle Progression, or DNA Damage Repair will be summarised. No suitable studies were published since starting the PhD project involving USP10 or USP34.

USP22 has emerged as a key regulator of both cell cycle progression and DNA damage repair. It is thought that USP22 acts in combination with RNF220 to stabilise the G1 cyclin D1 to promote cell proliferation in acute myeloid leukaemia (Pan et al., 2021). In addition, several studies have implicated USP22 in the DNA damage response. Notably, USP22 has been shown to be important for recruitment of PALB2, BRCA2, and RAD51 to sites of double strand breaks (Nardi et al., 2020). Moreover, depletion of USP22 has been shown to result in defects to γ-H2AX signalling and class switch recombination through non-homologous end joining (Li et al., 2018). Finally, a large-scale screen of prostate cancer samples identified the nucleotide repair protein XPC as an interactor of USP22 (McCann et al., 2020).

USP37 has emerged as one of the most interesting, with direct roles during both DNA replication and the DNA damage response. USP37 has been shown to deubiquitylate and stabilise CDT1 levels, predominantly during G1 and early S-phase of the cell cycle. CDT1 is required for the formation of MCM2-7 double hexamers on replication origins, and through its stabilisation, USP37 actively promotes origin licensing. Interestingly, the study also highlighted slowed replication fork speeds upon inducing depletion of USP37 (Hernández-Pérez et al.,

2016). In addition to roles during origin licensing, USP37 has been reported to also interact with the ReqQ helicase BLM (Wu et al., 2021), and CHK1 (Stromberg et al., 2021). Following induction of double strand breaks by Cisplatin treatment, USP37 is phosphorylated by ATM to promote the interaction and stabilisation of BLM; sustaining the DNA damage response (Wu et al., 2021). Moreover, USP37 knockouts have been found to also destabilise Checkpoint Kinase 1, resulting in increased DNA damage following the induction of replication stress (aphidicolin treatment) (Stromberg et al., 2021).

The E3 ubiquitin ligase TRIP12 has been shown to possess roles in cell cycle control as well as the cellular response to PARP inhibitors (Gatti et al., 2020; Larrieu et al., 2020). Recent work highlighted the requirements of the N-terminus of TRIP12 for chromatin binding (Larrieu et al., 2020). Moreover, the data presented implicates TRIP12 in mitotic entry as knockouts of TRIP12 by siRNA were shown to result in increased mitotic entry following G2 arrest and release (Larrieu et al., 2020). A second study identified TRIP12 to interact with, and ubiquitylate PARP1 on chromatin to limit the extent of PARP1 trapping after treatment with PARP inhibitors. Hence, the knockout of TRIP12 was subsequently shown to sensitise cells to PARP inhibition (Gatti et al., 2020).

RFWD3 has emerged as a prolific E3 ubiquitin ligase with several roles across DNA Replication and the DNA Damage response. Interestingly, bi-allelic mutations in RFWD3 have been reported to cause Fanconi Anaemia in patients (Knies et al., 2017). RFWD3 has been shown to be a key interactor of the DNA clamp PCNA during both unperturbed DNA replication, and upon the induction of DNA damage. As such, RFWD3 knockdowns result in a prolonged S-phase,

slowed replication fork speeds, G2/M cell cycle accumulation, as well as the accumulation of CDC45, RAD51, and RPA1 on chromatin (Lin et al., 2018). Similarly, the ubiquitylation of PCNA by RFWD3 is important for inducing the switch between replicative polymerases and those responsible for translesion synthesis; with RFWD3 knockout cell lines possessing TLS defects at ssDNA gaps (Gallina et al., 2021). Moreover, RFWD3 has also been implicated in ICL repair and homologous recombination, through interactions with RPA1 and RAD51 (Inano et al., 2017; Feeney et al., 2017), as well as the stabilisation of stalled replication forks in BRCA2 deficient cells (Duan et al., 2020). Finally, RFWD3 has been implicated in origin licensing through ORC stabilisation (Hsu et al., 2020)

Data from the Gambus group, alongside others, carried out since the start of the PhD project have implicated TRAIP in both DNA replication and the DNA damage repair processes. Notably, several papers over the last few years have shed light on the role of TRAIP during replisome disassembly (Moreno and Gambus, 2020; Deng et al., 2019; Wu et al., 2019; Sonneville et al., 2019; Villa et al., 2021). Briefly, if replisome disassembly was inhibited during S-phase, terminated replisomes were retained on chromatin until mitosis, where they were then unloaded. Data from our group suggested that, in this scenario, TRAIP ubiquitylates MCM7 with K-6 or K-63 linked ubiquitin chains (Moreno et al., 2019). The respective chains built during mitosis were recognised by the p97 segregase, resulting in CMG removal from chromatin. Furthermore, TRAIPs function in replisome disassembly during mitosis appears to be evolutionarily conserved, as similar roles were observed using *C. elegans* and mouse embryonic stem cells (Sonneville et al., 2019; Villa et al., 2021). Therefore, mitotic replisome disassembly appears to be a universal pathway, acting to remove any

post-termination or stalled replisomes still present on chromatin upon entry to mitosis. It is known that if replisomes are not removed, then the helicases can continue to translocate on double-stranded DNA (Low et al., 2020). During this translocation, the helicase can strip off proteins binding to chromatin. However, whether the terminated helicase remains active, facilitating DNA unwinding is unclear. Thus, if any retained replisomes were not unloaded prior to cell division, chromosome segregation may be impaired, either due to improper chromosome condensation, or the presence of bulky CMG remaining on DNA; potentially resulting in chromosome mis-segregation events, mitotic catastrophe, and overall cell viability defects.

Alongside mitotic replisome disassembly, TRAIP has also been suggested to have roles in both mitotic progression (See **1.6**) and mitotic DNA Synthesis (MiDAS). Mitotic defects have been widely reported in cells lacking TRAIP, however the respective underlying cause remained unknown. A recent study aimed to elucidate mechanisms for TRAIP during mitosis (Sonneville et al., 2019). This data revealed clear defects to the ability of cells to synthesise under-replicated regions of DNA (induced by aphidicolin treatment) by MiDAS in cells without TRAIP (Sonneville et al., 2019). Thus, TRAIP is important during the response to replication stress. Given our findings in *X. laevis*, that TRAIP is required to unload stalled replication forks during mitosis (Moreno et al., 2019), it may be that TRAIP also fulfils this role in mammalian cells, and that without TRAIP, replisomes are retained on chromatin, inhibiting MiDAS.

TRAIP has also been found to possess roles outside of mitosis. Work by Prof. Walter's group have shown using *X. laevis* egg extract that TRAIP can interact with the replisome upon

encountering blockages on DNA, namely DNA interstrand cross-links (ICLs) and DNA-protein cross-links (DPCs) (Wu et al., 2019; Larsen et al., 2019). Plasmids containing a single replication origin along with either ICLs or DPCs (M.HpaII cross-linked to fluorinated DNA sequences (Duxin et al., 2014)) were added to the egg extract. Following the DNA replication reaction, plasmids were isolated from egg extract and any respective products or associated proteins analysed. In the case of ICLs, it was shown that TRAIP ubiquitylates MCM2-7 upon convergence at the ICL site. The respective length of ubiquitin chains built by TRAIP were then deterministic of the respective downstream repair pathway. Short ubiquitin chains triggered NEIL3 glycosylase binding, ICL unhooking, and translesion synthesis. Whilst long ubiquitin chains resulted in CMG removal from chromatin and activation of the Fanconi anaemia pathway (Wu et al., 2019). In the case of DPCs, TRAIP was shown to be partly responsible for the ubiquitylation of the protein blockage on chromatin to trigger proteasome recruitment. Interestingly, in the absence of TRAIP, or if the protein blockage was situated on single stranded DNA (i.e. behind the replication fork), then DPC ubiquitylation was carried out by a second unknown ubiquitin ligase (Larsen et al., 2019).

In addition, TRAIP has recently also been shown to be required for ATM activation and the double-strand break response (Gleich et al., 2021). Mass spectrometry screening identified Ku70, Ku80, SMARCA5 and DNA-PK as TRAIP interacting partners. Following induction of DSB using neocarzinostatin, γ-H2AX and CHK2 phosphorylation were impaired after TRAIP depletion (Gleich et al., 2021). However, in all the studies detailed, the exact target of TRAIP remained unclear. It may be that TRAIP is required to remove replisomes at sites of DNA damage, to allow access of repair-associated proteins to chromatin. Previously published data

has shown that TRAIP is recruited specifically to sites of damage through interaction with PCNA (Feng et al., 2016; Hoffmann et al., 2016), suggesting potential interactions with stressed replication forks. Alternatively, TRAIP may be required for robust DNA damage signalling itself through a mechanism not requiring replisome association.

Chapter 4

The Generation and Characterisation of Conditional AID Degrons Against TRAIP and LRR1

4.1 Introduction

Having raised antibodies against a number of potentially interesting proteins, based on our work and emerging published data, TRAIP appeared to be the most interesting candidate to take forward. TRAIP is currently regarded as an important factor to protect against genomic instability. However, the majority of studies carried out in mammalian cell lines have focused on the requirements for TRAIP in response to DNA damaging agents. Upon the induction of replication stress, TRAIP was shown to promote genome stability in both S-phase and mitosis (Harley et al., 2016; Hoffmann et al., 2016; Feng et al., 2016; Sonneville et al., 2019). Furthermore, recent mechanistic data from the Gambus group and others demonstrated the

ability of TRAIP to drive mitotic replisome disassembly in *X. laevis* egg extract (Moreno et al., 2019; Deng et al., 2019), *C. elegans* (Sonneville et al., 2019), and mouse embryonic stem cells (Villa et al., 2021). On the other hand, during S-phase, TRAIP has been found to be required when the replisome encounters either DNA-protein crosslinks or inter-strand crosslinks (Wu et al., 2019; Larsen et al., 2019).

TRAIP is an essential gene for mouse embryonic development as well as in human somatic cell lines (Hart et al., 2015; Park et al., 2007), and it is known that mutations to TRAIP result in primordial dwarfism (Harley et al., 2016). However, the respective targets or roles of TRAIP during the unperturbed eukaryotic cell cycle remain unknown. This is an area I will address for the remainder of my PhD project. The primary aim going forward was to use immortalised human somatic cells to understand and characterise the essential role of TRAIP during the eukaryotic cell cycle, underpinning the associated cell lethality and primordial dwarfism phenotypes. Secondly, I would also like to explore whether the role of TRAIP in mitotic replisome disassembly is conserved in human somatic cells. However, study into the process of replisome disassembly in human cells is difficult as the S-phase nor the mitotic pathways have been elucidated. Therefore, prior to exploring the roles of TRAIP, validation of our existing understanding of replisome disassembly in human somatic cells is required. This chapter details the generation and subsequent characterisation of several mammalian cell lines for the investigation of TRAIP throughout the eukaryotic cell cycle.

4.2 Results

To study the roles of TRAIP at different stages of the cell cycle, we first needed to establish a suitable method of depleting TRAIP from cells. Common methods of doing so included CRISPR-Cas9 gene knockouts, siRNA/shRNA to prevent gene translation, or the use of several degron technologies (e.g. AID, SMASh, Halo, and TRIM) (Roth et al., 2019). The use of CRISPR-Cas9 gene knockouts was not feasible in this case due to the associated cellular lethality in cells lacking TRAIP. Using RNA interference (siRNA or shRNA) would result in sufficient protein depletion, as has been demonstrated previously: including, but not limited to Hoffmann et al. (2016); Harley et al. (2016); Gleich et al. (2021); and Chapard et al. (2014a). However, both siRNA and shRNA require at least 24 hours to facilitate sufficient protein depletion. Therefore, the use of RNAi would lead to incremental global protein loss over the entire cell cycle, and not at the specific required stages. Due to these reasons, we selected to use a conditional degron, namely, the rapid Auxin-Inducible Degradation (AID) system. AID cells were generated with the assistance of Prof. M. Kanemaki and Assistant. Prof. T. Natsume (Molecular Cell Engineering, National Institute of Genetics, Japan) as part of a Japanese Society for the Promotion of Science (JSPS) Fellowship.

4.2.1 Generation of Conditional Degron Cell Lines against LRR1

LRR1 degron cells were created with the idea of being an important positive control for the ligase known to ubiquitylate MCM7, driving replisome disassembly. At the stage of cell line generation, it was known that Cullin2^{LRR1} was required for the unloading of terminated replisomes from chromatin in *C. elegans* and *X. laevis* egg extract; while we hypothesised that TRAIP may possess similar roles. Moreover, to date, replication termination has not been

extensively characterised using human somatic cell lines. Specifically, the involvement of Cullin2^{LRR1} in MCM7 ubiquitylation during S-phase has only been demonstrated recently (Fan et al., 2021). Thus, prior to any investigation into the mitotic replisome disassembly pathway, we must first validate that the established S-phase mechanism is conserved in mammalian cell systems. Generated LRR1 degron cell lines, facilitating cell-cycle stage specific protein degradation, would fit this purpose.

The first stage of cell line generation was to consider the potential consequences of tag position, and select which terminus to target. Overall, little was known about the structure, function, or localisation of LRR1 in mammalian cells. Therefore, to select which terminus to tag, protein domain structures were studied. LRR1 contains 7 Leucine Rich Repeat regions as well as a C-terminal Cullin2 interacting motif. Due to the position of the Cullin2 interacting region it was possible that using C-terminal tags would interfere with Cullin2^{LRR1} complex formation, and so these were avoided.

Endogenous LRR1 was tagged N-terminally with either a mAID (mini-Auxin-Inducible Degron) or mAC (mAID-mCLOVER) tag, as described in **2.3.4**. CRISPR and DONOR plasmids were transfected into three parental cell lines: CMV-OsTIR1 (constitutive OsTIR1 expression), Tet-OsTIR1 (OsTIR1 expressed under a Tetracycline sensitive promoter), and F74G CMV-OsTIR1 (AID2 system; detailed in Yesbolatova et al. (2020)). Transfected cells were treated with Hygromycin to select cells incorporating the degron tag (Figure 4.1A). Bi-allelic gene tagging was confirmed through genomic PCR using two primer pairs (Figure 4.1B). Primer pair 1 recognised the respective gene of interest and a non-coding region of the genome upstream.

Primer pair 2 recognised the same site within the gene of interest, paired with oligonucleotides for the degron tag. It was expected that bi-allelic gene tagging would present as increased band size from primer pair 1, and the appearance of bands from primer pair 2 (Figure 4.1C). Examples from the screening to identify bi-allelically tagged degron clones are shown in Figures 4.1D-F. The successful clones are described in Table 2.6 (Materials and Methods). In addition to the cell lines described, I also attempted to generate LRR1 degron cells in a non-cancerous background (hTERT-RPE1); although no clones survived selection. Finally, efforts were made to create double-degron cell lines with C-terminal tagging, using the mAID-SMASh system, but only mono-allelically tagged clones were obtained (data not shown).

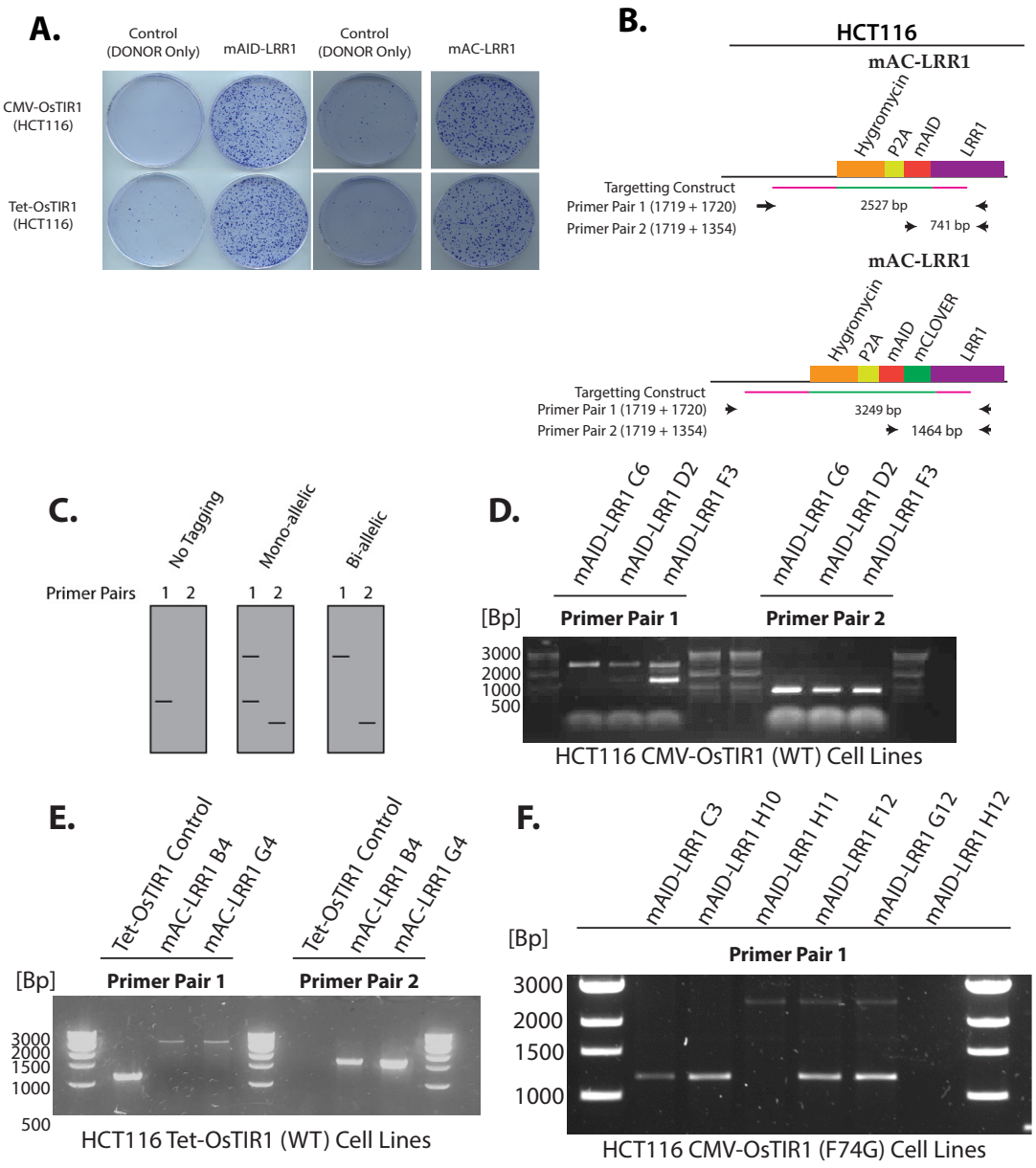


Figure 4.1: **Generation of Conditional LRR1 Degron Cells.** **A.** Cells colonies obtained after transfection for single-colony selection were stained with crystal violet stain for visualisation. **B.** Overviews of the tagging layouts. Endogenous LRR1 was tagged N-terminally with a degron tag, p2a self-cleavage site, and hygromycin resistance marker. The positions of the designed targetting construct used to tag endogenous LRR1 is shown. Pink lines represent homology arms recognising endogenous DNA sequences. Green lines represent sequences to be inserted. Details of the sequences covered by the targetting construct is included in the materials and methods. Arrows indicate the position of primers deigned to screen for bi-allelic gene tagging. Primers were designed to bind outside of the upstream and downstream targetting homology arms. Selection was carried out using Hygromycin B Gold, expressed by the endogenous LRR1 promoter. **C.** Diagram of the expected results from genomic PCR to check for bi-allelic tagging. Untagged control cell lines were used as reference controls. **D.** Example DNA agarose gel following genomic PCR to screen for cells in HCT116 CMV-OsTIR1 (WT) background. **E.** Example DNA agarose gel following genomic PCR to screen for cells in HCT116 Tet-OsTIR1 (WT) background. **F.** Example DNA agarose gel following genomic PCR to screen for cells in HCT116 CMV-OsTIR1 (F74G) background.

4.2.2 LRR1 is Degraded Following IAA Treatment

I next set out to confirm whether the endogenously tagged LRR1 could be degraded in cells following auxin treatment. To this end, HCT116 CMV-OsTIR1 mAID-LRR1 cell lines were treated with IAA for 24 hours and used for the creation of whole cell extracts, subsequently immunoblotted with antibodies against LRR1. Unfortunately, the antibody to detect the mAID tag was discontinued and it was not possible to detect endogenous LRR1 in HCT116 cells using several antibodies, both commercially available and raised in house. LRR1 is thought to possess particularly low expression levels in cells, which is also likely regulated by the cell cycle. It was therefore possible that the quantities of LRR1 in asynchronous whole cell extracts fell below detection limits. As a result, all attempts to detect mAID-LRR1 and associated degradation were unsuccessful (data not shown). To address this, we decided to enrich mAC-LRR1 from Tet-OsTIR1 parental cell lines using GFP-TRAP beads. Preliminary data revealed that this method was able to isolate endogenous mAC-LRR1 from cell extracts (Figure 4.2A). Furthermore, treatment of LRR1 degron cells for 24 hours with Doxycycline (OsTIR1 expression), followed by 24 hours of IAA treatment, was found to result in complete protein degradation (Figure 4.2B). Due to this, only the mAC-LRR1 conditional degron cell lines were used going forward. We also tested whether the fluorescent mCLOVER tag within the mAC-LRR1 cell lines could be detected, by immunofluorescence using fluorescent microscopy and flow cytometry. However, no differences in background fluorescent level could be detected with either method upon auxin treatment (data not shown). Whilst this was expected due to the lack of signal from the immunoblotting of whole cell extracts, it was still important to assess to avoid potential channel interference during future experiments, utilising fluorescence readouts.

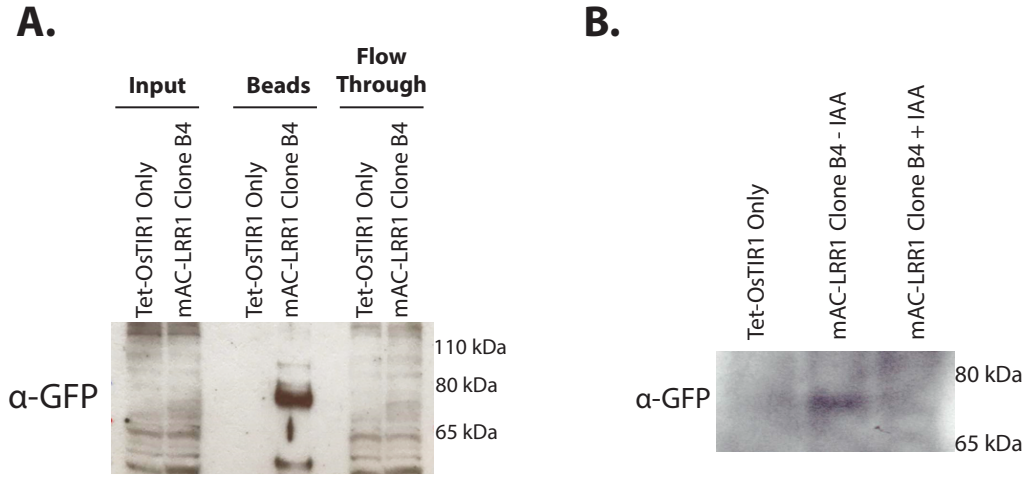


Figure 4.2: **mAC-LRR1 is Degraded Upon IAA Treatment. A.** To enrich mAC-LRR1 from whole cell extracts, GFP-TRAP beads were used. Shown is an example immunoblot from GFP-TRAP. mAC-LRR1 (approximately 80 kDa) was pulled out of cell extracts. No similar bands were observed in untagged controls, demonstrating assay specificity. Preliminary GFP-TRAP assays carried out by Dr. A. Reynolds-Winczura. **B.** mAC-LRR1 is degraded following doxycycline and IAA treatment. Cells were treated as described in **4.2.2.** GFP-TRAP assays were used to isolate mAC-LRR1, subsequently detected using GFP antibodies in immunoblotting experiments. Work carried out by Dr. S. Nath.

4.2.3 LRR1 is Important for Cell Viability

LRR1 is thought to be an essential protein, with gene knockouts lethal in embryonic mouse models (data not shown) and immortalised human somatic cells (Hart et al., 2015). Based on this, we expected that long term LRR1 degradation in the AID cells would have a similar result. To investigate the impact of mAC-LRR1 degradation on HCT116 cell viability, colony survival assays were used. Cells were plated at low seeding densities and incubated in the presence or absence of both doxycycline and IAA. Any resulting colonies were stained with methylene blue and counted. Colony quantification was normalised to the untreated control for comparison between cell lines. Very little difference could be detected when considering the proportions of colonies formed in untagged controls (Figure 4.3: Tet-OsTIR1), and the LRR1 degrons treated with doxycycline or IAA alone (Figure 4.3: red, light blue, and green bars). Conversely, clear defects to cell viability were found upon treatment of the mAID-LRR1 cell lines with both

doxycycline and IAA (Figure 4.3: dark blue bars). Furthermore, statistical analysis revealed that the reductions observed were statistically significant (see Figure 4.3 and associated legend). The phenotypes presented were also shared between two independent CRISPR clones, demonstrating that the differences were likely a result of LRR1 protein degradation and not off-target Cas9 activity. Surprisingly, the degradation of LRR1 did not completely abolish cell viability, as was expected for the depletion of essential proteins. This may be due to incomplete protein degradation following activation of the AID system. Alternatively, the colon cancer derived cell lines used may have defects to the mechanisms or cellular sensors associated with defective replication termination.

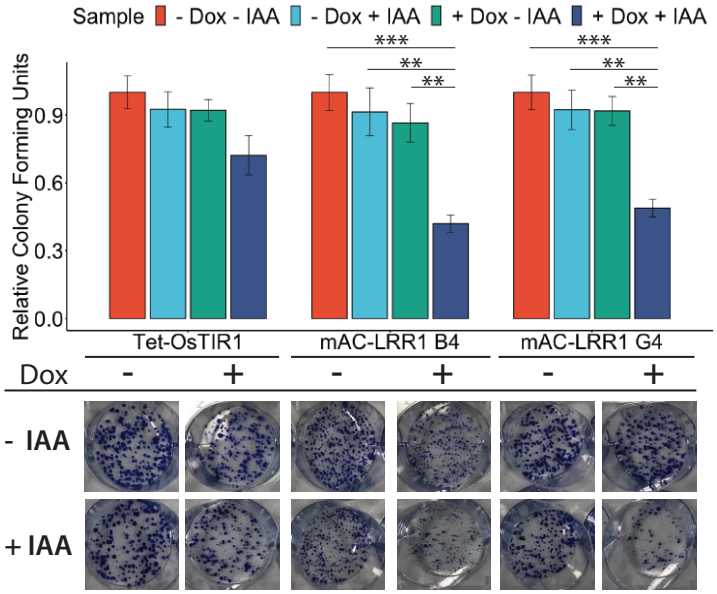


Figure 4.3: **LRR1 is Important for Cell Viability.** HCT116 Tet-OsTIR1 mAC-LRR1 cell lines were plated at different seeding numbers into individual wells of a 6-well plate. Approximately 24 hours later, 100 ng/µl of doxycycline was added as appropriate, followed by 100 µM IAA 24 hours after Dox addition. Treated cells were incubated for 7-11 days to allow colony formation and stained with methylene blue (bottom). Colonies were counted and normalised to untreated controls (top). Data shown was collected from 3 independent experimental repeats. Error bars depicting the standard error of the mean (SEM) are shown. Statistical analyses revealed normal data distribution and therefore parametric hypothesis testing was conducted (One-way ANOVA: Tet-OsTir1 F value = 2.675, p = 0.0749; mAC-LRR1 B4 F value = 10.21, p = 0.000274; mAC-LRR1 G4 F value = 11.24, p = 0.000154). Pairwise hypothesis testing was carried out between to further explore the differences identified within conditional LRR1 degron cells (Tukeys HSD), with significant differences shown on the plot.

4.2.4 Generation of Conditional Degron Cell Lines against TRAIP

Auxin-Inducible degron cells were also generated against the primary protein of interest for this PhD project, TRAIP. Previous work had highlighted that the N-terminal tagging of TRAIP altered its protein localisation when compared to both the reported endogenous location, and C-terminal tags; from the nucleolus to alternative punctate nuclear structures (Feng et al., 2016). Due to this, conditional TRAIP degron cells were generated with C-terminal mAID and mAC tags using the HCT116 CMV-OsTIR1 parental cell line (Figure 4.4). Genomic PCR was carried out with the primer pairs designed as detailed above (Figure 4.4B) to identify bi-allelically tagged clones (Figure 4.4C). Furthermore, to explore any potential roles for TRAIP in a non-cancerous background, conditional degrons were also created using hTERT-RPE1 Tet-OsTIR1 expressing parental cells (Figure 4.4D). Two TRAIP-mAID clones were shown to possess bi-allelic gene tagging in RPE1 cells. Of these, only 1 survived subsequent passaging. A full summary of the cell lines created is detailed in Table 2.6. Notably, for the entirety of the work conducted, the following clones were used: HCT116 TRAIP-mAID Clones C2 and D5, HCT116 TRAIP-mAC Clones C4 and F2, as well as RPE1 hTERT TRAIP-mAID; alongside the appropriate untagged control cell lines.

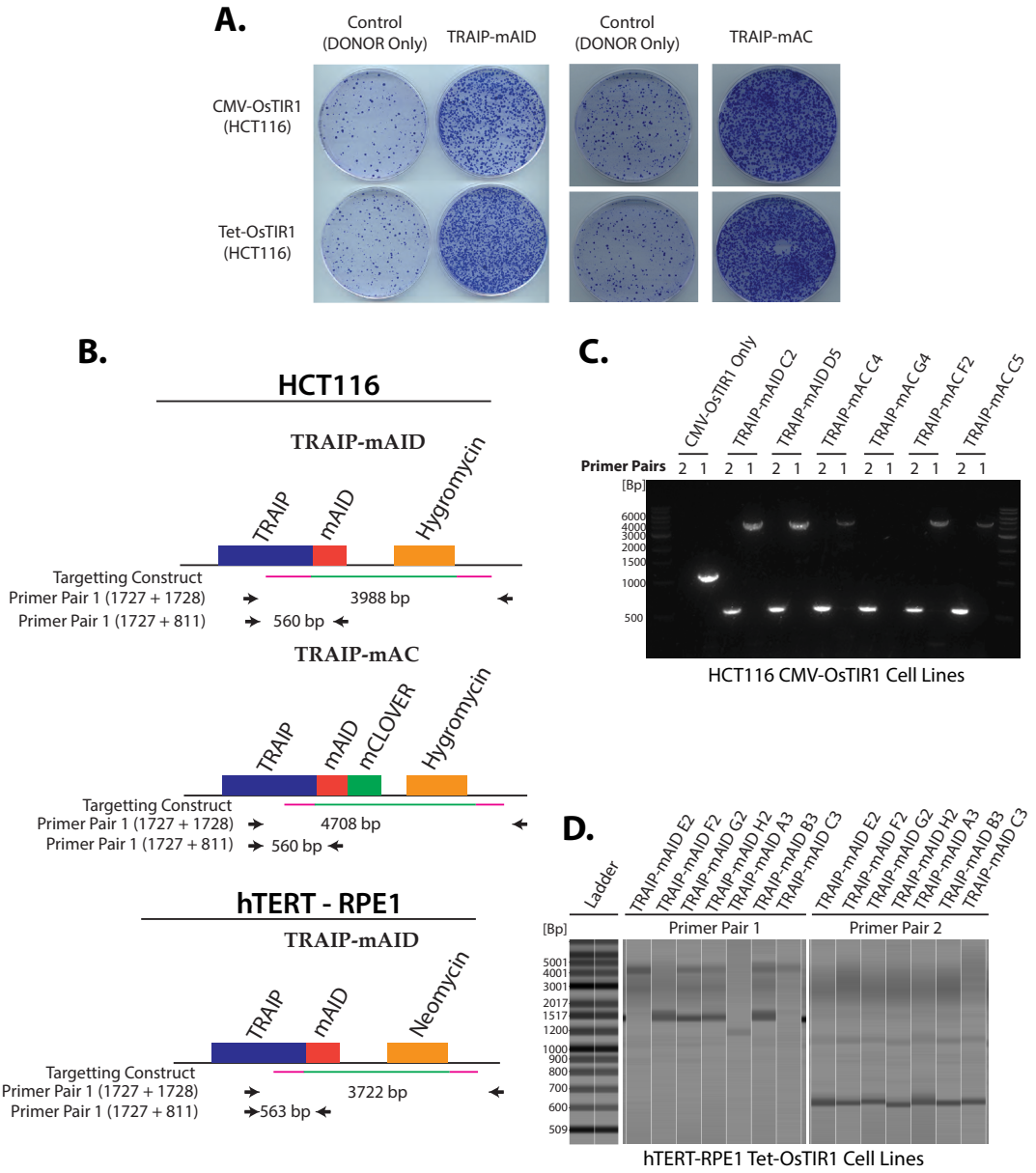


Figure 4.4: **Generation of Conditional Degron Cells Against TRAIP**. **A.** Cells colonies obtained after transfection for single-colony selection were stained with crystal violet stain for visualisation. **B.** Overviews of the tagging layouts. Endogenous TRAIP was tagged C-terminally with the appropriate degron tag along with an appropriate resistance marker. In HCT116 cells, hygromycin resistance was conferred by a phosphoglycerate kinase (PGK) promoter, encoded within the DONOR plasmid. In hTERT-RPE1 cells, neomycin/G418 resistance was conferred by a phosphoglycerate kinase (PGK) promoter, encoded within the DONOR plasmid. The positions of the designed targetting construct used to tag endogenous TRAIP is shown. Pink lines represent homology arms recognising endogenous DNA sequences. Green lines represent sequences to be inserted. Details of the sequences covered by the targetting construct is included in the materials and methods. Arrows indicate the position of primer pairs deigned to screen for bi-allelic gene tagging. Primers were designed to bind outside of the upstream and downstream targetting homology arms. **C.** Example DNA agarose gel following genomic PCR to screen for bi-allelic degron clones in a HCT116 CMV-OsTIR1 WT cell background. **D.** Example Multi-NA capillary electrophoresis result following genomic PCR to screen for bi-allelically tagged TRAIP degrons in an hTERT-RPE1 cell background.

4.2.5 TRAIP is Rapidly Degraded Following IAA Treatment

Following the generation and selection of bi-allelic TRAIP degron cells, I confirmed that the endogenously tagged protein could be degraded after auxin treatment. HCT116 TRAIP-mAID and TRAIP-mAC cells were treated with IAA for 24 hours and used to create whole cell extracts for immunoblotting. To detect TRAIP, we used an antibody created and kindly gifted by Prof. Niels Mailand (University of Copenhagen), used in Hoffmann et al. (2016). Figure 4.5A shows the resulting immunoblot from 24 hours IAA treatment. The ability of the provided antibody to recognise TRAIP was confirmed through band shifts, correlating to the approximate molecular weights of the degron tags used (mAID: 9 kDa, mAC: 35 kDa). In addition, no untagged protein was observed in TRAIP-mAID or TRAIP-mAC cell lines (53 kDa), confirming bi-allelic protein tagging. Furthermore, tagged TRAIP was found to be efficiently degraded after 24 hours of IAA treatment (Figure 4.5A). Although lower levels of TRAIP-mAID appeared to be expressed compared to other cell lines, this did not impair cell growth or viability.

Next, to further explore the kinetics of TRAIP degradation, timecourse experiments were carried out. Cells were treated with IAA over a 2-hour period and samples taken at the indicated times (Figure 4.5). Endogenously tagged TRAIP-mAID and TRAIP-mAC were found to be degraded, to below immunoblotting detection limits, in as little as 30 minutes (Figure 4.5B and Figure 4.5C). Importantly, the rapid nature of TRAIP degradation allows for protein depletion during specific cell cycle stages. Finally, as with LRR1, the included mCLOVER fluorescent tag could not be detected using either flow cytometry or fluorescent microscopy (data not shown).

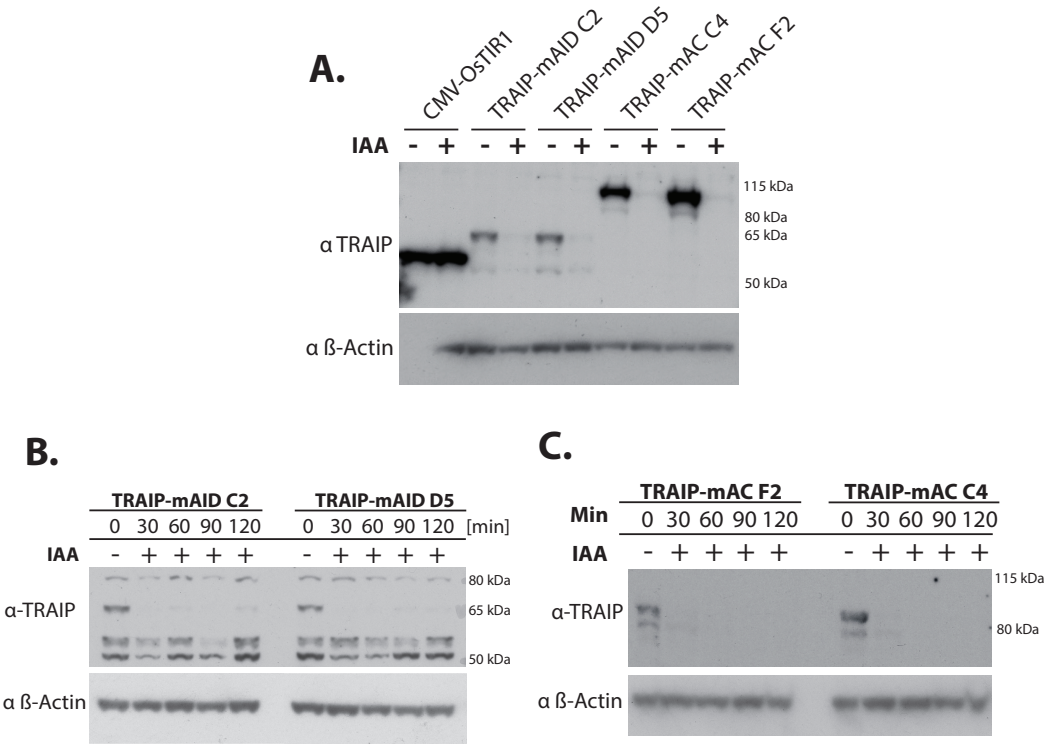


Figure 4.5: **TRAIP-mAID and TRAIP-mAC are Rapidly Degraded.** Immunoblotting experiments were carried out to understand the kinetics of TRAIP degradation. In all blots, TRAIP protein was detected using anti-TRAIP antibodies (Hoffmann et al., 2016). **A.** All cell lines were treated with IAA for 24 hours and analysed using immunoblotting. Band shifts, representative of the tag size, validated the antibody was able to recognise TRAIP. In all degron clones, endogenous TRAIP was shown to be efficiently degraded following IAA treatment. **B.** Timecourses of TRAIP degradation were carried out using TRAIP-mAID cell lines. TRAIP was revealed to be degraded after 30 minutes. **C.** Similar timecourse experiments were conducted in TRAIP-mAC cell lines, also degraded in 30 minutes.

4.2.6 TRAIP is Essential for Cell Viability

Before investigating any specific roles for TRAIP during individual cell cycle stages, we first aimed to understand the overarching consequences of TRAIP degradation. To explore this, we first utilised colony survival assays. HCT116 degron cells were plated at low seeding densities and treated with IAA for a period of 7-11 days. Following incubation, the cells were stained with methylene blue and counted as above for mAC-LRR1. In both the HCT116 TRAIP-mAID and TRAIP-mAC degron cell lines, long-term protein degradation was sufficient to completely abolish cell viability (Figure 4.6A-C). Moreover, as no such reductions were detected in

untagged control cell lines (Figure 4.6: CMV-OsTIR1), the observed defects appeared specific and not due to IAA cytotoxicity.

Whilst it was clear that TRAIP is an essential protein in HCT116 cells, it was not known whether these phenotypes also translated into a non-cancerous setting. To investigate this, similar cell viability assays were conducted using the hTERT-RPE1 TRAIP-mAID cell line. As the OsTIR1 expression in RPE1 cells was controlled by a tetracycline-sensitive promoter, the cells were first treated with doxycycline for 24 hours prior to IAA addition. Unsurprisingly, TRAIP-mAID degradation in RPE1 cells mirrored the phenotype shown in HCT116 cell lines, and the complete loss of cell viability was found (Figure 4.6D, red and dark blue bars). Interestingly, we also observed small reductions to the proportions of colonies following doxycycline addition only, not seen in the control cell lines (Figure 4.6D, red and green bars). It has been reported that the AID system can be 'leaky' (Yesbolatova et al., 2020), and the basal degradation of TRAIP in the absence of IAA was the most likely cause of the demonstrated sensitivity to doxycycline treatment.

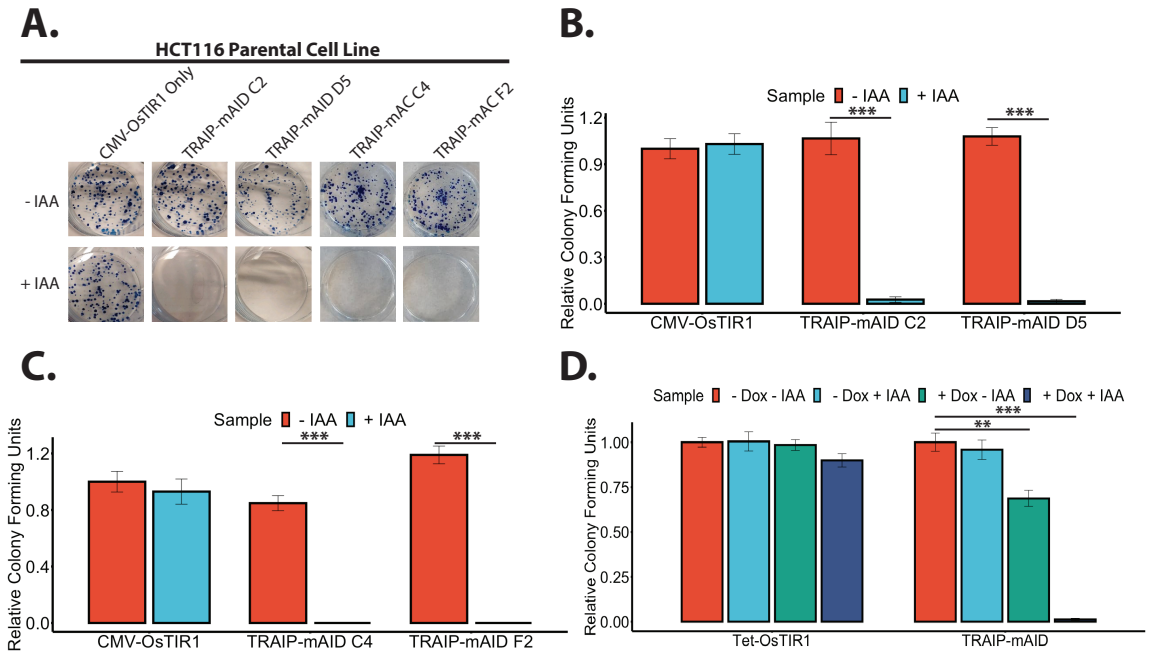


Figure 4.6: **TRAIP is Essential for Cell Viability.** To investigate the consequences of TRAIP degradation on cell viability, colony assays were used. Data shown was collected from three independent experimental repeats. **A.** Cells were treated with IAA for 7-11 days before being fixed, and stained with methylene blue. Shown are example images of representative samples from stained colony plates, used to calculate the relative colony forming units shown. **B.** Colony forming assays conducted in HCT116 TRAIP-mAID cells. Error bars depicting the standard error of the mean (SEM) are shown. Statistical analyses was carried out using T.tests. Significant differences were identified between TRAIP-mAID C2 ($p = 0.0002718$) and TRAIP-mAID D5 ($p = 0.0002739$). **C.** Colony forming assays conducted in HCT116 TRAIP-mAC cells. Error bars depicting the standard error of the mean (SEM) are shown. Statistical analyses was carried out using T.tests ($n = 3$). Significant differences were identified between TRAIP-mAC C4 ($p = 0.000161$) and TRAIP-mAID F2 ($p = 0.000159$). **D.** Colony assays in hTERt-RPE1 cells. Error bars depicting the standard error of the mean (SEM) are shown. Statistical analyses carried out using one-way ANOVA and Tukey's post hoc test. Relevant significant differences are shown (Untreated vs Dox: $p = 0.004$; Untreated vs Dox and IAA: $p = 0.0000011$).

4.2.7 TRAIP is Essential for Cell Proliferation and Cell Cycle Progression

TRAIP is Required for Cell Proliferation

The colony assays, exploring the effects of long-term protein degradation, revealed TRAIP to be an essential protein in both HCT116 and RPE1 cells. However, due to the associated lethality of this phenotype no additional information into the potential underlying factors could be determined. As a result, I next attempted to understand the respective impacts of shorter

periods of IAA treatment. Cells were plated at low seeding densities and treated with IAA over a 72-hour period, with samples taken and the total number of cells calculated every 24 hours. Due to the slower doubling time of RPE1 cells, proliferation curves were carried out using the faster cycling HCT116 cell lines only.

No differences were discovered, to relative cell numbers, between either the untreated and treated control cell lines (Figure 4.7 B-C, CMV-OsTIR1 only), or between control cell lines and the untreated TRAIP-mAID degron cells (Figure 4.7 A). Furthermore, the data presented correlated with that of the colony assays, demonstrating that the IAA treatment itself, or the inclusion of the degron tag, had no obvious effect on the cell's proliferative capacity. However, clear defects to cell proliferation were found following TRAIP degradation (Figure 4.7 B-C). Reductions to the total cell numbers were observed at all timepoints in the conditional TRAIP degrons treated with IAA. Subsequent statistical analysis revealed significant differences at all timepoints except at the 24-hour timepoint. This was likely a result of cells only having enough time to progress through the cell cycle once. The TRAIP-mAC and TRAIP-mAID curves were not directly comparable due to the experimental procedures being carried out at different times, with an alternative batch of FBS. Overall, this data suggested that TRAIP was directly required for cell proliferation, and that protein degradation over as little as 1-2 rounds of the cell cycle was sufficient to inhibit cell growth.

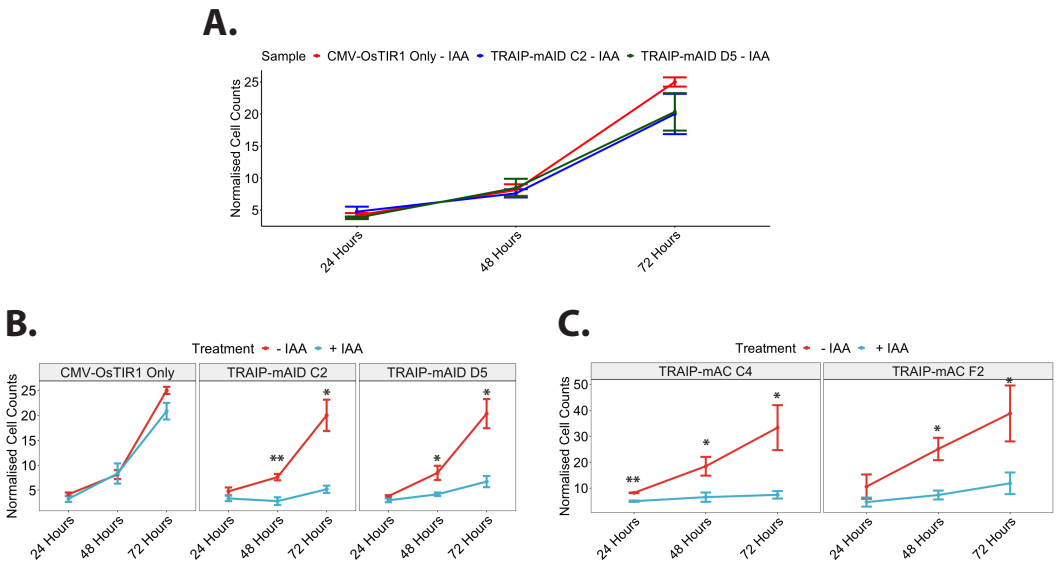


Figure 4.7: **TRAIP is Required for Cell Proliferation.** Growth curves were used to assess the impact of shorter term protein degradation on cell proliferation and growth. Cells were plated and treated with IAA before being incubated for 72 hours. Every 24 hours, samples were harvested and the total numbers of cells calculated. Cells were normalised to the seeding densities. Data collected from three independent experimental repeats was plotted. Error bars depicting the standard error of the mean (SEM) are shown. **A.** Untreated control cell lines were plotted alongside the two independent CRISPR TRAIP-mAID degron clones. No difference in growth at any timepoint was found. **B.** TRAIP-mAID cells were treated with IAA. Clear defects were observed to cell proliferation at all timepoints. Statistical significance was explored using T.tests for TRAIP-mAID C2 (48 hours: p = 0.0094; 72 hours: p = 0.03628) and TRAIP-mAID D5 (48 hours: p = 0.004; 72 hours: p = 0.3049). **C.** TRAIP-mAC cells were treated and plotted as in **B**. Similar to TRAIP-mAID, proliferation defects were also observed. Statistical significance was calculated using T.tests for TRAIP-mAC C4 (24 hours: p= 0.002158; 48 hours: p= 0.03; 72 hours: p= 0.04613) and TRAIP-mAC F2 (48 hours: p = 0.0399; 72 hours: p = 0.03326).

TRAIP is Required for Cell Cycle Progression

To investigate the impact of TRAIP on the cell cycle, samples were taken from each timepoint shown in Figure 4.7, stained with Propidium Iodide, and analysed using a flow cytometer. As with the previous data, no differences could be detected between untreated and treated controls (Figures 4.8-4.10, CMV-OsTIR1). Likewise, the fusion of the degron tag to TRAIP in HCT116 cells did not appear to impact cell cycle progression (Figures 4.8-4.10, red bars). Conversely, at all timepoints, cells lacking TRAIP were found to accumulate specifically during G2/M (Figures 4.8-4.10 D). Furthermore, reductions were also observed to the proportions of

cells residing in G1 and S-phase following TRAIP degradation (Figures 4.8-4.10 B-C). Statistical analysis revealed that the presented differences during G1 and G2/M were statistically significant in all clones and timepoints tested. However variations to the proportions of S-phase cells, characterised as any cell containing between 2N and 4N DNA content, were not. The differences in the total proportions of cells undergoing S-phase after TRAIP degradation were not observed consistently between all timepoints or across the four independent CRISPR clones. In addition, after 72-hours of TRAIP degradation, shifts to the DNA content of cells on the x-axis were seen (Figure 4.10 A). This was likely due to differences in the final harvested cell numbers, resulting from the loss of proliferation associated with TRAIP degradation (Figure 4.7). Differing cell numbers can result in slightly different staining conditions, often yielding different staining intensities and generating shifts in the signal detected.

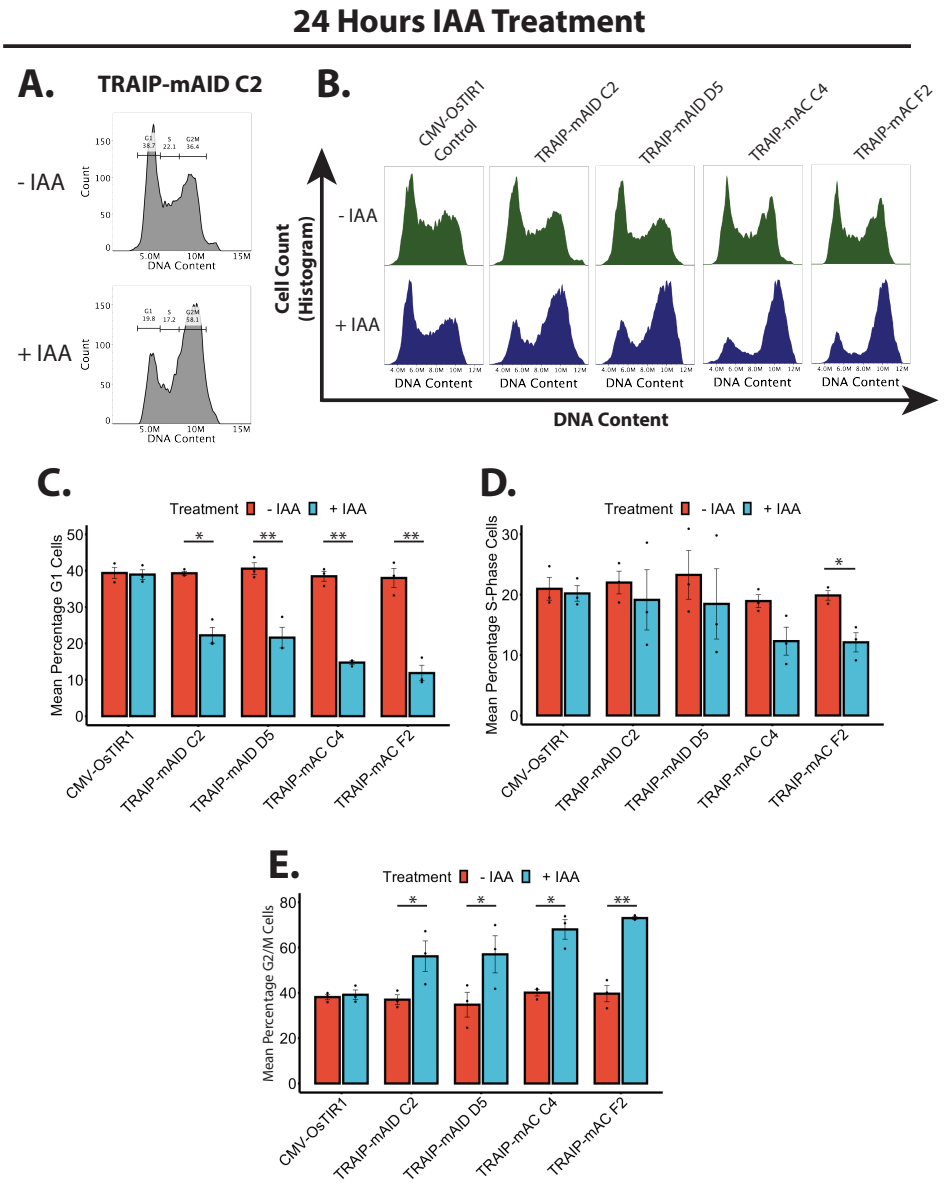


Figure 4.8: **Degradation of TRAIP leads to G2/M Cell Cycle Accumulation after 24 h of IAA Treatment.** Samples from the proliferation growth curves were analysed by flow cytometry to assess cell cycle progress. Data shown was collected from three independent experimental repeats. All error bars shown depict the standard error of the mean (SEM). **A.** Example of the gating strategy used. Raw data was initially gated as detailed in Figure 2.5. Histograms showing the total DNA content were then used to determine the relative proportions of cells in each cell cycle stage. Shown are G1 (2N DNA content), S-phase (2N < DNA content > 4N), and G2/M (4N DNA content) gates and associated quantification values for the representative example. **B.** Example plots obtained from the TRAIP degron cells treated with (blue) or without IAA (green) for 24 h. **C.** Quantification of the proportions of cells in G1 stage of the cell cycle. Differences were revealed in all degron clones: TRAIP-mAID C2 ($p = 0.0124$), TRAIP-mAID D5 ($p = 0.00873$), TRAIP-mAID C4 ($p = 0.00122$), and TRAIP-mAID F2 (0.00175). **D.** Quantification of the proportion of cells in S-phase. **E.** Quantification of the proportion of cells in G2/M. Differences were revealed in all degron clones: TRAIP-mAID C2 ($p = 0.0474$), TRAIP-mAID D5 ($p = 0.0483$), TRAIP-mAC C4 ($p = 0.0153$), TRAIP-mAC F2 ($p = 0.00978$).

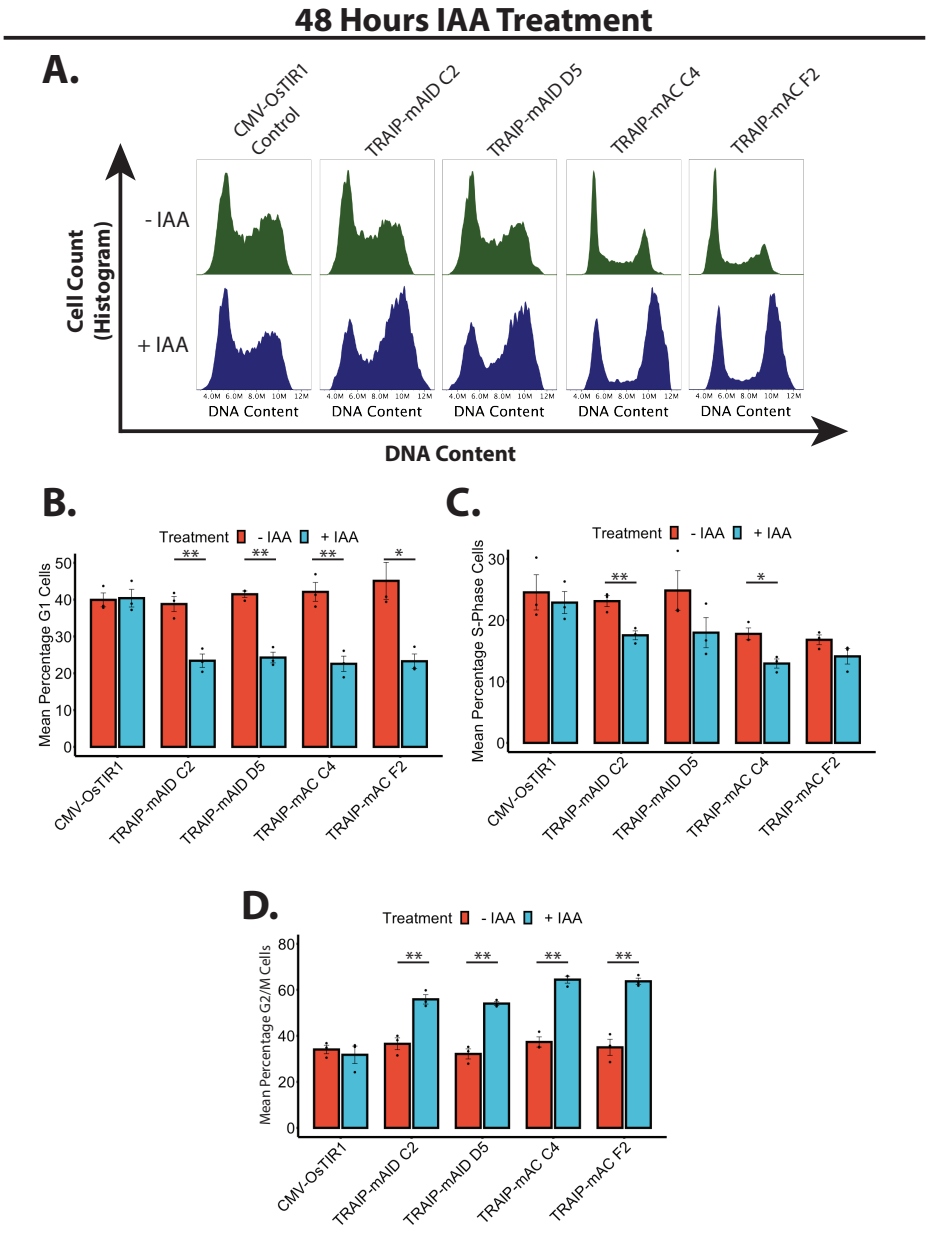


Figure 4.9: **Degradation of TRAIP leads to G2/M Cell Cycle Accumulation after 48 h of IAA Treatment.** Samples from the proliferation growth curves were analysed by flow cytometry to assess cell cycle progress. Data shown was collected from three independent experimental repeats. All error bars shown depict the standard error of the mean (SEM). The collected FACS data was gated as detailed in Figure 2.5 and 4.8A for quantification. **A.** Example plots obtained in samples treated with (blue) or without IAA (green). Example plots obtained in samples treated with (blue) or without IAA (green). A minimum of 10,000 cells were collected per condition within the cell cycle gate established (See Figure 2.5). **B.** Quantification of the proportions of cells in G1 stage of the cell cycle. Reductions after IAA treatment were revealed in all degron clones: TRAIP-mAID C2 ($p = 0.00510$), TRAIP-mAID D5 ($p = 0.00134$), TRAIP-mAID C4 ($p = 0.00470$), and TRAIP-mAID F2 (0.0352). **C.** Quantification of the proportion of cells in S-phase. Differences were found in TRAIP-mAID C2 ($p = 0.00978$) and TRAIP-mAC C4 ($p = 0.0188$). **D.** Quantification of the proportion of cells in G2/M. The accumulation of cells following TRAIP degradation was found in all degron clones: TRAIP-mAID C2 ($p = 0.00488$), TRAIP-mAID D5 ($p = 0.00478$), TRAIP-mAC C4 ($p = 0.00103$), TRAIP-mAC F2 ($p = 0.00754$).

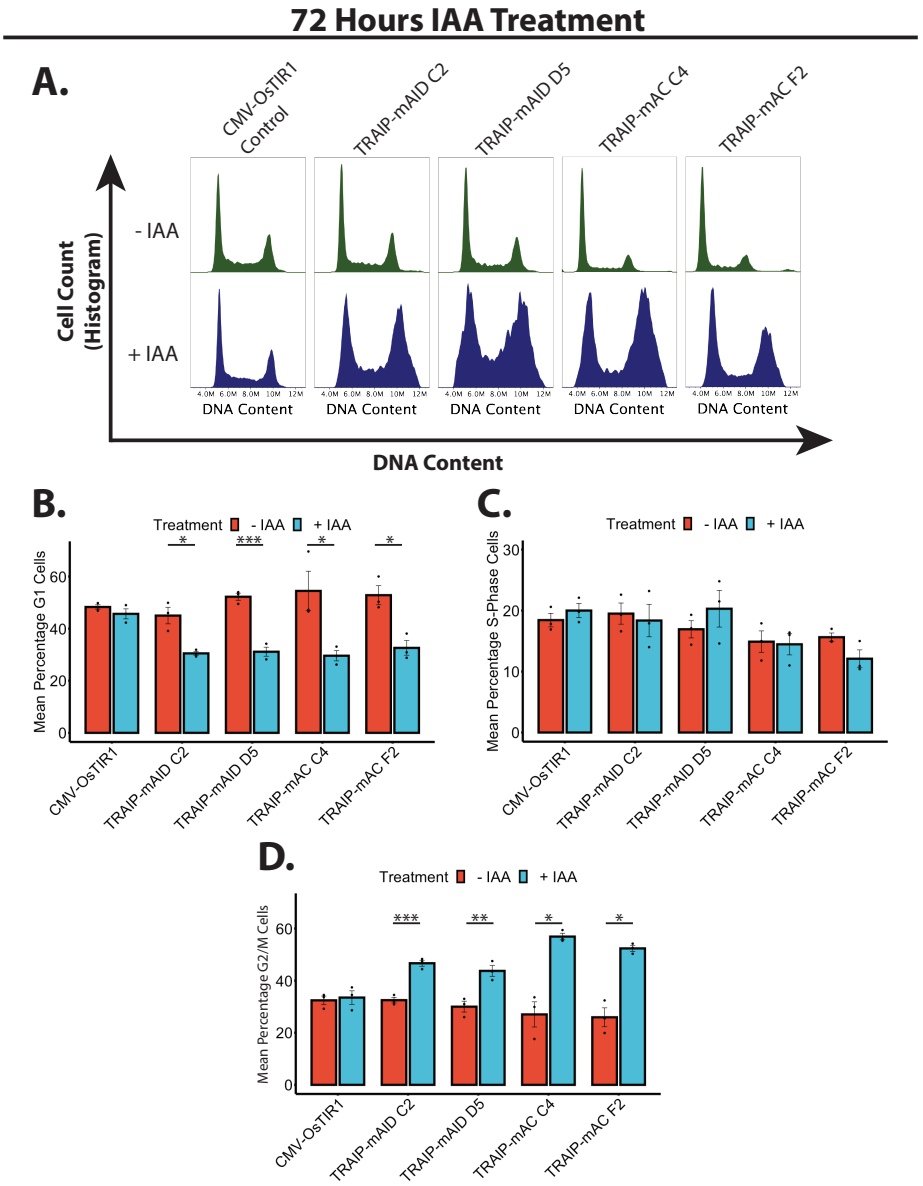


Figure 4.10: **Degradation of TRAIP leads to G2/M Cell Cycle Accumulation after 72 h of IAA Treatment.** Samples from the proliferation growth curves were analysed by flow cytometry to assess cell cycle progress. Data shown was collected from three independent experimental repeats. All error bars shown depict the standard error of the mean (SEM). The collected FACS data was gated as detailed in Figure 2.5 and 4.8A for quantification. **A.** Example plots obtained in samples treated with (blue) or without IAA (green). A minimum of 10,000 cells were collected per condition within the cell cycle gate established (See Figure 2.5). **B.** Quantification of the proportions of cells in G1 stage of the cell cycle. Reductions after IAA treatment were revealed in all degron clones: TRAIP-mAID C2 (p = 0.0380), TRAIP-mAID D5 (p = 0.000855), TRAIP-mAID C4 (p = 0.0364), and TRAIP-mAID F2 (0.0133). **C.** Quantification of the proportion of cells in S-phase. **D.** Quantification of the proportion of cells in G2/M. The accumulation of cells following TRAIP degradation was found in all degron clones: TRAIP-mAID C2 (p = 0.000890), TRAIP-mAID D5 (p = 0.00979), TRAIP-mAC C4 (p = 0.0197), TRAIP-mAC F2 (p = 0.0121).

Based on the data presented, it was concluded that the accumulation of cells during G2/M was

the primary phenotype of TRAIP degradation. Subsequently, due to this, and an overall lack of cycling cells, reductions were also observed to the proportion of cells in G1 and S-phase. Similarly, it was possible that a G2/M block during the cell cycle may have ultimately been causative of the losses shown to cell proliferation and cell viability. To gain further insight, any differences to the total numbers of cells containing abnormal DNA contents were recorded. DNA content lower than 2N is widely considered as a marker for cell death. On the other hand, any cells containing over 4N DNA content have likely undergone re-replication, a potential consequence of replication termination defects and common cause of genomic instability in cancer cell lines. Figure 4.11 summarises this data. Over the 72-hour IAA timecourse, cumulative increases to the proportion of cells displaying less than 2N DNA content were observed **??**. Statistical analysis revealed that, whilst general increases were found at every timepoint, the statistically significant differences were predominantly present after 72-hours of TRAIP degradation; likely when cells begin to undergo mechanisms for cell death. Next, investigation into cells undergoing re-replication found no effect upon TRAIP degradation (Figure 4.11 B, D, F). Significant differences were observed within a single sample set (TRAIP-mAC C4 treated with IAA for 48 hours), but this was not phenocopied by any other degron cell line, or at any other timepoint.

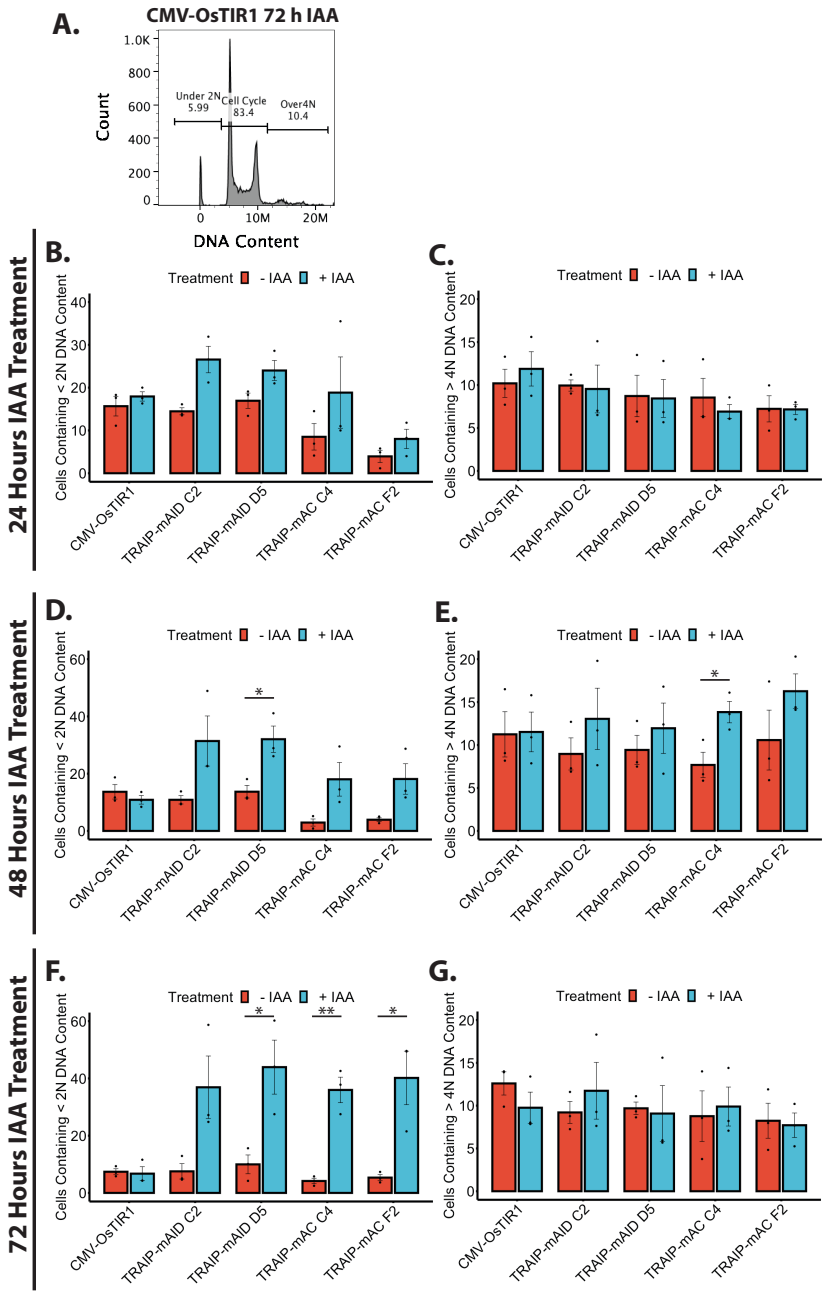


Figure 4.11: **TRAIP Depletion causes an Accumulation of Cells with < 2N DNA Content.** Cells treated with IAA were analysed by FACS to explore the emergence of cells with abnormal DNA content as a consequence of TRAIP degradation.Error bars shown depict the standard error of the mean (SEM). All data was parametric and so T-tests were used for statistical analysis (n = 3). **A.** Example gating strategy. Cells were gated as detailed in Figure 2.5 to obtain single-cell populations of interest. Populations of cells containing abnormal DNA contents were then quantified. Shown is CMV-OsTIR1 control cells treated with IAA for 72 h. **B.** Proportion of cells containing < 2N DNA content after 24 hours of IAA treatment. **C.** Proportion of cells containing > 4N DNA content after 24 hours of IAA treatment. **D.** Proportion of cells containing < 2 N DNA content after 48 hours of treatment. Statistical differences were shown between TRAIP-mAID D5 only (p = 0.0397). **E.** Proportion of cells containing > 4N DNA content after 48 hours of IAA treatment. Significant increases were shown in TRAIP-mAC C4 only (p = 0.0346). **F.** Proportion of cells containing < 2N DNA content after 72 hours of IAA treatment. Significant increases were shown in TRAIP-mAID D5 (p = 0.0282), TRAIP-mAC C4 (p = 0.00787), and TRAIP-mAC F2 (p = 0.0315). **G.** Proportion of cells containing > 4N DNA content after 72 hours of IAA treatment.

4.2.8 Cells without TRAIP accumulate in G2

Several studies have previously implicated TRAIP in key processes taking place during mitosis, including MiDAS, replisome disassembly, and the spindle assembly checkpoint (Sonneville et al., 2019; Moreno and Gambus, 2020; Chapard et al., 2014a). Given our observations, that cells without TRAIP accumulate during G2/M of the cell cycle, it was possible that these cells were arresting in mitosis due to mitotic problems. To test this, cells were treated with IAA for 24 hours and stained for the Serine 10 phosphorylation of Histone H3 (pH3), a marker of chromosome condensation during mitosis (Prigent and Dimitrov, 2003). The proportions of mitotic cells were then analysed using flow cytometry. This experiment was carried out using short IAA treatments (24 hours), allowing for most cells to complete the cell cycle only once. Due to the G2/M accumulation shown, it was possible that longer periods of IAA treatment, leading to fewer cycling cells, may have resulted in indirect impacts on the number of mitotic cells. Overall however, no differences in the total proportions of cells positive for pH3 could be identified following TRAIP degradation (Figure 4.12 A and B). To confirm this phenotype, cells were again treated with IAA for 24 hours, their DNA stained with DAPI, and imaged using a fluorescent microscope to detect cells with condensed chromosomes (mitotic index; Figure 4.12 C and D). This data mirrored the previous experiment, and no difference to the proportions of mitotic cells were detected. Furthermore, no evidence of mitotic catastrophe, a hallmark of mitotic problems, could be observed (data not shown). Altogether, cells without TRAIP were found to not accumulate in mitosis. Moreover, as we do not detect reductions to the proportions of mitotic cells it is also likely that TRAIP is not required for mitotic entry.

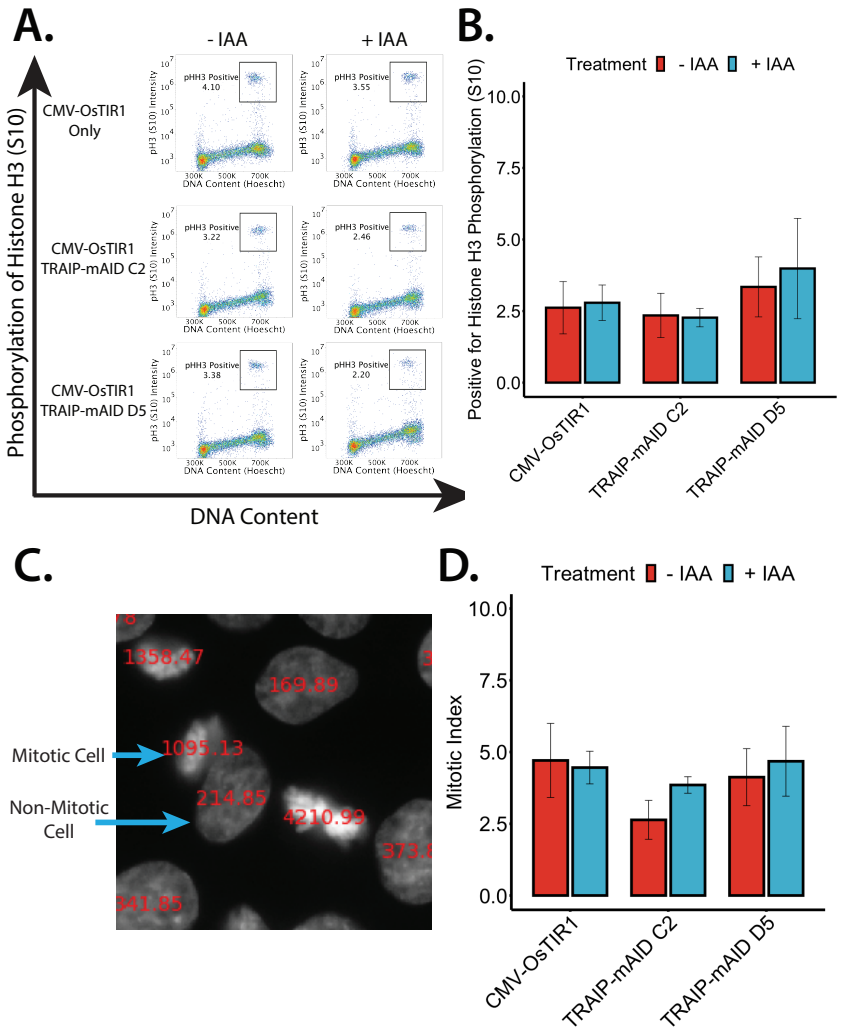


Figure 4.12: **Cells without TRAIP do not Accumulate in Mitosis.** To explore the proportion of cells in mitosis, degron cell lines were treated with IAA for 24 hours and stained for the Serine 10 phosphorylation of Histone H3; a marker of chromosome condensation. All figures were created using three independent experimental repeats. Data was found to be parametric, and so differences were analysed using T.tests. **A.** Example FACS plots for pH3 staining. Plots shown are the total DNA content (area) against the S10 pH3 intensity. The black box encapsulates those cells positive for mitosis. FACS data was collected from a minimum of 10,000 cells per condition passing the gating criteria in Figure 2.5. **B.** Quantification of the mean proportion of cells positive for S10 phosphorylation of Histone H3. Error bars shown depict the standard error of the mean (SEM). **C.** Example image from the mitotic index experiment. DAPI stained cells are shown with CellProfiler calculated pixel texture density shown in red text. Quantification was carried out using data from three experimental repeats (> 1000 nuclei per repeat). Cells found to contain a pixel texture density of > 1000 was considered mitotic. **D.** Quantification of the total proportions of cells found to contain condensed chromosomes by mitotic indexing. Error bars shown depict the standard error of the mean (SEM).

To explain the accumulation of cells in G2/M upon TRAIP degradation (Figure 4.8-4.10), cells lacking TRAIP must accumulate earlier in the cell cycle; specifically during very late S-phase or G2. To validate this, the degron clones were treated with IAA for 24 hours, stained for

two cell cycle markers: Mitosin/CENPF (G2 and mitosis) and pH3 (mitosis), and analysed using fluorescent microscopy. CENPF/Mitosin is a large kinetochore associated protein that is commonly used as a cell cycle marker due to its homogeneous nuclear distribution in G2 and mitosis (Rattner et al., 1993). By combining CENPF and pH3 staining, we were able to distinguish between cells in G2 (CENPF positive) and mitosis (CENPF and pH3 positive) (Figure 4.13 A). Only TRAIP-mAID degron cells were used for this experiment. Use of the TRAIP-mAC cells was avoided to prevent any potential contaminating signal from the mAC fluorescent tag, despite the preliminary testing indicating that we were unable to detect it (data not shown).

As observed above, no differences in the total proportions of cells in mitosis could be detected before or after TRAIP degradation, either by mitotic indexing or S10 pH3 staining (Figure 4.13 B and C, no WEE1i). Conversely, increased proportions of cells were found positive for CENPF, both with and without co-staining for pH3 (Figure 4.13 D and E, no WEE1i). Based on this, it was concluded that TRAIP degradation resulted in the specific accumulation of cells in G2 stage of the cell cycle. Moreover, treatment of cells with an inhibitor against WEE1 was sufficient to rescue the observed G2 accumulation (Figure 4.13 E, 1h and 3h WEE1i). In addition, increased proportions of mitotic cells were detected following 3 hours of inhibitor treatment, potentially due to the previously reported involvement of TRAIP in the spindle assembly checkpoint (Chapard et al., 2014a). WEE1 is a tyrosine kinase acting as a negative regulator for mitotic entry, and a key part of the G2/M cell cycle checkpoint (Ashwell, 2012). By inhibiting WEE1, cells in G2 of the cell cycle, particularly those under checkpoint control, would be forced into mitosis. Therefore, the rescue of the TRAIP-dependent G2 cell cycle accumulation by WEE1i treatment suggested that the conditional degron cells were arresting

due to checkpoint activation.

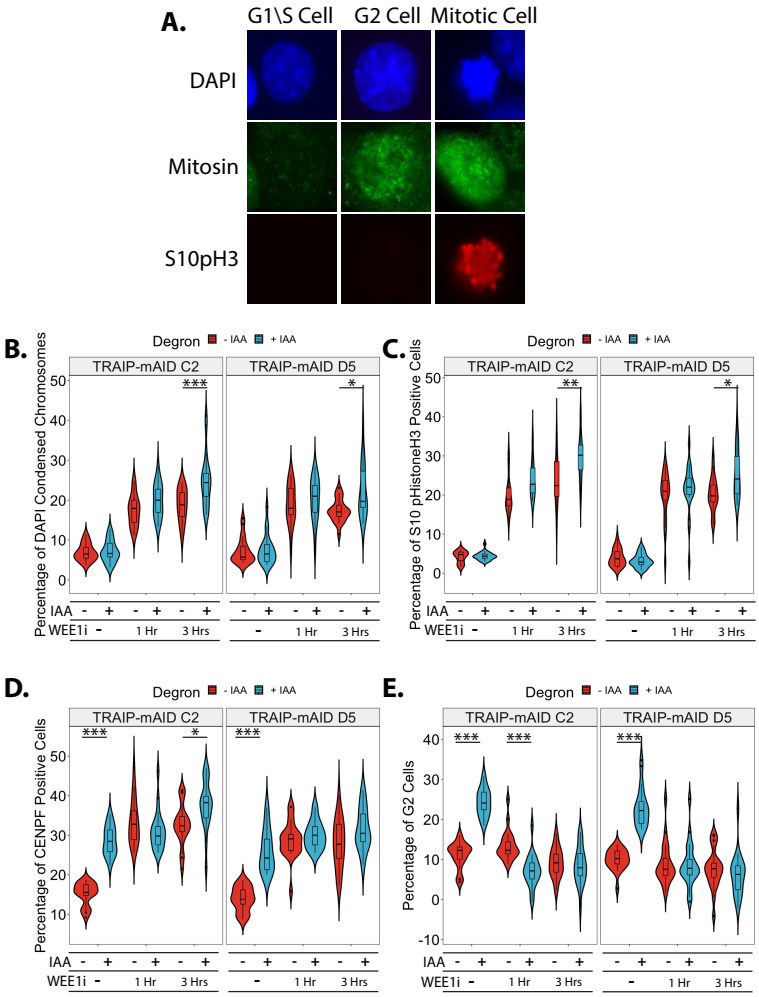


Figure 4.13: **Cells without TRAIP Accumulate in G2 by a WEE1 Dependent Mechanism.** Cells were treated with IAA for 24 hours and stained for CENPF (G2/mitosis) and S10 pH3 (mitosis). All data shown was collected over three independent experimental repeats. Statistical analyses were carried out using ANOVA followed by Tukey's post hoc test. Detailed pairwise values are Tukey's test results. An average of 1047 cells were quantified per condition, per repeat, to generate the plots shown. Plotted data is shown as violin plots, displaying the median and interquartile ranges as boxplots alongside the overall distribution of the data (violin). **A.** Example images. G2 cells were determined as those positive for CENPF and negative for S10 pH3. Mitotic cells were described as CENPF and S10 pH3 positive. **B.** Mitotic index was carried out on this data set. Significant increases in the proportions of mitotic cells were found after 3 hours of WEE1i treatment in both TRAIP-mAID C2 ($p = < 0.001$) and TRAIP-mAID D5 ($p = 0.0162$). **C.** Percentage of cells positive for S10 pH3 staining. Increases were found in both clones after IAA treatment and 3 hours of WEE1i treatment (TRAIP-mAID C2: $p = 0.00260$; TRAIP-mAID D5: $p = 0.0170$). **D.** Quantification of CENPF positive cells. Significant differences were shown between cells with or without TRAIP in TRAIP-mAID C2 Untreated ($p = < 0.001$), TRAIP-mAID C2 + Wee1i 3 hours ($p = 0.0294$), and TRAIP-mAID D5 untreated ($p = < 0.001$). **E.** Quantification of cells specifically in G2 (positive for CENPF, negative for S10 pH3). Significantly relevant differences were discovered in the following conditions: TRAIP-mAID C2 Untreated ($p = < 0.001$), TRAIP-mAID C2 1-hour WEE1i treatment ($p = < 0.001$), and TRAIP-mAID D5 Untreated ($p < 0.001$).

4.2.9 TRAIP-Dependent G2 Cell Cycle Arrest is Dependent on ATR but not ATM

In eukaryotic cells, the G2/M cell cycle checkpoints are governed by two master kinases: ATR or ATM. Typically, the ATM kinase is predominantly activated in response to double strand breaks. Alternatively, the ATR kinase is activated by a wide variety of sources, most notably replication stress (See **1.4**). However, regardless of the underlying mechanism, the treatment of arrested cells with WEE1 inhibitors would likely force mitotic entry. To attempt to identify the kinase responsible for the WEE1 dependent G2 arrest, cells were first treated with IAA in combination with inhibitors against ATR or ATM. The resulting cell cycle profiles were then assessed using flow cytometry. Treatment of TRAIP depleted cells with ATR inhibitors was sufficient to rescue the G2M cell cycle accumulation, whilst use of ATM inhibitors was not (Figure 4.14 A and B). Moreover, higher proportions of cells were found to accumulate in G2/M following treatment with both IAA and ATM inhibitors, when compared to IAA treatment alone. Overall, this data indicated that the G2 cell cycle arrest following TRAIP degradation was due to factors related to ATR kinase activation.

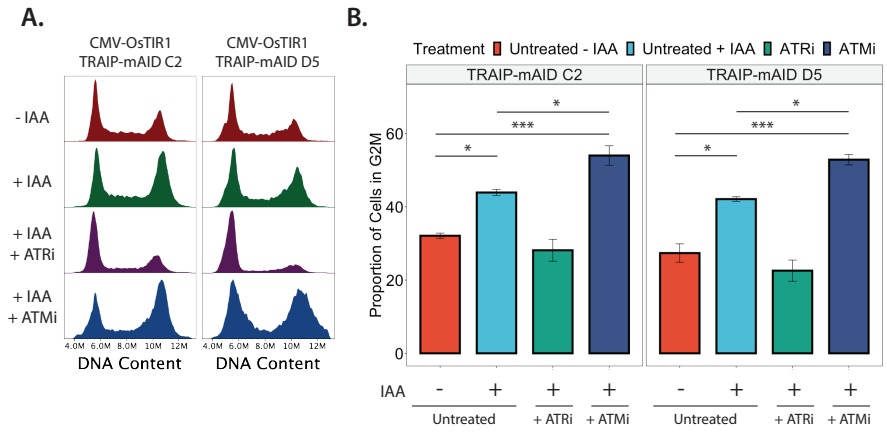


Figure 4.14: **TRAIP-Dependent G2 Cell Cycle Arrest is Rescued by ATR Inhibition.** To identify the kinase responsible for the G2 arrest caused by loss of TRAIP, cells were treated with IAA in combination with ATR or ATM inhibitors. Data was analysed using flow cytometry, and statistical analyses conducted using one-way ANOVA and Tukey post-hoc testing. A minimum of 10,000 cells were quantified per condition. Cells were gated to quantify the proportions of cells in G2/M (containing 4N DNA content) as detailed in Figure 2.5 and 4.8A. Data collected from three independent experimental repeats. **A.** Example cell cycle profiles. **B.** Quantification of the proportion of cells with G2/M DNA content. Plots show the mean percentage of cells in G2/M -/+ the standard error of the mean (SEM). IAA treatment alone caused G2M cell cycle arrest, as detailed previously (TRAIP-mAID C2: p = 0.0163; TRAIP-mAID D5: p = 0.00445). Treatment of cells with ATR inhibitor was shown to rescue the cell cycle arrest. Conversely, treatment with ATM inhibitor did not. Combined treatment with ATM inhibitors and IAA resulted in increased proportions of G2M cells, when compared to untreated control cell lines (TRAIP-mAID C2: p = 0.000332; TRAIP-maid D5: p = 0.000109), and those treated with + IAA alone (TRAIP-mAID C2: p = 0.0360; TRAIP-mAID D5: p = 0.0258).

4.2.10 Cells without TRAIP Exhibit Increased Cell and Nuclear Size

Whilst investigating the cellular consequences of TRAIP degradation, it became apparent that cells lacking TRAIP increased in size. To quantify this phenotype, I first reanalysed the flow cytometry data collected as part of the proliferation curves. TRAIP-mAID and TRAIP-mAC cells treated with IAA for 24 - 72 h were plotted based on the recorded forward scatter (marker of overall cell size) and side scatter (marker of cell granularity). Gates for cell sizes (Figure 4.15 A) were positioned using the main cell population identified in untagged controls (CMV-OsTIR1) and applied to all conditional degron cell lines. The gating strategy was established so that the main population of cells resided in the bottom left quadrant, with enlarged cells in the top right quadrant. Any cells in the other two quadrants showed non-linear growth, likely

possessing irregular cell size/granularity ratios, and were therefore not quantified. In all TRAIP degron clones treated with IAA, we observed increased proportions of enlarged cells (Figure 4.15).

Following this, I aimed to understand whether the increases to overall cell size translated to analogous increases in nuclear size. To this end, cells were treated with IAA for 24 - 72 h and DNA stained with DAPI for imaging using fluorescent microscopy. Nuclei were identified using an automated segmentation programme (CellProfiler), and the total nuclear pixel volume calculated. Comparable to the flow cytometry data, these experiments highlighted an overall increase in nuclear size following TRAIP degradation (Figure 4.16 A and B). Density plots of the data highlighted the pattern of enlarged nuclei. Overall shifts were observed from the untreated cell lines at all timepoints following IAA treatment, not seen in untagged control cell lines. Furthermore, 48 h of TRAIP degradation appeared to be the timepoint resulting in the maximal increase to nuclei size (Figure 4.16 C-E). It is well reported that G2 cells are larger than G1 or S-phase cells. However, the size increases shown appeared to extend beyond the natural fluctuations existing during the cell cycle. Therefore, it was likely that the increase of cell size was a direct result of TRAIP degradation, and not an indirect phenomenon caused by G2 cell cycle accumulation.

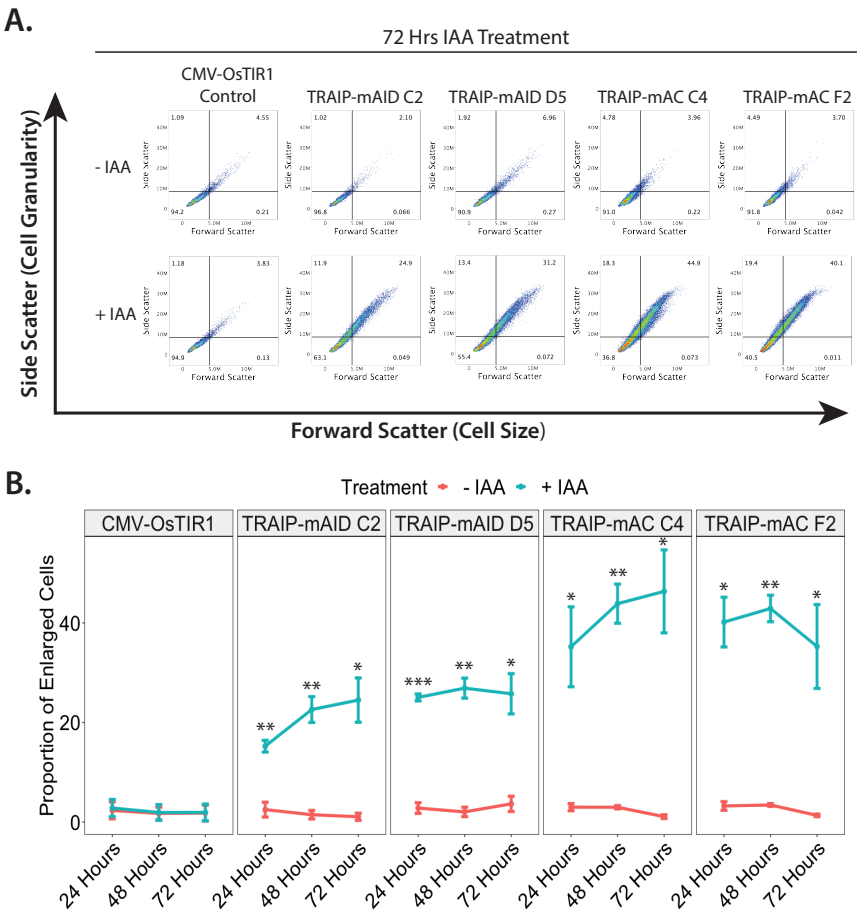


Figure 4.15: **Cells without TRAIP Exhibit Increased Cell Size.** Overall changes to cell size were quantified using Flow Cytometry Forward Scatter (cell size) and Side Scatter (cell granularity). A minimum of 10,000 cells were collected within the cell cycle gate established (See Figure 2.5). Quantification of the mean proportion of enlarged cells identified is shown on the plot (top right quadrant). Data shown is representative of three independent experimental repeats. **A.** Example FACS plots for all cell lines following 72 hours of IAA treatment. Enlarged cells were identified as those shifting into the top right quadrant. **B.** The proportion of enlarged cells. Plots were created using the mean percentage of enlarged cells -/+ standard error of the mean (SEM). Data were identified to be parametric, and so t-tests were used to assess significance. Increases to the proportion of abnormally large cells were shown at all timepoints for TRAIP-mAID C2 (24 hrs: $p = 0.00306$; 48 hrs: $p = 0.00906$; 72 hrs: $p = 0.0314$), TRAIP-mAID D5 (24 hrs: $p < 0.001$; 48 hrs: $p = 0.00193$; 72 hrs: $p = 0.0211$), TRAIP-mAC C4 (24 hrs: $p = 0.0279$; 48 hrs: $p = 0.00848$; 72 hrs: $p = 0.0320$), and TRAIP-mAC F2 (24 hrs: $p = 0.0155$; 48 hrs: $p = 0.00418$; 72 hrs: $p = 0.281$).

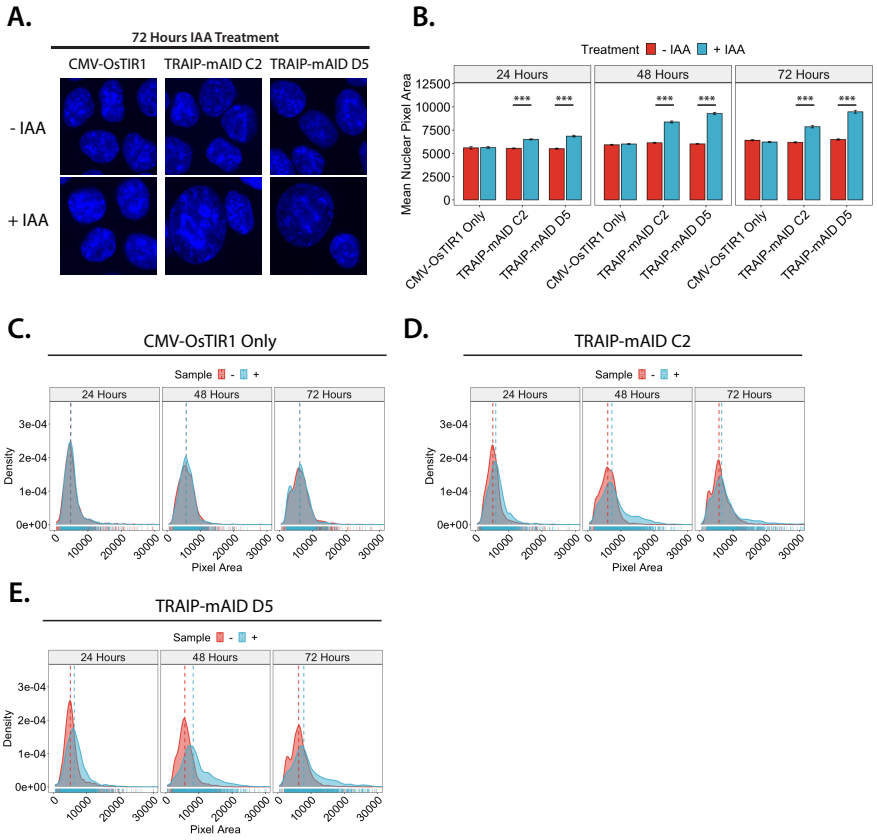


Figure 4.16: **Cells without TRAIP Exhibit Increased Nuclear Size .** Shown are data from three independent experimental repeats. An average of 674 cells were quantified per condition, per repeat. Overall changes to nuclei size were quantified using CellProfiler from DAPI stained cells imaged using a fluorescent microscope. The collected images were first segmented to identify nuclei, and then the average pixel area calculated. **A.** Example images showing the typical size increases found after 72 hours of IAA treatment. **B.** Mean pixel area for the nuclei is shown. Significant increases to nuclear area were shown in all degron clones at all timepoints tested ($p < 0.001$). Data is shown as the mean pixel area -/+ standard error of the mean (SEM). **C.** Density distribution of all nuclei detected. Shown are CMV-OsTIR1 control cells with (blue) or without (red) IAA at 24, 48, and 72 h timepoints. The median value is indicated by the dotted lines. **D.** Density distribution of all nuclei detected. Shown are TRAIP-mAID C2 control cells with (blue) or without (red) IAA at 24, 48, and 72 h timepoints. The median value is indicated by the dotted lines. **E.** Density distribution of all nuclei detected. Shown are TRAIP-mAID D5 control cells with (blue) or without (red) IAA at 24, 48, and 72 h timepoints. The median value is indicated by the dotted lines.

4.2.11 Cells Lacking TRAIP Exit the Cell Cycle in G2/M through Senescence

One major question remaining was to identify the mechanism underpinning the loss of proliferative capacity following TRAIP degradation. Intriguingly, reductions to cell proliferative capacity, cell cycle arrest, and increased cell size were all hallmarkers of senescence. Cell senescence describes the permanent prevention of proliferation through cell cycle exit,

classically occurring during G1 due to age-associated telomere shortening. However, more recently, data has emerged identifying senescence as a potential tumorigenesis protection mechanism, preventing damaged cells from dividing. Moreover, in the case of accumulating replication stress, G2-specific senescence has been reported to be associated with ATR and ATM activation (Gire and Dulic, 2015). To check whether TRAIP deficient cells were exiting the cell cycle by senescence, I utilised a β-galactosidase assay, as the hydrolase β-galactosidase is widely expressed in senescent cells. Through the addition of a modified substrate, cleavable by β-galactosidase to produce a fluorescent signal, the detection of senescent cells within a population was achieved (Figure 4.17A). TRAIP-mAID cells were treated with IAA for 24 to 72 h, the β-galactosidase substrate added for 45 min immediately before harvesting, and any cells positive for β-galactosidase activity assessed using flow cytometry. Due to the signal emitted following substrate breakdown in the FITC channel, TRAIP-mAC cells were not used. At all timepoints tested, the presence of senescent cells was discovered (Figure 4.17 B). Furthermore, the comparison of the senescent population of cells, with total DNA content, revealed these cells to reside in G2/M stage of the cell cycle (Figure 4.17 C). Altogether, the presented data suggested that G2-associated cell cycle exit was the ultimate consequence of TRAIP degradation, and the causative factor of the loss of proliferative capacity.

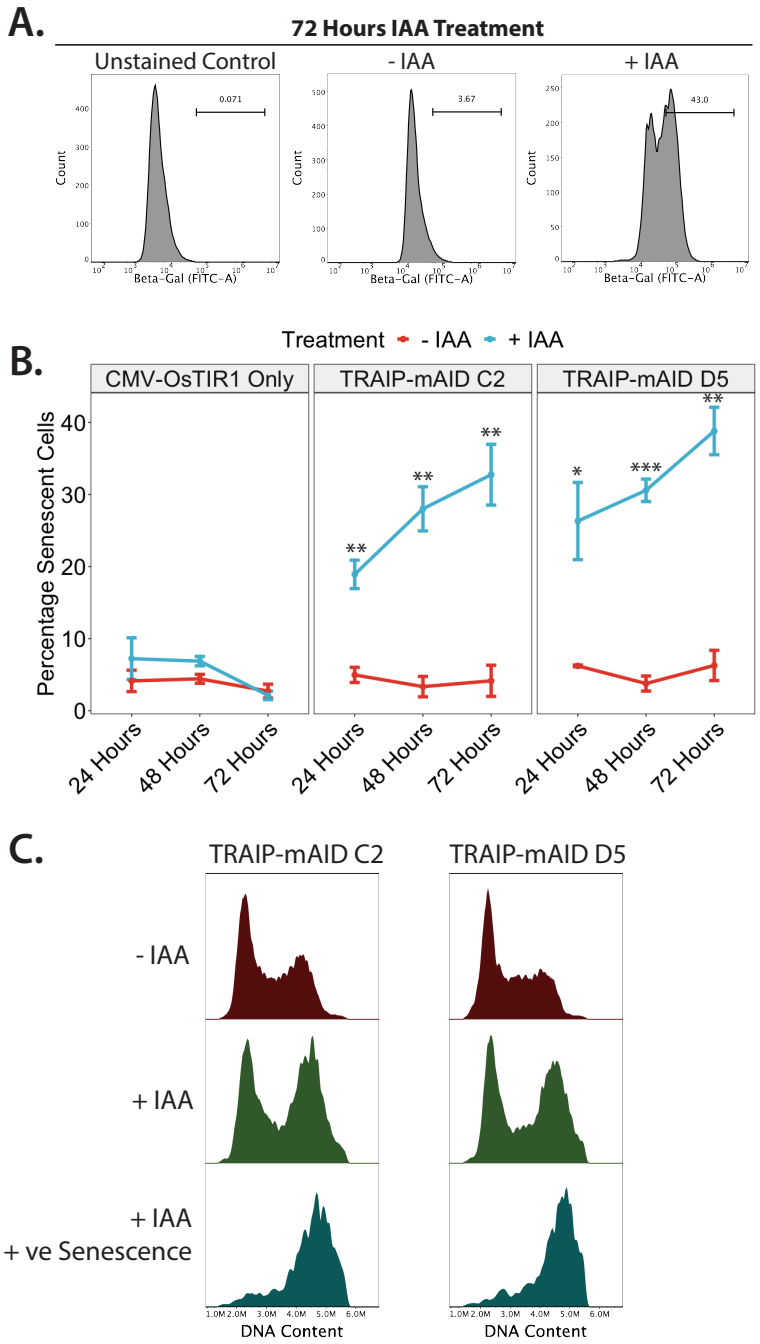


Figure 4.17: **Cells Lacking TRAIP Exit the Cell Cycle in G2/M *via* Senescence.** β- galactosidase assays were used to detect the presence of senescent cells following TRAIP degradation. A minimum of 10,000 cells within the cell cycle gate established (See Figure 2.5) were used for quantification. All data shown was collected from three independent experimental repeats **A.** Example FACS histograms for detectable β-galactosidase activity. Shown are untreated control cells, and TRAIP-mAID C2 cells treated with and without IAA for 72 hours. Positive peaks of signal are indicated by the gated regions. **B.** Quantification of the proportions of senescent cells within the cell population. Data is shown as the mean percentage cells -/+ standard error of the mean (SEM). Data was parametric and so t-tests were used to compare -/+ IAA at each respective timepoint. Significant increases were shown for TRAIP-mAID C2 (24 hrs: p = 0.00118; 48 hrs: p = 0.00651; 72 hrs: p = 0.00925) and TRAIP-mAID D5 (24 hrs: p = 0.003; 48 hrs: p = < 0.001; 72 hrs: p = 0.00220). **C.** To identify where in the cell cycle cells were entering senescence, the senescent populations of cells were compared with the total DNA content. Cells were shown to be leaving the cell cycle specifically in G2M.

4.2.12 TRAIP Degradation does not Induce Apoptosis in HCT116 Cell Lines

Whilst G2-associated senescent cells explained the observed cell cycle accumulation and loss of cell proliferation following TRAIP degradation. It did not offer clarification as to the increased proportions of cells containing < 2N DNA content (Figure 4.11A, C, and E). Cells that contain reduced amounts of total DNA content commonly have fragmented nuclei; a key phenotype associated with apoptosis. Therefore, we asked whether there was a secondary population of apoptotic cells present after TRAIP degradation. To detect apoptotic cells, cell impermeable fluorescent conjugates specific for Annexin V were used. Annexin V is a phospholipid binding protein associated with the cytoplasmic surface of the plasma membrane in healthy cells. Upon the induction of apoptosis, structural changes result in the translocation of Annexin V, from the intracellular plasma membrane surface, to the extracellular side for macrophage recognition (Demchenko, 2013). Harvested cells were incubated with conjugates for Annexin V recognition before being analysed by flow cytometry. Hydroxyurea treatment was used as a positive control, resulting in the detection of an apoptotic proportion of cells (Figure 4.18A). Conversely, no differences could be found to the proportions of cells entering apoptosis, between either the control cell lines or TRAIP-mAID degrons treated with or without IAA (Figure 4.18 A and B). This result was not necessarily surprising, as senescence is known to inhibit cells from entering apoptosis (Gire and Dulic, 2015). However, the cause of the increased proportion of cells found containing < 2N DNA contain was not known. It was likely that this was an ultimate read-out of cell death following TRAIP degradation, although the precise mechanisms involved remained unclear.

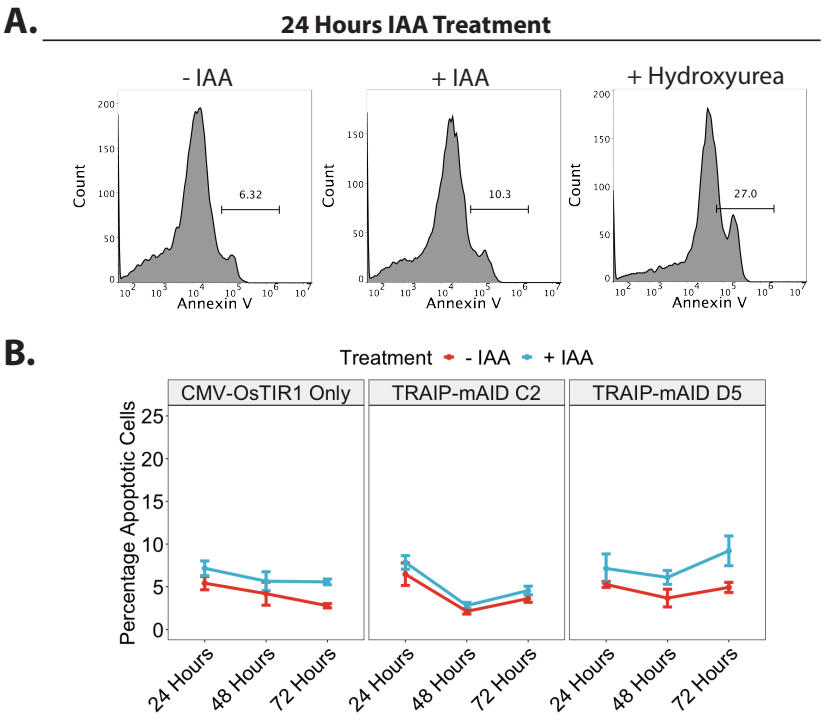


Figure 4.18: **TRAIP degradation does not lead to high levels of apoptosis in HCT116 cells.** To understand whether the proportion of cells containing < 2N DNA content following TRAIP degradation were due to apoptosis, Annexin V FACS assays was used. Cells were treated with IAA for 24 to 72 hours. Data shown was collected from three independent experimental repeats. A minimum of 10,000 cells were quantified per condition. **A.** Example FACS plots showing the detected signal for Annexin V. The gated regions highlight positive signal. No differences were detected between – and + IAA treatment. Conversely, a clear positive population of apoptotic cells was found upon hydroxyurea treatment. **B.** quantification of the mean percentage positive for apoptosis. Data is shown as the mean percentage cells -/+ standard error of the mean (SEM). Significance was assessed using t.tests, but no differences were found.

4.3 Discussion

Throughout this chapter, several conditional degron cell lines against two key proteins involved in replisome disassembly were established. Due to the essential nature of processes associated with DNA replication, it was imperative to generate a mammalian cell model enabling cell-cycle stage specific protein degradation. Alternative methods of protein depletion (e.g., siRNA or shRNA), facilitating incremental protein loss over prolonged periods of time, may have led to the appearance of indirect secondary phenotypes due to defective DNA replication

and associated recovery mechanisms. In addition, many ubiquitin ligases target different substrated at different stages of the cell cycle. For example, Cullin2^{LRR1} has been shown to ubiquitylate the cell cycle regulator p21 independently of the reported replisome disassembly mechanisms (Fan et al., 2021; Starostina et al., 2010). Moreover, TRAIP has also been implicated in processes specific for both S-phase and mitosis. Therefore, methods inducing global protein depletion over several rounds of the cell cycle would likely affect multiple pathways, potentially antagonistically or additively to phenotypes caused by replication defects.

Auxin-inducible degradation was the system of choice to induce protein degradation, primarily because of the rapid 20-minute half-life reported (Natsume et al., 2016). Over recent years several degron technologies have emerged exploiting existing cellular mechanisms to mediate the degradation of proteins of interest. Notably, these techniques often revolve around the use of CRISPR-Cas9 to modify the respective protein of interest, and commonly utilise functional ubiquitin-proteasome pathways. Importantly, facilitating protein degradation instead of gene expression level overcomes several limitations of alternative techniques (e.g., off-target effects and the requirement for protein turnover) (Roth et al., 2019). Several different degron technologies are available, including systems where ligand addition directly induces protein degradation (e.g., PROTAC, AID, and SMASh), and those where proteins of interest are degraded in the absence of stabilising compounds (e.g., FKBP12 and UnaG) (Banaszynski et al., 2006; Chung et al., 2015; Navarro et al., 2016; Paiva and Crews, 2019). As an alternative to AID, one system of note is the HaLo tag; allowing for both protein degradation as well as fluorescent labelling or protein purification through the addition of modified ligands (Buckley

et al., 2015).

LRR1 was tagged N-terminally for the creation of Auxin-Inducible Degrons using HCT116 parental cell lines. Interestingly, fewer clones were detected during the generation of LRR1 degron cells when compared to TRAIP (compare Figure 4.1A and 4.4A). The N-terminal tags used comprised of the mAID degron as well as a respective antibiotic selection marker, separated by a self-cleavage P2A domain. As a result, the expression of the selection marker was under endogenous promoter control. Whereas during C-terminal tagging, the selection marker was expressed from an exogenous constitutive promoter inserted into the genome adjacent to the degron. It was possible that, due to the low LRR1 expression levels (see **4.2.2**), transfected cells were not entirely resistant to the selection drug used. This may also explain why it was not possible to generate conditional LRR1 degrons using a non-cancerous background (hTERT-RPE1 cells). Similarly, attempts to create double-degrons using C-terminal SMASh-mAID tags were also unsuccessful. Recently, the tertiary structures for LRR1 in complex with Cullin2 have been resolved in *X. laevis*, *S. cerevisiae*, and mammalian cells. This data confirmed the requirements of the LRR1 C-terminus for Cullin2 complex formation. In addition, zinc finger domains required for protein stability were also discovered close to the C-terminus. On the other hand, N-terminal regions were poorly resolved, not directly required for Cullin2 interaction, and reported to be mostly unstructured (Jenkyn-Bedford et al., 2021; Zhou et al., 2021). Given this, it was likely that the inclusion of tags onto the C-terminus of LRR1 would prevent $Cullin2^{LRR1}$ complex formation and were therefore not viable.

The role of LRR1 in replisome disassembly has been well characterised previously using

X. laevis egg extracts, *C. elegans*, and *S. cerevisiae* (see **1.3.4**). However, the requirements for LRR1 in mammalian cells is less well understood. A recent study by Fan et al. (2021) identified LRR1 as a CDK4/6 regulated gene required for DNA replication and mitosis in human cells. Using RPE1 cells, and existing gene fitness data (Hart et al., 2015), the authors demonstrated LRR1 to be an essential gene (Fan et al., 2021). On the other hand, the depletion of LRR1 using siRNA did not affect cell viability (Starostina et al., 2010). Similarly, in our data, the degradation of mAC-LRR1 did not completely abolish cell viability, as was expected for the loss of essential proteins. This may be due to incomplete protein degradation following IAA treatment, with small proportions of LRR1 potentially capable of fulfilling the respective cellular role. Alternatively, the colon cancer derived cell lines used for making degrons may be less sensitive to LRR1 degradation than the non-cancerous RPE1 cell line.

Previous work has highlighted TRAIP to be an essential gene, for both mouse embryonic development and immortalised human cell culture (Hart et al., 2015; Park et al., 2007). Similarly, the degradation of TRAIP-mAID and TRAIP-mAC in both HCT116 and RPE1 cells led to the abolishment of cell viability. Interestingly, however, gene knockouts of TRAIP in mouse oocytes or immortalised mouse embryonic stem cells did not possess the associated lethality (Villa et al., 2021; Yuan et al., 2016). Despite this cells without TRAIP were reported to exhibit slowed rates of proliferation (Park et al., 2007; Villa et al., 2021; Yuan et al., 2016). In patients, TRAIP mutations causing primordial dwarfism (Seckel Syndrome) are also characterised by limited cell proliferation (Harley et al., 2016). Analogously, short-term TRAIP-mAID and TRAIP-mAC degradation in HCT116 cells was found to inhibit proliferation, likely through the observed G2 cell cycle accumulation. Increased proportions of G2/M cells following TRAIP

depletion have also been reported previously using RNAi (Feng et al., 2016; Harley et al., 2016; Hoffmann et al., 2016). Overall, the phenotypes of TRAIP degradation corroborate with that of previously published data. Therefore, the generated conditional TRAIP degron cells are a viable model for investigation into the mechanism of action for TRAIP during the unperturbed eukaryotic cell cycle.

The observed G2 cell cycle accumulation in cells without TRAIP offered clarification for the underlying mechanisms surrounding the reductions to cell proliferation. Moreover, the accumulating population of cells was rescued by ATR and WEE1 inhibitor treatment, suggesting that these cells were arresting due to G2 checkpoint activation (ATR-WEE1-CHK1 axis). ATR predominantly functions in response to stalled replication forks as part of the replication stress response. In support of this path of thinking, TRAIP has been previously reported to interact with key components of the replication fork to promote genomic stability following the induction of replicative stress and DNA damage (Deng et al., 2019; Feng et al., 2016; Hoffmann et al., 2016; Harley et al., 2016). Notably, TRAIP is required specifically at barriers to the replication fork that would otherwise block CMG progression (Larsen et al., 2019; Wu et al., 2019). Alternatively, TRAIP may possess direct roles in the DNA damage response, independent of any replisome-association. TRAIP interacts directly with the double-strand break repair proteins Ku70-80, SMARCA5, and DNA-PK (Gleich et al., 2021). In addition, cells depleted of TRAIP were found to exhibit reduced levels of ATM activation following the induction of double-strand breaks (Gleich et al., 2021). The treatment of our conditional TRAIP degrons with ATM inhibitors did not rescue the G2/M cell cycle accumulation. However, higher proportions of cells were observed accumulated in G2/M following TRAIP degradation

and ATMi treatment. This suggested that, whilst any interactions between TRAIP and ATM were not the primary cause of the losses to cell proliferation, additional interactions may have been present. It is known that prolonged replication fork stalling can eventually result in fork collapse and double-strand break formation (Petermann and Helleday, 2010; Zeman and Cimprich, 2014). Therefore, the phenotypes observed may have been representative of increased fork collapse, and the requirement for increased double-strand break repair in cells treated with IAA.

In addition to the reported roles for TRAIP during S-phase, mitotic aberrations have also been previously observed following TRAIP depletion (increased micronuclei and chromosomal rearrangements) (Deng et al., 2019; Feng et al., 2016; Hoffmann et al., 2016). It is possible that the mitotic phenotypes demonstrated were representative of further mechanisms of TRAIP throughout the cell cycle, alongside roles in mitotic DNA synthesis and the spindle assembly checkpoint (Chapard et al., 2014a; Sonneville et al., 2019). Alternatively, high levels of replicative stress during S-phase can persist into mitosis, and often result in increased frequencies of micronuclei, anaphase bridges, and chromosomal rearrangements (Fenech et al., 2011). However, persisting replication stress also commonly induces cell death through mitotic catastrophe, not detected in our work.

The ultimate consequence of TRAIP degradation in the HCT116 cells appeared to be G2/M cell cycle exit by senescence. Traditionally, senescence was thought to be triggered during G1 stage of the cell cycle by increasing DNA damage. This leads to the activation of the CDK inhibitors p21 and p16, preventing Rb phosphorylation and cell cycle progression (Gire and Dulic, 2015).

However, p21 was also shown to be a key regulator for sustaining G2 cell cycle arrest induced by the DNA damage checkpoint (Bunz et al., 1998; Dulić et al., 1998), raising the possibility of a G2 cell cycle exit programme. Since this discovery, a number of studies have demonstrated the existence of G2-stage cell senescence. First, large proportions of human fibroblasts entering replicative senescence were found to possess 4N DNA content. Subsequent analyses of this population revealed mono-nucleated cells only, confirming G2 cell cycle exit and ruling out the possibility of G1-associated senescence following mitotic bypass (Mao et al., 2012). Second, G2-cell senescence has also been highlighted following prolonged exposure to the genotoxic agents ICRF-193 (topoisomerase inhibitor) and bleomycin (induces DSB) (Baus et al., 2003). In both cases, G2-cell cycle exit occurred by a mechanism dependent on p21, p53, and the phosphorylation of retinoblastoma proteins. Similar G2-cell cycle phenotypes have also been observed following γ-irradiation (Flatt et al., 2000), infrared irradiation (Krenning et al., 2014), in telomerase negative cells (Jullien et al., 2013), and *in vivo* using human congenital naevi (Michaloglou et al., 2005). Despite this work, the practical existence of G2-stage cell cycle exit is highly debated. Specifically, whether these cells are truly in G2 stage of the cell cycle, or in G1 with 4N DNA content due to mitotic bypass mechanisms. In my work, I could not detect any clear signs of multi-nucleated cells likely indicative of this; although more robust microscopy techniques, incorporating cytoplasmic markers, should be conducted to confirm these observations. Altogether, G2 cell cycle exit has been proposed to safeguard against adaptation to long-term G2 arrest, that may otherwise result in eventual mitotic entry (Gire and Dulic, 2015).

The loss of cell proliferation induced by senescence may also form an important

anti-tumorigeneses mechanism. Patients presenting with TRAIP mutations (Seckel syndrome) do not possess increased cancer disposition, commonly associated with mutations to genes involved in DNA replication and DNA damage repair (Harley et al., 2016). Furthermore, TRAIP does not appear to be highly mutated across different cancer types (< 1% overall) (Tate et al., 2019). The G2/M senescence reported following the loss of TRAIP, therefore, may be antagonistic to tumour development. It would be of interest to explore the extent of TRAIP-mediated cell senescence further. Increased β-galactosidase has been reported in both cell senescence (permanent cell cycle exit) and quiescence (temporary cell cycle exit) (Terzi et al., 2016). In addition, as no defects to the mitotic proportions of cells following TRAIP degradation could be detected, cells accumulating in G2 may eventually be able to progress into mitosis. To address this, the population of senescent cells following TRAIP degradation should be confirmed using a second method (such as detecting p16 or p21 levels in cells). Following this, experiments exploring whether TRAIP deficient cells can re-enter the cell cycle should be conducted. Senescence has also been reported to inhibit apoptosis (Vicencio et al., 2008). The degradation of TRAIP-mAID and TRAIP-mAC was did not induce apoptosis in HCT116 cell lines, despite the presence of increased proportions of cells possessing < 2N DNA content (fragmented nuclei). Due to this, the ultimate mechanism of cell death taking place in G2 arrested cells could not be identified, and additional work is required to understand TRAIP-mediated cell death.

Chapter 5

TRAIP is Essential during S-Phase for the Resolution of DNA Replication - Transcription Conflicts

5.1 Introduction

Characterisation of the TRAIP conditional degron cell lines revealed the overall consequences of TRAIP degradation. Altogether, the presented data provided a clear overview of the possible mechanisms underlying the cell lethality and primordial dwarfism phenotypes associated with TRAIP. Cells lacking TRAIP were shown to possess impaired proliferative ability, resulting in their accumulation specifically in G2 due to checkpoint activation. Furthermore, the ultimate consequence of TRAIP degradation appeared to be G2/M cell cycle exit via senescence. However, the precise molecular mechanism underpinning the observed phenotypes remained unclear.

This chapter builds upon the described work to understand the primary cellular processes requiring TRAIP. For this, three objectives were established. First, we set out to understand the underlying cause of the G2 cell cycle arrest observed. Second, any differential requirements for TRAIP during individual cell cycle stages was determined; and the specific stage TRAIP is essential for was identified. Finally, we aimed to explore the essential mechanism of TRAIP, underpinning the associated lethality and primordial dwarfism phenotypes during the unperturbed eukaryotic cell cycle.

5.2 Results

5.2.1 The Loss of TRAIP Results in the Accumulation of DNA Damage

TRAIP has been previously implicated in the maintenance of genomic stability and efficient DNA damage repair (Feng et al., 2016; Harley et al., 2016; Hoffmann et al., 2016; Gleich et al., 2021; Soo Lee et al., 2016). Similarly, our data demonstrated that the G2 cell cycle arrest caused by TRAIP degradation could be overcome using ATRi. Thus, it was likely that increased replicative stress was the causative factor. We therefore wondered whether TRAIP degradation led to the accumulation of DNA damage. To test this, cells were treated with IAA for 24 hours before being stained for the DNA damage markers γ-H2AX (Serine 139) and 53BP1. Any accumulation of these markers was then assessed using immunofluorescence. The phosphorylation of Histone H2AX at Serine 139 acts as the first step in the recruitment of repair proteins to DNA lesions, and stressed replication forks (Kuo and Yang, 2008). On the other hand, 53BP1 is recruited specifically to double strand breaks (Panier and Boulton, 2013). No differences could be

detected between treated and untreated control cell lines (Figure 5.1, CMV-OsTIR1), or between untagged controls and untreated degron cell lines (Figure 5.1A-C, - IAA). Conversely, TRAIP degradation was shown to result in the subtle but general accumulation of both γH2AX and 53BP1 foci (Figure 5.1A-C, TRAIP-mAID C2 and D5).

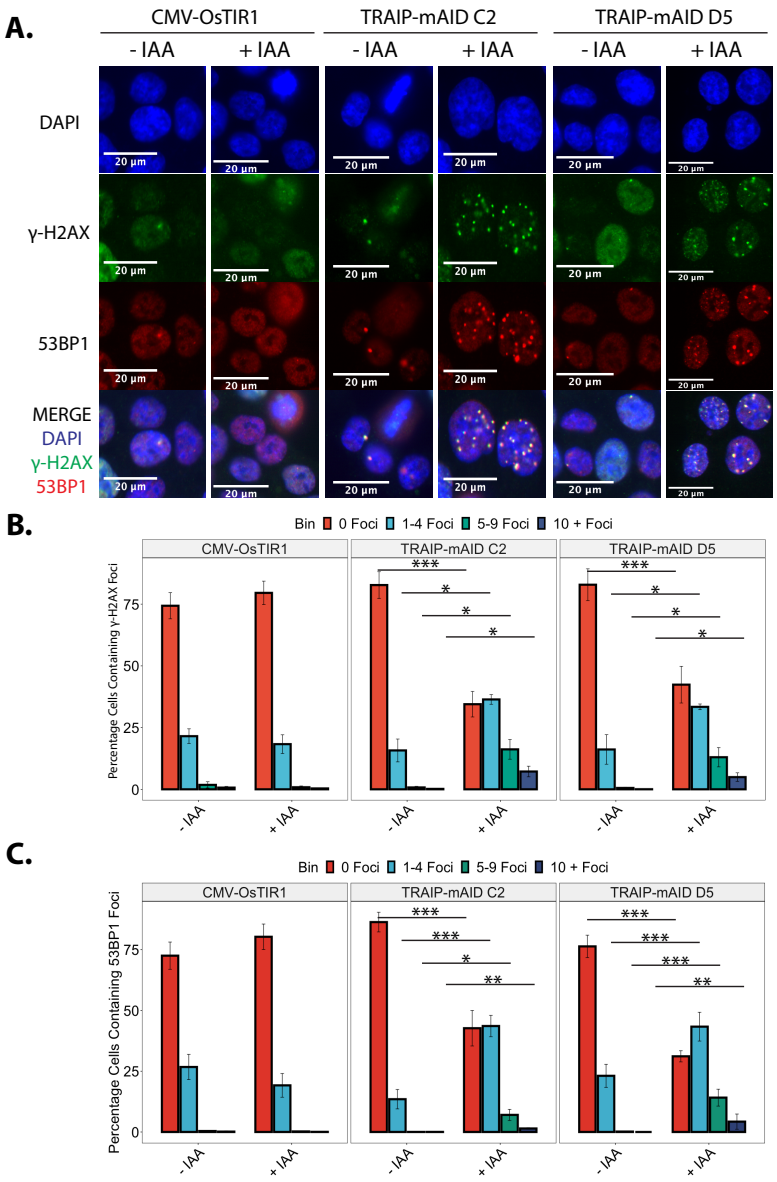


Figure 5.1: **The Loss of TRAIP Results in Accumulating DNA Damage Foci.** TRAIP-mAID cell lines and appropriate controls were treated with IAA for 24 hours. Cells were then fixed in 4% paraformaldehyde and stained for the general replication stress marker γH2AX (S139) as well as the double strand break specific 53BP1. Foci were quantified using CellProfiler: first, nuclei masks were created to identify regions of interest. The respective γ-H2AX signal was then enhanced through background noise reduction (rolling ball algorithm). Finally, foci were identified and related to parent nuclei. All data shown was collected from three independent experimental repeats (average of 942 cells per condition, per repeat). **A.** Example microscopy images. Shown are example cells from the three channels used: Blue – DAPI (DNA), Green – γH2AX, Red – 53BP1. Also shown is a scale bar for reference. **B.** Quantification of γH2AX foci. Cells containing γH2AX were binned into different categories and plotted using bar charts, showing the mean proportion of cells in each category +/- the SEM. Statistical analyses was carried out using one-way ANOVA and Tukey post-hoc testing. Significant differences from the post-hoc testing are shown for TRAIP-mAID C2 (0 Foci: $p = < 0.001$; 1-4 Foci: $p = 0.015$; 5-9 Foci: $p = 0.029$; 10 + Foci: $p = 0.039$) and TRAIP-mAID D5 (0 Foci: $p < 0.001$; 1-4 Foci: $p = 0.038$; 5-9 Foci: $p = 0.0046$; 10+ Foci: $p = 0.041$). **C.** Quantification of 53BP1 foci. Cells containing 53BP1 foci were binned into different categories and plotted using bar charts, showing the mean proportion of cells in each category +/- the SEM. Statistical analyses was carried out using one-way ANOVA and Tukey post-hoc testing. Significant differences from the post-hoc testing are shown for TRAIP-mAID C2 (0 Foci: $p = < 0.001$; 1-4 Foci: $p < 0.001$; 5-9 Foci: $p = 0.0168$; 10 + Foci: $p = 0.0059$) and TRAIP-mAID D5 (0 Foci: $p < 0.001$; 1-4 Foci: $p < 0.001$; 5-9 Foci: $p = 0.0046$; 10+ Foci: $p = 0.078$).

5.2.2 TRAIP does not Appear to be Required for Progression through G2/M

TRAIP has been implicated in key processes taking place during S-phase and mitosis, both of which have the potential to cause increased DNA damage and subsequent cell cycle arrest. Consequently, I next aimed to understand whether TRAIP was required for the entirety of the cell cycle, or for a specific stage. Given the observed G2 cell cycle accumulation, we first explored any role for TRAIP during G2. The conditional degron cell lines were arrested in G1 using Lovastatin and released into S-phase (Figure 5.2A). IAA was optionally added 15-hours post release, when most cells resided in late S-phase (Figure 5.2B); facilitating TRAIP degradation prior to progression through G2. Timepoints were taken at 20- and 24- hours post release, corresponding to G2/M of the first cell cycle, or G1 of the second. The total proportions of cells in each cell cycle stage was then quantified by Propidium Iodide staining, analysed by flow cytometry. We hypothesised that, if TRAIP was required specifically for G2, then the degradation of TRAIP during late S-phase would result in cell cycle accumulation. However, no such accumulation could be detected following the degradation of TRAIP in late S-phase, at either timepoint (Figure 5.2C-E).

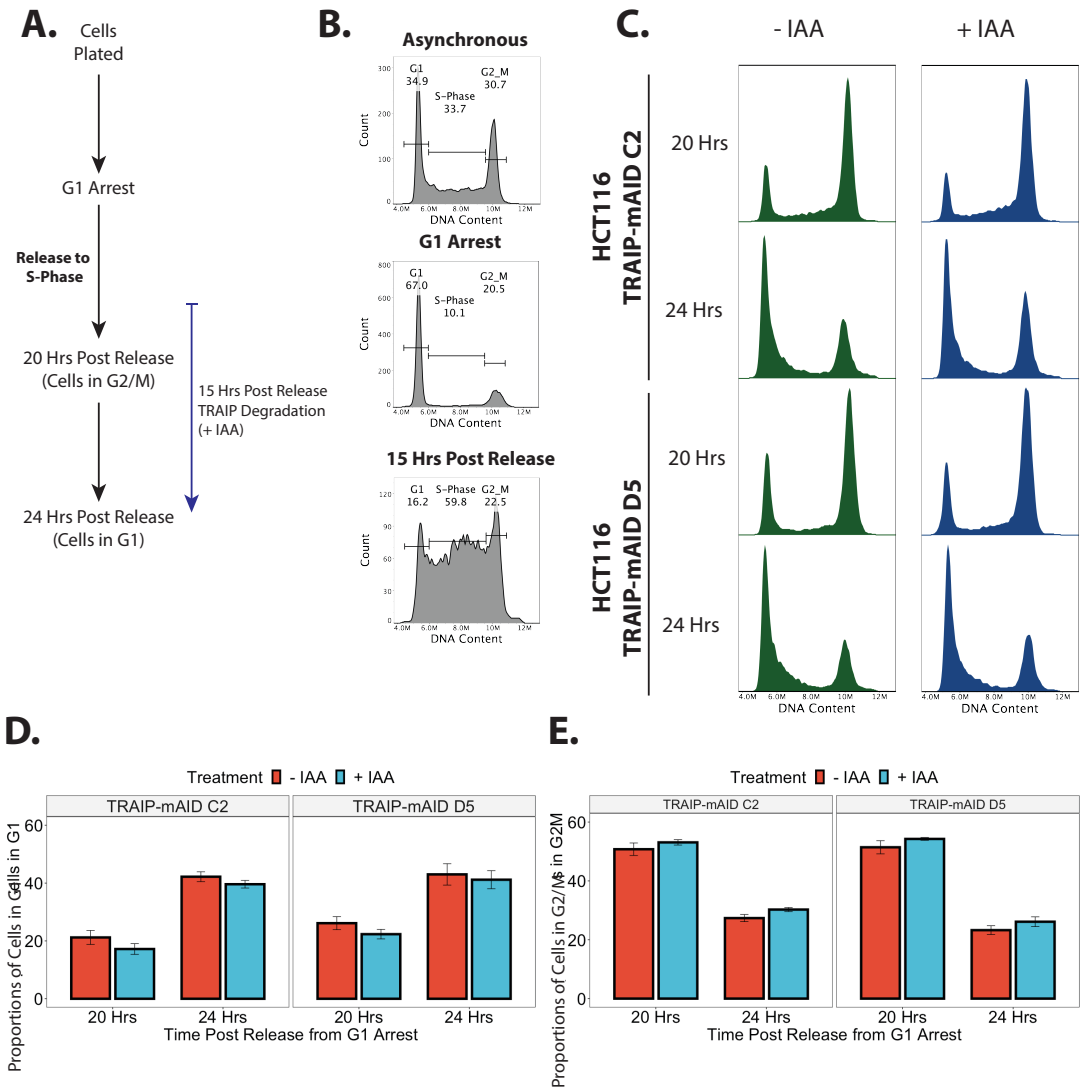


Figure 5.2: **TRAIP does not Appear to be Required for Progression through G2/M.** To understand whether TRAIP was needed specifically for cell cycle progression during G2, IAA treatment was combined with established cell synchronisation techniques and the previously reported G2 arrest phenotype. Data shown was collected over three independent experimental repeats. Cells were gated as detailed in the materials and methods (See Figure 2.5). **A.** Experiment schematic. Cells were arrested in G1 and released into S-phase. IAA was added to degrade TRAIP 15 hours post release, and timepoints taken at 20- and 24-hrs post release. Harvested cells were fixed in ethanol and stained with Propidium Iodide. The proportions of cells in each cell cycle stage were analysed using a flow cytometer, described in the materials and methods. **B.** Control synchronisation samples. Shown are asynchronous cells, G1 arrested cells, as well as 15 hours post release where IAA was added. Gates established to determine the proportion of cells in each cell cycle stage, used for quantification, are shown. The gates set using the asynchronous control sample were applied to all samples. **C.** Example cell cycle distributions for the cells with and without TRAIP at each of the timepoints tested. Cells in green contained TRAIP, whilst those in blue were lacking TRAIP. **D.** Total proportions of cells in G1 stage of the cell cycle (containing 2N DNA content). Data is displayed as the mean proportions +/- the SEM. Statistical significance testing was carried out using t. tests, and no differences between untreated and treated cells was found. **E.** Total proportions of cells in G2/M stage of the cell cycle (containing 4N DNA content). Data is displayed as the mean proportions +/- the SEM. Statistical significance testing was carried out using t. tests, and no differences between untreated and treated cells was found.

5.2.3 TRAIP is Essential for S-Phase

TRAIP did not appear to be required for cell cycle progression specifically through G2 and mitosis. Therefore, it was likely that the phenotypes observed following TRAIP degradation were due to problems during S-phase. To this end cells were again arrested in G1 and released into S-phase. However, to understand the requirement for TRAIP specifically during S-phase, IAA was added 1 hour prior to release from the G1 arrest (Figure 5.3A). In this situation, when cells progressed through the entirety of S-phase without TRAIP, G2/M cell cycle accumulation was observed (Figure 5.3B and D). Furthermore, corresponding reductions to the proportions of cells in G1 stage of the cell cycle were also detected (Figure 5.3C), analogous to that observed in asynchronous cells following TRAIP degradation (Figure 4.8- 4.10).

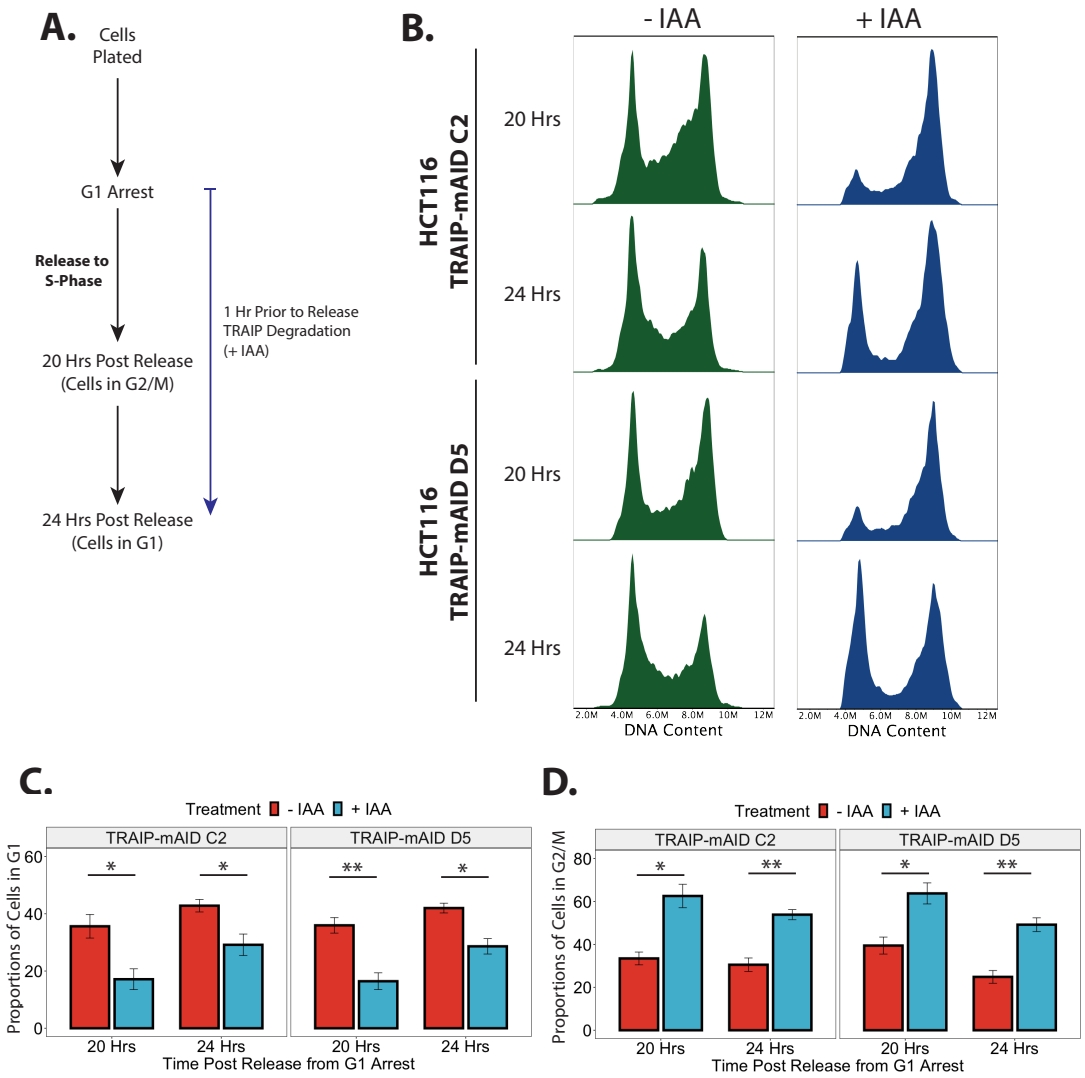


Figure 5.3: **TRAIP is Important for S-Phase Progression.** To understand whether TRAIP was needed specifically during S-phase, IAA treatment was combined with established cell synchronisation techniques and the analysis of previously reported G2 arrest phenotype. Data shown was collected over three independent experimental repeats. Quantification was carried out using a minimum of 10,000 cells per repeat. Gates were established onto control samples to quantify the populations of cells in each cell cycle stage; detailed in Figure 5.2B and Figure 2.5. **A.** Experiment schematic. Cells were first arrested in G1. Approximately 1 hour prior to release into S-phase, IAA was added to degrade TRAIP. Following TRAIP degradation, cells were released into S-phase, and timepoints taken at 20- and 24-hrs post release. Harvested cells were fixed in ethanol and stained with Propidium Iodide. The proportions of cells in each cell cycle stage were analysed using a flow cytometer, described in the materials and methods. **B.** Example of cell cycle distributions for the cells with and without TRAIP at each of the timepoints tested. Cells in green contained TRAIP, whilst those in blue were lacking TRAIP. **C.** Quantification of proportion of cells in G1 stage of the cell cycle (containing 2N DNA content). Data is displayed as the mean proportions +/- the SEM. Statistical significance testing was carried out using t. tests, and significant differences are shown on the plots (TRAIP-mAID C2 – 20 Hrs: p = 0.0288, 24 Hrs: p = 0.0465; TRAIP-mAID D5 – 20 Hrs: p = 0.00825, 24 Hrs: p = 0.0196). **D.** Quantification of proportions of cells in G2/M stage of the cell cycle (containing 4N DNA content). Data is displayed as the mean proportions +/- the SEM. Statistical significance testing was carried out using t. tests, and significant differences are summarised on the plots (TRAIP-mAID C2 – 20 Hrs: p = 0.0171, 24 Hrs: p = 0.00514; TRAIP-mAID D5 – 20 Hrs: p = 0.0198, 24 Hrs: p = 0.00512).

Whilst it was clear that TRAIP was required for S-phase progression, it was possible that the previously reported mitotic roles for TRAIP contributed to the observed genomic instability and G2/M accumulation. To exclude this possibility, a reciprocal experiment was carried out to those detailed in Figure 5.2 and 5.3. Cells were arrested in G2 using RO-3306. During the final hour of G2 cell cycle arrest, IAA was optionally added to degrade TRAIP, and the cells released into mitosis (5.4A). Approximately 3 hours later, when most cells resided in G1 of the cell cycle (Figure 2.3), IAA was optionally removed from the cell media to enable TRAIP re-synthesis during G1. Samples were then harvested 24 hours later, and the resulting cell cycle profiles assessed as described above. When cells progressed through mitosis, G1, and S-phase without TRAIP, G2/M cell cycle accumulation was observed (Figure 5.4C and E, + IAA). Conversely, no such accumulation could be detected when cells progressed through mitosis only without TRAIP (Figure 5.4C and E, + IAA WASH samples). Furthermore, as with the previous cell cycle data, all G2/M effects were accompanied by corresponding changes to the proportions of cells in G1 (Figure 5.4D). Overall, the presented data revealed that the essential mechanism of TRAIP was carried out during S-phase. In addition, the degradation of TRAIP for a single S-phase was sufficient to inhibit cell proliferation.

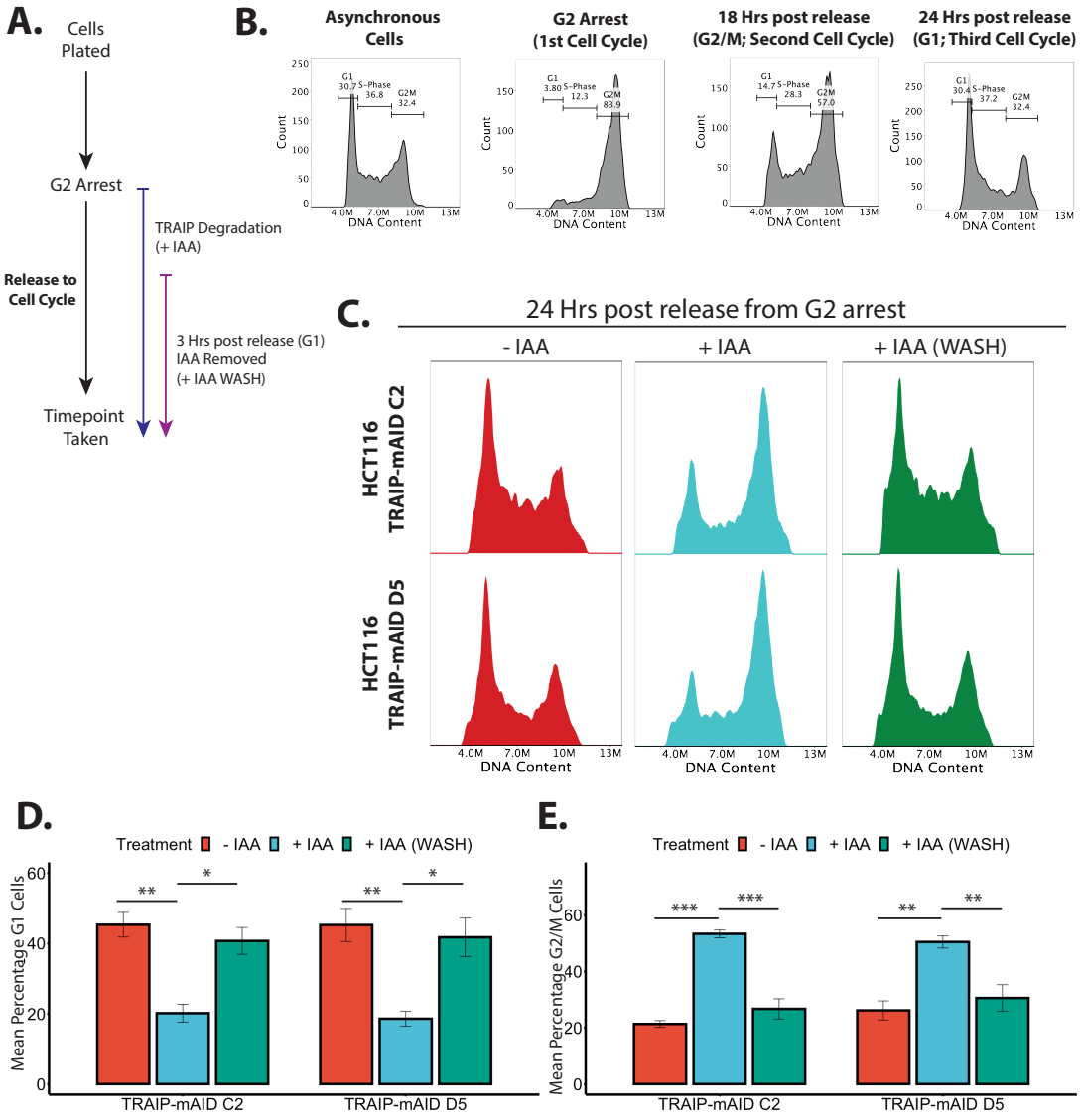


Figure 5.4: **TRAIP Function in Mitosis does not Impact on the G2 Cell Cycle Arrest Observed Upon TRAIP Degradation.** To further understand the requirements of TRAIP during the cell cycle, a G2 arrest and release experiment was conducted. Data shown was collected over three independent experimental repeats. **A.** Experiment schematic. Cells were arrested in G2 using the CDK1 inhibitor RO-3306. IAA was added to degrade TRAIP 1 hour prior to release from G2 arrest. Following the degradation treatment, cells were released back into the cell cycle. Approximately 3 hours post release, when cells were in G1, IAA was optionally removed to allow TRAIP re-synthesis. Samples were harvested 24 hours post-release and analysed by flow cytometry. **B.** Examples of cell synchronisation stages. Shown are asynchronous cells, G2 arrested cells, 18 hours post-release, and 24 hours post-release. Samples were gated as detailed in the materials and methods to isolate single-cell populations (Figure 2.5). Additional gates were then established using the asynchronous control cells to define G1, S-phase, and G2/M populations (shown). Gates were then applied to all samples for quantification. **C.** Example FACS plots. Shown are both TRAIP-mAID C2 and D5 clones for – IAA (red), + IAA (blue), and + IAA washed off in G1 (Green). **D.** Quantification of the total proportion of G1 cells (containing 2N DNA content -/+ SEM). Statistical analysis was carried out using one-way ANOVA and Tukey's post-hoc test. Significant differences are summarised on the plot (TRAIP-mAID C2: - IAA vs + IAA, $p = 0.00632$; - IAA vs + IAA WASH, $p = 0.953$; + IAA vs + IAA WASH, $p = 0.0259$. TRAIP-mAID D5: - IAA vs + IAA, $p = 0.00403$; - IAA vs + IAA WASH, $p = 0.985$; + IAA vs + IAA WASH, $p = 0.0116$). **E.** Quantification of the total proportion of G2/M cells (containing 4N DNA content -/+ SEM). Statistical analysis was carried out using one-way ANOVA and Tukey's post-hoc test. Significant differences are summarised on the plot (TRAIP-mAID C2: - IAA vs + IAA, $p < 0.001$; - IAA vs + IAA WASH, $p = 0.800$; + IAA vs + IAA WASH, $p < 0.001$. TRAIP-mAID D5: - IAA vs + IAA, $p = 0.00107$; - IAA vs + IAA WASH, $p = 0.898$; + IAA vs + IAA WASH, $p = 0.00554$).

5.2.4 TRAIP does not Appear to be Required for DNA Synthesis

Given that TRAIP was essential specifically for S-phase, we wondered whether the loss of TRAIP resulted in any defects to global DNA replication. Cells with and without TRAIP were pulsed with the thymidine analogues BrdU or EdU for 1 hour immediately prior to cell fixation. Both BrdU and EdU can be readily incorporated into replicating DNA and thus act as measures for the total amount of DNA synthesis undertaken per cell. The resulting analogue incorporation was measure by flow cytometry (BrdU, Figure 5.5) and immunofluorescence (EdU, Figure 5.6). In both cases, overall reductions to the total proportions of cells incorporating BrdU/EdU were found following TRAIP degradation (Figure 5.5B and 5.6B). However, the relative amounts of BrdU/EdU incorporated per cell (fluorescence intensity) remained unchanged (Figure 5.5C and 5.6C). Based on this, it is likely that the reductions to the proportions of cells incorporating each analogue were due to fewer S-phase cells, caused by the highlighted cell proliferation defect and cell cycle arrest. As the intensities of each respective thymidine analogue was not affected by IAA treatment, it was also likely that TRAIP degradation itself did not induce changes to the amounts of DNA synthesis undertaken. However, as a caveat, the incorporation of thymidine analogues shows only global changes to DNA replication, and is not sensitive enough to detect events taking place in specific sub-sets of cells.

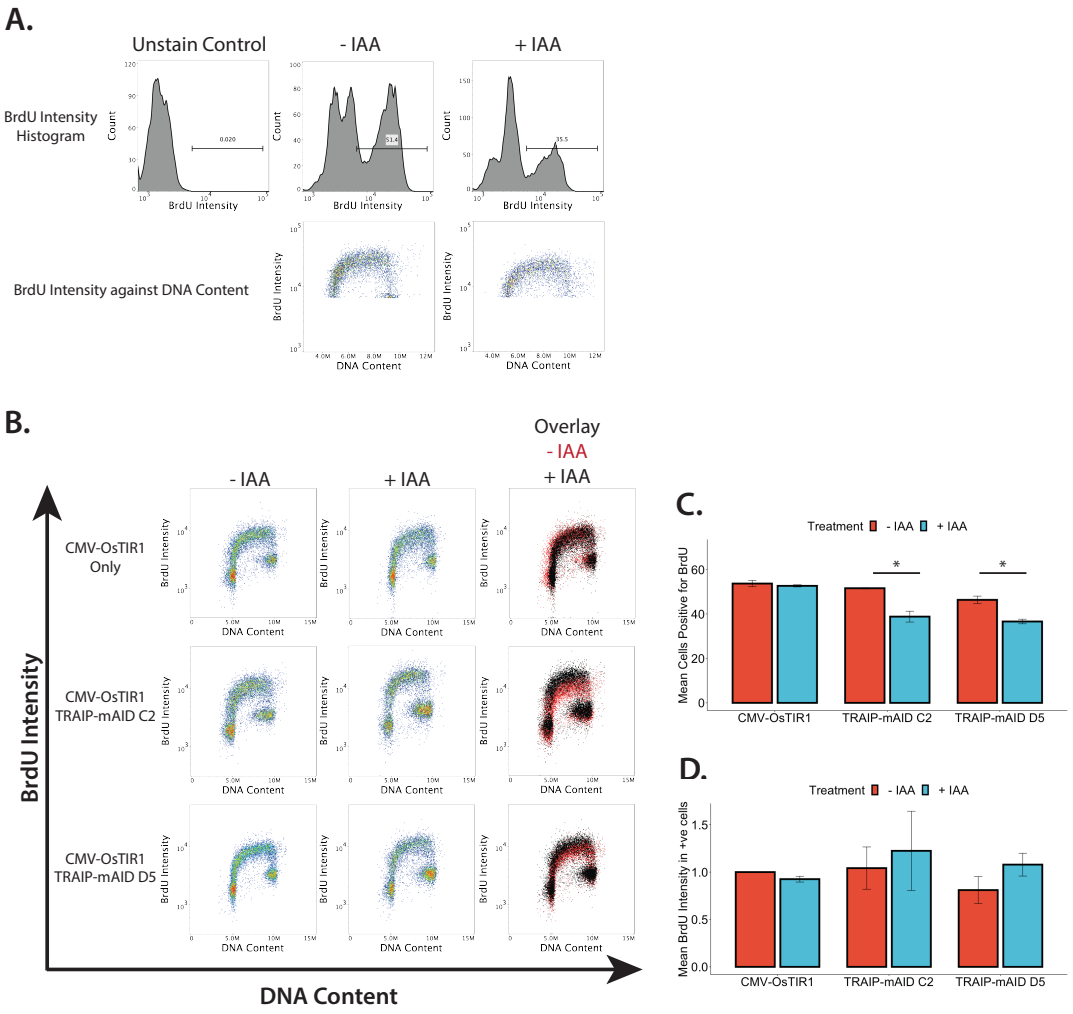


Figure 5.5: **TRAIP Degradation does not Change Global DNA Replication Levels: BrdU.** To understand whether the loss of TRAIP led to any defects in the total amount of DNA synthesis performed, cells were first treated with IAA to degrade TRAIP. Approximately 23 hours after IAA treatment, the cells were pulsed for 1 hour with the thymidine analogue BrdU. Following this, cells were harvested, fixed, and prepared as detailed in the materials and methods. Data shown was collected from three independent experimental repeats. **A.** Example Gating strategy. A minimum of 10,000 cells were quantified within the cell cycle gates described previously (See Figure 2.5). To detect BrdU positive cells, gates were placed to detect the positive population using unstained controls (top). The regions encapsulated by the gates contained all cells positive for BrdU, throughout the cell cycle (bottom). **B.** Example FACS plots showing the patterns of BrdU incorporation (y-axis) throughout the cell cycle (x-axis). Overlays of the two cell populations are also shown (- IAA: red, + IAA: black). **C.** Quantification of the total proportions of cells incorporating BrdU. The mean proportions of BrdU positive cells (as shown in A) were plotted as bar charts, displaying the mean and SEM. Statistical analysis was carried out using t. tests, and any significant differences discovered is summarised on the plot (TRAIP-mAID C2: p = 0.0331; TRAIP-mAID D5: p = 0.0126). **C.** Quantification of the average BrdU intensity per cell. The mean BrdU intensity of the positive populations (shown in A) was calculated and plotted. Shown is the mean BrdU intensity and associated error (SEM). Statistical analyses was conducted using t. tests, but no significant differences were found.

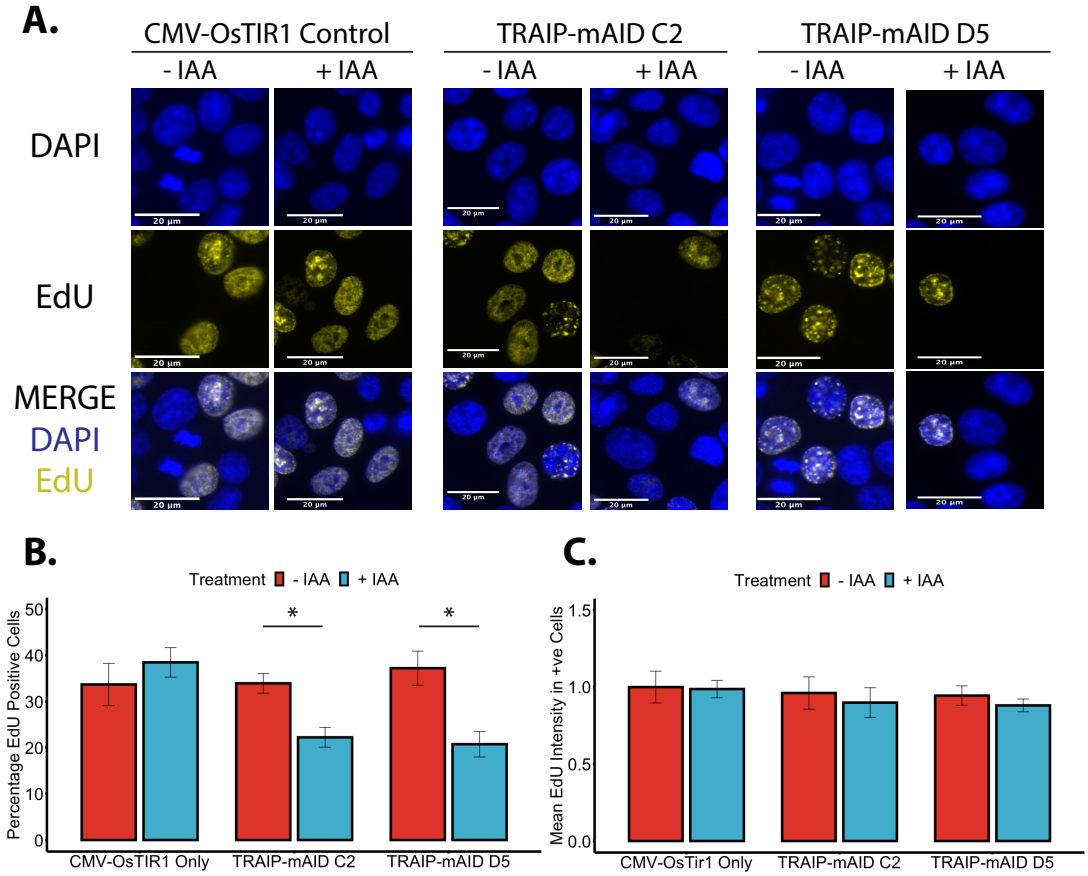


Figure 5.6: **TRAIP Degradation does not Change Global DNA Replication Levels: EdU.** To understand whether the loss of TRAIP led to any defects in the total amount of DNA replication undertaken, cells were first treated with IAA to degrade TRAIP. Approximately 23 hours after IAA treatment, the cells were pulsed for 1 hour with the thymidine analogue EdU. Following this, cells were harvested, fixed, and prepared using the Click-IT reaction, as detailed in the materials and methods. Shown are data collected over three experimental repeats (average: 835 cells quantified per condition, per repeat). **A.** Example images showing the EdU incorporation (yellow) into nuclei (blue). Merged images showing overlays of the two channels are also depicted. **B.** Quantification of the total proportion of cells incorporating EdU. The positive cells were identified using Cell Profiler, setting an intensity threshold for detection. The resulting proportions were then plotted using the mean and SEM. Statistical analyses was carried out on the data using t. tests and significant differences are summarised on the plots (TRAIP-mAID C2: p = 0.0178; TRAIP-mAID D5: p = 0.0264). **C.** Quantification of the average EdU intensity per cell. The total integrated intensity of the positive cells was measured using Cell Profiler. Data was then normalised to the untreated control, and the mean with SEM plotted. Statistical analyses were carried out using t. tests, but no differences were found.

During S-phase, it is thought that TRAIP can be recruited to both active and stalled replisomes to promote genomic stability. Recent work has shown that TRAIP can interact directly with the replisome to facilitate replisome disassembly upon CMG encountering blockages on chromatin. Therefore, we wondered whether TRAIP was also important for replisome

disassembly in otherwise unperturbed conditions. To this end, cells with and without TRAIP were pre-extracted using CSK buffer (Forment and Jackson, 2015), before being analysed using a flow cytometer. Use of the CSK buffer functioned to remove the cytoplasmic fraction, as well as soluble proteins from the nucleus. The extracted nuclei were then stained with antibodies against MCM7 to visualise the replisome. A summary of the MCM7 binding patterns to chromatin are shown in Figure 5.7. Consistent with published models, MCM7 was found to bind to chromatin during G1. Throughout S-phase, the levels of the MCM7 decreased as active and dormant origins were unloaded before reaching a negative level in G2/M. Comparison of the MCM7 signals from cells with and without TRAIP did not reveal any large visual differences, and it appeared that TRAIP does not possess a major role in S-phase replisome disassembly nor dormant origin unloading. Further exploration of TRAIP's role during DNA replication is addressed in Chapter 6 of this PhD thesis.

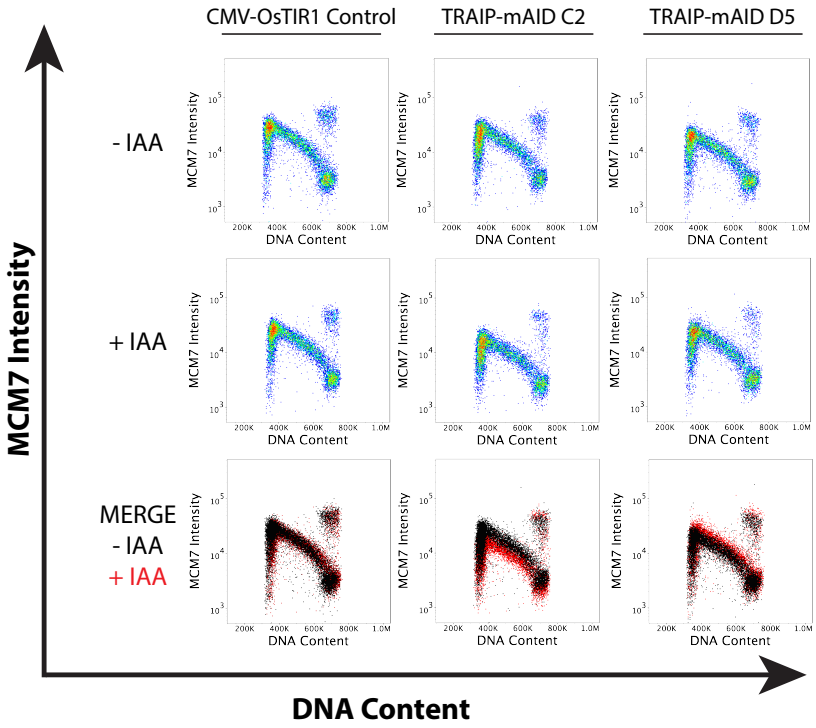


Figure 5.7: **TRAIP does not Appear to be Required for Unperturbed Replisome Disassembly.** To explore the effects of TRAIP degradation on MCM7 chromatin binding pattern, we utilised the methods published in Forment and Jackson (2015). Cells were treated with IAA for 24 hours, before the soluble fraction was extracted using CSK buffer. Extracted cells were fixed in Paraformaldehyde before being stained with antibodies against MCM7 and Hoechst (DNA). Shown is representative data from three independent experimental repeats. Cells were gated as described previously (see Figure 2.5). Cells encompassed by the applied gates were plotted to display the MCM7 intensity (y axis) against the total DNA content (x axis). In addition, overlays were generated to directly compare the signals (- IAA: black, + IAA: red).

5.2.5 γ-H2AX ChIP-Sequencing Reveals Links Between TRAIP and Transcription

TRAIP is not required for the completion of bulk DNA synthesis. Despite this, we have demonstrated that the essential role for TRAIP exists specifically during S-phase (Figure 5.2 - 5.4) through a mechanism important for the maintenance of genomic stability (Figure 5.1). Next, to gain additional insight into the potential roles of TRAIP, we aimed to exploit the described phenotypes and map genome wide the location of accumulating DNA damage

(γ-H2AX ChIP-Seq).

Cells without TRAIP Accumulate DNA Damage Specifically During S-Phase

Prior to conducting γ-H2AX ChIP sequencing, I first confirmed that the previous observations of generated DNA damage were indeed specific to S-phase. For this, a similar experimental set-up was used as detailed in Figure 5.3A. Cells were arrested in G1 of the cell cycle where TRAIP was degraded through 1 h IAA treatment. Following this, the cells were released into S-phase and timepoints taken (Figure 5.8A). A total of 5 timepoints were selected: G1 arrest, 13 hours post release (early-mid S phase), 16 hours post release (mid-late S phase), 20 hours post release (G2/M), and 24 hours post release (next G1). At each point, cells were harvested and stained with antibodies against γ-H2AX (S139). In addition, representative samples were also taken and stained with Propidium Iodide (DNA) for analysis using a flow cytometer (Figure 5.8B). Example microscopy images are shown in Figure 5.9. The associated quantification is depicted in Figure 5.8C. No differences to the proportions of y-H2AX foci could be found to cells during the G1 arrest. Following entry into S-phase, cells lacking TRAIP were observed to accumulate genomic instability (Figure 5.8C). Subsequent quantification of the relative numbers of γ-H2AX foci revealed that the overall DNA damage levels peaked at 16 hours post release (mid-late S phase); consistent with S-phase problems. As cells then entered G2 and the following G1, slight reductions in the total proportions of damaged cells were shown, when compared to the 16 h peak. However, significantly more damaged cells remained at these timepoints when compared to untreated controls. Thus, it was possible that the accruing DNA damage was retained during mitosis and through cell division. Although, the increased levels of genomic instability could have equally originated from the enlarged G2/M population after

IAA treatment.

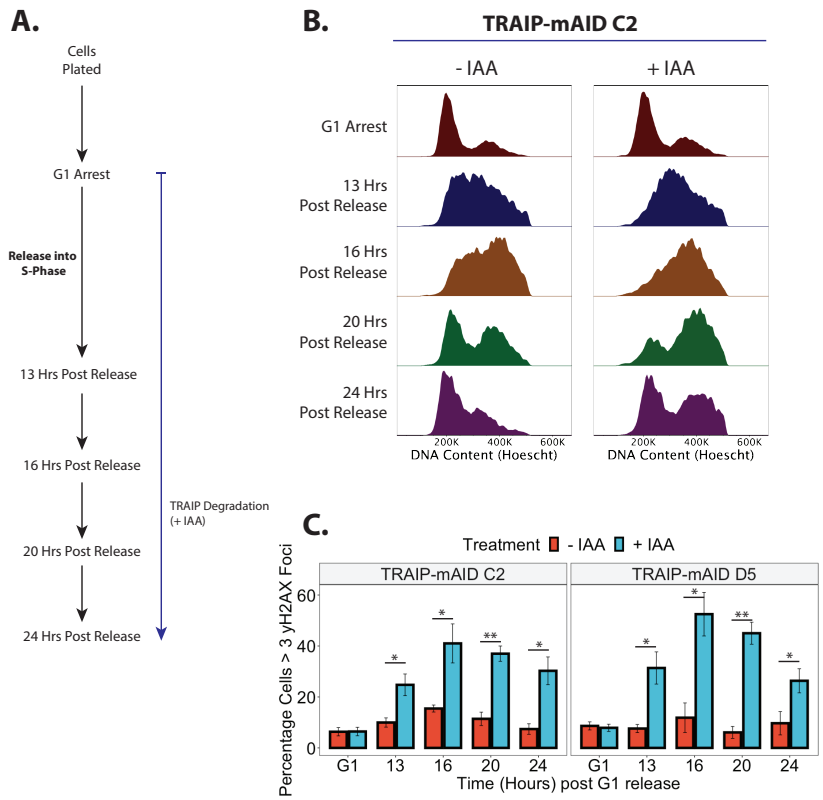


Figure 5.8: **TRAIP is Important for the Prevention of DNA Damage in Otherwise Unperturbed Cells (I).** To confirm that the previously observed accumulation of DNA damage was specific for S-phase, a G1 arrest and release experiment was conducted. Data shown was collected over three independent experimental repeats. **A.** Experiment schematic. Cells were arrested in G1 using Lovastatin, as detailed in the materials and methods. IAA was added to G1 arrested cells for 1 hour to degrade TRAIP. Cells with or without TRAIP were then released into S-phase, and timepoints taken. At each timepoint, cells were harvested and stained with antibodies against γ-H2AX (S139) for immunofluorescence. In addition, representative samples were taken, stained with Propidium Iodide, and run on a Flow Cytometer to assess the cell cycle profiles at each timepoint. **B.** Representative cell cycle profiles. Cells were gated as described previously (see Figure 2.5). Shown are example cell cycle profiles from each timepoint. Progression through S-phase is demonstrated following release from G1 arrest. **C.** Quantification of γ-H2AX foci. Data was analysed as described previously in Figure 5.1. The resulting proportions of cells containing over 3 foci were calculated and plotted, using the mean and SEM. Data shown was collected from three independent experimental repeats, with an average of 735 cells per condition/repeat quantified. Statistical analysis revealed the data to be normally distributed. As the treatment with IAA was to be compared between each timepoint individually, t. tests were used. Significant differences are summarised on the graph for TRAIP-mAID C2 (13 Hrs post release: p = 0.028; 16 Hrs post release: p = 0.037; 20 Hrs post release, p = 0.0016; 24 Hrs post release, p = 0.019) and TRAIP-mAID D5 (13 Hrs post release: p = 0.028; 16 Hrs post release, p = 0.010; 20 Hrs post release, p = 0.0019; 20 Hrs post release, p = 0.032).

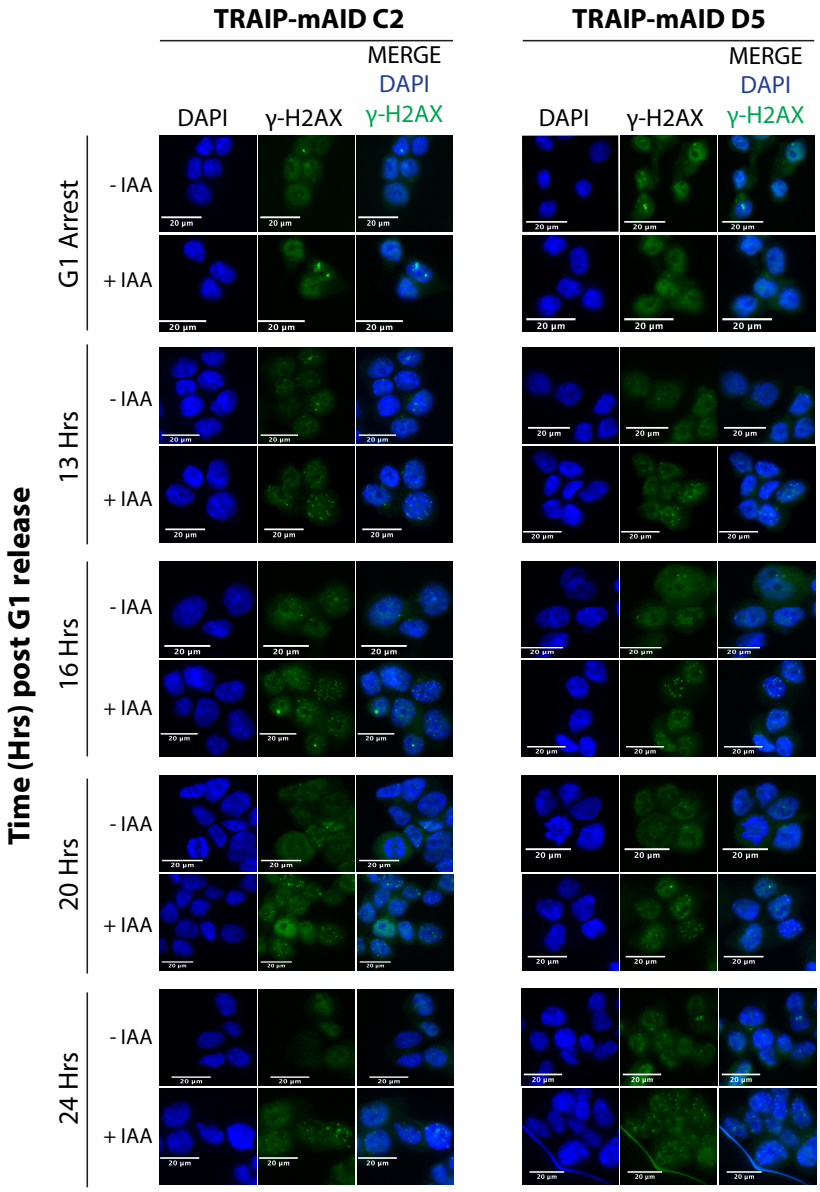


Figure 5.9: **TRAIP is Important for the Prevention of DNA Damage in Otherwise Unperturbed Cells (II).** Shown are example microscopy images for the experiment detailed in Figure 5.8. Data shown is representative of three independent experimental repeats, with an average of 735 cells per condition/repeat quantified in Figure 5.8. Cells were stained with DAPI (DNA, blue) and antibodies against γ-H2AX (S139, Green, marker of replication stress). Also shown are overlays of the two signals, for correlation of the respective γ-H2AX foci per parental nucleus.

TRAIP-Dependent Replication Stress is Associated with Transcription Start Sites

Having confirmed that the accumulating DNA damage signal was specific for S-phase, γ-H2AX ChIP-sequencing was conducted. Cells were treated as detailed in Figure 5.8A and samples

prepared for sequencing at mid-late S-phase (16 h following G1 arrest). The 16-hour timepoint was selected to capture the maximal accumulation of γ-H2AX on chromatin. Small amounts of each sample were taken for protocol optimisation. Briefly, sonication settings were trialled to determine the conditions resulting in DNA fragments between 300-600 bp (data not shown). In addition, quantitative PCR using primers against the actin housekeeping gene validated the material isolated through the immunoprecipitation protocol (data not shown). H2AX ChIP-sequencing was carried out simultaneously using the same samples for data normalisation.

Two independent sequencing experiments were carried out to ensure reproducibility. Unfortunately, the level of γ-H2AX signal increase in the ChIP samples from TRAIP-mAID C2 following IAA treatment was not as strong as TRAIP-mAID D5. Investigation into the potential causes revealed incomplete protein degradation following IAA treatment in the second repeat (data not shown). As a result, TRAIP-mAID C2 was removed from the data set and only TRAIP-mAID D5 analysed. Overall, higher proportions of y-H2AX were captured in cells lacking TRAIP, corroborating our previous results (example peak in Figure 5.10A). To begin to understand where in the genome the TRAIP-mediated DNA damage was located, we cross-referenced the detected γ-H2AX signal with known features of DNA replication mapped by alternative techniques in HCT116 cells, including initiation and termination zones (Zhao et al., 2020) as well as common fragile sites (Fungtammasan et al., 2012). However, no correlations could be found in any comparison (Figure 5.10B-D).

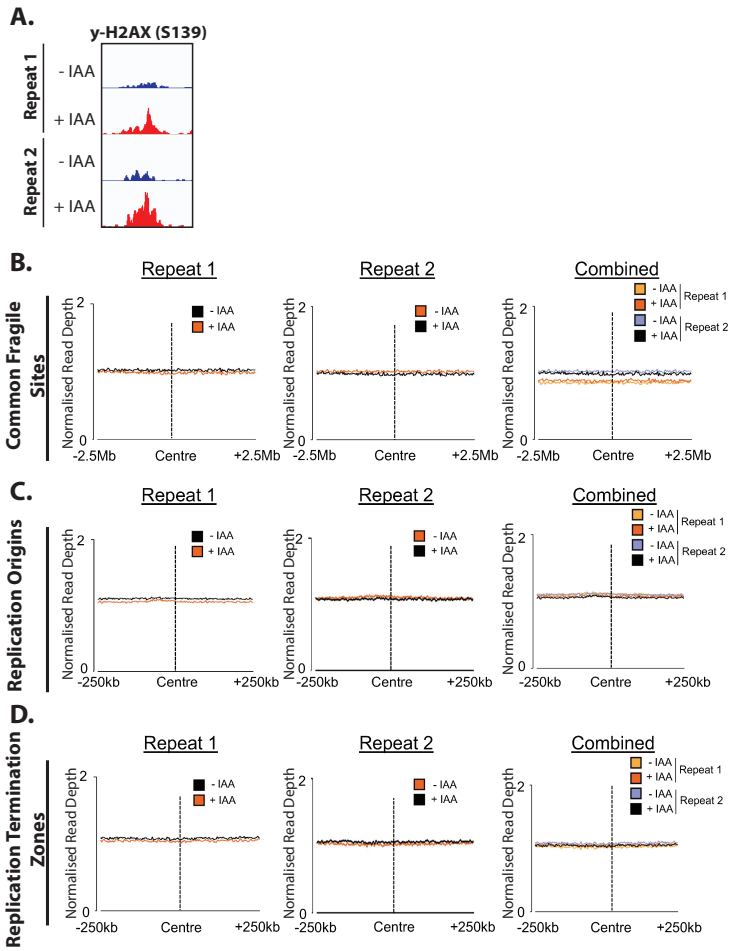


Figure 5.10: **Accumulating γ-H2AX was not Associated with Known Replication Features. A.** Example γ-H2AX ChIP peaks detected. Two experimental repeats are shown, either with (blue) or without (red) TRAIP. Clear increases in the γ-H2AX signal following IAA treatment were found. **B.** The detected γ-H2AX signal was overlaid onto known common fragile sites (Fungtammasan et al., 2012). The dotted line indicates CFS centre. Left: Repeat 1. Middle: Repeat 2. Right: Merged Data. **C.** The detected γ-H2AX signal was overlaid onto known origins of replication (Zhao et al., 2020). The dotted line indicates origin centre. Left: Repeat 1. Middle: Repeat 2. Right: Merged Data. **D.** The detected γ-H2AX signal was overlaid onto known replication termination zones (Zhao et al., 2020). Termination zones were defined as regions in-between two neighbouring replication origins. The dotted line indicates termination zone centre. Left: Repeat 1. Middle: Repeat 2. Right: Merged Data. ChIP-Seq data analysis was carried out by Dr. M. Saponaro.

To further attempt to identify genomic locations possessing increased γ-H2AX signal, we next utilised a peak-calling algorithm to label hotspots of γ-H2AX. Any region possessing 8-fold increase in γ-H2AX signal (+ IAA compared to - IAA) was called as a peak. In total 1700 and 5984 peaks were identified from repeats 1 and 2, respectively. Interestingly, 545 peaks were discovered to be conserved between the two repeats (Figure 5.11A). Initial analysis of

these shared peaks revealed that approximately 95.77% of the detected peaks were closely associated with RNA polymerase II transcripts (-/+ 2kb from the transcription start site, Figure 5.11B). Importantly, when we overlaid all the detected γ-H2AX signal over all transcribed genes, clear correlations emerged between TRAIP-dependent DNA damage and the transcription start site; irrespective of whether the detected γ-H2AX met stringent peak calling thresholds (Figure 5.11C and D).

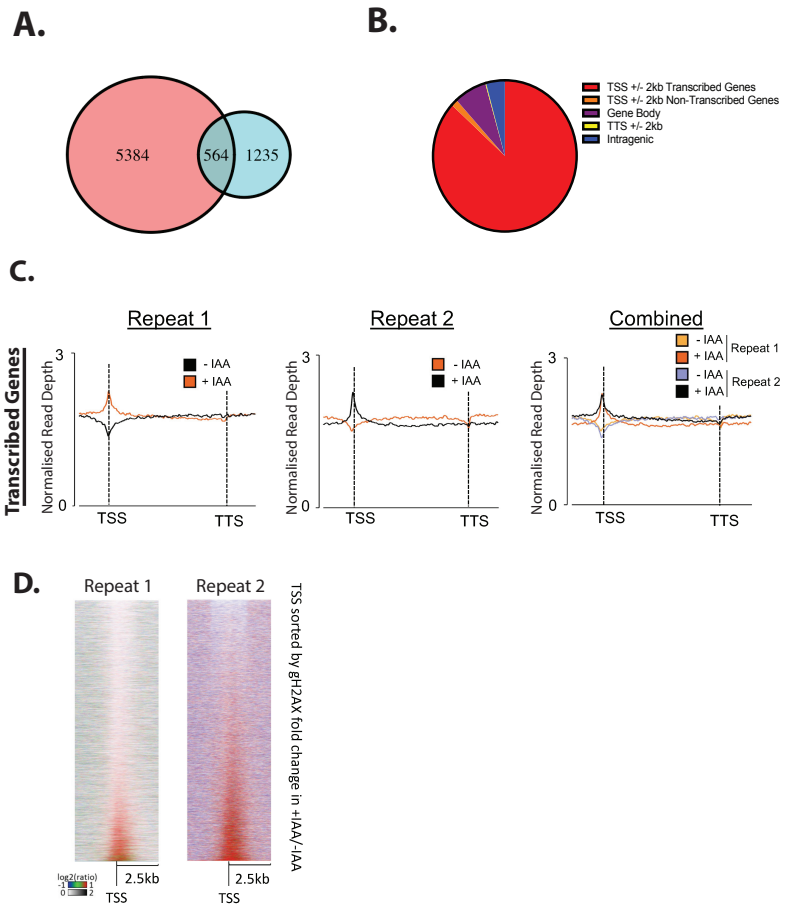


Figure 5.11: **TRAIP Dependent γ-H2AX is Associated with Transcription Start Sites. A.** Summary of the peaks detected in each repeat (Repeat 1: Blue; Repeat 2: pink). **B.** Genomic Locations of all peaks. Overall, the majority of detected peaks resided within 2kb of the transcription start sites (TSS) at transcribed genes. Other sites shown: Transcription start sites of non-transcribed genes, Gene body, Transcription Termination Sites (TTS), and intragenic regions. **C.** All γ-H2AX signal was overlaid onto of all transcribed genes. The dotted line indicates transcription start site (TSS) and transcription termination sites (TTS). Left: Repeat 1. Middle: Repeat 2. Right: Merged Data. Overall, increased damage was observed specifically at the TSS. **D.** Heatmaps focused on the transcription start site showing γ-H2AX accumulation in both repeats. ChIP-Seq data analysis was carried out by Dr. M. Saponaro.

However, not all transcription start sites (TSS) possessed increased levels of DNA damage. Hence, we next set out to understand the characteristics of the damaged TSS, and how these regions differed from the undamaged TSS, by focusing on the 545 conserved peaks identified. Functional sequence analysis of the genes immunoprecipitated from chromatin by γ-H2AX antibodies excluded any specific gene dependencies potentially underpinning the data (Table 5.1). Moreover, no correlation could be detected between those sites of DNA damage and gene length, or level of transcriptional activity (Figure 5.12A and B). Interestingly when we compared the replication dynamics (Zhao et al., 2020) at the identified peaks, we found that of the 545 conserved γ-H2AX, approximately 80% were preferentially replicated during early S-phase (Figure 5.12C).

Table 5.1: **Summary of the Significant GOTerms Identified from Genes Isolated by γ-H2AX ChIP-sequencing.** Analysis conducted by Dr. M. Saponaro. Shown are the significant GOTerms hits from three search criteria: Biological Process (BP), Cellular Component (CC), and MF (Molecular Function). Only significant hits are reported (Corrected p-value < 0.05).

Analysis Type	Gene Ontology Term	Count (# Genes)	Frequency (%)	Corrected P-Value (Benjamini)
Biological Process (GOTerm BP)	positive regulation of transcription from RNA polymerase II promoter	55	10.5	0.0014
Biological Process (GOTerm BP)	negative regulation of transcription from RNA polymerase II promoter	42	8	0.0077
Biological Process (GOTerm BP)	ephrin receptor signaling pathway	12	2.3	0.013
Biological Process (GOTerm BP)	vascular endothelial growth factor receptor signaling pathway	11	2.1	0.013
Biological Process (GOTerm BP)	transcription from RNA polymerase II promoter	31	5.9	0.034
Biological Process (GOTerm BP)	transcription, DNA-templated	81	15.4	0.045
Biological Process (GOTerm BP)	regulation of actin cytoskeleton organization	8	1.5	0.071
Biological Process (GOTerm BP)	covalent chromatin modification	12	2.3	0.071
Biological Process (GOTerm BP)	protein phosphorylation	27	5.1	0.08
Molecular Function (GOTerm MF)	protein binding	289	55	0.0026
Cellular Component (GOTerm CC)	nucleus	206	39.2	0.000000016
Cellular Component (GOTerm CC)	nucleoplasm	114	21.7	0.000047
Cellular Component (GOTerm CC)	cytoplasm	175	33.3	0.0041
Cellular Component (GOTerm CC)	cytosol	117	22.3	0.017
Biological Process (GOTerm BP)	positive regulation of transcription from RNA polymerase II promoter	55	10.5	0.0014

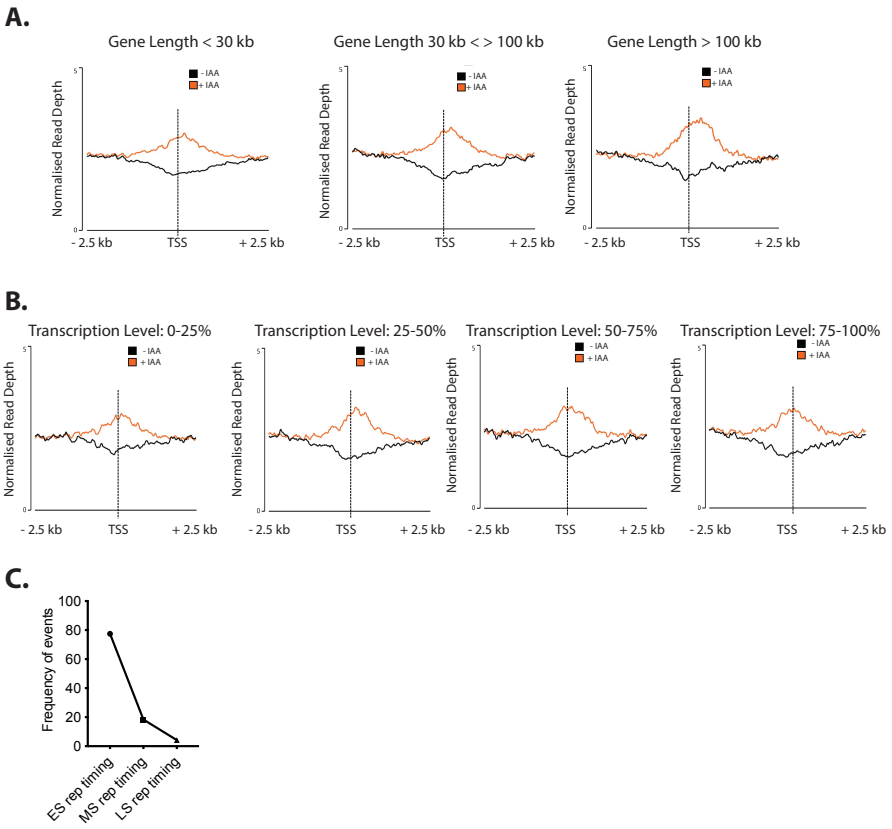


Figure 5.12: **The Conserved Peaks are Replicated During Early S-Phase. A.** All γ-H2AX data from repeat 1 overlaid onto all transcribed genes sorted by length. Left: < 30 kb. Middle: 30 kb< > 100 kb. Right > 100 kb. **B.** All γ-H2AX data from repeat 1 overlaid onto genes ranked by the relative level of transcriptional activity. **C.** Replication timing from Zhao et al. (2020) was used to determine the replication dynamics of the conserved peaks. Shown are frequencies of genes replicated in early (ES), mid (MS), or late (LS) S-phase. ChIP-Seq data analysis was carried out by Dr. M. Saponaro.

Due to the established link between TRAIP-mediated γ-H2AX and the transcription start site, we next decided to explore any association with the transcription machinery, specifically RNA Polymerase II. For this, we utilised a previously published RNA Polymerase II ChIP-seq data set (Figure 5.13A) (Erickson et al., 2018). All detected γ-H2AX signal was overlaid onto the RNA Pol II ChIP-seq data and focused on the transcription start sites. The resulting overlays indicated that the detected γ-H2AX peaks were located just ahead of the RNA Polymerase II surrounding the transcription start site (Figure 5.13B). Bimodal distributions were observed for RNA Pol II at the TSS identified. Moreover, it appeared that the TRAIP-dependent DNA damage resided

directly in the path of elongating transcription complexes.

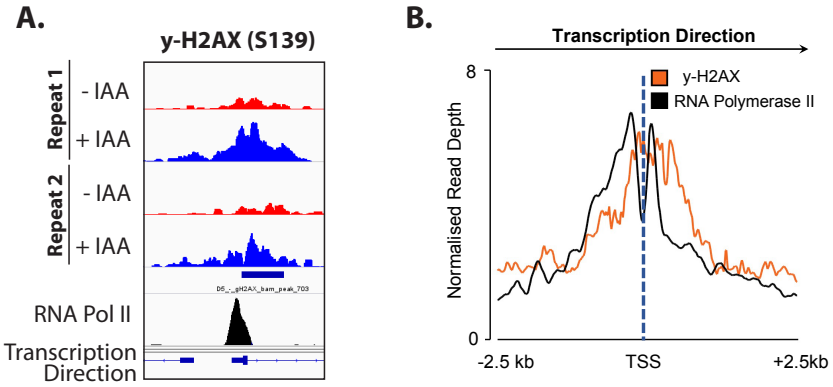


Figure 5.13: **TRAIP-Dependent γ-H2AX Appeared to Correlate with RNA Polymerase II. A.** RNA Polymerase II ChIP-sequencing (Erickson et al., 2018) was combined with our γ-H2AX ChIP-sequencing data set. Shown are example DNA damage peaks along with the RNA Pol II position. **B.** γ-H2AX peaks resided ahead of the RNA Polymerase II at the transcription forks. All DNA damage (orange) was overlaid onto all RNA-Pol II signal (black).

TRAIP is important when the replisome encounters blockages on chromatin (Larsen et al., 2019; Wu et al., 2019). Given the association between TRAIP, the TSS, and RNA Polymerase II, we wondered whether RNA Polymerase II would present as a barrier to replisome progression. If the cell processed CMG – RNA Pol II conflicts similarly to DPC's, it was likely that TRAIP was required. To start to test this hypothesis, we identified the closest replication origin to each conserved γ-H2AX damage peak using a published Polymerase Usage Sequencing (Pu-Seq) data set carried out in HCT116 cells (Koyanagi et al., 2021). γ-H2AX peaks were found to be 28 kb away from the closest replication origin, whereas transcription sites possessing low γ-H2AX signal resided approximately 41 kb away (Figure 5.14A, compare All Peaks and All Genes with low γ-H2AX signal). Furthermore, by considering the directionality of both replication and transcription at these sites we were able to determine whether the replisome will encounter RNA Polymerase II in a head-on or co-directional manner (Figure 5.14A). This data suggested that the γ-H2AX peaks were predominantly at the first transcription start site encountered by

the replication fork progressing from the nearest origin; whilst the TSS with low γ-H2AX signal were less likely to be at the first TSS encountered by the replisome (Figure 5.14B). Moreover, it was equally likely for the damaged TSS to contain co-directional or head-to-head replication transcription conflicts (Figure 5.14B).

It is well reported that head-to-head replication-transcription collisions are more damaging than co-directional conflicts (Saponaro, 2022). Our data suggested equal contributions of both orientations. However, the RNA polymerase ChIP seq data overlaid onto the γ-H2AX data set demonstrated bimodal RNA Pol II distributions at the damaged TSS, suggesting bi-directional transcription. To test this, we combined our ChIP sequencing data with published precision run-on sequencing (PRO-Seq) data, exploring strand specific nascent transcription (Andrysik et al., 2021). In total, 98.25% of all genes with a γ-H2AX peak possessed bi-directional transcription start sites (example peak in Figure 5.14D). To then investigate these sites further, the ratio of antisense to sense transcription was calculated within 1000 bp of the TSS. A value close to 1 represented equal proportions of sense and antisense transcription (bi-directional activity at the TSS). Values closer to 0 represented sites with more sense than antisense transcription (predominantly single-direction transcriptional activity). Compared to all transcribed genes, those TSS possessing conserved γ-H2AX peaks possessed more equal levels of antisense to sense transcription; suggesting increased bi-directional transcriptional activity and thus higher probabilities of damaging head-to-head replication-transcription collisions irrespective of which site the replication fork arrives at the TSS (Figure 5.14C). Similar results were found when we compared the conserved γ-H2AX peaks with regions of low γ-H2AX immunoprecipitated during our ChiP-Seq experiment (Figure 5.14C). The same calculations

were also carried out using the published RNA Polymerase II ChIP-Seq data (Erickson et al., 2018), yielding analogous results (Figure 5.14C). Overall, this data indicated that without TRAIP, transcription start sites in general become hotspots for genomic instability. But it is predominantly the first TSS possessing bi-directional transcriptional activity encountered by the replisome, preferentially replicated during early S-phase, that creates persisting problems.

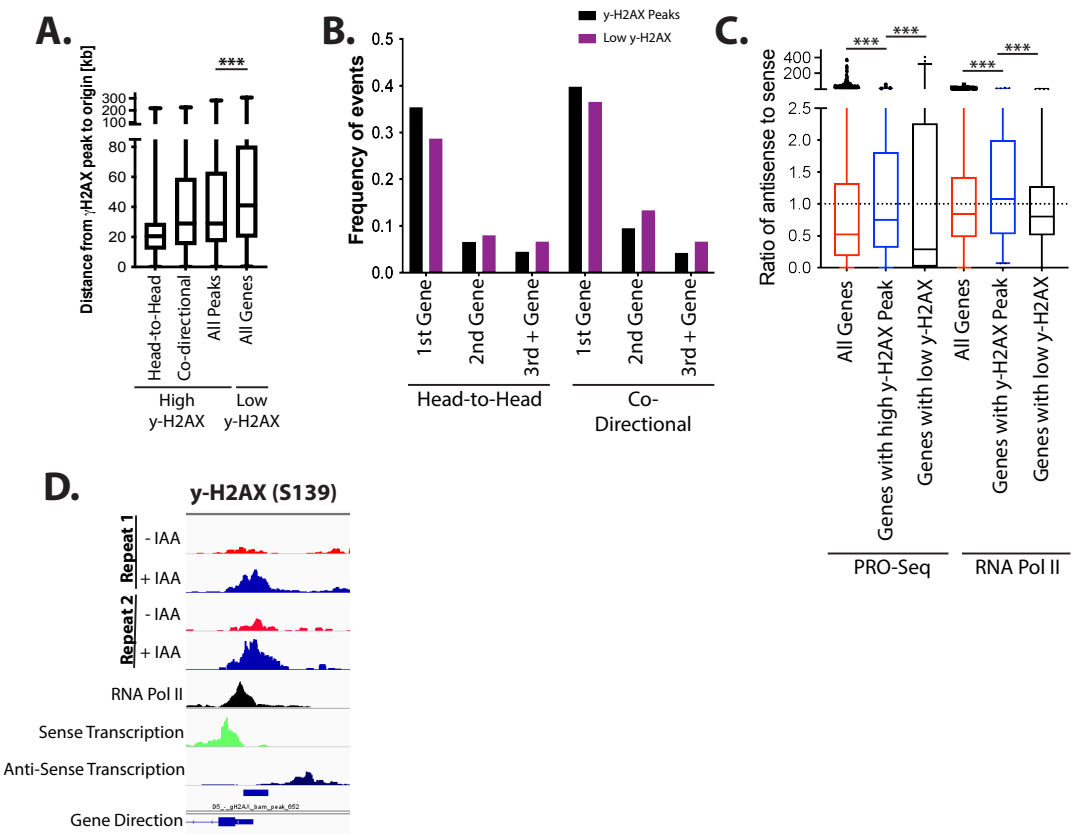


Figure 5.14: **TRAIP-Dependent γ-H2AX Accumulates at the First TSS Possessing Bi-Directional Transcription Encountered by the Replisome.A.** The closest replication origins to damaged TSS were determined (Zhao et al., 2020). Overall, damaged TSS were found to reside closer to the nearest replication origin in comparison to all genes (Mann Whitney Test: $p < 0.001$). **B.** Damaged TSS are often the first gene encountered by the replisome, with equal frequencies of head-to-head and co-directional conflicts. Damage signal was separated into γ-H2AX peaks (black) and regions possessing low γ-H2AX signal (purple). Shown are the frequencies of damaged TSS at the first, second and third or greater gene encountered by the replisome. **C.** Antisense to sense transcriptional ratio. Shown are two comparisons. Left γ-H2AX peaks, separated into peaks and low damaged sites in comparison to all genes using the PRO-Seq data set (Andrysik et al., 2021). Right, γ-H2AX peaks and low damaged sites in comparison to all genes, and genes with low γ-H2AX peaks, using the RNA Pol II data set (Erickson et al., 2018). Statistical analysis carried out using Mann Whitney tests ($p < 0.001$ for all indicated comparisons). **D.** Example γ-H2AX ChIP-seq peaks following the combination of our data with that of PolII ChIP-seq data and Pro-Seq data.

5.2.6 TRAIP Degradation does not Increase Global Transcription

The γ-H2AX ChIP-sequencing identified the genomic location of TRAIP-associated DNA damage. In addition, in-depth analysis of the detected peaks revealed a potential mechanism of action: mediating conflicts between DNA replication and transcription in proximity to promoters. Alternatively, however, TRAIP could be directly involved in upregulation of transcription. The hyper-activation of transcription due to misregulation has been previously demonstrated to result in increased levels of genomic instability (Bowry et al., 2021). To investigate whether TRAIP degradation led to a hyper-transcriptional phenotype, Eu incorporation assays were used. Eu (5-ethynyl uridine) is an alkaline nucleoside that can be readily incorporated into nascent RNA and detected by immunofluorescence, offering a method to measure global transcription levels. The conditional degron cell lines were arrested in G1, treated with IAA for 1-hour, and cells released into S-phase. Approximately 13 hours after release, when the cells were in early S-phase, Eu was added for 30 minutes. Following the incubation in Eu, the cells were fixed and stained as detailed in the materials and methods before being analysed using fluorescent microscopy. The transcription inhibitor triptolide was added to cells for 90 minutes as a positive control, shown to result in overall reductions to Eu intensity (Figure 5.15). It is worth noting that that triptolide did not completely abolish transcription. Eu can be incorporated into nascent mRNA by all three RNA polymerases, whilst triptolide only acts to inhibits RNA Pol II. Interestingly comparison of the total Eu intensity in cells with and without TRAIP did not reveal a hyper-transcription phenotype. Instead, the opposite occurred, and TRAIP degradation led to slight reductions in the global amounts of transcription undertaken (Figure 5.15). Given this result, the experiment should also be repeated using untagged control cell lines (CMV-OsTIR1 only) to confirm that the observed results were due to TRAIP degradation itself, and not IAA.

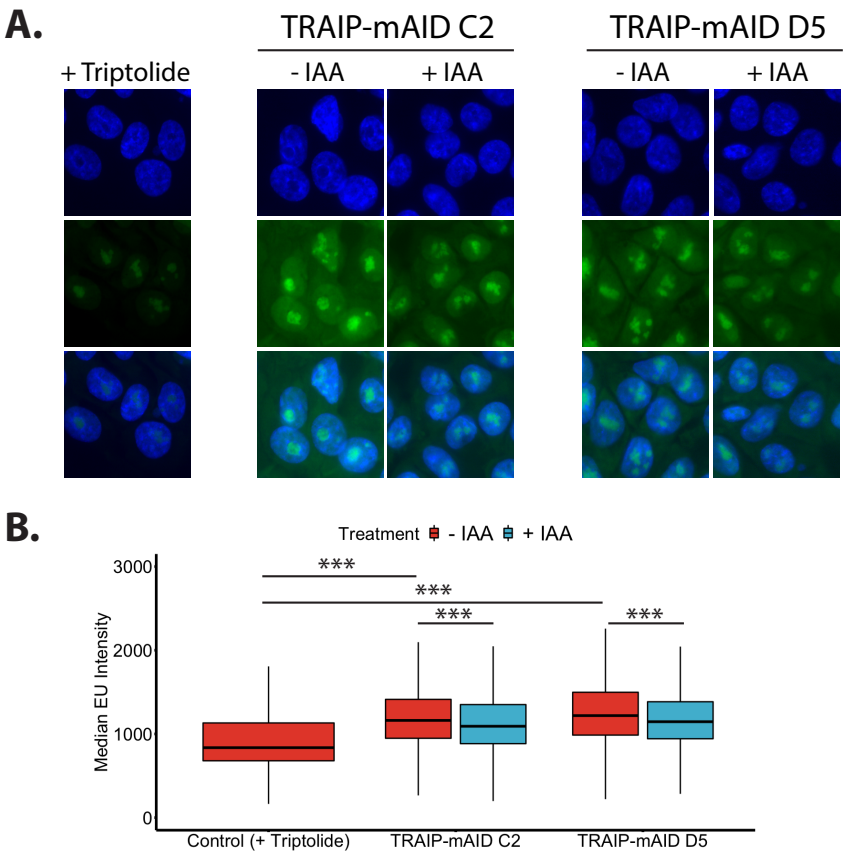


Figure 5.15: **TRAIP Degradation does not Induce Excessive Transcription Levels.** To test whether IAA treatment led to hyper-transcription, cells were synchronised in G1 and treated with IAA for 60 minutes to degrade TRAIP. Following protein degradation, the cells were released into S-phase for 13 hours before being supplemented with Eu for 30 minutes. Cells were then fixed and Eu visualised using Click-iT chemistry, detailed in the materials and methods. The transcription inhibitor triptolide was used as a positive control. Data shown was collected over three independent experimental repeats, with an average of 960 nuclei quantified per condition, per repeat. **A.** Examples of the immunofluorescence experiment. Shown are the two channels utilised: Blue (DNA/DAPI), Green (Eu), and overlays of both. **B.** Quantification of the integrated Eu intensity per cell. Regions of interest were identified based on the DAPI signal, and the integrative Eu intensity measured. Boxplots were then generated to show the median intensity values and interquartile ranges. Data was determined to be normally distributed, so parametric tests (ANOVA and Tukey Post-hoc) were used for statistical comparison. Significant differences are shown on the plot (for all conditions $p < 0.001$).

5.2.7 TRAIP's Mechanism of Action Requires RNA Polymerase II

The loss of TRAIP during S-phase did not induce major changes to the overall level of transcriptional activity in degron cells. Therefore, I next aimed to further investigate the relationship between TRAIP, RNA Polymerase II, and accumulating replication stress proposed

through our ChIP-sequencing data. S-phase cells with and without TRAIP were treated with two different transcription inhibitors: triptolide and DRb. The TFIIH inhibitor triptolide functions to block RNA Polymerase II loading (Erickson et al., 2018). On the other hand, the CDK9 inhibitor DRb leads to the RNA Pol II stalling at the TSS, preventing progression into the gene (Saponaro et al., 2014). The respective impact of each inhibitor was determined through any changes to the accumulating DNA damage levels as previously shown. Strikingly, the treatment of cells with the two inhibitors had different effects. The addition of triptolide for 90 minutes to S-phase cells was sufficient to rescue any accumulating DNA damage caused by TRAIP degradation (Figure 5.16). The treatment time of 90 minutes for triptolide treatment was selected as this has been reported to have no effect on DNA replication progression (Kotsantis et al., 2016), similarly demonstrated in our experiments using EdU to label replicating cells (Figure 5.16D and E). Conversely, DRb did not appear to rescue the accumulating DNA damage phenotype (Figure 5.17A-C). However, the treatment of cells with DRb itself has been previously highlighted to induce DNA damage (Stoimenov et al., 2011). As a result, it was difficult to ascertain whether any relationship existed between IAA and DRb treatment. Although TRAIP degradation was not shown to act additively with DRb, suggesting that DRb targets the same pathway requiring TRAIP to maintain genomic stability.

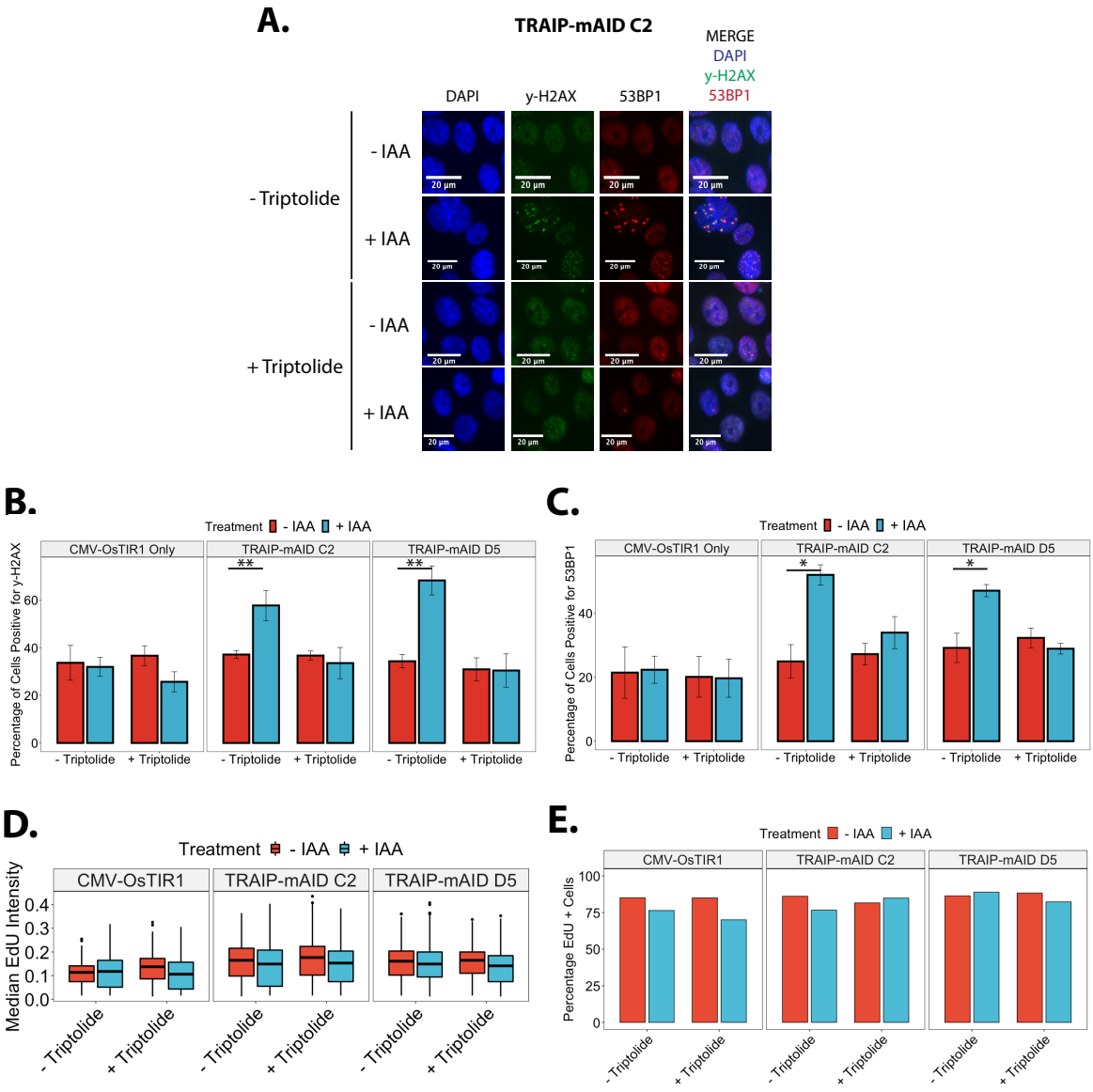


Figure 5.16: **DNA Damage Induced by TRAIP Degradation Requires RNA Polymerase II on Chromatin.** To understand any association between TRAIP and active transcription and RNA Pol II, the degron cells were treated with transcription inhibitor triptolide. Cells were arrested in G1, TRAIP degraded, and released into S-phase. In early S-phase triptolide was added for 90 minutes and cells harvested for microscopy. DNA damage, specifically γ-H2AX and 53BP1 foci, were used as a read-out. Shown are the respective impacts of triptolide on TRAIP-associated replication stress. Shown is data collected from three independent experimental repeats, with an average of 1400 nuclei analysed per condition, per repeat. **A.** Example cells (TRAIP-mAID C2 cell lines). Nuclei regions of interest were identified, and any foci within this region counted using CellProfiler. **B.** Quantification of the cells positive for γ-H2AX (S139) foci. Data was discovered to be normally distributed, therefore pairwise comparison (t.tests) were used to understand the impact of IAA on transcription inhibition. Significant differences are shown on the plots (TRAIP-mAID C2 – Triptolide: p = 0.00622; TRAIP-mAID D5 – Triptolide: p = 0.00798). **C.** Quantification (n = 3) of the cells positive for 53BP1 foci. Data was discovered to be normally distributed, therefore pairwise comparison (t.tests) were used. Significant differences are shown on the plots (TRAIP-mAID C2 – Triptolide: p = 0.0424; TRAIP-mAID D5 – Triptolide: p = 0.0474). **D.** Median EdU intensity per cell following Triptolide and IAA treatment (n = 1). **E.** Proportion of cells positive for EdU following Triptolide and IAA treatment (n = 1).

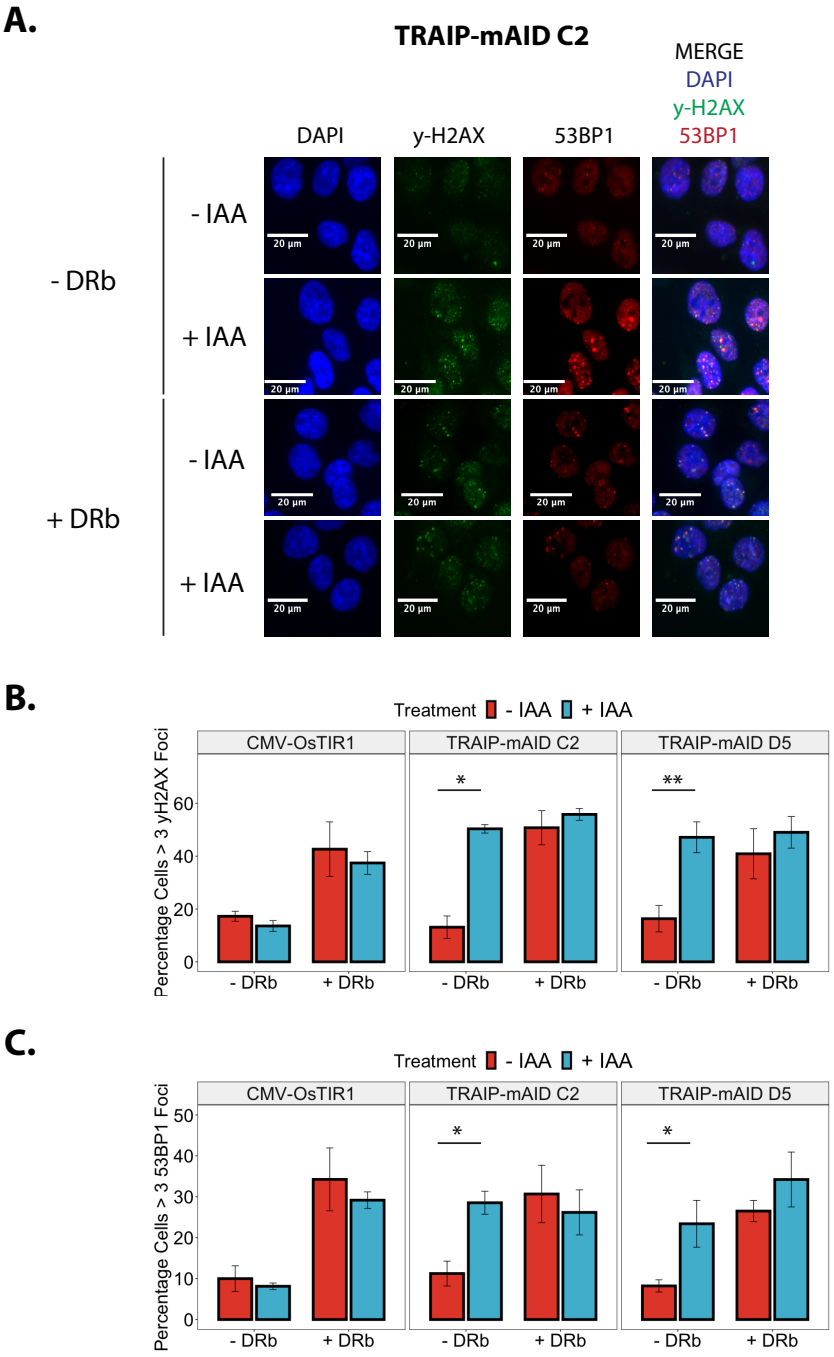


Figure 5.17: **DNA Damage Induced by TRAIP Degradation is Epistatic with Transcription Inhibition by DRb.** Cells were arrested in G1, TRAIP degraded, and released into S-phase. Approximately in early S-phase, the transcription inhibitor DRb was added for 90 minutes, and cells harvested for microscopy. DNA damage, specifically γ-H2AX and 53BP1 foci, were used as a read-out. Shown is data collected from three independent experimental repeats, with an average of 1215 nuclei analsed per condition, per repeat. **A.** Example cells (TRAIP-mAID C2 cell lines). Nuclei regions of interest were identified, and any foci within this region counted using Cell Profiler. **B.** Quantification of the cells containing > 3 γ-H2AX (S139) foci. Data was discovered to be normally distributed, therefore pairwise comparison (t.tests) were used to understand the impact of IAA on transcription inhibition. Significant differences are shown on the plots (TRAIP-mAID C2 – Triptolide: p = 0.0146; TRAIP-mAID D5 – Triptolide: p = 0.00738). **C.** Quantification of the cells containing > 3 53BP1 foci. Data was discovered to be normally distributed, therefore pairwise comparison (t.tests) were used. Significant differences are shown on the plots (TRAIP-mAID C2 – Triptolide: p = 0.0243; TRAIP-mAID D5 – Triptolide: p = 0.0259).

5.2.8 TRAIP Degradation Leads to Increased DNA Replication - Transcription Collisions

The data presented strongly suggested that the mechanism requiring TRAIP involved RNA polymerase II present on chromatin. Furthermore, our γ-H2AX ChIP sequencing data implicated DNA replication – transcription conflicts at the first gene encountered by the replisome, possessing bi-directional transcription activity, as the potential genomic location. Consequently, I next aimed to directly visualise DNA replication-transcription collisions following TRAIP degradation. For this, proximity ligation assay (PLA) was used. PLA identifies interactions between two substrates, in this case nascent DNA (EdU) and elongating RNA polymerase II (Serine 5 CTD phosphorylated); each recognised by primary and secondary antibodies, the latter of which were conjugated to DNA oligonucleotides. If the two substrates are within close proximity, then the oligonucleotides are hybridised into a closed loop. Subsequent rolling circle assays amplifies any hybridised structures, detectable using fluorescent complimentary DNA sequences.

The conditional degron cells were synchronised in G1, treated with IAA for 1 hour, and then released into S-phase. When cells were in early S-phase (12 hours post release), known to be the stage of maximal transcription and replication levels, EdU was added for 20 minutes to label nascent DNA (Figure 5.18B). Cells were then fixed and prepared for PLA as described in the materials and methods. Any resulting foci, representing the presence of elongating RNA Polymerase II in proximity of newly synthesised DNA, were quantified using CellProfiler (Figure 5.18A). Overall, no differences to the total proportions of cells exhibiting PLA foci could be detected (Figure 5.18C). However, when we explored further the cells possessing high

proportions of PLA events (> 5 per cell; Figure 5.18D), TRAIP-dependent variations emerged. Specifically, TRAIP degradation led to the increased presence of RNA polymerase II in proximity to the replication fork. Therefore, the loss of TRAIP either directly caused an increased frequency of replication-transcription collisions, or led to defects in their resolution.

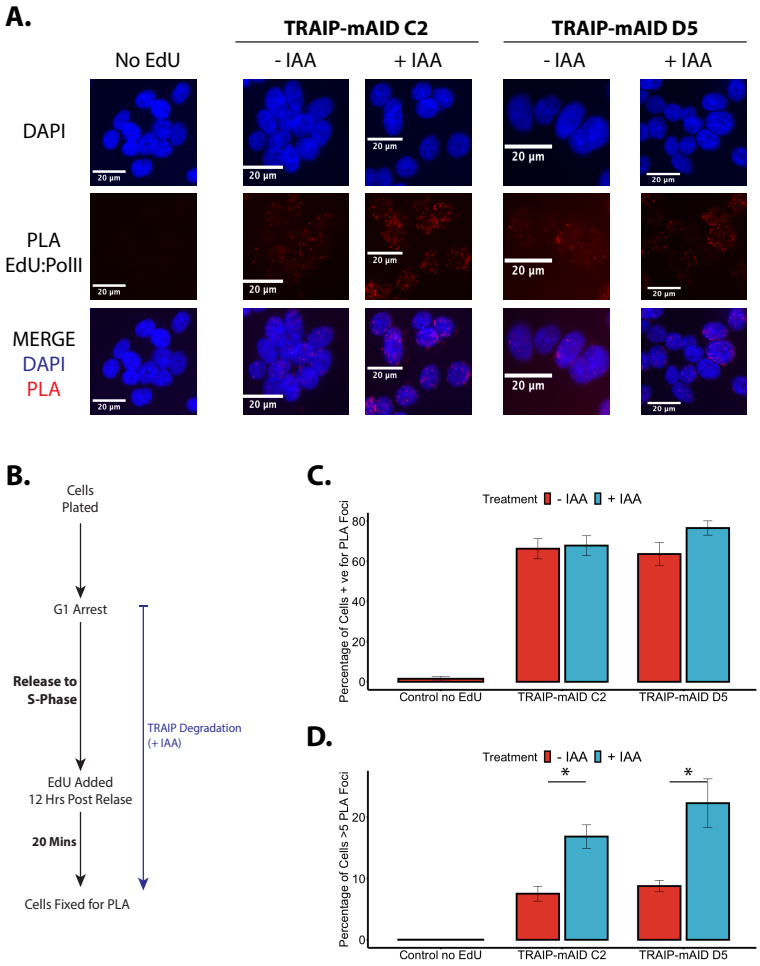


Figure 5.18: **Loss of TRAIP leads to Increased Presence of RNA Polymerase II on Nascent DNA.** To understand whether TRAIP was required for the resolution of conflicts between replication forks (nascent DNA) and active RNA Polymerase II, PLA assay were used. S-phase cells were treated with EdU to label nascent DNA, subsequently detected using Click-iT chemistry and anti-biotin antibodies along with anti-Serine 5 phosphorylation of CTD. Shown is data collected over three independent experimental repeats, with an average of 983 nuclei analysed per condition, per repeat. **A.** Example images, showing PLA events detecting the presence of RNA polymerase II in proximity to newly synthesised DNA. Staining depicted is DAPI (blue) and PLA (red). **B.** Experimental schematic used. **C.** Quantification of the total proportion of cells positive for PLA events. Cells were quantified using CellProfiler, described previously. **D.** Quantification of the total proportions of cells containing > 5 PLA foci. Data was determined to be normally distributed and therefore T-tests were used. Significance is displayed on the plot (TRAIP-mAID C2: p = 0.02; TRAIP-mAID D5: p = 0.0442).

5.2.9 TRAIP and ATR Show Possible Interactions in Inducing DNA Damage

Previously, I have shown that the G2 cell cycle arrest caused by TRAIP degradation was rescued following treatment of the cells with ATR inhibitors. Furthermore, treatment with ATM inhibitors led to increased G2 accumulation, suggesting the potential sensitisation of cells to ATM inhibition following TRAIP degradation (Figure 4.14). The rescue of the G2 cell cycle arrest with ATR inhibitors does not necessarily mean that any created damage is resolved, as cells are less efficient at responding to increasing replicative stress without ATR. To understand this phenotype further and highlight any therapeutic potential of TRAIP as a druggable target, the conditional degron cell lines were treated with both IAA and either ATRi or ATMi for 24 hours. Any resulting sensitisation of cells without TRAIP, to the respective inhibitors, was determined through quantification of the numbers of formed DNA damage foci (γ-H2AX S139 or 53BP1; Figure 5.19).

Both γ-H2AX and 53BP1 foci were found to accumulate following IAA treatment, irrespective of the inhibitor used. ATM inhibition alone was found to not lead to increased DNA damage, nor was it shown to act in an additive or antagonistic manner with TRAIP degradation. Conversely, ATR inhibition itself was found to result in the accumulation of both γ-H2AX and 53BP1 foci. When ATR inhibition was used in combination with TRAIP degradation, differences were observed. When considering the formation of 53BP1 foci, the results presented suggest that TRAIP degradation has an additive relationship with ATR inhibition, leading to increased DNA damage. Conversely, much lower increases were observed in γ-H2AX foci formation; with differences only reported in the D5 clone. However, we must also consider that those cells treated with ATRi alone also show increased levels of damage. This raises the possibility of an

antagonistic relationship, as the approximate increases in cells positive for damage is reduced after ATRi treatment when compared to the untreated controls (-/+ IAA). However, more work will be required to follow up on these observations, and ascertain whether TRAIP has any interplay with ATR in inducing DNA damage.

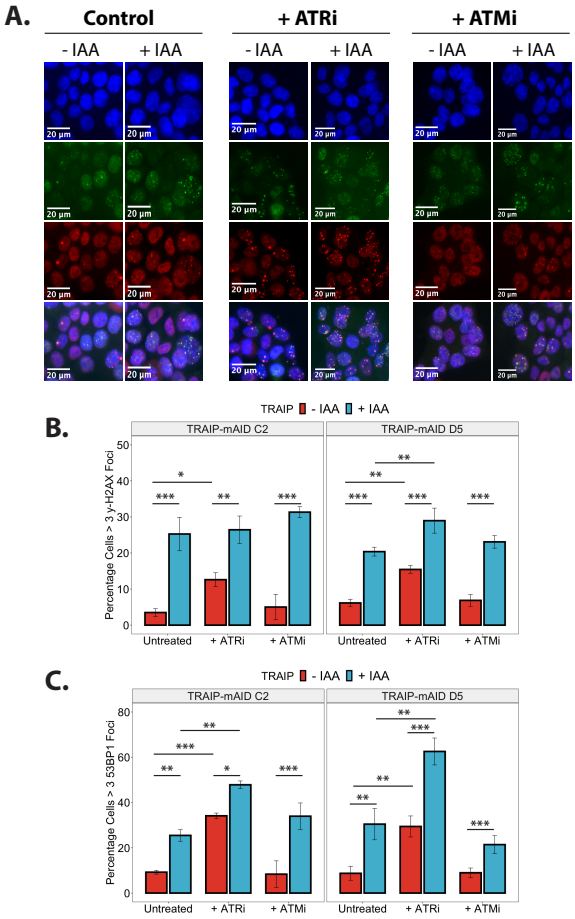


Figure 5.19: **TRAIP and ATR Show Possible Interactions in Inducing DNA Damage.** To understand any interplay between TRAIP and ATR/ATM inhibition, cells were treated for 24 hours with both IAA and a respective inhibitor against the respective kinase of interest. Date was collected over three independent experimental repeats, with an average of 1534 nuclei quantified per condition per repeat. **A.** Example cells. Shown is staining for DNA (DAPI: blue), γ-H2AX (S139; green), and 53BP1 (red) following the appropriate cell treatment. **B.** Quantification of the γ-H2AX foci. Any formed foci were quantified using Cell Profiler, and the proportions of damaged cells (> 3 foci) quantified. Data shown as the mean -/+ SEM. Statistical analysis was carried out using parametric tests (ANOVA and pairwise comparisons). Significance is summarised on the plots for TRAIP-mAID C2 (Untreated – IAA vs Untreated + IAA: $p < 0.001$; + ATR – IAA vs + ATR + IAA: $p = 0.00741$; + ATM – IAA vs + ATM + IAA: $p < 0.001$; Untreated – IAA vs + ATR – IAA: $p = 0.00280$) and TRAIP-mAID D5 (Untreated – IAA vs Untreated + IAA: $p < 0.001$; + ATR – IAA vs + ATR + IAA: $p < 0.001$; + ATM – IAA vs + ATM + IAA: $p < 0.001$; Untreated – IAA vs + ATR – IAA: $p = 0.00461$; + IAA vs + ATR + IAA: $p = 0.00751$). **C.** Quantification of the 53BP1 foci. Any formed foci were quantified using Cell Profiler, and the proportions of damaged cells (> 3 foci) quantified. Data shown as the mean -/+ SEM. Statistical analysis was carried out using parametric tests (ANOVA and pairwise comparisons). Significance is summarised on the plots for TRAIP-mAID C2 (Untreated – IAA vs Untreated + IAA: $p = 0.00859$; + ATR – IAA vs + ATR + IAA: $p = 0.0214$; + ATM – IAA vs + ATM + IAA: $p < 0.001$; Untreated – IAA vs + ATR – IAA: $p < 0.001$; + IAA vs + ATR + IAA: $p = 0.001$) and TRAIP-mAID D5 (Untreated – IAA vs Untreated + IAA: $p = 0.00702$; + ATR – IAA vs + ATR + IAA: $p < 0.001$; + ATM – IAA vs + ATM + IAA: $p < 0.001$; Untreated – IAA vs + ATR – IAA: $p = 0.00933$; + IAA vs + ATR + IAA: $p = 0.0044$).

5.3 Discussion

The characterisation of TRAIP degradation presented a clear overview of the cascade inhibiting cell proliferation. The loss of TRAIP in otherwise unperturbed cells led to the accumulation of DNA damage, which in turn, activated the ATR-WEE1-CHK1 checkpoint axis. However, the respective molecular mechanisms causative of the increased DNA damage, underpinning the cell proliferation defects, remained unknown. To begin to explore this, it was imperative to first understand where in the cell cycle TRAIP was required. By combining the rapid nature of TRAIP-mAID degradation with cell synchronisation and our established read-out of G2 accumulation, we revealed that TRAIP was specifically required for S-phase. A single round of S-phase without TRAIP was sufficient to halt cell proliferation. In addition, cells that underwent mitosis without TRAIP, and then re-synthesised TRAIP before the following S-phase, did not accumulate during G2/M. Finally, cells lacking TRAIP-mAID were found to accumulate DNA damage throughout S-phase, that appeared to persist to the following G1. Altogether, this data suggested that the mitotic roles for TRAIP were not the primary mechanism required for cell viability, which instead occurred in S-phase.

During S-phase, TRAIP is thought to be required for the maintenance of genomic stability. Notably, much of the work surrounding TRAIP has focused on the response to DNA damage or replication stress-inducing agents (Feng et al., 2016; Harley et al., 2016; Hoffmann et al., 2016; Soo Lee et al., 2016). On the other hand, the current understanding as to the role of TRAIP during unperturbed conditions, is comparably poor. Despite reported interactions between TRAIP and key replisome components, specifically PCNA and CMG (Feng et al., 2016; Hoffmann et al., 2016), we detected no defects to either the total amount of replication undertaken by

the cell, of the binding pattern of the replisome. Given this and our observation of increased DNA damage during S-phase, we decided to carry out γ-H2AX ChIP-sequencing to map where in the genome TRAIP-dependent DNA damage was accumulating. We hypothesised that the resulting data would have one of two possible outcomes. If the detected damage was randomly dispersed throughout the genome, then it was likely that TRAIP was an important DNA damage repair protein, and the lack of TRAIP would lead to an inability to process endogenously forming DNA lesions. Conversely, if the ChIP-Sequencing resulted in the identification of specific genomic locations susceptible to TRAIP-dependent DNA damage, these may point towards an alternative mechanism of action responsible for cell viability.

The γ-H2AX ChIP-sequencing identified TRAIP-dependent DNA damage to be closely associated with RNA Polymerase II transcripts, at transcription start sites. Consideration as to any potential features nearby that may explain the observed damage highlighted that the conserved peaks were close to replication origins. This result, in itself, was not surprising as it is well established that replication origins are typically positioned close to transcription start sites, particularly in highly transcribed genes (Chen et al., 2019). In bacterial systems, it has been reported that this relationship facilitates co-operation between replication and transcription, both traversing DNA in the same direction to avoid head-to-head conflicts between the two processes (Srivatsan et al., 2010). Less is known in human cell systems. Although data is emerging to suggest that replication initiates near transcription start sites possessing RNA Polymerase II, conferring similar genome organisation (Chen et al., 2019). Also, TSS usually reside in more open regions of chromatin, and thus may be preferred locations for ORC binding and replication origin establishment. Interestingly, the TSS with

high levels of γ-H2AX following TRAIP degradation resided closer to replication origins than regions with low γ-H2AX, and when compared to all transcribed genes. Moreover, the sites of conserved γ-H2AX were shown to possess clear evidence of transcription progressing in both directions from the start site, and were preferentially located at the first TSS encountered by the replisome. This is consistent with a model where upon the progressing replisome will encounter RNA polymerase II close to the TSS. Without TRAIP, the data indicated that these conflicts remained unresolved, resulting in the accumulation of replication stress and probable fork stalling. Analogous to this, siRNA depletions of TRAIP have been shown to result in asymmetric replication forks using DNA fibre assays, representative of single fork stalling (Hoffmann et al., 2016).

Aside from direct conflicts between RNA polymerase II and CMG, a further source of transcription associated genomic instability is the formation of RNA:DNA hybrids (R-Loops) (Skourti-Stathaki and Proudfoot, 2014). Previous work has shown that R-loops can impair replisome progression, although CMG is able to overcome encountering R-loops on chromatin, often with the assistance of accessary helicases (e.g., PIF1) (Brüning and Marians, 2020; Schauer et al., 2020). Given our data, we wondered whether TRAIP may be involved in the resolution of CMG – R-Loop conflicts. We could detect no large changes to the presence of R-loops in the degron cells before and after IAA treatment (data not shown). However, to visualise R-loops we utilised immunofluorescence approaches using the S9.6 antibody. Use of the S9.6 antibody is generally not recommended for immunofluorescence due to non-specific binding (Smolka et al., 2021). As a result, whilst our data suggested no role for TRAIP in R-loop resolution, further work would be required, using more robust techniques (e.g., using

DNA-R-Loop Immunoprecipitation or mutant RNASE H2 to label R-loops) (Chédin et al., 2021).

Overall, the data suggested that TRAIP was required for a mechanism at TSS, correlating with likely sites of DNA replication – transcription conflicts. Alternatively, it was possible that TRAIP was directly involved in transcriptional regulation. In several forms of cancer, oncogene deregulation has been shown to stimulate excessive gene transcription, creating more conflicts and resulting in genome instability (Bowry et al., 2021; Kotsantis et al., 2016). Intriguingly, TRAIP degradation was found to instead reduce the global levels of transcription undertaken. It was possible that, if TRAIP was required for resolving replication – transcription collisions, then without TRAIP, conflicts would result in both replication and transcription machineries stalling. Whilst replication fork stalling following TRAIP degradation has been shown (Hoffmann et al., 2016), any respective impact on polymerase progression remained unclear. Thus, future work should aim to address this. Excessive DNA polymerase stalling may lead to the reductions in transcriptional activity shown, and could be confirmed through qPCR screens using primers specific to the conserved genes found to possess γ-H2AX peaks.

Any accumulating DNA damage caused by TRAIP degradation was shown to be rescued through triptolide treatment, suggesting that the respective mechanism involved required RNA Polymerase II loaded at TSS. Similarly, when we prevented the progression of RNA Pol II into the gene body (DRb treatment), additive effects with IAA were not found. To attempt to understand why different results were observed using different transcriptional inhibitors, the respective mechanisms of action must be considered. Triptolide is a transcription factor II H (TFIIH) inhibitor that prevents the loading of RNA Polymerase II onto gene promoters

(Erickson et al., 2018). Mechanistically, triptolide inhibits transcription initiation through inducing degradation of the major RNA Polymerase II sub-unit Rbp1 (Wang et al., 2011). DRB, on the other hand, inhibits the phosphorylation and release of RNA Polymerase II into the gene body (Stoimenov et al., 2011). Our ChIP-sequencing data suggested that particularly crowded transcription start sites preferentially exhibit high γ-H2AX levels. It may be that the differences observed arised from the variable protein levels at these sites after treatment with the two inhibitors. On the other hand, studies have demonstrated that DRB treatment triggers the efficient removal of RNA Polymerase II from gene promoters (Erickson et al., 2018). DRB treatment has also been implicated in increased R-loop formation at sites of paused transcription (Chen et al., 2017); potentially increasing the number of barriers for the replisome to overcome without TRAIP, resulting in the increased levels of genomic instability found. Alternatively, there may be a DNA damage dependency. The HCT116 cells treated with DRB only exhibited higher levels of DNA damage than those treated with triptolide. TRAIP degradation was not additive with this treatment. RNA Polymerase II has been shown to be ubiquitylated by several proteins in human cells (including BRCA1, von Hippel-Lindau proteins, and NEDD4) (Ingham et al., 2004; Kuznetsova et al., 2003; Starita et al., 2005). This highlights the possibility of multiple mechanisms processing RNA Polymerase II under different circumstances. It may be that, in the case of RNA Polymerase II stalling upon DRB treatment, the mechanisms involving TRAIP have redundancies with alternative pathways stimulating RNA Polymerase II removal. Further work is therefore required to dissect the precise mechanisms underpinning the TRAIP-dependent differences discovered upon transcriptional inhibition. Specifically exploring R-loop resolution and more closely the types of DNA damage formed following TRAIP degradation. In addition, it would be interesting to explore the effects of

α-amanatin (RNA Polymerase II inhibitor).

Altogether, this data links the TRAIP mechanism of action specifically with RNA polymerase II activity, further corroborating the ChIP-sequencing data. It would be interesting to explore whether experiments could be carried out to upregulate transcription in combination with TRAIP degradation. However, the stimulation of transcription artificially in mammalian cells is difficult and will often have impacts on other cellular processes. In addition, as not every transcription start site possessed high levels of DNA damage without TRAIP, global changes in transcriptional activity may not affect the specific regions identified to require TRAIP. We therefore attempted to identify whether any conserved genes were expressed through hormone receptor binding or similar. Unfortunately, no such genes were discovered in the data set.

Finally, proximity ligation assays confirmed increased replication-transcription conflicts following TRAIP degradation. Altogether, the loss of TRAIP led to the increased presence of elongating RNA polymerase II on nascent DNA, close to the replication fork. The roles identified during this chapter highlighted TRAIP as a key promoter of genomic stability at sites of transcription associated replication stress. The phenotypes presented underpin the losses to cell viability following TRAIP degradation and offer a clear mechanism responsible for the observed G2 arrest and cell cycle exit. Moreover, defective replication-transcription conflict resolution would potentially block both replication fork and transcription progression, offering explanation as to why patients with TRAIP mutations are characterised by reduced cell proliferation and dwarfism phenotypes (Harley et al., 2016); instead of the classical Fanconi

Anaemia syndromes often associated with defective ICL repair proteins (Moreno et al., 2021), as TRAIP has been reported (Wu et al., 2019).

Chapter 6

The Role of TRAIP in Replisome Disassembly

6.1 Introduction

TRAIP was originally selected for study during this PhD project as it had been identified to accumulate with terminating replisomes upon the inhibition of S-phase replisome disassembly. Chapter 1 of this PhD thesis contributed to the elucidation of TRAIPs role during mitotic replisome disassembly using *X. laevis* egg extracts, shown by our group and others (Deng et al., 2019; Moreno et al., 2019). Analogous roles for TRAIP have also been demonstrated using *C. elegans* (Sonneville et al., 2019) and mouse embryonic stem cells (Villa et al., 2021). Furthermore, during mitosis TRAIP has been shown to be important for mitotic DNA synthesis (Sonneville et al., 2019); although it is currently unclear whether this role encompasses replisome disassembly at sites of under-replicated DNA. As a result, I next aimed to explore whether the reported mitotic roles for TRAIP were conserved in human somatic cells. In addition, we were interested in understanding whether any mechanism for TRAIP during mitosis was independent from those reported in S-phase, or part of a more generalised

pathway for promoting genomic stability. However, until recently, the process of replisome disassembly had not been studied in mammalian cell systems (Fan et al., 2021; Villa et al., 2021). Due to this, before carrying out work to investigate the role of TRAIP, our existing knowledge of the replisome disassembly pathways from model organisms were validated in human immortalised cancer cell lines using the generated HCT116 cell lines.

6.2 Results

6.2.1 The Role of p97 in Replisome Disassembly

The p97 segregase is thought to be essential for both S-phase and mitotic replisome disassembly. Work from several groups has shown that, upon replisome convergence and MCM7 ubiquitylation, p97 is recruited to the formed ubiquitin chains to facilitate CMG unloading. Thus, to begin to understand the mechanisms regulating replisome disassembly in human somatic cells, we first asked whether p97 was similarly indispensable. HCT116 control cells (CMV-OsTIR1 only) were treated with the p97 inhibitor CB5083 for 6 hours, sufficient to allow any S-phase cells to complete DNA replication. The cells were then harvested and extracted with CSK buffer to remove soluble fractions, described previously (Forment and Jackson, 2015). Subsequent staining with antibodies against MCM7 allowed for visualisation of the binding pattern of the replisome to chromatin (See **Figure 4.4**). Overall, the treatment of asynchronous HCT116 cells with p97i for 6-hours had no observable effect on the cell cycle as no differences could be detected to the proportions of cells in G1, S, or G2/M using the total DNA content (Figure 6.1A-D). Visually, it initially appeared that more cells were present in S-phase, however the observed differences only translated to minor increases (approximately

10% in the quantification values included in the example, shown in Figure 6.1B) that were not statistically significant nor consistent across all three repeats. Differences were also observed to the total numbers of cells collected following p97i treatment, highlighted by differences to the histogram y-axis not found in other experiments (Figure 6.1B). Conversely, consideration of the proportion of cells positive for pH3S10 (marker of condensed chromosomes) revealed significantly less mitotic cells following p97i treatment (Figure 6.1E and F). As a result, we were unable to explore the mitotic replisome disassembly pathways with this experimental approach and further optimisation was required.

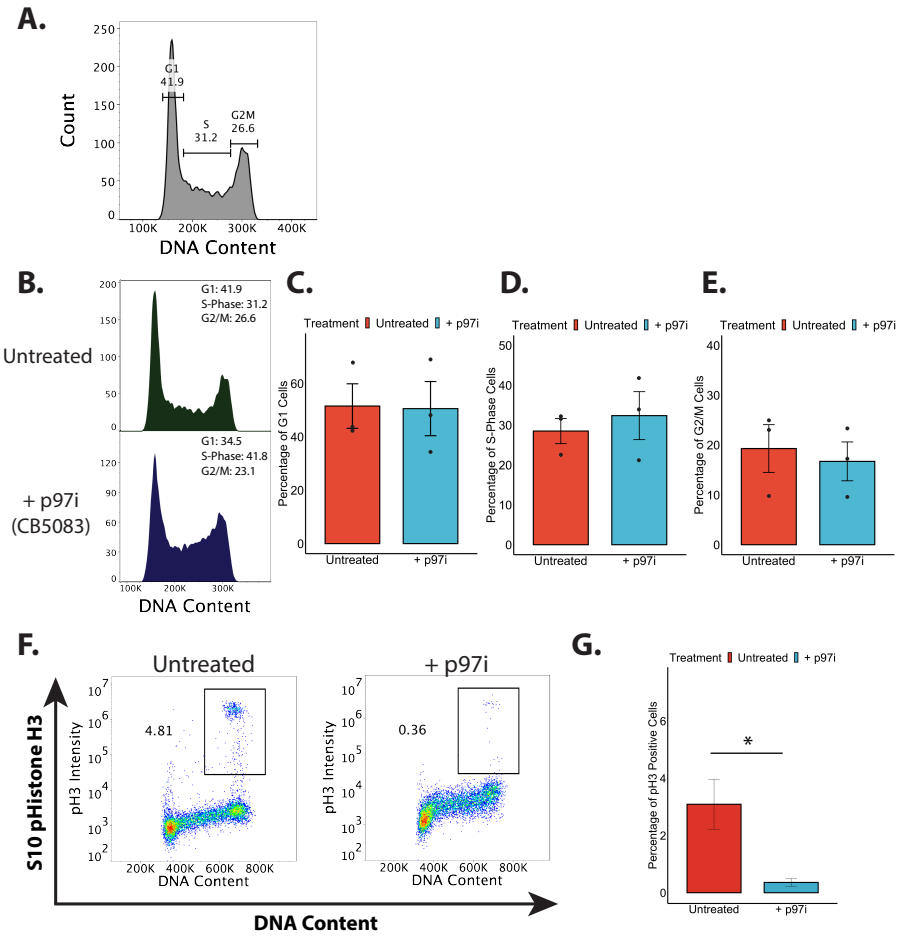


Figure 6.1: **p97 Inhibition Leads to Reductions in the Mitotic Cell Population.** To understand the impacts of p97 inhibition throughout the cell cycle, asynchronous cells were treated for 6 hours with the p97i CB5083. Cells were then extracted using CSK buffer and fixed. Fixed cells were stained with antibodies against S10 Histone H3 phosphorylation (mitotic marker), and with Hoechst to label the total DNA content. Data shown was collected over three independent experimental repeats. **A.** Example of the gating established to determine the proportions of cells in each cell cycle stage. Cells were gated as previously detailed to isolate the single-celled populations of interest (see Figure 2.5), capturing a minimum of 10,000 cells per condition per repeat within the cell cycle. Cells in G1, S-phase, and G2/M were then quantified by placing gates in the positions shown. Gates were set using untreated control samples before being applied to all samples. **B.** Example cell cycle profiles. Shown are untreated controls (green) and p97i treated (blue) cells. **C.** Quantification of the total proportion of G1 cells. Shown is the mean percentage G1 cells -/+ SEM. **D.** Quantification of the total proportion of G1 cells. Shown is the mean percentage S-phase cells -/+ SEM. **E.** Quantification of the total proportion of G1 cells. Shown is the mean percentage G2/M cells -/+ SEM. **F.** Example plot showing of the total proportion of cells positive for S10 Histone H3 phosphorylation. The positive cell population is indicated by the black box. Associated percentages are displayed to the left of the applied gate. **G.** Quantification of the proportion of mitotic cells from E. Shown is the mean percentage of cells positive for S10 Histone H3 phosphorylation. Error bars are displayed as the SEM. Clear defects were observed following p97i treatment (t.test p = 0.0431).

Despite the loss of the mitotic cell population following CB5083 treatment, we were still able to explore the effects of p97 inhibition on the binding pattern of the replisome to chromatin

(Figure 6.2). Cells were treated, extracted using CSK buffer, and stained for MCM7 as described above. Visual comparison of the overall MCM7 intensity between untreated and treated controls highlighted defects to both replisome loading (G1), and replisome disassembly (G2/M). During G1 stage of the cell cycle, we observed cells undergoing origin licensing, represented by increasing MCM7 intensity below the main, fully licensed, G1 population (Figure 6.2A). Interestingly, the addition of p97i to the cells resulted in the loss of cells with this intermediary MCM7 signal. Subsequent quantification of the total proportions of G1 cells with high (completed origin licensing) or low (undergoing origin licensing) MCM7 intensity (Figure 6.2A) confirmed this observation (Figure 6.2B). MCM2-7 double hexamers are loaded onto chromatin during late mitosis and G1 (Moreno and Gambus, 2015) and the overall reductions in mitotic cells after p97i was the most likely reason for the lack of intermediary MCM2-7 signal.

During S-phase, both active and dormant origins are disassembled. p97i treatment had no impact on the removal of dormant origins, demonstrated by the steady reduction of MCM7 signal throughout S-phase (Figure 6.2C, top panel). Hence, to understand the respective impact of p97 inhibition on active CMG, we instead focused on the G2/M cell population. In control cell lines, during G2/M, neither active nor dormant origins should be present on chromatin. Therefore, the G2/M MCM7 intensity in the controls was used to set gates encompassing all cells negative for MCM7 (Figure 6.2C, bottom panel). The established gates were then applied to p97i treated samples, revealing overall increases in MCM7 intensity during G2/M, represented by the upwards shift of the main cell population (Figure 6.2C and D). Altogether, the data suggested that p97 was required for replisome disassembly during S-phase, analogous to previously published roles. Although, caveats within the data set

required addressing. First the loss of the mitotic cell population, and G1 cells undergoing origin licensing, required exploring further. Second, whilst we observed defects to unloading during G2/M, we were unable to investigate mitotic replisome disassembly due to the lack of mitotic cells.

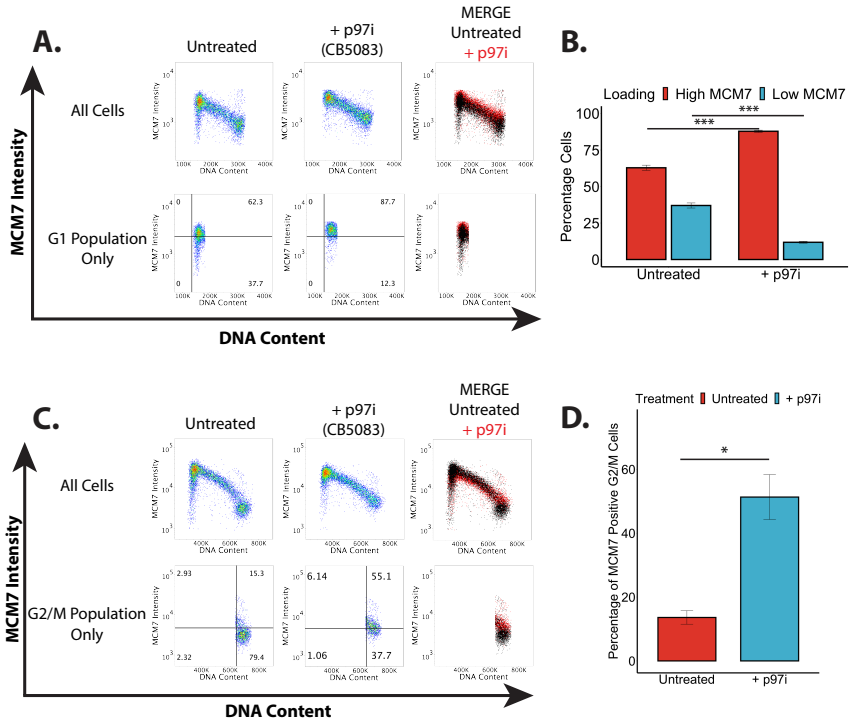


Figure 6.2: **p97 is Important for MCM7 Binding Throughout the Cell Cycle I.** To understand any role of p97 in replisome disassembly, asynchronous cells were treated for 6 h with CB5083. Cells were extracted using CSK buffer, fixed, and the binding pattern of the replisome visualised through immunofluorescence using MCM7 antibodies. Cells were gated as described in the materials and methods (see Figure 2.5). Shown is data collected from three independent experimental repeats, with a minimum of 10,000 cells captured within the cell cycle gate per condition, per repeat. **A.** Example FACS plots showing the replisome binding pattern (MCM7 intensity; y axis) throughout the cell cycle (DNA content; x axis). All cells are shown (top) for reference, alongside G1 cells only (2N DNA content; bottom). The gates applied to quantify the proportion of MCM7 during G1 are shown. Cells were classified as possessing either high MCM7 (top right quadrant) or low MCM7 (bottom right quadrant). **B.** Quantification of the high and low MCM7 levels observed in G1 cells after CB5083 treatment. Data was plotted showing the mean percentage of cells within each quadrant -/+ SEM. Statistical analysis revealed increases to the proportions of cells containing high MCM7 intensity, and reductions to the cells with low MCM7 intensity (ANOVA: $p > 0.001$; Tukey post-hoc test: $p > 0.01$ for both comparisons). **C.** Example FACS plots showing the reference replisome binding pattern (as detailed in A) and the proportion of MCM7 bound to chromatin specifically during G2/M (bottom). The gates applied to quantify the proportion of MCM7 during G2/M are shown; with cells positive for MCM7 residing in the top right quadrant. **D.** Quantification of the proportion of MCM7 retained into G2/M following p97i. The mean percentage of cells positive for MCM7 were plotted alongside the SEM. Pairwise comparison discovered increased MCM7 retention following 6 h CB5083 treatment (t. test: $p = 0.025$).

The loss of the mitotic cell population, combined with reductions to cells undergoing origin licensing during G1 stage of the cell cycle, suggested that p97 inhibition led to defective cell cycle progression. However, analysis of the total DNA content following p97i treatment did not reveal any cell cycle perturbations. Therefore, to further understand the role of p97 during the eukaryotic cell cycle, I utilised BrdU pulse chase assays to track S-phase progression. Asynchronous cells were first treated with CB5083 and BrdU. After 1-hour of BrdU treatment, labelling S-phase cells, the BrdU was removed (Figure 6.3A) and CB5083 maintained. Approximately 5 hours later cells were harvested and prepared for flow cytometry as described in the materials and methods. If p97 was required only for mitotic entry it was likely that inhibitor treatment would have no effect on S-phase progression, and the cell cycle position of BrdU labelled cells would match that of untreated controls. Alternatively, if p97 was important for S-phase, then defects would become apparent. Gates were established using control cell lines harvested immediately following BrdU treatment (Figure 6.3C) and applied to all samples. In untreated controls, the BrdU positive cells were shown to progress from S-phase into G2/M as expected. On the other hand, p97i treated cells were found to predominantly remain in early to mid S-phase. Correspondingly, reductions were observed to the proportions of BrdU positive cells in late S-phase and G2/M after p97 inhibition. The population of BrdU positive G1 cells in untreated controls likely represented cells that, upon BrdU treatment, were in late-S phase and consecutively progressed through mitosis. This G1 population of BrdU positive cells was also lost in samples treated with CB5083. Altogether, this data indicated that the inhibition of p97 perturbed cell cycle progression and induced slowed or arrested S-phase.

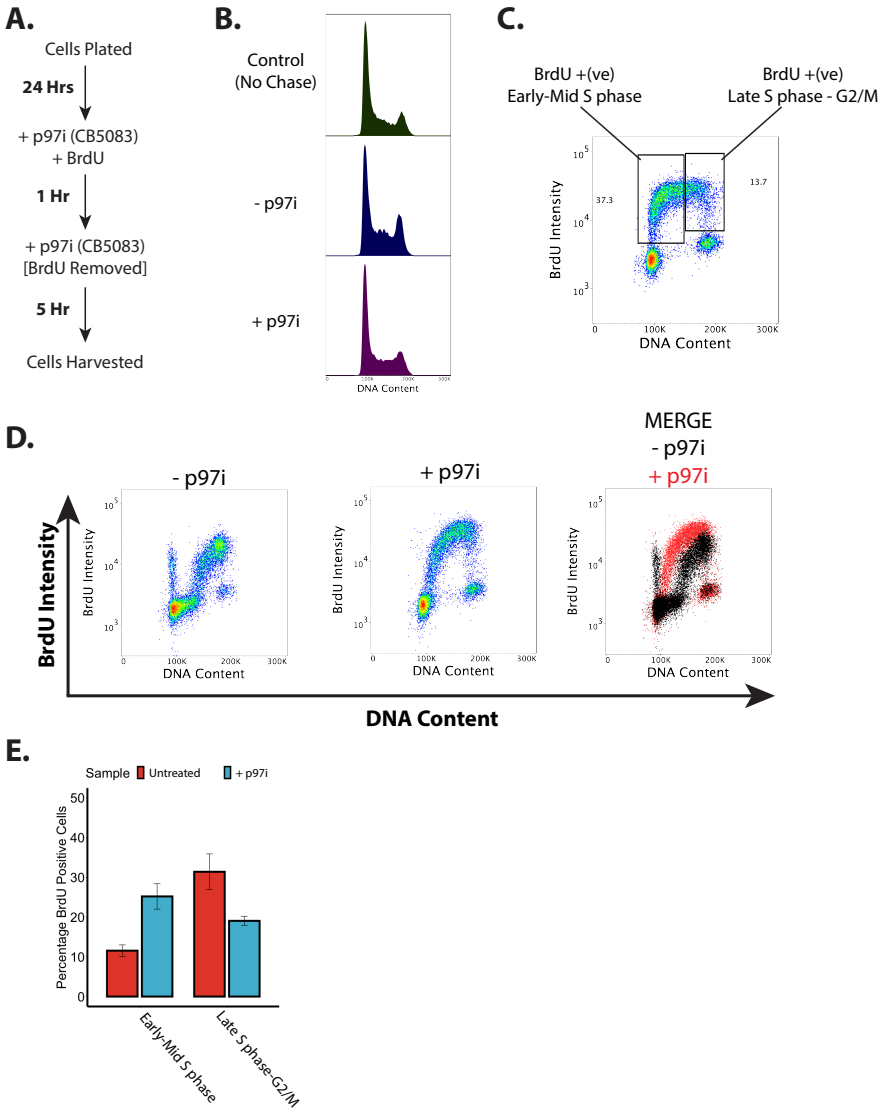


Figure 6.3: **p97 is Required for S-Phase Progression.** To understand the underlying cause of the reductions to mitotic entry following CB5083 treatment, we used BrdU-pulse chase to explore S-phase progression. Data shown was collected through two independent experimental repeats. **A.** Experimental Schematic. **B.** Cell cycle profiles showing total DNA content. Cells were gated as described previously in the materials and methods (see Figure 2.5), and data from a minimum of 10,000 cells falling within the cell cycle gate collected. Shown are control samples (taken 1-hour following BrdU addition without the chase; green), - p97 inhibitor (5-hour pulse, blue) and + p97 inhibitor (5-hour pulse, purple). **C.** Gating set-up. Gates were established based on the control cell lines to capture BrdU positive cells in G1/S and G2/M. **D.** Example FACS plots showing total DNA content plotted against the BrdU intensity. **E.** Quantification of the proportions of BrdU positive cells over two repeats. p97 inhibition was shown to result in the accumulation of cells in early-mid S phase as well as a reduction in cells in late S phase and G2/M. Shown is the mean percentage BrdU positive cells -/+ SEM. No statistical comparison was carried out due to only having two experimental repeats for this data set.

The slowed cell cycle progression and loss of mitotic cells following p97i prevented any analysis of the requirements for p97 in mitotic replisome disassembly. We next attempted, therefore,

to push cells into mitosis using the WEE1 inhibitor MK-1775. Use of this inhibitor was found to effectively overcome TRAIP-dependent G2 cell cycle arrest. As a result, it was hoped that WEE1 inhibition would have similar results on cells treated with p97i. However, with respect to replisome disassembly, it was important to first confirm that WEE1i had no effect on the overall binding pattern of MCM7 to chromatin as it has been previously shown to induce excessive dormant origin firing during S-phase (Moiseeva et al., 2019a). Asynchronous cells were treated with MK-1775 for between 30-120 minutes and prepared for flow cytometry as previously described. No major changes were observed to either the cell cycle profile, or replisome unloading pattern, between cells with and without MK-1775 (WEE1i) treatment (Figure 6.4A). Importantly, increased proportions of mitotic cells (positive for pH3S10) were found across all treatment times (Figure 6.4B). Notably, 30 and 60-minutes of WEE1i resulted in the maximal increase of mitotic cells. Thus, 60-minute treatment time was selected as this fit best with the established protocols followed previously to explore replisome unloading.

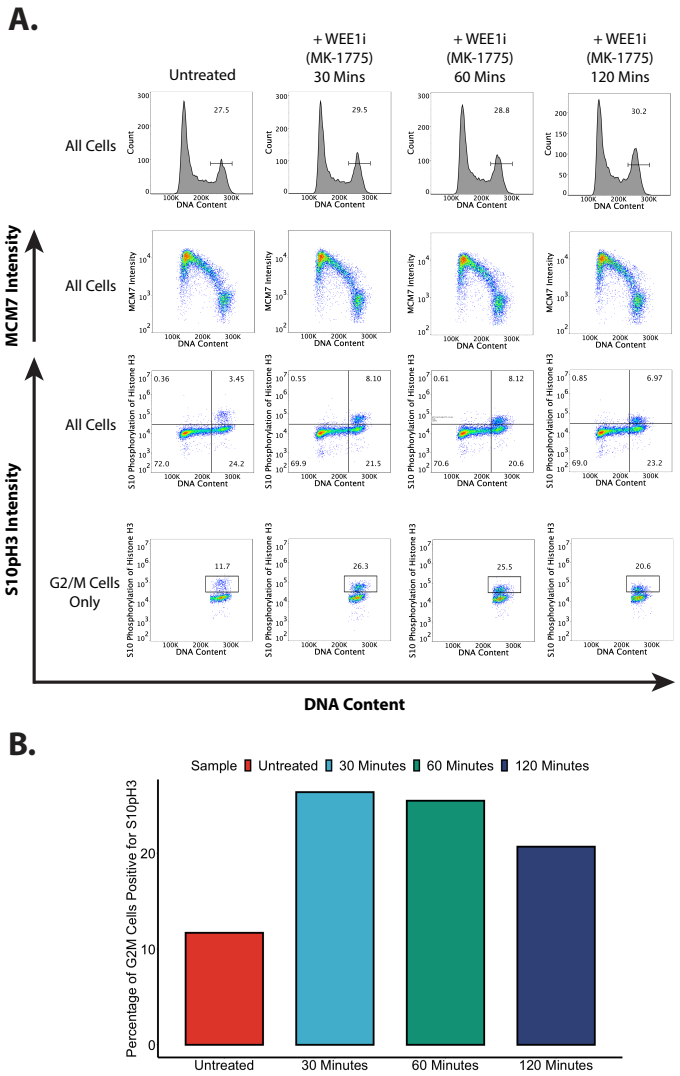


Figure 6.4: **WEE1 Inhibition Pushes Cells into Mitosis.** To select the optimal timepoint to use for WEE1 inhibitor treatment a timecourse was carried out. Asynchronous cells were treated with MK-1775 for 30, 60, and 120 minutes. Cells were harvested and prepared for flow cytometry as described in the materials and methods, staining for DNA content, MCM7, and pH3S10. Data from one experimental repeat is shown. To obtain the cell cycle profiles, cells were gated as detailed in the materials and methods (Figure 2.5). **A.** Example FACS images are shown: the cell cycle profiles (top), with the proportions of G2/M cells highlighted; the replisome binding pattern on chromatin following WEE1 inhibitor treatment (middle); the proportion of G2/M mitotic cells following WEE1 inhibitor treatment as indicted by histone H3 S10 phosphorylation (bottom two panels), the mitotic cells are indicated in the box. **B.** Quantification of the proportion of G2/M cells positive for pH3S10. The 60-minute treatment time was selected. No statistical comparison was conducted as the experiment was for validation purposes, and only one repeat was conducted.

Following validation of the ability of short WEE1 inhibitor treatments to push cells into mitosis without affecting the binding pattern of MCM7 to chromatin, nor the overall cell cycle distribution, the previous p97i experiment was repeated. Asynchronous cells were treated with

the p97i CB5083 for 6 hours, and WEE1i MK-1775 added for the final hour. The cells were then subjected to CSK extraction and stained as described previously. Similar to our earlier data, no differences were detected between the proportions of cells in G1, S, or G2/M following p97 and WEE1 inhibition (Figure 6.5A-D). Moreover, whilst MK-1775 treatment was able to push some cells into mitosis, defects to mitotic entry after p97 inhibition remained (Figure 6.5E and F). Despite this, as we were able to detect mitotic cells (pH3S10 positive) in both conditions, mitotic replisome disassembly was explored (Figure 6.6). The addition of the WEE1i MK-1775 was sufficient to rescue the previously highlighted defect to origin licensing (Figure 6.6B), confirming that this observation was a consequence of impaired cell cycle progression (compare Figure 6.6B and 6.2B). In addition, comparison of the total MCM7 intensity in all G2/M cells revealed a signal shift, corroborating our previous work and signifying replisome retention from S-phase into G2/M (Figure 6.6A and C). Moreover, consideration of the MCM7 intensity specifically in mitotic cells (positive for pH3S10) revealed a similar increase (Figure 6.6A and D), suggesting that p97 was also important for mitotic replisome disassembly. However, the increase to MCM7 intensity in mitotic cells were minor, and not the complete retention of MCM7 expected. It was possible that many of the cells retaining MCM7 could not progress into mitosis irrespective of MK-1775 treatment. Alternatively, there may be additional pathways facilitating replisome removal independently of p97 action, yet to be elucidated.

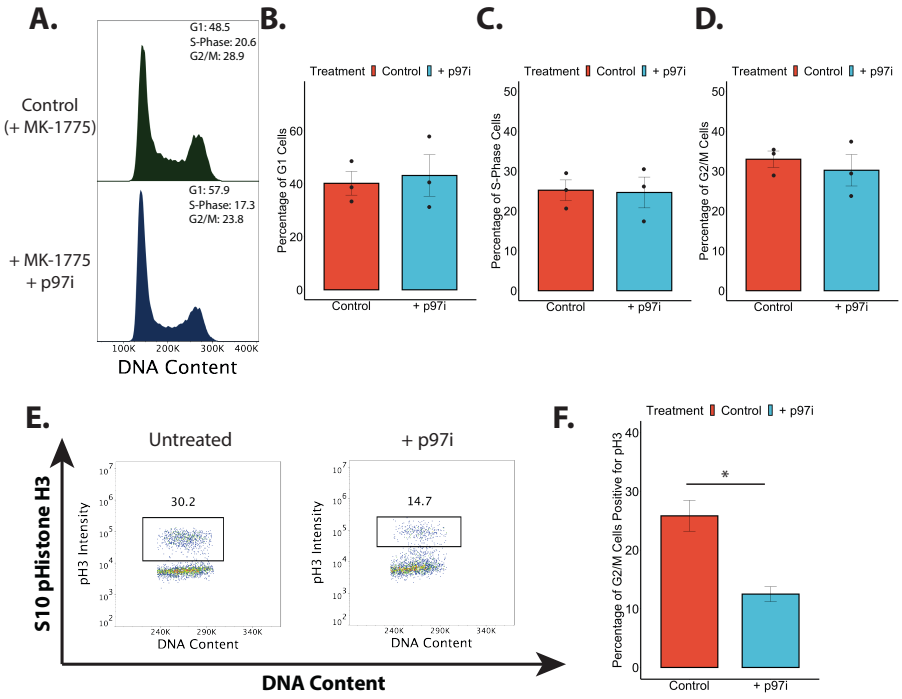


Figure 6.5: **p97 Inhibition Leads to Reductions in the Mitotic Cell Population II.** To explore mitotic replisome disassembly following p97 inhibition, cells were treated with CB5083 for 6 hours, adding the WEE1 inhibitor MK-1775 1 hour prior to harvesting. Cells were fixed and prepared as detailed previously (Figure 6.1). Cells were gated to quantify the populations of cells in G1 (2N DNA content), S-phase (2N > DNA content < 4N), and G2/M (4N DNA content) as depicted in Figures 2.5 and 6.1A. Data shown was collected from three independent experimental repeats. **A.** Example cell cycle profiles. Shown are cells treated only with WEE1i MK-1775 (Dark Green) and cells treated with p97i CB5083 and WEE1i MK-1775 (Dark Blue). **B.** Quantification of the proportion of cells in G1. Plotted is the mean percentage of cells -/+ SEM. **C.** Quantification of the proportions of cells in S-phase. Plotted is the mean percentage of cells -/+ SEM. **D.** Quantification of the proportions of cells in G2/M. Plotted is the mean percentage of cells -/+ SEM. **E.** FACS plots detecting the total proportion of G2/M cells positive for pH3S10. Mitotic cells are identified within the black box, and percentage shown above. **F.** Quantification of the total proportion of mitotic cells. Plotted is the mean percentage of cells -/+ SEM. Despite the use of WEE1 inhibitor to push cells into mitosis, significant reduction in the proportion of mitotic cells remained in comparison to control cells (t. test: p = 0.0215).

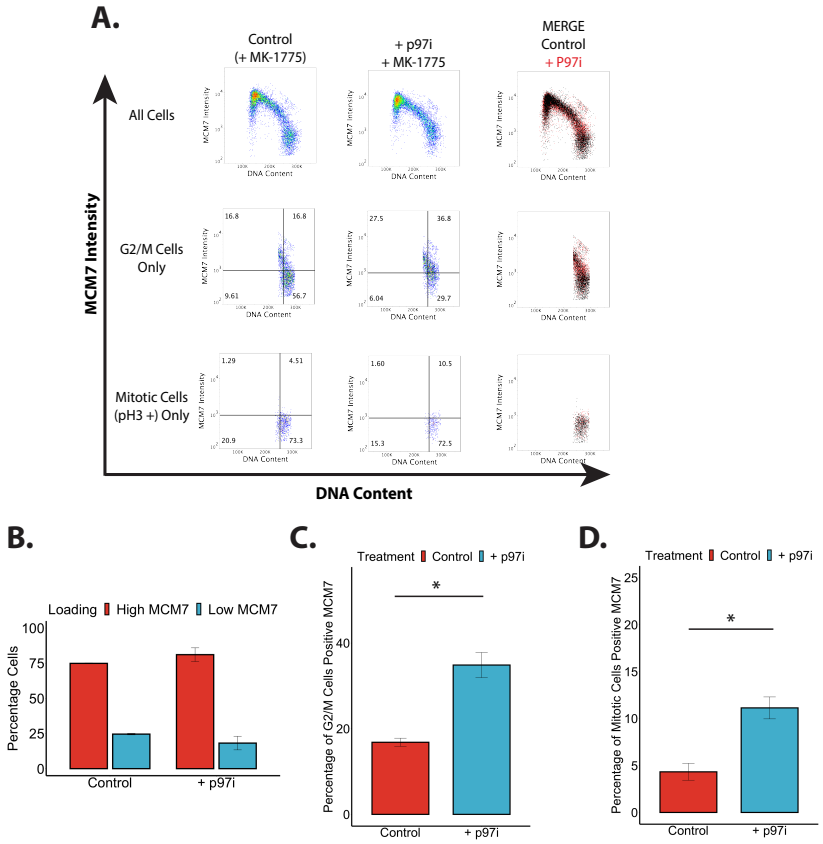


Figure 6.6: **p97 is Important for MCM7 Binding Throughout the Cell Cycle II.** Cells were prepared as detailed in Figure 6.2. Data shown is from three independent experimental repeats. **A.** Comparison of the replisome binding patterns for untreated cells as well as following p97 inhibition. The total DNA content was plotted against MCM7 intensity, for all cells (top), G2/M cells only (middle), or mitotic cells (bottom). **B.** Quantification of MCM7 intensity in G1 cells. Cells were defined as having either high MCM7 (main cell population) or low MCM7 intensity ('tail' of decreasing MCM7 intensity). Shown is the mean percentage of cells -/+ SEM. Statistical comparison revealed overall differences within the data set (ANOVA: $p < 0.001$). However, subsequent pairwise comparisons highlighted no differences between High and Low MCM7 intensity with respect to the cell treatment. **C.** Quantification of G2/M cells positive for MCM7. The gates shown in A were used, and the resulting proportions of positive cells plotted -/+ SEM. Pairwise comparisons were carried out using t. tests, depicting significant increases in positive cells following CB5083 treatment ($p = 0.0177$). **D.** Quantification of mitotic (pH3S10 positive) cells positive for MCM7. The gates shown in A were used and resulting proportions of cells plotted -/+ SEM. Pairwise comparisons were carried out using t. tests, depicting significant increases in replisome retention following CB5083 treatment ($p = 0.0115$).

6.2.2 The Role of Cullin-Type Ubiquitin Ligases in Replisome Disassembly

Whilst p97 is required universally for replisome disassembly, the ubiquitin ligase responsible for MCM7 modification differs between pathways. Specifically, work using several model systems has identified Cullin2^{LRR1} and TRAIP to be responsible for CMG ubiquitylation during

S-phase and mitosis, respectively (Deng et al., 2019; Moreno et al., 2019; Sonneville et al., 2017). Until recently, the involvement of Cullin2^{LRR1} during replisome disassembly was not clear in human somatic cells (Fan et al., 2021). Moreover, to date, no clear evidence exists for mitotic replisome disassembly in human cells. Therefore, I next aimed to validate the S-phase unloading using HCT116 cells. To this end, asynchronous cells were treated for 6 hours with the neddylation inhibitor MLN4924 to prevent Cullin activation, blocking the ubiquitylation of MCM7 during S-phase by Cullin2^{LRR1}. The treatment of cells with MLN4924 was shown to result in the accumulation of cells with G1/early S-phase DNA content (Figure 6.7A-D). Corresponding reductions were also observed to the proportion of cells with G2/M DNA content and specifically in mitosis (pH3S10 positive) (Figure 6.7E and F).

Comparison of the total MCM7 intensities across the cell cycle found MLN4924 treatment to result in a very different binding pattern to that observed after p97 inhibition (compare Figures 6.8A and 6.2A). MLN4924 targets all Cullin-type ubiquitin ligases, and previously published work has highlighted MLN4924 to induce large amounts of re-replication through the stabilisation of Cdt1 levels (Cullin1 and Cullin4 specific degradation) (Lin et al., 2010). Consequently, it was likely that the apparent loss of MCM7 unloading observed was instead constant reloading of MCM2-7 due to Cdt1 action. However, no clear signs of re-replication could be detected in our data (defined as cells possessing > 4N DNA content; Figure 6.8C). As we observed increased proportions of cells in G1 stage of the cell cycle by total DNA content, it was possible that not enough cells progressed through S-phase efficiently enough to allow for the detection of cells with > 4N DNA content. The isolation of G2/M cells using the total DNA content revealed significantly higher MCM7 levels in cells treated with MLN4924 (Figure 6.8A

and B); most likely caused through a combination of MCM2-7 re-loading and the inhibition of S-phase replisome unloading.

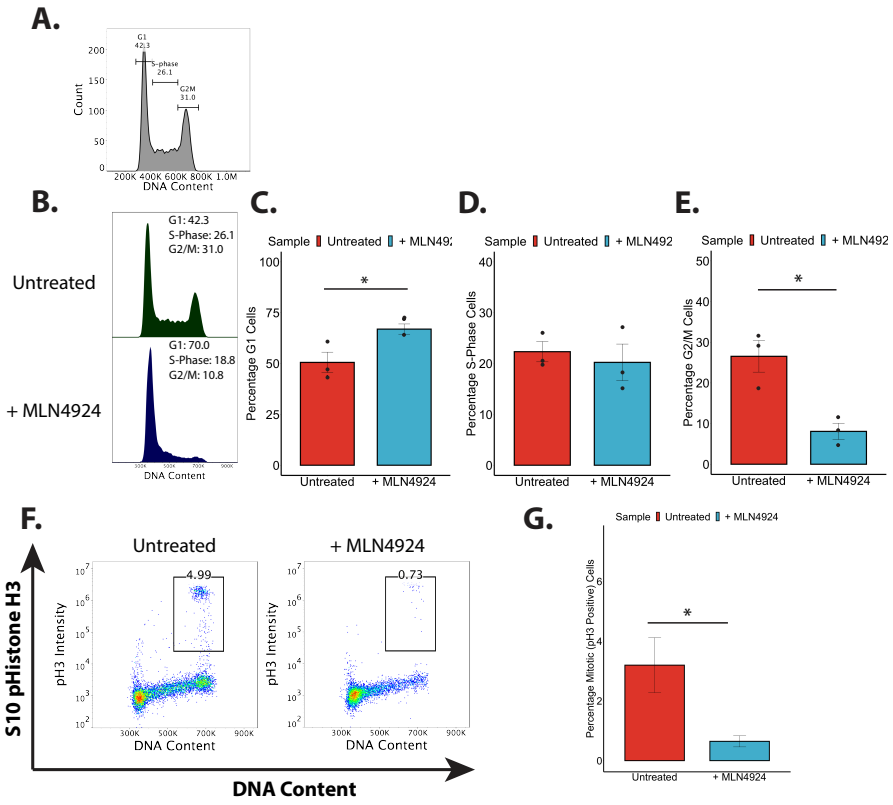


Figure 6.7: **MLN4924 Treatment Causes G1 Cell Cycle Accumulation.** To attempt to inhibit S-phase MCM7 ubiquitylation, cells were treated with the Cullin inhibitor MLN4924 for 6 hours. Following inhibitor treatment, cells were prepared as described previously (Figure 6.1). Data shown is from three independent experimental repeats. **A.** Gates were set up as previously detailed using untreated controls to determine the relative proportions of cells in each cell cycle stage (Figure 2.5), and subsequently applied to all samples. **B.** Example cell cycle profiles following 6 h of MLN4924 treatment. Shown are untreated (green) and treated (blue). **C.** Quantification of the proportion of cells in G1. Shown is the mean percentage cells -/+ SEM (t.test: p = 0.0313). **D.** Quantification of the proportions of cells in S-phase. Shown is the mean percentage cells -/+ SEM. **E.** Quantification of the proportions of cells in G2/M. Shown is the mean percentage cells -/+ SEM (t.test: p = 0.0245). **F.** Example FACS plots showing the identification of mitotic cells using antibodies against S10 Histone H3 phosphorylation. Total DNA content was plotted against pH3S10 intensity. Mitotic cells (positive for pH3S10) are shown in the black boxes. **G.** Quantification of mitotic cells. Shown is the mean percentage cells -/+ SEM. MLN4924 treatment was shown to reduce the proportion of mitotic cells (t. test: p = 0.0278).

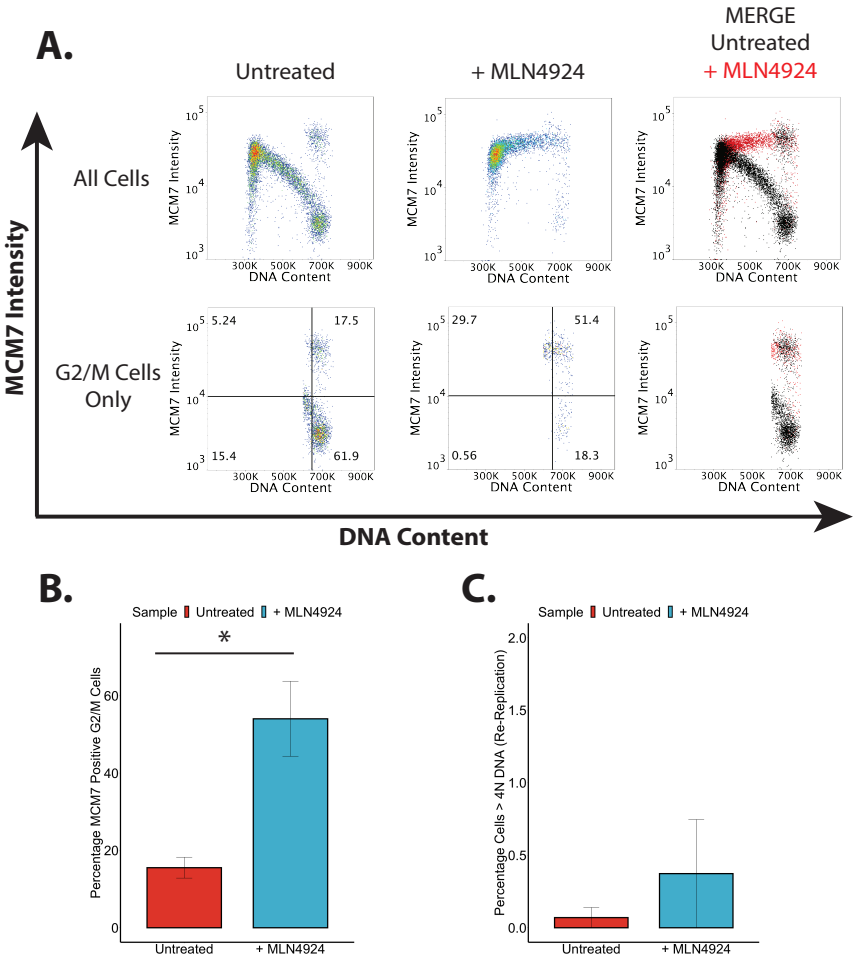


Figure 6.8: **MLN4924 Treatment Induces MCM7 Retention on Chromatin**. To explore the binding pattern of MCM7 throughout the cell cycle following MLN4924 treatment, cells were treated as detailed in Figure 6.2. Data shown was collected from three independent experimental repeats. **A.** Example FACS plots. Shown is the total DNA content plotted against the total MCM7 intensity; Untreated (left), + MLN4924 (right). To quantify any replisome retention into G2/M, those cells were first isolated using the cell cycle gates established (see Figure 2.5), and thresholds applied (quadrants, bottom). Any G2/M cells remaining positive for MCM7 resided in the top right quadrant. **B.** Quantification of the percentage G2/M cells positive for MCM7, identified through the gates in A. Shown is the mean positive cell populations -/+ SEM. Increased replisome retention was observed following MLN4924 treatment (t. test: p = 0.0247). **C.** Quantification of the cells possessing > 4N DNA content. Shown are the mean cell populations -/+ SEM.

The use of the neddylation inhibitor MLN4924 perturbed the cell cycle progression, resulting in the loss of the mitotic cell population. As a result, we were unable to investigate the mitotic replisome disassembly pathway. To address this, we decided to combine MLN4924 treatment with WEE1 inhibition, as described above. Analogous to our previous results, use

of MK-1775 was sufficient to push cells into mitosis (FIgure 6.9C and D). Furthermore, the reported accumulation of MLN4924-treated cells with 2N DNA content was rescued using MK-1775 (Figure 6.9A and B, compare with Figure 6.7B); whilst the observed reductions to cells with 4N DNA content remained unchanged (Figure 6.9A and D, compare with Figure 6.7D). Moreover, unlike p97i treatment, no defects to mitotic entry were detected when MLN4924 was combined with MK-1775 (Figure 6.9E and F, compare with Figure 6.7F).

Following validation of the use of MK-1775 in combination with MLN4924, I next explored any replisome retention from S-phase into G2 or mitosis. Irrespective of MK-1775 treatment, MLN4924 was found to result in MCM2-7 re-loading onto chromatin (Figure 6.10A). Furthermore, the isolation of G2/M cells using total DNA content found significant increases to the proportion of cells positive for MCM7, as described previously (compare Figures 6.10 and 6.8). Conversely, no differences were detected in total MCM7 intensity specifically in mitotic cells (Figure 6.10A and C). The data shown initially suggested increases to the proportions of MCM7 retained on chromatin into mitosis after MLN4924 treatment. However statistical analysis could not identify any significant changes, thus it must be assumed that there was no difference between conditions. Therefore, these data suggested that the mitotic replisome disassembly was indeed conserved from lower eukaryotes, into human somatic cell lines. Upon the inhibition of S-phase replisome disassembly by prevention of Cullin activation, CMG was retained onto chromatin into mitosis, where it was then unloaded in a mechanism dependent on p97 but not Cullin type ubiquitin ligases. The over-loading of MCM2-7 double hexamers due to MLN4924 treatment is detrimental to cells entering mitosis (Figure 6.7F). Overall, the large numbers of both active and dormant replicative helicases present on chromatin require

removing from chromatin before cell division, and not all cells may be capable of this after WEE1i treatment (bypassing the G2 checkpoint), resulting large signal variations (Figure 6.10C).

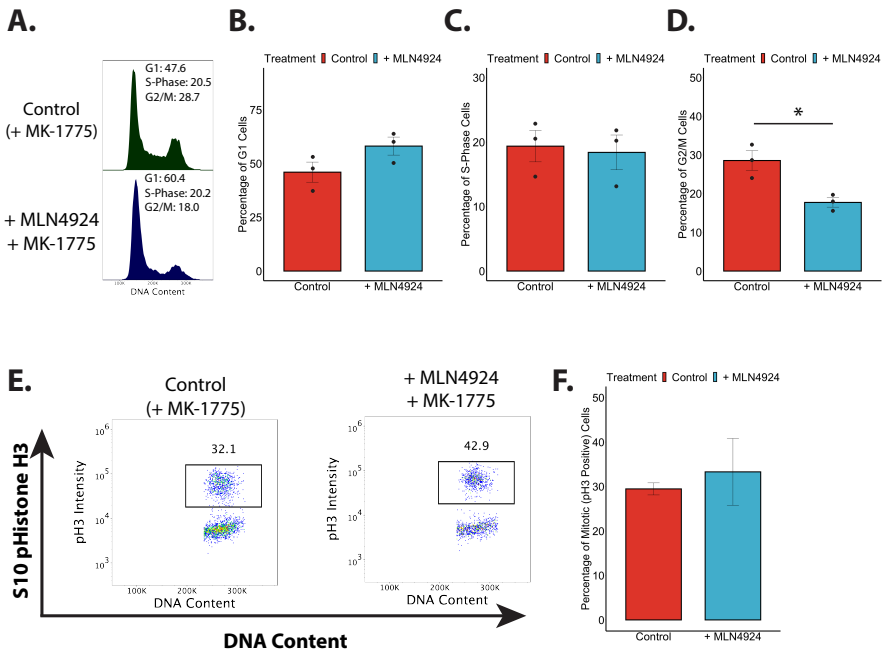


Figure 6.9: **MK-1775 Treatment Overcomes MLN4924-induced G1 Cell Cycle Accumulation.** Asynchronous cells were treated for 6 h with MLN4924. 1 hour prior to harvesting, cells were optionally supplemented with MK-1775, fixed, and prepared for flow cytometry. Cells were gated to quantify the proportion of cells in each cell cycle stage as detailed previously (Figure 2.5 and 6.7A). Data shown was collected over three independent experimental repeats. **A.** Example cell cycle profiles. Shown is the total DNA content for cells treated with WEE1i MK-1775 only (green) and WEE1i MK-1775 and CULi MLN4924 treated (blue) cells. **B.** Quantification of the total proportions of cells in G1. Shown is the mean percentage of cells -/+ SEM. **C.** Quantification of the total proportions of cells in S-phase. Shown is the mean percentage of cells -/+ SEM. **D.** Quantification of the total proportion of cells in G2/M. Shown is the mean percentage of cells -/+ SEM (t.test: p = 0.00335). **E.** Example FACS plots showing the proportion of G2/M cells positive for pH3S10. Shown is the total DNA content plotted against pH3S10 intensity. Mitotic cells are indicated in the black box, with percentages shown above. **F.** Quantification of the proportion of G2/M cells positive for pH3S10. Shown is the mean percentage of cells -/+ SEM.

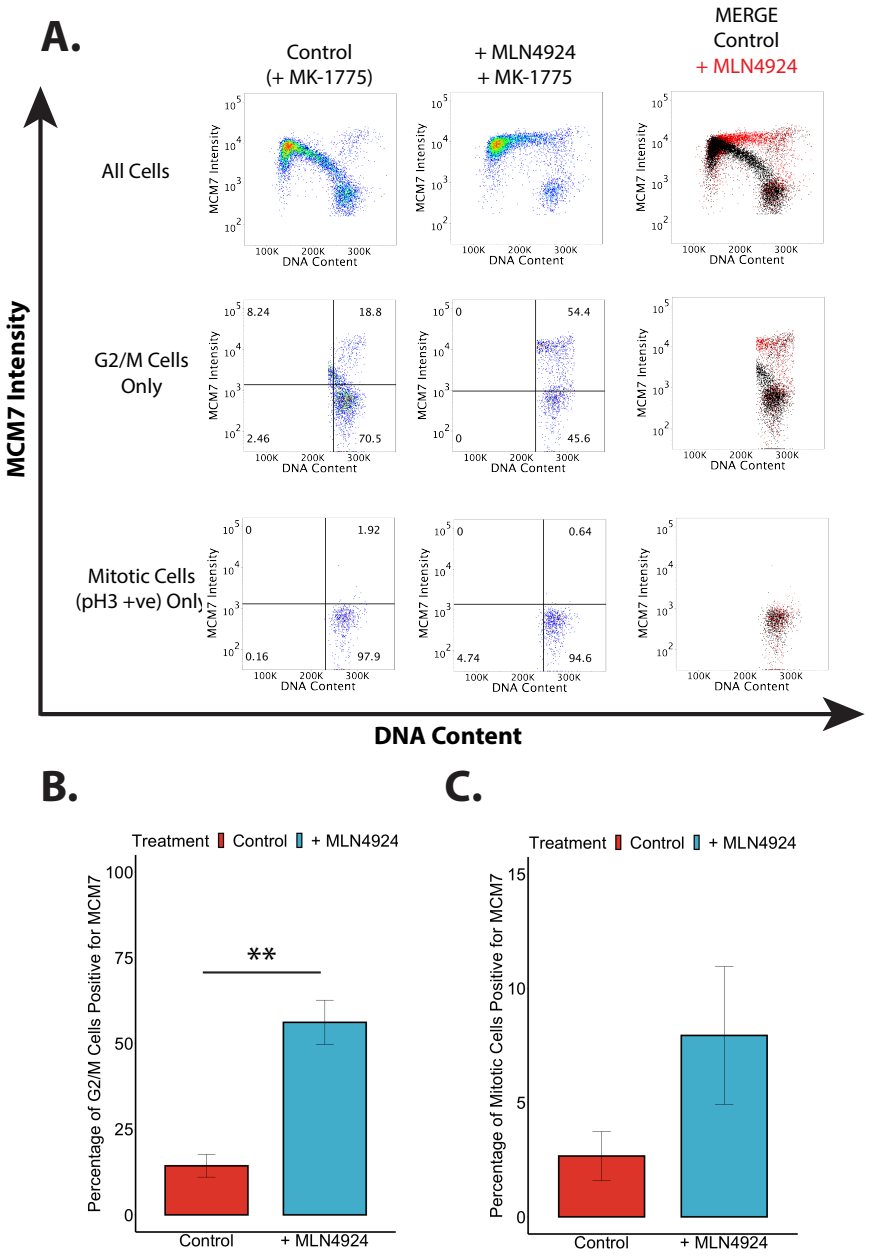


Figure 6.10: **Mitotic Replisome Disassembly Appears to be Conserved in HCT116 Cells.** Asynchronous cells were treated for 6 hours with MLN4924, additionally supplemented with MK-1775 for the last hour to push cells into mitosis. Cells were then fixed and prepared for flow cytometry as described previously (Figure 6.1). Data shown was collected from three independent experimental repeats. Cells were gated to isolate the cell cycle (Figure 2.5), with a minimum of 10,000 cells quantified per condition, per repeat. **A.** Example FACS plots. Shown are FACS plots depicting the total DNA content against MCM7 intensity for all cells (top), G2/M cells only (middle), and mitotic cells only (bottom). Gates were established based on the control cells and applied to all samples (quadrants). **B.** Quantification of the total proportions of G2/M cells positive for MCM7. Shown is the mean percentage of cells positive for MCM7 -/+ SEM. Significant increase was found using pairwise hypothesis testing (t. test: p = 0.00519). **C.** Quantification of the total proportions of mitotic cells positive for MCM7. Shown is the mean percentage of cells positive for MCM7 -/+ SEM. The mean of number of mitotic cells positive for MCM7 suggest an increase after MLN4924 treatment. However, this was not consistent in all experimental repeats (see example shown in A, bottom panel). Subsequent statistical analysis found no significant changes in the data sets (t.test: p = 0.2). Hence, we must conclude that there are no differences in MCM7 intensity between conditions.

6.2.3 The Role of TRAIP in Replisome Disassembly

Preliminary characterisation of the replisome disassembly mechanisms in human somatic cells revealed that our existing knowledge from alternative model organisms, is likely analogous to mammalian cell systems. The treatment of cells with inhibitors against either p97 or Cullin-type ubiquitin ligases resulted in replisome retention from S-phase into G2/M. Moreover, in the case of MLN4924 treatment, any replisomes re-loaded and retained appeared to be removed during mitosis. Work from several groups has demonstrated that TRAIP is the ubiquitin ligase driving mitotic replisome disassembly (Moreno et al., 2019; Sonneville et al., 2019; Deng et al., 2019; Villa et al., 2021). Therefore, we next aimed to understand this role further using the conditional degron cell lines. As p97 is universally required for all known replisome disassembly pathways, it was expected that combination of TRAIP-degradation and p97i treatment would yield no differences in the proportions of cells retaining MCM7 on chromatin, as both pathways should be fully blocked with p97i. On the other hand, it was envisaged that MLN4924 inhibitor treatment would block just the S-phase pathway opening the window of opportunity to visualise the importance of TRAIP for the mitotic replisome disassembly, analogous to that shown in other model systems. Initially, the previous flow cytometry experimental setups were carried out in the TRAIP degron cells. Asynchronous cells were treated with IAA alongside CB5083 or MLN4924 for 6 hours. The WEE1 inhibitor MK-1775 was also included for the final hour to overcome the respective defects to cell cycle progression induced by the inhibitors, as well as the previously observed TRAIP-dependent G2 cell cycle arrest.

Consideration of the proportions of cells in each cell cycle stage was analogous to that

described above (Figure 6.11A and B-D). Higher proportions of cells were found to be positive for MCM7 during G2/M of the cell cycle after treatment with either MLN4924 or CB5083, compared to untreated controls (Figure 6.11B and E). MCM7 retention was also observed specifically during mitosis after treatment with CB5083, but not MLN4924; suggesting the backup replisome disassembly pathway was active as shown above (Figure 6.11B and F). Again, as previously demonstrated, MLN4924 treatment resulted in an apparent increase to MCM7 intensity during mitosis. However subsequent statistical analysis found no differences and thus it must be concluded that the MCM7 intensities were not different from untreated controls. TRAIP degradation had no effect on the total MCM7 intensities on chromatin after neither p97i nor Cullin inhibitor treatment. This result was expected for p97i as p97 is required for all replisome unloading. However, we hoped that inhibition of all cullins with CULi MLN4924 would block S-phase replisome disassembly allowing us to visualise the requirement for TRAIP activity in mitosis. The over-loading of MCM2-7 during S-phase, resulted in non-significant increases to replisome retention into mitosis even in control cells. As a result, it was difficult to ascertain active replisome retention over the high background signal detected. The over-loading of MCM2-7 in response to CULi MLN4924 is specific to human somatic cells, and is not induced to that extent in other systems (Moreno et al., 2019; Sonneville et al., 2017). Therefore, further work was required to understand any role for TRAIP during replisome disassembly in human somatic cells.

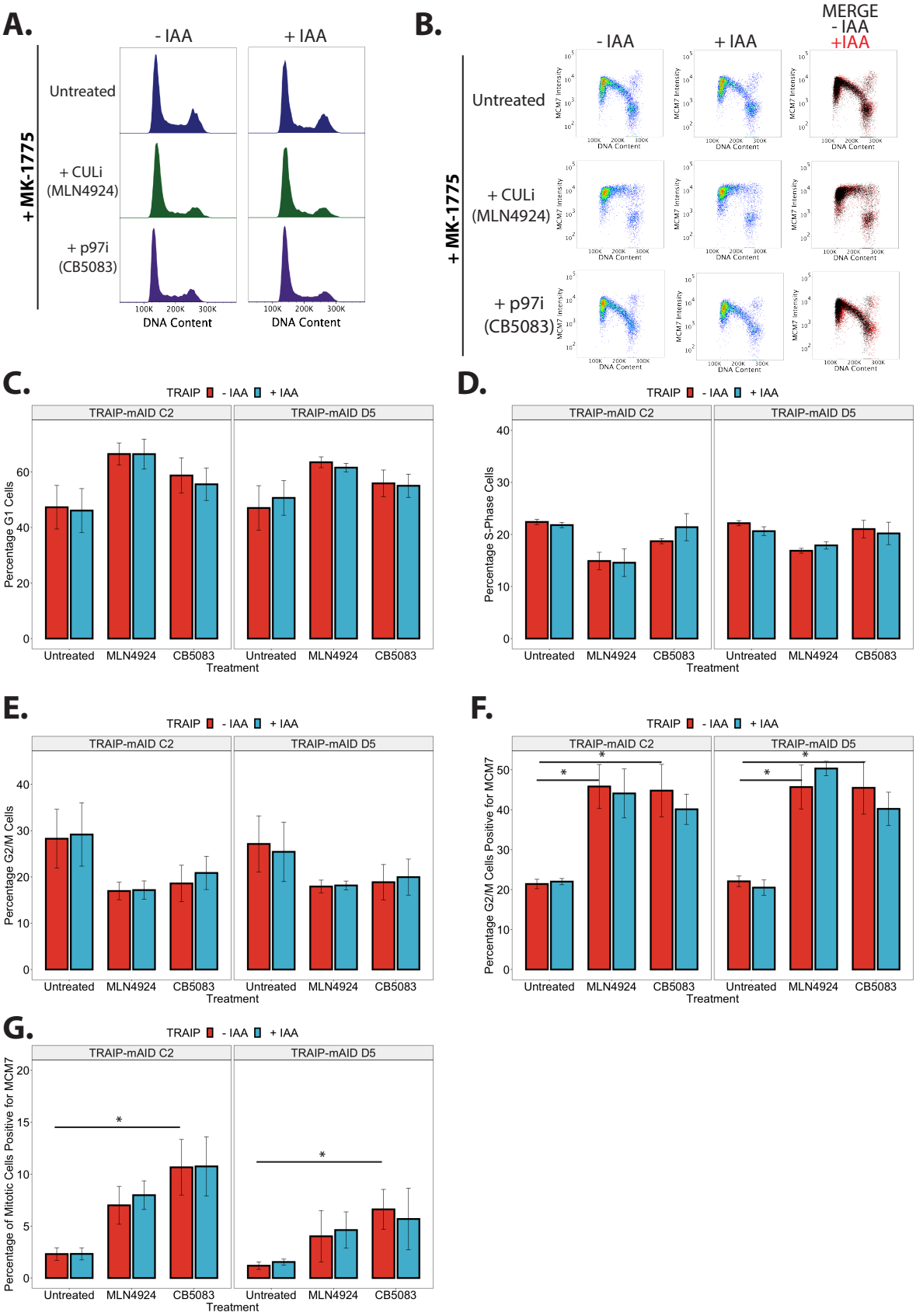

A.
- IAA
+ IAA
+ MK-1775
Untreated
+ CULi (MLN4924)
+ p97i (CB5083)
100K 200K 300K
DNA Content
B.
MERGE
- IAA
+IAA
MCM7 Intensity
C.
TRAIP - IAA + IAA
TRAIP-mAID C2
TRAIP-mAID D5
Percentage G1 Cells
Untreated MLN4924 CB5083
Treatment
D.
Percentage S-Phase Cells
E.
Percentage G2/M Cells
F.
Percentage G2/M Cells Positive for MCM7
G.
Percentage of Mitotic Cells Positive for MCM7

Figure 6.11 *(previous page)*: **TRAIP has no Detectable Impact on MCM2-7 Levels by Flow Cytometry.** Cells were treated with MLN4924 or CB5083 in combination with IAA for 6 h. For the last hour prior to harvesting, MK-1775 was added. Cells were prepared for flow cytometry as detailed previously. Cells were gated as shown in Figure 2.5. To determine the proportions of cells in each cell cycle stage, gates were established on control samples using the total DNA content and applied to treated samples; for examples of gating placement, see Figure 2.5, 6.1A, and 6.7A. Data shown was collected over three independent experimental repeats. **A.** Example cell cycle profiles using the total DNA content. Shown are untreated (blue), CULi MLN4924 treated (green) and p97i CB5083 treated (purple) cells -/+ IAA. **B.** Example FACS plots for the data as detailed in A, plotting the total MCM7 intensity against total DNA content. **C.** Quantification of the proportion of cells in G1. Shown is the mean percentage of cells -/+ SEM. **D.** Quantification of the proportion of cells in S-phase. Shown is the mean percentage of cells -/+ SEM. **E.** Quantification of the proportions of cells in G2/M. Shown is the mean percentage of cells -/+ SEM. **F.** Quantification of the G2/M cells (identified by total DNA content) positive for MCM7. Gates to determine the proportion of cells in G2/M positive for MCM7 were established as shown in figures 6.6A and 6.10A. Shown is the mean percentage of cells -/+ SEM. Statistical comparisons were carried out using ANOVA (TRAIP-mAID C2: p = 0.00445; TRAIP-mAID D5: p = 0.000596). Pairwise testing was carried out using Dunns post-hoc testing, the significant comparisons are indicated on the plot (TRAIP-mAID C2 – IAA: untreated vs MLN4924: p = 0.020; untreated vs CB5083: p = 0.0341. TRAIP-mAID D5 – IAA: untreated vs MLN4924: p = 0.014; untreated vs CB5083: p = 0.0153). **G.** Quantification of the mitotic cells (G2/M cells positive for S10 phosphorylation of Histone H3) positive for MCM7. Gates to determine the proportion of cells in G2/M positive for MCM7 were established as shown in figures 6.6A and 6.10A. Shown is the mean percentage of cells -/+ SEM. Statistical comparisons were carried out using ANOVA (TRAIP-mAID C2: p = 0.0214; TRAIP-mAID D5: p = 0.000596). Pairwise testing was carried out using Dunns post-hoc testing, the significant comparisons are indicated on the plot (TRAIP-mAID C2 – IAA: untreated vs CB5083: p = 0.04. TRAIP-mAID D5 – IAA: untreated vs CB5083: p = 0.029).

The flow cytometry methods employed to study replisome disassembly involved the visualisation of MCM7 binding throughout the entire cell cycle. However, due to the vast quantities of dormant MCM7 present on chromatin throughout G1 and S-phase, it was unlikely that minor signal shifts correlating to the partial retention of replisomes would be detected over the background signal. Moreover, the inhibition of Cullin2 activation led to the re-loading of MCM2-7 to chromatin, resulting in higher levels of background noise, potentially masking specific signals from retained replisomes. To attempt to overcome these caveats, and further investigate the role of TRAIP during replisome disassembly, we next aimed to focus on active replisomes only. Several antibodies were trialled to detect the active replisome, including GINS, AND-1 (Ctf4), and CDC45. None of the tested antibodies worked using flow cytometry. Hence, we instead utilised fluorescent microscopy, and of the antibodies trialled, only CDC45 was found to result in the detection of a fluorescent signal above the background fluorescence (data not shown, CDC45 antibodies demonstrated previously in Fan et al. (2021). Cells were

treated as detailed above and prepared for microscopy as described in the materials and methods. Only MLN4924 treatment was tested, as we expected no differences in MCM7 retention between cells with and without TRAIP after p97 inhibition. Finally, preliminary data testing these methods with MCM7 antibodies suggested that, regardless of the inhibitor used, most replisomes were disassembled upon chromosomal condensation (i.e. no MCM7 detected in cells with highly condensed chromosomes, detected with DAPI staining; not shown). Due to this, it was also possible that replisomes may be disassembled prior to the S10 phosphorylation of Histone H3. Therefore, in this experiment, G2/M cells were isolated using CENPF/Mitosin staining (Figure 6.12A).

TRAIP degradation alone did not result in increased CDC45 on chromatin during G2/M, suggesting that the S-phase, replisome disassembly pathway was sufficient to unload active replisomes following replication termination. Importantly, this data corroborates that shown previously, demonstrating that TRAIP is not needed whilst LRR1-driven replisome disassembly is active. On the contrary, significant reductions to the detected CDC45 intensity in G2/M cells was observed following IAA treatment in TRAIP-mAID D5 (Figure 6.12C). Although, this was not phenocopied in TRAIP-mAID C2, and therefore it was unclear whether this was representative of S-phase replication defects. Similarly, we identified a decrease to the CDC45 intensity following MLN4924 treatment only in TRAIP-mAID C2 (Figure 6.12B). Despite this descrepancies, we found significantly higher CDC45 levels in G2/M cells treated with both IAA and MLN4924 in both CRISPR degron clones (Figure 6.12B and C). This indicated that TRAIP was indeed functioning in a mitotic replisome disassembly pathway. Altogether, the data presented formed a first indication of the potential role of TRAIP during mitotic replisome

disassembly, however further work is required. First, it will be important to understand the kinetics of mitotic replisome disassembly, and to determine precisely when active replisomes are disassembled by TRAIP. Second, the mitotic replisome disassembly mechanisms should be tested when TRAIP is degraded specifically during G2, to account of any impacts of the reported S-phase functions of TRAIP.

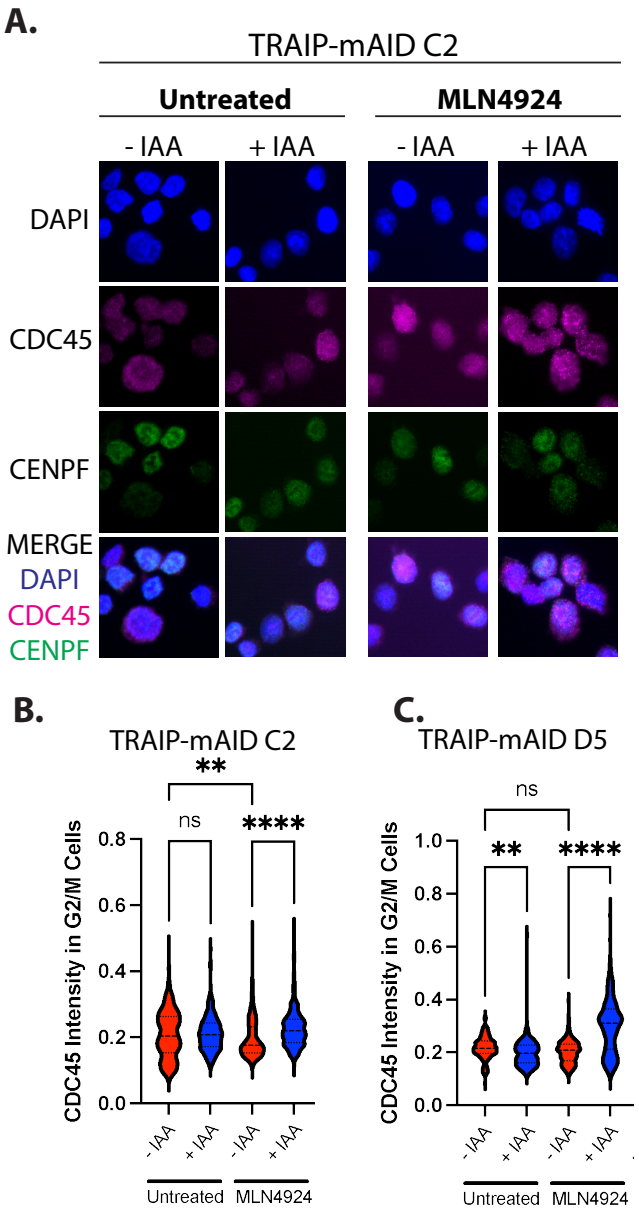


Figure 6.12: **The TRAIP Mitotic Replisome Disassembly Pathway Appeared to be Active in Human Somatic Cells.** Asynchronous cells were treated with combinations of IAA and MLN4924 inhibitor for 6 hours. MK-1775 was added for the final hour of this incubation to overcome the previously described cell cycle defects. Cells were then fixed and prepared for immunofluorescence as detailed in the materials and methods. Shown is data from three independent experimental repeats, with an average of 350 CENPF positive cells analysed per condition, per repeat. **A.** Example images. Cells were stained with DAPI (total DNA content: blue) and antibodies against CDC45 (purple), CENPF (green). Also shown is overlays of all channels. **B.** Quantification of the median CDC45 intensity in G2/M cells (CENPF positive) from TRAIP-mAID C2. Data shown as median violin plots and associated interquartile ranges. Any differences between the groups were determined using one-way ANOVA and subsequent pairwise comparisons, with significance indicated on the plot (one-way ANOVA $p < 0.0001$; Sidak multiple comparison, - IAA untreated vs + IAA untreated: $p = 0.014$; - IAA MLN vs + IAA MLN: $p < 0.0001$). **C.** Quantification of the median CDC45 intensity in G2/M cells (CENPF positive) from TRAIP-mAID D5. Data shown as median violin plots and associated interquartile ranges. Any differences between the groups were determined using one-way ANOVA and subsequent pairwise comparisons, with significance indicated on the plot (one-way ANOVA $p < 0.0001$; Sidak multiple comparison, - IAA untreated vs + IAA untreated: $p = 0.052$; - IAA MLN vs + IAA MLN: $p < 0.0001$).

6.2.4 TRAIP Degradation Prolongs DNA Replication into G2

Alongside the reported roles for TRAIP during mitotic replisome disassembly, TRAIP is also thought to be necessary for mitotic DNA synthesis (Sonneville et al., 2019). Intriguingly, the requirements for TRAIP during MiDAS may revolve around the removal of the replication machinery to facilitate the recruitment of MiDAS factors to chromatin (Wu et al., 2021). Given our data, indicating that TRAIP is likely to be required for human somatic replisome disassembly in mitosis, we wondered whether similar MiDAS phenotypes could be observed in the conditional degron cell lines. Furthermore, we were interested in understanding whether any requirements for TRAIP during MiDAS were due to independent mitotic mechanisms, or compounding S-phase defects. We aimed therefore to observe the effects of low level aphidicolin treatment in cells going through S-phase, or only G2 stage of the cell cycle, without TRAIP. The experimental schematic followed is depicted in Figure 6.13A. Cells were first arrested in G1 and optionally treated with either IAA, aphidicolin, or both. After 1 hour of drug treatments cells were released into S-phase, maintaining the appropriate inhibitor treatments, and arrested again during G2 of the cell cycle using RO-3306, where samples were also optionally supplemented with IAA. Finally, all cells were released from G2 arrest in the presence of the thymidine analogue EdU to label replicating cells and timepoints taken 30- and 60-minutes post release.

Fluorescent microscopy was used to assess any MiDAS-like phenotypes. Overall limited proportions of cells were found to be in mitosis, and this population was further reduced following aphidicolin treatment (Figure 6.14). Furthermore, in the few cells presenting with highly condensed chromosomes, no clear MiDAS foci (EdU distinct foci) could be detected in

any condition. It was clear, therefore, that the current experimental set-up required additional optimisation to firstly enhance the proportion of mitotic cells, and then facilitate the detection of conventional MiDAS markers. The inclusion of mitotic shake-off techniques would allow the specific isolation of mitotic cells. Alternatively, treatment with the WEE1 inhibitor MK-1775 demonstrated previously may overcome any restricted mitotic entry induced by aphidicolin or IAA treatment

However, visualisation of the global EdU content of all cells released from the G2 arrest yielded unexpected results. In control samples (no IAA or aphidicolin), approximately 30% of the cells released from G2 cell cycle arrest were found to possess pan-nuclear EdU staining suggesting that, to some extent, DNA replication was active during late G2 and early mitosis. Moreover, this presence of G2/M replicating cells was significantly enhanced when cells were treated with aphidicolin throughout S-phase (Figure 6.13C-D). Strikingly, similar increase to the proportion of EdU positive cells after release from G2 arrest was also observed in both clones lacking TRAIP throughout the entirety of S-phase (Figure 6.13C-D), and this was not recapitulated when TRAIP was instead degraded during G2. Thus, it was possible that the loss of TRAIP throughout S-phase resulted in prolonged DNA replication, extending into G2 and mitosis. Conversely, no differences were detected between G1 or G2 TRAIP degradation in samples treated with both IAA and aphidicolin. Although, aphidicolin treatment did appear to act additively to the effects of TRAIP degradation during S-phase at the 60-minute timepoint, suggesting that aphidicolin and TRAIP degradation impacted different mechanisms.

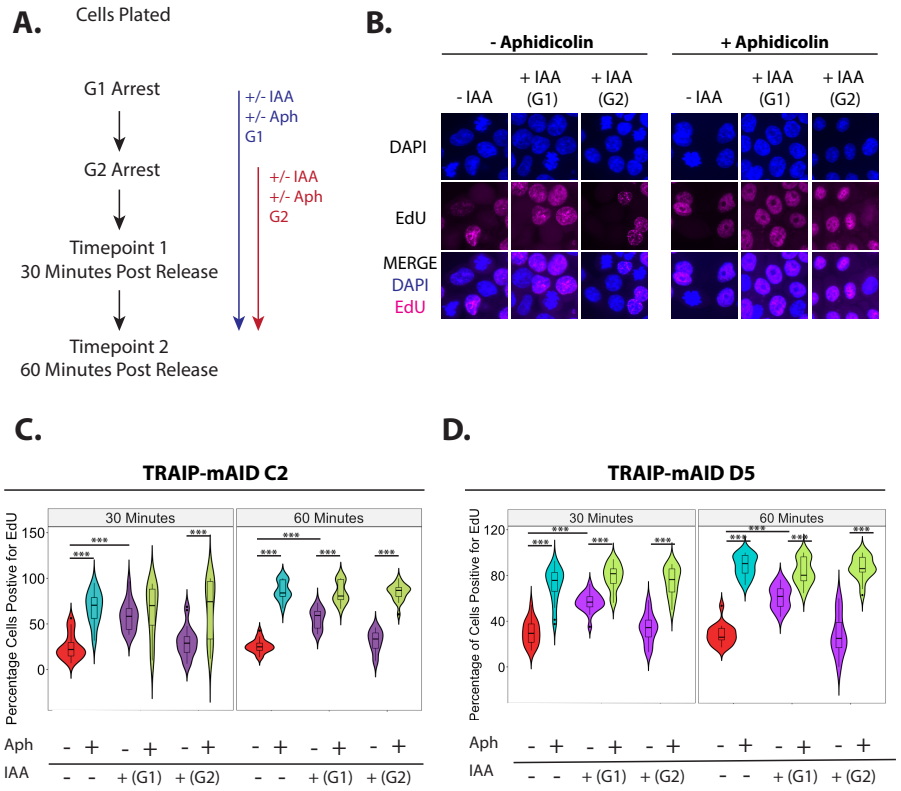


Figure 6.13: **TRAIP Degradation Prolongs DNA Replication into G2.** Shown are data from three independent experimental repeats from > 500 cells per condition, per repeat. **A.** Experimental Schematic used. **B.** Example images. Shown are TRAIP-mAID C2 cells stained with DAPI (DNA: blue) or for antibodies against EdU (purple). Overlays of all channels is also shown. **C.** Quantification of the total proportion of cells positive for EdU incorporation for experiments using TRAIP-mAID C2. Data shown as violin plots, displaying the median, interquartile ranges, and overall spread of the data. Any differences between groups were determined using one-way ANOVA testing and post-hoc pairwise comparisons, indicated on the plots ($p > 0.001$ for all comparisons shown). **D.** Quantification of the total proportion of cells positive for EdU incorporation for experiments using TRAIP-mAID D5 (n = 3). Data shown as violin plots, displaying the median, interquartile ranges, and overall spread of the data. Any differences between groups were determined using one-way ANOVA testing and post-hoc pairwise comparisons, indicated on the plots ($p > 0.001$ for all comparisons shown).

6.2.5 TRAIP is Important for Mitotic Progression

TRAIP has also been shown to be important for the progression of cell division during mitosis by the regulation of mitotic timing through the spindle assembly checkpoint. To understand whether this role was independent of the S-phase mechanisms identified in this PhD project, G2 arrest and release experiments were carried out. The conditional degron cells were arrested in G2 using the potent CDK1 inhibitor RO-3306, as described in the materials and

methods. Arrested cells were treated with IAA to degrade TRAIP before being released into mitosis. Timepoints were then taken 30- and 60-minutes post release to track the entry and progression of cells through the cell cycle. Aphidicolin treatment, known to cause mitotic problems through the accumulation of stalled replication forks, was used as a control. Early and late mitotic cells were quantified using fluorescent microscopy, defined by condensed (early) and segregated (late) chromosomes using DAPI staining (Figure 6.14A).

As expected, aphidicolin treatment resulted in fewer mitotic cells when compared to all conditions (Figure 6.14B-C). Analysis of the impact of TRAIP degradation revealed that, whilst all cells started mitosis (condensed chromosomes) at a similar rate, defects were observed to timing of chromosome segregation. Segregating cells could not be detected 30 minutes post-release, as this timepoint was likely too short for the cells to reach anaphase. However, at the 60 minute timepoint, samples without TRAIP possessed fewer segregating cells, suggesting that they may progress through mitosis either slower or faster than controls. Thus, it was concluded that TRAIP was important for mitotic progression and timing. In addition, during this experiment, cells were also stained for the helicase BLM to detect DNA bridges. However, no such accumulation, of either ultrafine or anaphase bridges, could be detected (data not shown). Moreover, increased micronuclei formation was also not evident (data not shown).

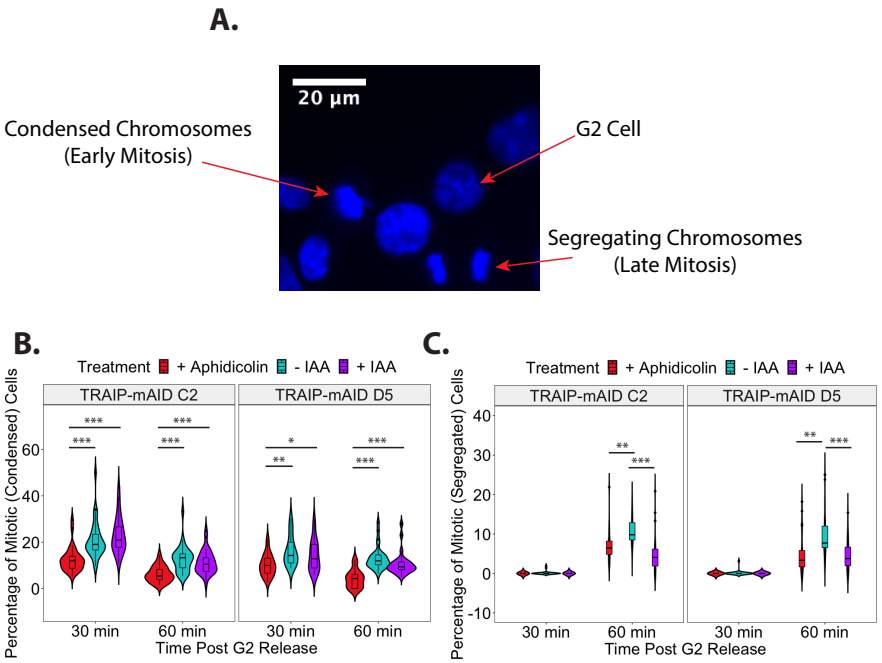


Figure 6.14: **TRAIP is Important for Mitotic Progression.** To investigate the effect of TRAIP degradation on mitotic progression, cells were arrested in G2 and treated with IAA. Following 1 h treatment to facilitate TRAIP degradation, cells were released into mitosis and mitotic progression tracked through visual observation of chromosome condensation (DAPI) staining. Data shown was collected over three independent experimental repeats, with > 500 cells analysed per condition, per repeat. **A.** Example DAPI stained image depicting the quantification carried out. Cells were either classified as early mitosis (condensed chromosomes) or late mitosis (segregating cells). **B.** Quantification of the proportion of early mitotic cells, displaying condensed chromosomes. Shown are aphidicolin treated controls (red), - IAA (blue), and + IAA (purple). Data shown as violin plots, displaying the median, interquartile range, and spread of the data. Statistical analysis carried out using one-way ANOVA and pairwise post-hoc tests, with significance indicated on the plot (for all indicated comparisons, $p > 0.001$). **C.** Quantification of the proportion of late mitotic cells, displaying segregating chromosomes. Data shown as violin plots, displaying the median, interquartile range, and spread of the data. Shown are aphidicolin treated controls (red), - IAA (blue), and + IAA (purple). Statistical analysis carried out using one-way ANOVA and pairwise post-hoc tests, with significance indicated on the plot (TRAIP-mAID C2 60 mins + aphidicolin control vs – IAA: $p = 0.00117$, - IAA vs + IAA: $p < 0.001$; TRAIP-mAID D5 60 mins + aphidicolin control vs – IAA: $p = 0.00209$; - IAA vs + IAA: $p < 0.001$).

6.3 Discussion

As a process essential for the propagation of life, the respective mechanisms involved in DNA replication are conserved throughout eukaryotic evolution. Previous work from our group and others have demonstrated the core steps underpinning replisome disassembly using several model organisms, including *X. laevis* egg extract, *C. elegans*, *S. cerevisiae*, and recently,

mammalian cell lines (Deng et al., 2019; Moreno et al., 2019, 2014; Sonneville et al., 2017, 2019; Villa et al., 2021). However, in mammalian cell systems, studies have primarily focused on using mouse embryonic stem cells. The use of embryonic systems possesses several advantages when it comes to studying DNA replication, including faster doubling times and larger proportions of replicating cells (Villa et al., 2021). Conversely, progression through the cell cycle in embryonic stem cells differs from that seen in somatic immortalised cell lines. Notably, these cells lack the ability to trigger G1/S phase cell cycle arrest, as well as exhibiting only limited G2/M checkpoint activation upon the induction of DNA damage (Suvorova et al., 2016) and are somehow less sensitive to perturbations during S-phase. Furthermore, the regulation of DNA replication itself also differs in embryonic systems. It has been reported that the stabilisation of Cdt1 alone in the embryonic *X. laevis* egg extract does not trigger re-replication, whilst the opposite was observed in mammalian cell lines (Lin et al., 2010; Sonneville et al., 2017). In addition, in embryonic stem cells, both ATR and ATM are required to regulate origin firing; compared to just ATR in somatic cell lines (Blakemore et al., 2021). Due to this, it was important to first understand the regulation of the two replisome disassembly mechanism in our conditional degron cells, and validate that these were indeed analagous to that previously published using alternative models.

The protein segregase p97 is thought to be essential for replisome disassembly, recruited to ubiquitylated MCM7 to facilitate CMG unloading from chromatin (Moreno and Gambus, 2020). Moreover, recent work has highlighted analagous roles for p97 in mouse embryonic stem cells (Villa et al., 2021). Similarly, we also observed retention of the replisome component MCM7 during both G2/M and specifically mitosis following the treatment of HCT116 cells with

p97 inhibitor. This data suggested that p97 is universally required for both S-phase and mitotic replisome disassembly. Although similar observations could also be a result of alternative S-phase defects induced by inhibition of p97 function in S-phase, such as impaired replication fork progression. It is known that low-dose CB5083 treatment result in G1 cell cycle arrest, reduced cell viability, and increased apoptosis in several cancerous somatic cell lines, both *in vitro* and when used to generate mouse tumour models (Zhao et al., 2020). In this PhD project, the use of the p97 inhibitor CB5083 was shown to directly inhibit cell proliferation. We did not observe clear signs of G1 accumulation, and this was probably due to the short (6 h) treatment times used (Figure 6.1). On the other hand, clear defects to mitotic entry were found (Figure 6.1). Further work then identified that the underlying cause of the highlighted cell cycle defect was S-phase cell cycle slowing or arrest (Figure 6.3).

During S-phase, p97 has a wide array of substrates, and the loss of p97 has been highlighted to result in the accumulation of high numbers of ubiquitylated proteins on chromatin (Vaz et al., 2013). Notably, p97 has been reported to be essential for DNA replication, DNA damage repair, and the regulation of transcription (Franz et al., 2016a). With respect to DNA replication, one prominent role for p97 is the removal of the licensing factor Cdt1 from chromatin. In mammalian cells this is orchestrated through the p97 co-factor FAF1, and FAF1 depletions blocking this mechanisms were found to result in stalled replication forks, ATR checkpoint activation, and excessive dormant origin firing (Franz et al., 2011, 2016b). Interestingly, p97 appeared to be specifically targetted to chromatin-bound CDT1 and its inhibition does not lead to similar MCM2-7 re-loading as shown following MLN4924 inhibitor treatment. Furthermore, interactions between p97 and CDT1, were shown to be independent to that of the p97-MCM7

interaction during replication termination (Franz et al., 2016b). It is difficult, therefore, to untangle the direct effects of p97 function on the disassembly of terminated replisomes from other roles impacting replication fork progression, as both result in the accumulation of active CMG on chromatin. It was also particularily difficult to analyse the impact of p97 inhibition on mitotic replisome disassembly, taking into account the defects to cell cycle progression. Hence, it was concluded that CB5083 inhibitor treatment was not optimal for the study of DNA replication in human somatic cells. Further work is required to identify less damaging methods of inhibiting the mechanimsms of replisome unloading. Our group has recently shown in *X. laevis* egg extract that the p97 co-factor UBXN7 functions to reduce the ubiquitin threshold needed for p97 binding to CMG (Tarcan et al., 2021). It has been demonstrated in the case of Ubxn-3 (FAF1 *C. elegans* homologue), that depletion of the Ubxn-3 co-factor possessed similar phenotypes to that shown after p97 depletion (Franz et al., 2011, 2016b). Therefore, it would be worthwhile understanding whether this function of UBXN7 is conserved in human somatic cells; and whether the depletion of UBXN7 is capable of delaying or preventing replisome disassembly in S-phase to an extent that the mitotic pathway would be activated.

Cullin2^{LRR1} ubiquitylation of MCM7 upon replisome convergence acts as the cellular signal for p97 binding and CMG disassembly. Commonly, the protein neddylation inhibitor MLN4924 has been used to block Cullin2 activation and thus MCM7 ubiquitylation in model systems (Deng et al., 2019; Moreno et al., 2019; Sonneville et al., 2019; Villa et al., 2021). But, in human somatic cell lines, MLN4924 has also been reported to cause re-replication, leading to the loss of cell proliferation (Lin et al., 2010). Whilst we did not detect any specific evidence of re-replication in HCT116 cells treated with MLN4924, the constant re-loading of MCM2-7

double hexamers throughout S-phase was observed (Figure 6.8). Thus, the highlighted accumulation of MCM7 on chromatin was therefore likely a sum of new dormant origins and retained active replisomes. In addition, MLN4924 also induced cell cycle accumulation of cells possessing 2N DNA content, and corresponding reductions to cells with a 4N DNA content, as well as mitosis specifically (Figure 6.7). Unlike p97i, the losses to the mitotic proportions of cells resulting from MLN4924 were rescued by inhibiting the G2 checkpoint kinase WEE1 (Figure 6.9). Through this, any replisomes retained into G2/M appeared to be unloaded during mitosis; indicating that both the mitotic replisome disassemby pathway was active in human somatic cell lines, and that this pathway was sufficient to unload the high levels of replisomes present on chromatin (Figure 6.10).

Despite these observations, the use of MLN4924 was also not optimal for studying replisome disassembly due to MCM7 re-loading and cell cycle defects. Re-loading of large quantities of MCM2-7 double hexamers onto chromatin during S-phase led to increased replisome retention in mitosis even in control cell lines. It was likely that cells were unable to fully resolve this prior to mitotic entry, especially when pushed through G2 using MK-1775. Hence, we observed large variations in the amounts of MCM7 retained into mitosis, and this was likely not an endogenously relavent scenario, thus unsuitable for studying replisome disassembly. Alternative methods to inhibit the S-phase disassembly pathway may include LRR1 or Cullin2 depletion. Although in all cases, using RNA interference to achieve protein knockdown would likely involve multiple rounds of the cell cycle with gradually depleting protein levels, the consequences of which for replisome disassembly are not clear. The depletion of both Cullin2 or LRR1 by siRNA was shown to have no effect on cell cycle progression by total DNA content

(Starostina et al., 2010). This may have been due to inneficient protein knockdowns, and residual proportions of either LRR1 or Cullin2 may fulfill its respective cellular role. However, especially in the case of LRR1, it is extremely difficult to verify the efficiency of protein knockdown due to low expression levels. In this case, using a rapid degron tag would be particularly advantageous, offering both degradation in a specific cell cycle stage and a means by which to isolate endogenous protein and validate its depletion.

Further work is required to determine whether the generated LRR1 degron cells would be suitable for these purposes. Preliminary data not shown found no clear defects to replisome disassembly upon the degradation of LRR1 using the cell lines generated. Published work since the start of this PhD has suggested that the role of LRR1 is conseved in human somatic cells however. Fan et al. (2021) utilised transient transfections of small CRISPR-guide RNA to deplete LRR1 and explored the resulting phenotypes exerted on the cell. The authors found that upon LRR1 depletion, replisomes were retained on chromatin into G2 where cells arrested due to ATR-mediated checkpoint activation (Fan et al., 2021). This checkpoint activation upon the inhibition of replisome disassembly has not been reported previously using embryonic systems. Using the generated LRR1 conditional degron cells, we were unable to observe similar phenotypes, and no such G2 cell cycle accumulation was found following LRR1 degradation (data not shown).). In addition, it was also reported that the loss of replisome disassembly led to overall reductions to DNA replication due to the loss of replication machinary recycling (Fan et al., 2021); a secondary phenotype also not reported previously in embryonic systems. Hence, it is likely that the regulation surrounding replisome disassembly in somatic cells is complex and requires additional factors not needed in embryonic systems. Embryonic cell

systems are known to have large quantities of replication factors to sustain rapid cell cycles with limited gap phases (Kermi et al., 2017). Conversely, in somatic cell systems, replication factors are typically transcribed during these gap phases and rapidly turned over. As a result, the respective replication capability of a cell is linked to its transcriptional activity (Pennycook et al., 2020). Therefore, somatic cells also require replication component recycling of rate limiting components (e.g., CDC45) to sustain DNA synthesis (Köhler et al., 2016). However, despite these differences between model systems, the primary mechanisms and factors involved appear to be conserved.

Following validation of the core established mechanisms of S-phase replisome disassembly, we next investigated the mitotic replisome disassembly mechanisms and the role of TRAIP in this process. No differences could be detected to the proportions of MCM7 retained on chromatin in cells with or without TRAIP using flow cytometry (Figure 6.11). Large quantities of MCM7 are present on chromatin throughout the cell cycle, only a subset of which are converted into active replisomes. As a result, it was likely that any retention of active replisomes would only present as minor signal shifts. The extent of this was particularly apparent following p97i treatment, preventing all replisome removal, both in S-phase and in mitosis (Figure 6.2 and 6.6). Given this, it was likely that flow cytometry was not sensitive enough to detect the retention of subsets of active replisomes. In *X. laevis* egg extracts, caffeine is added to the reactions to induce origin firing and thus increase the proportions of active replisomes on chromatin. Hence, it would be interesting to explore whether similar phenotypes could be induced in human somatic cells. WEE1 and ATR inhibitors have been reported to induce increased origin firing (Moiseeva et al., 2019b), although the additional affects on cell cycle

checkpoints likely make these unsuitable for use for the study of replisome disassembly. We also found that the huge quantities of re-loaded MCM2-7 upon CULi MLN4924 treatment made it even more difficult to use whole MCM2-7 population as a readout of active replisomes (Figures 6.8 and 6.10). In the high noise of MCM2-7 bound on chromatin we could detect no significant effects of TRAIP activity in mitosis (Figure 6.11).

To overcome the sensitivity problems associated with flow cytometry, we turned to microscopy techniques. Immunofluorescence experiments using MCM7 antibodies were not conclusive (data not shown). However, CDC45 antibodies allowed the detection of active replisomes, described previously (Fan et al., 2021). Using these, we observed increased replisome retention specifically in G2/M following TRAIP degradation in cells treated with MLN4924, demonstrating that the mitotic replisome pathway is likely to be conserved in human somatic cells (Figure 6.12). However, use of the CDC45 antibodies generated an, unexpected, pan-nuclear staining pattern. Whilst this was analagous to the results observed by Fan et al. (2021), it differed from studies visualising alternative components of the replisome (Sld5-GFP; large foci-like structures at heterochromatic regions) (Villa et al., 2021). It may be that this difference was due to antibody amplification of signal vs the detection endogenously expressed GFP-tagged protein. Alternatively Villa et al. (2021) explored replisome retention specifically during late S-phase. It is known that the staining of replication proteins or nascent DNA does differ throughout S-phase. For example, short EdU pulses result in pan-nuclear staining during early and mid S-phase, and foci during late S-phase (Aparicio et al., 2012). Similarly, PCNA antibody staining may also be used to stage S-phase cells due to the differing signals observed in early (foci), mid (pan-nuclear), and late (heterochromatic regions, large

patches) S-phase cells (Madsen and Celis, 1985). Therefore, it would be interesting carrying out experiments to understand the staining pattern for the CDC45 antibody used throughout S-phase. In our work, CDC45 intensity was shown to be vastly reduced upon entry into mitosis, suggesting the visualisation of ongoing replication. Nevertheless, additional steps aiming to validate the specificity of this antibody should be carried out; primarily investigating whether the pan-nuclear staining is truly representative of replication, or a combination of CDC45 and non-specific (background) labelling. It would also be interesting to co-stain these cells with markers for heterochromatin to try recapitulate those results observed by Villa et al. (2021), specifically looking at late S-phase DNA replication.

Furthermore, work is needed to fully explore the role of TRAIP in this process. Due to the demonstrated roles of TRAIP in S-phase, it would be important to understand whether similar proportions of active replisomes were retained when TRAIP is instead degraded specifically during G2, and not impacted by the highlighted checkpoint activation or cell cycle arrest. In addition, due to the described caveats associated with MLN4924 inhibitor treatment, TRAIP degradation should be combined with more specific mechanisms of blocking S-phase disassembly, such as LRR1 or Cullin2 depletion. Although, in studies using mouse embryonic stem cells, siRNA degradation was combined with MLN4924 treatment, indicating that one alone may not be sufficient to block S-phase replisome disassembly (Villa et al., 2021).

TRAIP has also been shown to be important for MiDAS in human somatic cells, and cells without TRAIP were found to display reduced amounts of MiDAs following aphidicolin treatment to induce under-replicated regions of DNA (Sonneville et al., 2019). We therefore

attempted to understand whether similar phenotypes could be observed in our degron cell lines. Furthermore, by using the rapid protein degradation facilitated by the AID system, we aimed to understand whether the reported roles were indeed a independent mitotic mechanism, or caused by S-phase problems. Unfortunately, the experiment did not work as expected, and too few mitotic cells were identified for quantification; further reduced by aphidicolin treatment. In the future, increased starting numbers of cells should be combined with mitotic shake off techniques to account for this. However, through ommitting mitotic shake offs in our experiment, we did encounter unexpected results. TRAIP degradation during S-phase was found to prolong DNA replication into G2/M, to a similar extent as aphidicolin treatment (Figure 6.13). This phenotype was specific to S-phase roles of TRAIP as similar results were not seen when TRAIP was instead degraded during G2. Moreover, the effects of aphidicolin and TRAIP degradation in S-phase appeared to be additive; suggesting that these two act in different pathways. The exact cause of TRAIP-mediated replication delays were not clear and further work was warranted. During S-phase, we have shown that TRAIP is required specifically at transcription start sites for the promotion of genomic stability. It was possible, therefore, that without TRAIP, these sites become particularly difficult to replicate. Moreover, without TRAIP, the ATR-dependent checkpoint was activated which is known to restrict origin firing and potentially slowed DNA replictation. It would be interesting to see whether similar results persisted upon inhibition of checkpoint activation using ATR inhibitors. In addition, it has been shown that TSS possessing high transcriptional activity, including the increased rates of anti-sense transcription also found in our work, are also replicated during G2/M (Wang et al., 2021). Without TRAIP, therefore, it was possible that these sites remained unprocessed until gene transcription was completed. Such a situation may suggest ubiquitylation and

removal of the replisome upon the conflict as a mechanism of action. Conversely, when we cross-references the TSS identified in this project with known locations of G2/M TSS replication, we found no correlation (data not shown). In all situations, however, EdU levels were found to be reduced upon chromosome condensation, suggesting that the prolonged replication is completed before mitotic entry (data not shown).

The final mechanism of TRAIP addressed during mitosis was possible roles in mitotic progression. Cells without TRAIP have been reported to progress through mitosis faster due to defects in mitotic spindle checkpoint regulation (Chapard et al., 2014a). We also see problems with mitotic timing following TRAIP degradation. The specific degradation of TRAIP during G1 was found to have no effect on mitotic entry and the condensation of chromosomes. Conversely, reduced rates of cells exhibiting chromosomal segregation was then found in cells without TRAIP. Due to the singular timepoint taken, it was equally possible that TRAIP degradation prolonged or increased the speed of segregation to result in the observations made. Although, the reduced rates found appeared to be similar to that found upon aphidicolin treatment during S-phase, known to slow the progression through mitosis. To fully understand the impact of TRAIP degradation during mitosis, live cell imaging should be carried out to calculate precise timings associated with cytokinesis.

Chapter 7

Discussion

This work has built upon, and extended, our current knowledge of the roles of TRAIP throughout the eukaryotic cell cycle. At the start of this project, the mechanisms underpinning the loss of cell proliferation following TRAIP knockout, or hypomorphic mutation, were unclear. Overall, we reveal that TRAIP is important for cell cycle progression through a mechanism exerted during S-phase (Figure 5.3, 5.4). γ-H2AX ChIP sequencing identified the likely genomic locations for this mechanism: transcription start sites possessing bi-directional transcriptional activity (Figures 5.11 - 5.14). The presence of RNA Polymerase II on chromatin was found to be important for the S-phase role of TRAIP (Figure 5.16). Moreover, the data generated also suggested TRAIP may also have interplay with DNA replication. When TRAIP was degraded specifically during S-phase, replication was extended into G2, to a similar extent as observed following aphidicolin treatment (Figure 6.13). In addition, the loss of TRAIP led to increased RNA Polymerase II presence near the replication fork (nascent DNA, Figure 5.18). Overall, due to the described observations and previously reported roles, we hypothesised that TRAIP was required for the resolution of DNA Replication-Transcription conflicts.

It is known that transcription start sites are typically difficult to replicate regions (Wang et al., 2021). Without TRAIP, we propose that the ability of cells to duplicate crowded transcription start sites is further perturbed, resulting in increased DNA damage (Figure 5.1 and 5.8-5.9), ATR-mediated G2 arrest (Figure 4.13 and 4.14), and G2/M cell cycle exit by senescence (Figure 4.17). On the other hand, whilst the described S-phase roles for TRAIP were likely responsible for the associated cell lethality and reduced proliferative capacity previously demonstrated, additional mitotic roles also exist. Cells without TRAIP show defects to mitotic progression between chromosome condensation and segregation (Figure 6.14). In addition, validation of the core mechanisms of replisome disassembly throughout the cell cycle (Figures 6.1-6.10)) indicated that the previously demonstrated, TRAIP-driven, mitotic pathway was also likely to be active in human somatic cell lines (Figures 6.11 and 6.12).

7.1 The Essential Role of TRAIP during S-Phase

The mechanism involving TRAIP, important for the prevention of genomic instability and potentially underpinning perturbation of cell viability, was proposed to be the resolution of DNA replication - transcription conflicts. Previous work carried out by multiple groups have highlighted a number of features portraying likely sites of DNA Replication-Transcription encounters. Briefly, it is thought that likely conflict sites contain either high densities of protein complexes associated with chromatin, or DNA sequences preferentially forming secondary structures (e.g., R-loops, G-quadruplexes) (Germain et al., 2021). Thus, transcription start sites appear to be key locations for interactions between DNA replication and transcription. Analogously to this, we discovered that TRAIP depletion resulted in the creation of DNA

damage close to transcription start sites possessing more equal levels of antisense to sense transcription, indicative of bi-directional transcription (Figures 5.10 - 5.14). It is also thought that efficient replication origins are often located near gene promoters (Cayrou et al., 2015). We found that, in case of conserved hotspots of TRAIP induced damage, these hotspot TSS were positioned closer to an origin than genes without increased DNA damage and therefore potentially portrayed sites with an increased chance of collisions. Altogether, it was clear that the mechanism of TRAIP strongly correlated with the known locations of DNA replication transcription conflicts.

Next, we demonstrated direct links between TRAIP and RNA polymerase II. Accumulating RNA Polymerase II has been associated with difficult to replicate regions (Wang et al., 2021), potentially suggesting the inability of the replisome to efficiently traverse regions possessing large amounts of RNA Pol II, such as the transcription start site. By combining our ChIP-sequencing with previously published data sets (Erickson et al., 2018), we were able to map the location of RNA polymerase II in HCT116 cells and found a correlation of bi-modal RNA Pol II in close proximity to the detected DNA damage (Figure 5.13). Moreover, the DNA damage caused by TRAIP degradation was rescued upon the inhibition of RNA polymerase II loading onto transcriptional promoters by Triptolide (Figure 5.16). In addition, this DNA damage accumulation was also perturbed when we blocked RNA polymerase II progression into the gene body using DRB (Figure 5.17). Finally, increased presence of RNA polymerase II was found close to active replication forks after TRAIP degradation (Figure 5.18).

As TRAIP has been reported to have several substrates on chromatin during S-phase,

two mechanisms were proposed for its role at replication-transcription collisions: revolving around the ubiquitylation of either the replisome or RNA polymerase II (Figure 7.1). Work by Prof Walter's lab has suggested that TRAIP is a part of the active replisome, situated in such a way so that it can ubiquitylate components ahead of the replication fork whilst being sterically inhibited from ubiquitylating behind the fork (Wu et al., 2019). In this scenario, TRAIP was shown to ubiquitylate replisomes from neighbouring origins to trigger disassembly upon convergence at an ICL (Wu et al., 2019). Nascent chromatin capture has been used to identify TRAIP to be enriched on nascent chromatin, supporting the idea that TRAIP is part of the active replication fork in mammalian cells (Wessel et al., 2019). Furthermore, TRAIP has also been shown to ubiquitylate a protein blockage (DPC) ahead of the replication fork, resulting in the recruitment of the proteasome and SPRTN to the blockage (Larsen et al., 2019). Given this, it was feasible that TRAIP could ubiquitylate RNA polymerase II ahead of the replication fork (Figure 7.1, left).

Previously published work has established that irreversible RNA polymerase II stalling, often after encountering lesions on the transcribed strand of DNA, results in the ubiquitylation of RNA polymerase II and its eventual degradation by the proteasome (Bregman et al., 1996; Ratner et al., 1998; Somesh et al., 2005; Tufegdzic Vidakovic et al., 2019). The best understood model for RNA Polymerase II polyubiquitylation was described using budding yeast, and only the largest RNA polymerase II subunit Rpb1 was found to be ubiquitylated. Briefly, Rpb1 is ubiquitylated by Rsp5 to form K63-linked ubiquitin chains, subsequently cleaved to mono-ubiquitylation by the Rsp5 associated deubiquitinating enzyme Ubp2. Finally, the Elongin-complex ubiquitin ligase Elc1-Cullin3 is recruited to the mono-ubiquitin mark and

mediates the attachment of K48-linked chains onto Rpb1 to recruit the proteasome (Tufegdzic Vidakovic et al., 2019; Wilson et al., 2013). This reaction was also dependent on the action of the E2-conjugation enzyme Ubc5 for substrate recognition (Somesh et al., 2007). Conversely, in human cells, less is known and RNA Polymerase II is thought to be ubiquitylated by multiple ligases. Rsp5 has several homologues, including the NEDD4 family of HECT-type ubiquitin ligases (Ingham et al., 2004). However, of these, only NEDD4 itself has been directly shown to ubiquitylate RNA polymerase II (Anindya et al., 2007). Other proteins have been implicated in RNA pol II ubiquitylation, however, including BRCA1 and von Hippel-Lindau proteins (Kuznetsova et al., 2003; Starita et al., 2005). Furthermore, the p97 segregase has been shown to be recruited to ubiquitylated RNA Polymerase II after UV induced DNA-damage, potentially indicating its removal from chromatin (He et al., 2017). Given this, it would be worthwhile exploring these findings further with respect to our data. TRAIP has been previously uncovered to be capable of forming lysine-linked ubiquitin chains, including K6 and K63 (Moreno et al., 2019; Shi et al., 2018). However, the respective E2-conjugation enzyme catalysing this reaction remains unclear. Work should be carried out to understand whether TRAIP can interact with any human homologues of Ubc5, the UBC5 family of E2-conjugation enzymes (Ube2D1 – Ube2D4) (Stoll et al., 2011) to build either K48- or K63- linked ubiquitin chains. Interestingly, we have previously demonstrated the ability of *X. laevis* TRAIP to autoubiquitylate *in vitro* using Ube2D1 (UBCH5) (Moreno et al., 2019). In addition, in yeast, the RNA Polymerase II ubiquitylation sites have been mapped *in vitro*, and were found to be conserved in human RNA Pol II (Somesh et al., 2007). Thus, it may be of interest to explore if expressing mutations of these sites possessed similar phenotypes to TRAIP degradation.

Alternatively, large scale proteomics screens, and our work in *X. laevis* egg extract, has consistently identified TRAIP to be enriched at stressed replication forks (Dungrawala et al., 2015; Moreno et al., 2019; Wessel et al., 2019). Additional studies have used immunofluorescence to highlight the recruitment of TRAIP specifically to sites of induced replication stress and DNA damage (Feng et al., 2016; Hoffmann et al., 2016). Therefore, it was also a possibility that TRAIP may ubiquitylate the replisome at replication-transcription conflicts to trigger CMG disassembly in a similar mechanism to that reported during mitosis (Figure 7.1, right) (Deng et al., 2019; Moreno et al., 2019; Sonneville et al., 2019). It has already been shown that TRAIP is capable of driving CMG disassembly through MCM7 ubiquitylation during S-phase at sites containing ICLs (Wu et al., 2019). Furthermore, unpublished preliminary data from our lab also suggests that TRAIP accumulates directly with CMG during S-phase upon the inhibition of replisome disassembly (not shown). To investigate this possibility further, the association of TRAIP and MCM7 should first be validated, before any respective ubiquitylation sites on MCM7 by TRAIP during S-phase should be determined.

Several questions remained surrounding the role of TRAIP in the resolution of replication – transcription collisions. First, it will be imperative that any requirement for TRAIP's ubiquitin ligase activity is explored. To this end, IAA treatment should be combined with the re-introduction of WT and catalytically inactive mutants of TRAIP. Following the elucidation of any requirement for protein ubiquitylation, the respective substrate should be also identified. Doing so will facilitate further work into the function of any formed ubiquitin chains. For example, does protein ubiquitylation stimulate the removal of a substrate from chromatin at replication - transcription conflicts? What linkage-type is utilised? And,

what are the consequences of preventing this ubiquitylation (i.e., by introducing Lysine-null substrate mutants)? However, only a small proportion of the total number of complexes of RNA polymerase II and CMG on chromatin will collide at any given time. In addition, both components are ubiquitylated and disassembled from chromatin upon their termination or encountering sources of stress. Therefore, it is difficult to study this process in a cycling population of cells. To overcome this, it is likely that known conflict sites must be introduced and the isolation, or visualisation of single replication-transcription collision will be required. A clear candidate for this would be to use single molecule imaging to replicate and transcribe plasmid DNA simultaneously. In mammalian cells, the Tus-Ter plasmid system has been used to study replication fork stalling in HEK293T cells (Willis et al., 2014), allowing uni-directional plasmid replication and artificial blockage insertion. It may be possible, therefore, to adapt this system to insert a gene promoter site to facilitate transcription in either direction. In addition, utilising a plasmid system would also enable the inclusion of sequences likely to form R-loops or secondary DNA structures (e.g. A-T rich repeats) (Germain et al., 2021), to start to understand whether TRAIPs role is specific for RNA Polymerase II, R-loops, or all replisome blockages on chromatin.

Second, what are the steps following TRAIP substrate ubiquitylation? One prospective candidate is the recruitment of the p97 segregase and subsequent removal of the respective complex from chromatin. p97 has been shown to be capable of both removing RNA polymerase II and CMG from chromatin in mammalian cell lines (He et al., 2017; Tufegdzic Vidakovic et al., 2019; Villa et al., 2021). To attempt to answer this, we analysed any differences in DNA damage accumulation following the treatment of cells with combinations of p97i, triptolide, and IAA.

The results, however, were inconclusive, likely due to the reported S-phase problems caused by CB5083 inhibitor treatment (Figure 6.1 - 6.3). In budding yeast, the p97 co-factors Ubx4 and Ubx5 were identified to partially stabilise Rpb5 after UV-induced DNA damage (Verma et al., 2011), potentially with similar mechanisms as described for the co-factor Ubxn7 during replisome disassembly (Tarcan et al., 2021). Hence, it would be interesting to establish whether similar roles exist for the human homologues ASPL/TUG (Ubx4) (Madsen et al., 2014) and UBX5 (Ubx5), and whether depletion of either co-factor stabilised RNA Polymerase II on chromatin.

Third, what is the most damaging consequence of the replication-transcription collisions that leads to the loss of cell proliferation? Under-replication of DNA due to extensive replication fork stalling has been shown to lead to chromosome mis-segregation, DNA damage, and ultimately cell death (Bertolin et al., 2020). If unresolved, persisting replication-transcription conflicts may have resulted in extensive fork stalling and increased replication stress, ATR-mediated checkpoint activation, and the proliferation defects observed. Our work highlighted that the sites of conserved DNA damage following TRAIP degradation were usually replicated in early S-phase, and that the loss of TRAIP appeared to prolong DNA replication into G2/M; potentially linking TRAIP degradation to impaired replication. On the other hand, transcription stalling and the loss of gene expression of key cell cycle regulators may also stop cell proliferation (Engeland, 2017). However, GOTerms analysis of the genes containing conserved DNA damage did not reveal such trends (Table 5.1), and so it was most likely that impaired replication and accumulating replication stress was the primary cause of the cell proliferation defects. Given this, the described replication phenotypes should first be explored further. It was possible that the prolonged DNA replication was a result of checkpoint activation and reduced origin firing. If

true, the inclusion of ATRi should rescue the observed defects. Importantly, these phenotypes should also be associated with transcription. TRAIP depleted cells have been shown to cause increased replication fork stalling (Hoffmann et al., 2016). It would be interesting to repeat this experiment in the degron cells, including triptolide and ATRi, to assess whether the replication fork stalling was due to transcription-replication collisions or checkpoint control.

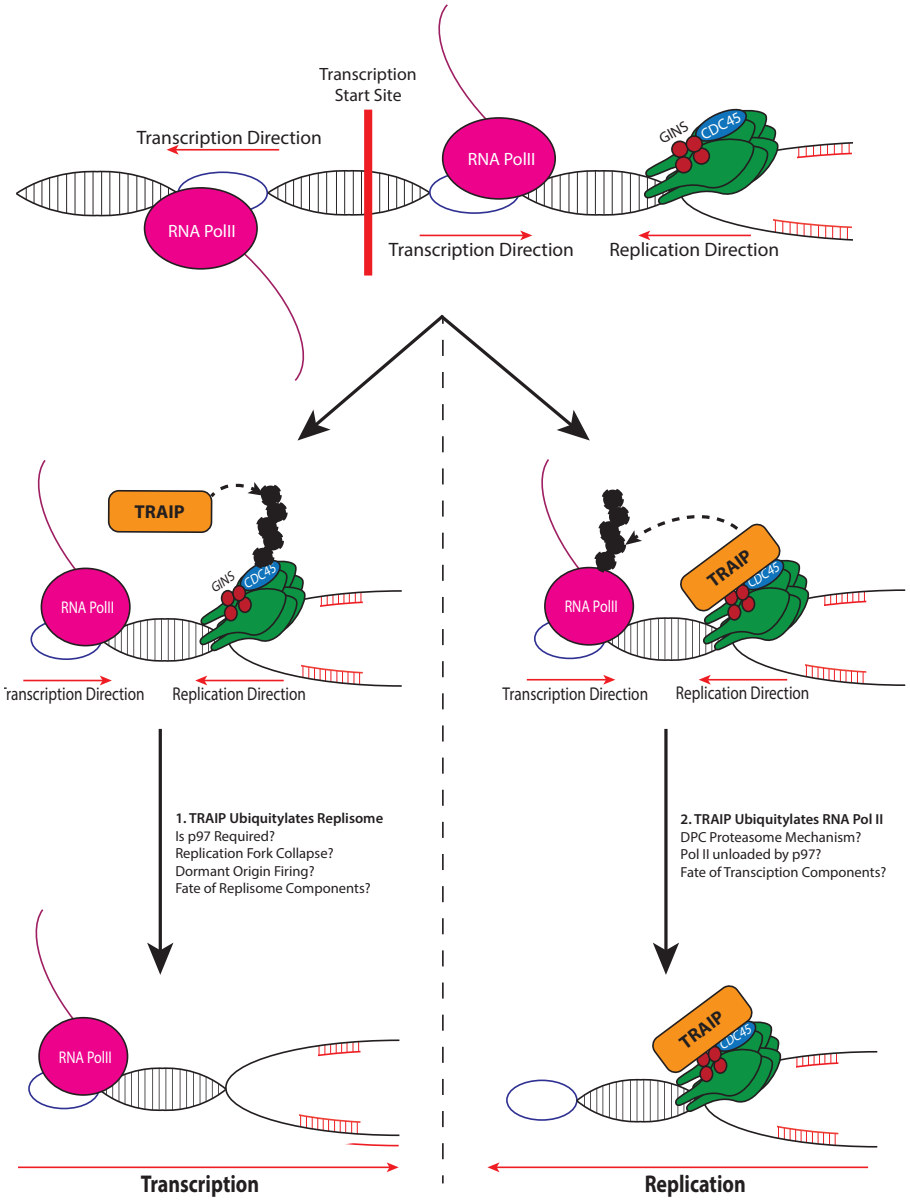


Figure 7.1: **The proposed mechanism of action for TRAIP during DNA replication-transcription conflicts.**. TRAIP is required preferentially at bi-directional transcription start sites with nearby replication origins, indicating head-on replication conflicts. We propose that upon collisions between CMG and RNA Pol II TRAIP will ubiquitylate either the active CMG or RNA polymerase II. In either situation, the subsequent steps likely involve complex removal from chromatin and continuation of the other process.

7.2 Roles of TRAIP During Mitosis

Prior to the start of this PhD, TRAIP had been reported to possess expression levels peaking in mitosis, and was implicated in the regulation of the spindle assembly checkpoint (Chapard et al., 2014a, 2015). Our lab identified TRAIP to accumulate with terminating replisomes upon the inhibition of S-phase replisome disassembly in *X. laevis* egg extract (Moreno et al., 2019). To then build on this, I aimed to utilise the degron cell lines generated to understand any involvement of TRAIP in human replisome disassembly. We could detect no direct involvement for TRAIP in the removal of unperturbed replisomes during S-phase (Figure 5.7).

To start to understand the mechanisms of human replisome disassembly, I first explored any defects to the proportions of MCM2-7 bound to chromatin following treatment with small molecule inhibitors against p97 and Cullin-type ubiquitin ligases. Importantly, the inhibitors selected had been extensively used previously in model organisms and mouse embryonic stem cells for the study of DNA replication termination. However, the use of these inhibitors led to complex phenotypes, likely caused by numerous wide-ranging effects on cell cycle dynamics (Figures 6.1-6.3 and 6.7-6.8).

MLN4924 is a potent inhibitor of NEDD8-activating enzymes, commonly used to prevent the activation of Cullin-type ubiquitin ligases (Soucy et al., 2009). In my work, this inhibitor was used to inhibit the Cullin2-mediated ubiquitylation of MCM7 during DNA Replication Termination. Alongside this, however, several other mechanisms would also be affected. The Cullin proteins form the largest family of E3 ubiquitin ligases in human cells, with roles in a myriad of essential cellular processes. Protein ubiquitylation by Cullin-type ligases is

essential for DNA replication, cell cycle progression, and proteasomal-mediated protein degradation (Emanuele et al., 2011). Of particular note is the role of Cullin-1 and -4 in the degradation of CDT1. The inhibition of this mechanism stabilises CDT1, leading to the re-loading of MCM2-7 and DNA re-replication (Lin et al., 2010). The high levels of MCM7 retention observed on chromatin following MLN4924 treatment was likely representative of this mechanism. In addition, although the activation of Cullin-type ubiquitin ligases is the most well described function of protein neddylation, other substrates exist. A recent proteomics screen identified cannonical neddylation sites in 431 unique proteins involved in a wide range of cellular functions: including DNA Replication, mRNA surveillance, and interactions with the proteasome and spliceosome (Lobato-Gil et al., 2021). A further 131 substrates were also identified following the induction of proteotoxic stress (Lobato-Gil et al., 2021). Thus, it is possible that the use of MLN4924 will cause additional phenotypes due to the direct functional importance of protein neddylation itself; alongside those indirect effects caused by the loss of Cullin-mediated protein ubiquitylation.

To inhibit the activity of the p97 segregase, a highly selective and potent inhibitor was used (CB-5083) (Zhou et al., 2015). We envisaged that the inhibition of p97 would prevent the removal of terminated replisomes from chromatin. However, the replisome is not the only substrate for p97 extraction, and use of this inhibitor has been shown to result in the accumulation of ubiquitylated proteins on chromatin, with wide ranging effects (Vaz et al., 2013). This was discussed previously (see Chapter 6.3). Due to these considerations, it was difficult to untangle the impact of p97 inhibition on replisome disassembly when also considering any impacts from other affected mechanisms. The downstream consequences of

these compounding effects became particularly apparent when investigating any defects to S-phase progression following p97i; with our data suggesting that cells stall during S-phase after CB-5083 treatment (Figure 6.3). To attempt to overcome this, and alleviate the cell cycle accumulation phenotypes observed following both CB-5083 and MLN4924 treatment, we selected to inhibit the WEE1 checkpoint kinase using MK-1775. Identified as a key regulator of the G2 DNA damage checkpoint, WEE1 phosphorylates and inactivates CDK1 to prevent entry into mitosis, allowing the repair of any DNA lesions before cell division (Matheson et al., 2016). I observed that the inhibition of WEE1 was able to overcome the G2 cell cycle arrest induced by TRAIP degradation. However, MK-1775 has also been reported to have additional effects during G1, potentially influencing the interpretation of the data collected. Specifically, WEE1 is thought to suppress CDK2-mediated activation of the replicative helicase. The use of MK-1775, therefore, leads to excess dormant origin firing upon entry into S-phase (Moiseeva et al., 2019b). Interestingly, such an effect may be exploited for the study of DNA replication. In *X. laevis* egg extract, caffeine is often included in reactions to increase origin firing, ultimately resulting in more termination events (Marheineke and Hyrien, 2004). It would be interesting to explore whether MK-1775 treatment may allow a similar approach in human cell lines.

Nevertheless, the data obtained using the described inhibitor treatments are consistent with the motion that mechanisms of replisome disassembly established in model systems are also active in human somatic cell lines. Furthermore, immunofluorescence experiments provided the first insight into the mechanism of action, suggesting that TRAIP was indeed responsible for driving replisome removal during G2/M following the inhibition of S-phase replisome disassembly.

In addition to work exploring replisome disassembly, we were interested to understand whether the previously reported mitotic roles of TRAIP (Chapard et al., 2014a, 2015; Sonneville et al., 2019) were independent to the reported S-phase mechanisms (Feng et al., 2016; Harley et al., 2016; Hoffmann et al., 2016; Larsen et al., 2019; Wu et al., 2019). Correlating with published data (Chapard et al., 2014a), we observed defective mitotic timing following the specific degradation of TRAIP during G2-phase, indicating that the role of TRAIP in mitotic progression was separate to that observed in S-phase. Conversely, the siRNA depletion of TRAIP was shown to result in increased micronuclei formation (Hoffmann et al., 2016) not found in our conditional TRAIP degron cell lines. This may have been due to the shorter IAA treatments used when compared to requirements for siRNA (typically 24 h IAA vs 48-72 h siRNA). Alternatively, there may be differences in micronuclei formation between cell lines; Hoffmann et al. (2016)) utilised U2OS cells which are well known to be polyploid and therefore may be more susceptible to micronuclei formation due to possessing more unstable genomes (Garribba and Santaguida, 2022; Kneissig et al., 2019). The reported requirements of TRAIP for MiDAS have been suggested to encompass replisome disassembly to enable nuclease access to DNA and stimulate replication fork breakage (Wu et al., 2021). Given this, the question remains as to what is the main target of TRAIP in unperturbed cells, and is the reported requirement for TRAIP in MiDAS due to its mitotic function or functions earlier in cell cycle during S-phase? Aphidicolin treatment was required to explore the role of TRAIP during MiDAS previously (Sonneville et al., 2019). However, mitotic defects have been found following the degradation of TRAIP alone (micronuclei, mis-aligned chromosomes), potentially resultant from the genome alterations caused by the loss of TRAIP-mediated S-phase problems or mitotic replisome disassembly (Deng et al., 2019). Thus, it is possible that TRAIP is important

for CMG removal during S-phase in response to endogenous replication stress and that is consequently responsible for the phenotypes observed in mitosis. One such candidate may be the replication-transcription conflicts proposed in our work.

Another pertinent question remaining with regards to TRAIPs roles in two different stages of the cells cycle is what drives and regulates these different specificities and functions of TRAIP? Prof Walter's model during S-phase suggests that TRAIP cannot ubiquitylate the fork it is associated with (Wu et al., 2019). In agreement with this, we suggest that TRAIP will most likely ubiquitylate RNA polymerase II ahead of the fork during a replication-transcription conflict. However, during mitosis, TRAIP can remove both terminated and stalled replication forks by directly ubiquitylating MCM7 (Deng et al., 2019; Moreno et al., 2019). In this situation, TRAIP may modify the replication fork it is associated with, as it is unlikely that there will always be an opposing replisome ahead of the fork. Work in mammalian cell lines has shown that TRAIP can re-localise to sites of replication stress (Feng et al., 2016; Hoffmann et al., 2016). Large scale proteomics screens have corroborated this observation, with TRAIP shown to accumulate specifically with the replication fork following the induction of replication stress (Dungrawala et al., 2015; Wessel et al., 2019). Therefore, it was possible that TRAIP was recruited specifically to replisomes in trouble, acting as part of the replication stress response. If true, this role of TRAIP in promoting genomic stability may be active throughout the entire cell cycle.

Alternatively, protein ubiquitylation is an extremely flexible post-translational modification regulated by several components. The respective E2 conjugation enzymes interacting with TRAIP has not been reported in any system and it is possible that different E2 enzymes

are determinative of the different lysine-linked ubiquitin chains reported to be formed by TRAIP. On the other hand, TRAIP itself is directly modified by phosphorylation during mitosis (unpublished work from our lab) that may induce changes to its activity or respective cellular target. If left unregulated, TRAIP would likely have disastrous effects on cell viability. DNA replication is regulated so that no more MCM2-7 double hexamers can be loaded onto chromatin following entry into S-phase (Moreno and Gambus, 2015). Given the roles of TRAIP in driving replisome disassembly, it is possible that its disregulation may lead to the aberrant removal of replisomes throughout S-phase. The canonical S-phase pathway for replisome disassembly incorporates mechanisms to prevent this, and $Cullin2^{LRR1}$ is inhibited from binding to the non-terminated CMG by the excluded leading strand (Jenkyn-Bedford et al., 2021; Zhou et al., 2021). It is not currently known whether similar regulation impacts TRAIP.

7.3 Is TRAIP a Druggable Target?

Objective 4 of this PhD project initially aimed to understand whether TRAIP was a viable drug target for therapeutic purposes. The expression of TRAIP is tightly regulated throughout the cell cycle by the E2F transcription factor, and as such, cancers with upregulated E2F transcriptional activity often also possess TRAIP over-expression (Chapard et al., 2015). Specifically, TRAIP over-expression has been reported in breast epithelial cancer cell lines and tumours (Yang et al., 2006; Zhou and Geahlen, 2009), basal cell carcinomas (Almeida et al., 2011), melanoma (Chapard et al., 2015), liver cancer (Guo et al., 2020), and osteosarcoma (Li et al., 2021). The precise role of TRAIP in tumour development and progression, however, is conflicting, with both oncogenic and tumour suppressive functions reported. It is possible that the over-expression of TRAIP in these cases was a secondary effect from aberrant E2F activity,

but evidence also exists correlating TRAIP overexpression with poorer patient prognosis (Guo et al., 2020). Conversely, TRAIP has also been shown to be downregulated or mutated in several types of cancer, including colorectal and large B-cell carcinoma (Cerami et al., 2012; Gao et al., 2013). Intriguingly, mutations to TRAIP impairing its' ubiquitin ligase activity do not appear to portray increased cancer predisposition and instead limit cell proliferation to cause primordial dwarfism phenotypes (Harley et al., 2016); an outcome not commonly associated with proteins involved in ICL repair.

Our work indicated that, if TRAIP was indeed regulating processing of the DNA replication – transcription conflicts, it may form a viable therapeutic target to prevent tumorigenesis. The conditional degron cell lines were generated from colorectal cancer parental cell lines. Importantly, in this background, the loss of TRAIP led to ATR-mediated cell cycle arrest. Furthermore, TRAIP degradation ultimately led to cell senescence, not complimentary with increased proliferative states. Alongside our data, TRAIP knockdowns have also shown to reduce cell viability in other tumour models (Guo et al., 2020). The inhibition of ATR, promoting genomic instability, is emerging as a promising candidate for cancer therapies (Barnieh et al., 2021). Importantly, it has been shown that the inhibition of ATR may sensitise cancer cells to replicative stress inducing agents to increase cell death by apoptosis or senescence (Bartkova et al., 2006; Weber and Ryan, 2015). As TRAIP degradation led to increased replicative stress and cell senescence alone, we wondered whether TRAIP was antagonistic to tumour growth. On top of this, the loss of ATR functionality may enhance the TRAIP-dependent losses to cell viability and further promote cell death. It is possible that, in cancers displaying increased transcriptional activity (Bowry et al., 2021), TRAIP was also overexpressed to preserve the

processing of DNA replication-transcription conflicts. Thus, inhibition of this mechanism may induce replication stress and ultimately cell death. Interestingly, when exploring the hotspots for TRAIP-mediated DNA damage due to unprocessed replication transcription conflicts, the conserved genes identified correlated with regions of increased copy number alterations in cancers deficient for TRAIP (Figure 7.2); suggesting a link between TRAIP and cancer cell proliferation.

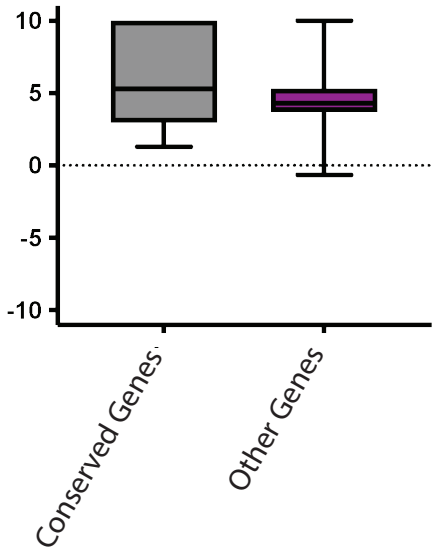


Figure 7.2: **Sites of Conserved TRAIP-Dependent DNA Damage have more Copy Number Aberrations in TRAIP-Defective Cancer Models.** Copy number aberrations in TRAIP-deficient colorectal cancers from cBioportal were compared to our ChIP sequencing data. Shown is the frequency of copy number aberrations in those genes possessing conserved DNA damage peaks (grey), and all other genes (purple). Analysis carried out by Dr. Marco Saponaro.

The ubiquitin-proteasome system, underpinning protein turn-over, has long been studied for the development of novel inhibitors for cancer treatments. Inhibitors have been developed against all components of the protein ubiquitylation pathway (Shen et al., 2013), or the proteasome itself (Hungria et al., 2019). Prominently, several of these inhibitors aimed to prevent the degradation of wild-type p53 by aberrant regulatory pathways to promote the apoptotic response (Shen et al., 2013). To understand whether TRAIP may act as a viable

therapeutic target, a high throughput screen was designed with collaborators at Astra Zeneca to test approximately 100,000 likely compounds for TRAIP inhibition. Although this work could not be completed during this PhD project, it is our intention that this screen will be carried out as part of future work. Briefly, the *in vitro* ability of recombinant TRAIP to autoubiquitylate has been shown (Besse et al., 2007; Moreno et al., 2019). Using this information, a multi-step screening cascade was designed (Figure 7.3). Briefly, we will first run *in vitro* autoubiquitylation assays in the presence of each compound and measure any reduction in activity through the acoustic mist ionisation mass spectrometry (AMI-MS) platform to facilitate high throughput capabilities (Belov et al., 2020). AMI-MS has an approximate molecular weight cut-off of 15-20 kDa, and would effectively ionise free ubiquitin in the reaction. By only using a rate-limiting amount of ubiquitin, we will determine any inhibition by the respective loss of this free ubiquitin pool.

Confirmation assays will then be carried out to refine the hits identified from the high throughput screen. First, we will similarly use AMI-MS to explore whether promising compounds can also inhibit the TRAIP-driven ubiquitylation of biologically relevant targets (mapped MCM7 ubiquitylation sites acting in the mitotic replisome disassembly pathway). Second, biochemical confirmation of each hit, alongside dose response, will be carried out using a Homogeneous Time Resolved Fluorescence (HTRF) approach. HTRF utilises standard FRET to identify protein interactions *in vitro*, in this case we will utilise fluorescently tagged ubiquitin and TRAIP. However, unlike standard FRET, HTRF is accompanied by small time delays to the emitted signal to overcome the major limitation of background signal from FRET, not feasible with large scale screens (Degorce et al., 2009).

Finally, the specificity of the selected pool of small inhibitory compounds will be refined to ensure the specific inhibition of TRAIP, and not other components of the ubiquitylation cascade. Measuring any inhibition of E1 activation enzymes is routinely carried out using standard ATP consumption assays adapted from techniques originally designed for measuring kinase activity (Koresawa and Okabe, 2004). Conversely, assays investigating the activity of the E2 conjugation enzymes are more complex. For this, we envisaged repeating the *in vitro* ubiquitylation assays using a panel of E2 conjugation enzymes and E3 ubiquitin ligases alongside the TRAIP assay. Following completion of the screen, any compounds (expected: 1-10 from 100,000 starting pool) will be screened using a combination of *X. laevis* egg extract and cancerous cell lines.

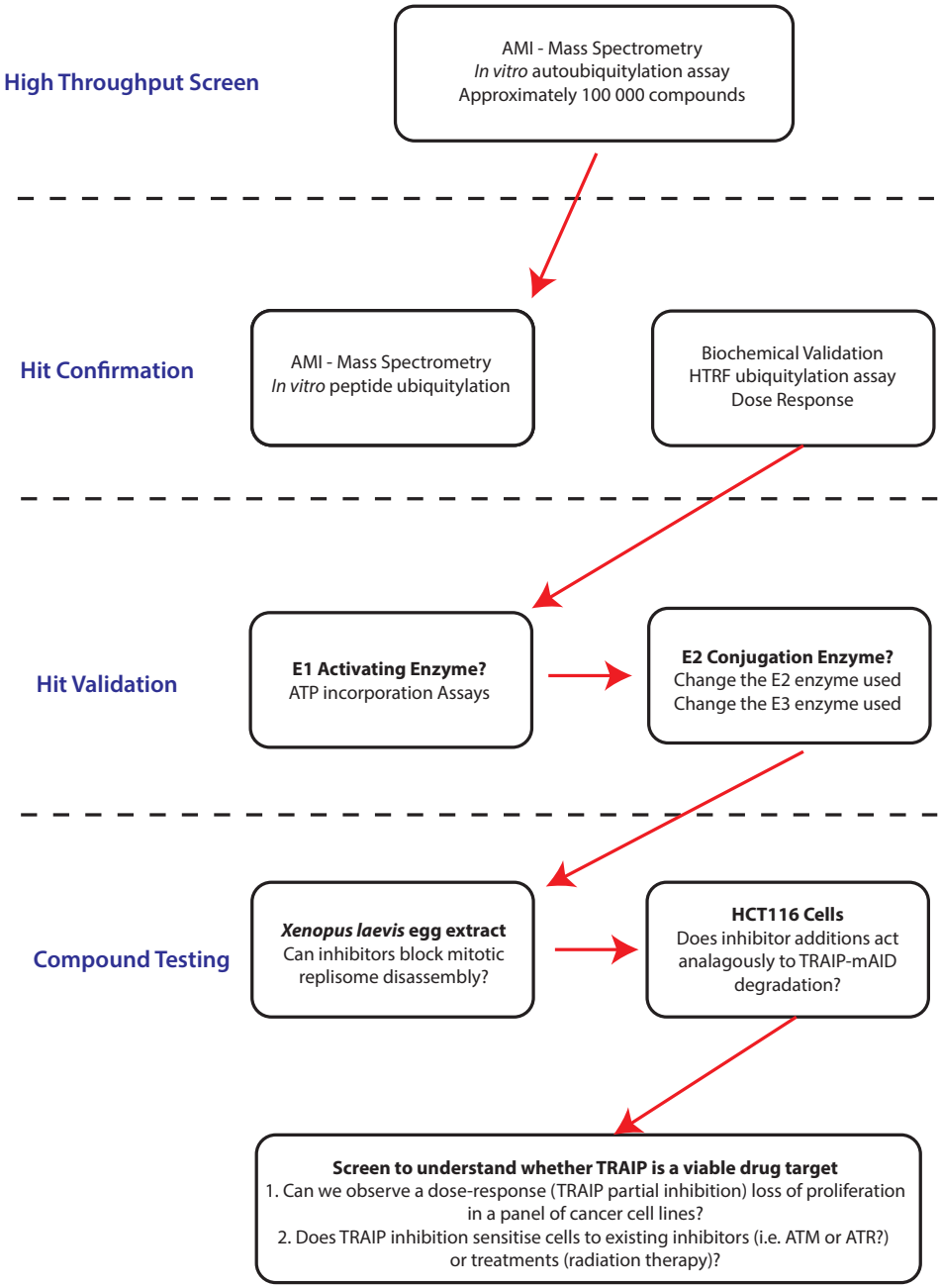


Figure 7.3: **A Summary of the Designed High Throughput Screen to Identify Small Molecule Inhibitors of TRAIP.** Screen will be carried out as part of a future project in collaboration with Astra Zeneca. Shown are the detailed steps for the high throughput screen, hit confirmation, hit validation, and subsequent compound testing.

7.4 Conclusion

Overall TRAIP has emerged as a key regulator of genomic stability. For the first time, we have implicated TRAIP in active transcription through several means. Additional work carried out during this PhD and other labs have also highlighted the importance of TRAIP for the processing of the replisome during multiple cell cycle stages. Therefore, it is likely that TRAIP plays a role as part of a wider replisome-associated network for the specific protection of the replisome upon encountering barriers on chromatin. Whilst in unperturbed cells, this is predominantly exerted during replication-transcription encounters, it is clear that TRAIP is important in facilitating the replisome bypassing several types of blockages. Through these mechanisms, TRAIP is pivotal for the unperturbed eukaryotic cell cycle, potentially protecting against tumorigenesis and thus acts as a potentially viable target for the treatment of several diseases. However, several questions remain surrounding the regulation of TRAIP, and the exact targets of TRAIP ubiquitylation, types of chains built during S-phase in human cells, or the respective linkage type used for formed ubiquitin chains remains unclear. Thus, further work is required to explore the precise mechanistic processes catalysed by TRAIP activity.

Appendix A

Plasmid Constructs and Expression Sequences

A.1 Plasmid constructs and sequences used for recombinant protein expression and purification

To purify recombinant proteins of interest during this PhD project, vectors were generated by DC Biosciences (Dundee), inserting the desired DNA sequence of interest into PET28 plasmid backbones. Detailed below is a summary of the background construct used (Figure A.1), and insert sequences for each respective candidate.

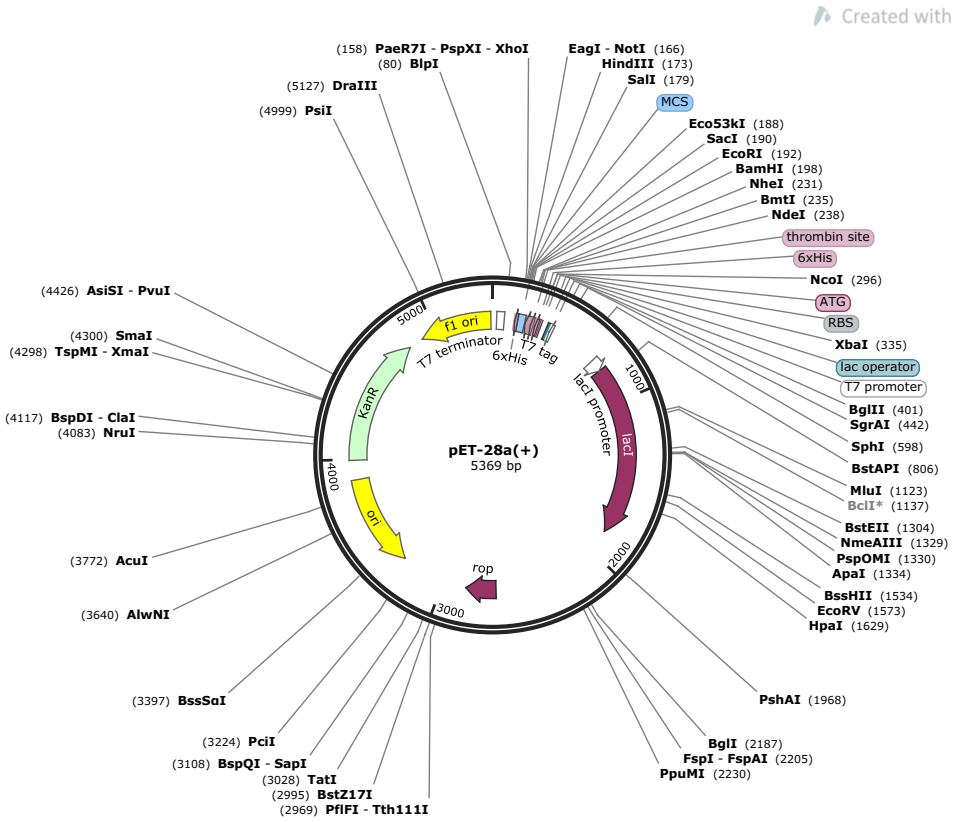


Figure A.1: **pET28 Plasmid Map**. Shown is the pET28 plasmid backbone used by DC Biosciences to generate expression plasmids for the production of recombinant candidate proteins in *E. coli*. DNA sequences of interest were inserted using molecular cloning techniques within the Multiple Cloning Site (MCS), facilitating protein expression of both expression of recombinant protein from a T7 promoter and inclusion of a 6X His-tag onto the N-terminus of respective recombinant proteins of interest. Plasmid backbone sequence was acquired from the SnapGene public resource database (available at snapgene.com). Figure generated using SnapGene (Insightful Science; available at snapgene.com).

A.1.1 USP10 Insert Sequence

Insert length: 690 bp

Sequencing primers used to confirm insertion: T7 Promoter / T7 Terminator

Restriction Sites Used: NdeI / HindIII

Antibiotic Selection: Kanamycin

Insert Sequence: CATATGGCATCCCCGTCCGAACAGTACATCTTCGGCGAATTCTCCGACGACGAAT

TCAAACAGTTCTTCGTAACGGCACGTTGCACGGTAGAACTGCCGCCGTACAACGAACACTTCTTCCCG

TGCGGCCCGCAGTCCTCCGGCGACTTCCAGGACGACATGCACCTGAAATTCTCCGAAGTAATCCACG

GCATCTCCGGCGAAGAATGCCCGCGTATCGAATTCGGCATCGAAGAAGTAATCGACCACAACACGAC

GCTGCCGAACAACACGGACTACTCCATCTCCTCCAACCTGAACCCGCAGGCACCGGAATTCATCCTGA

CGTGCTCCTCCTCCCCGAAAGACTCCAACAACGTACTGCACGAAAACAACTTCGACGCAATCGACTGC

CAGTTCTCCGAATCCTCCATCCCGGACGGCTCCGGCAACGCAGACTCCGACGGCACGTCCGGCACGG

GCCAGCGTGAACGTAAAAAAAAAAAAAAACGTCCGCCGGGCTACTACTCCTACCTGGAAGGCGTAG

GCGACGTACCGTCCGAAACGCTGCTGAACGGCCACGCAAACTCCGCAGGCCTGAACTCCATCTCCAC

GGACGACCCGGACCTGGCAGAAGACATCCCGATCTCCACGACGTCCCCGCGTACGTGCACGTCCCCG

GACAACTTCGTAGACCTGAACTAAAAGCTT

A.1.2 USP22 Insert Sequence

Insert length: 1584 bp

Sequencing primers used to confirm insertion: T7 Promoter / T7 Terminator

Restriction Sites Used: NheI / XhoI

Antibiotic Selection: Kanamycin

Insert Sequence: GCTAGCATGTCCCCGGCAGGCTGCTCCCACGTAAACTCCTTCAAAGTAGAAAACT

GGAAACAGAACCTGCGTGTAATCTACCAGTGCTTCGTATGGTCCGGCACGCCGGAAACGCGTAAACG

TAAAGCAAAATCCTGCATCTGCCACATGTGCGGCGCACACCTGAACCGTCTGCACTCCTGCCTGTACT

GCGTATTCTTCGGCTGCTTCACGAAAAAACACATCCACGAACACGCAAAAAACAAACGTCACAACCTG

GCAATCGACCTGCTGTACGGCGGCATCTACTGCTTCATGTGCCAGGACTACATCTACGACAAAGACAT

GGAACAGGTAGCAAAAGAAGAACAGCGTAAAGCATGGAAACTGCAGGTATTCTCCCCGGCACTGGT

ATCCCCGTACCAGTACACGATGACGGGCGTAGGCGAAAAATACTCCACGTGGGAACCGACGAAACG

TGAACTGGAACTGCTGCAGCACAACCCGAAACGTCGTAAAATCACGACGAACTGCACGATCGGCCTG

CGTGGCCTGATCAACCTGGGCAACACGTGCTTCATGAACTGCATCGTACAGGCACTGACGCACACGC

CGCTGCTGCGTGACTTCTTCCTGTCCGACCGTCACAAATGCGAAATGCAGTCCCCGAACTCCTGCCTG

GTATGCGAAATGTCCACGCTGTTCCAGGAATTCTACTCCGGCCACCGTTCCCCGCACATCCCGTACCG

TCTGCTGCACCTGGTATGGACGCACGCACGTCACCTGGCAGGCTACGAACAGCAGGACGCACACGA

ATTCCTGATCGCAGCACTGGACGTACTGCACCGTCACTGCAAAGGCGACGACAACGGCAAAAAAGCA

AACAACCCGAACCACTGCAACTGCATCATCGACCAGATCTTCACGGGCGGCCTGCAGTCCGACGTAA

CGTGCCAGGTATGCCACGGCGTATCCACGACGATCGACCCGTTCTGGGACATCTCCCTGGACCTGCC

GGGCTCCTCCACGCCGTTCTGGCCGCTGTCCCCGGGCTCCGACGCAGGCGTAGTAAACGGCGAATCC

CACGTATCCGGCACGACGACGCTGACGGACTGCCTGCGTCGTTTCACGCGTCCGGAACACCTGGGCT

CCTCCGCAAAAATCAAATGCTCCGGCTGCCACTCCTACCAGGAATCCACGAAACAGCTGACGATGAA

AAAACTGCCGATCGTAGCATGCTTCCACCTGAAACGTTTCGAACACTCCGCAAAACTGCGTCGTAAAA

TCACGACGTACGTATCCTTCCCGCTGGAACTGGACATGACGCCGTTCATGGCATCCTCCAAAGAATCC

CGTATGAACGGCCAGTACCAGCAGCCGTCCGACTCCCTGCACAACGACAACAAATACTCCCTGTTCGC

AGTAGTAAACCACCAGGGCACGCTGGAATCCGGCCACTACACGTCCTTCATCCGTCAGCACAAAGAC

CAGTGGTTCAAATGCGACGACGCAATCATCACGAAAGCATCCATCAAAGACGTACTGGACTCCGAAG

GCTACCTGCTGTTCTACCACAAACAGTTCCTGGAATACGAATAACTCGAG

A.1.3 USP34 Insert Sequence

Insert length: 690 bp

Sequencing primers used to confirm insertion: T7 Promoter / T7 Terminator

Restriction Sites Used: NdeI / HindIII

Antibiotic Selection: Kanamycin

Insert Sequence: CATATGTGCGAAATGTGCGCAGAACTGCTGCTGCTGCTGAACGACATCTCCGACT
CCGAAGGCTCCGACGGCCTGCAGCTGCGTAAAGAACACGCACTGAAAATCTTCGCATACATCAACTC
CTGGGCACAGCGTCAGTGCCTGTGCTGCTTCAAAGAATACAAACACCTGGAAATCTTCAACCAGGTA
GTATGCGCACTGATCAACCTGGTAATCGGCCAGGTACAGGCACTGCAGGACCAGCTGGTAAAAATCG
TAACGACGTCCCCGGAATCCAACTGGCAGGACGAACACAAACCGTCCGAAGAAGAACTGCTGAACG
TAGAAAAAGAACCGCAGGACGAAGAAGAAGAAGGCGAAGAACGTGGCAACCCGCAGGAAAAAACG
CTGGACAACGCACGTACGTGCAACCCGACGGAAGAAGAATCCATCAAATCCACGGAAACGTTCCACC
TGTGGTCCACGGACGAAAAAGAAAAACTGCTGCTGTGCGTAGCAAAAATCTTCCAGATCCAGTTCCC
GCTGTACACGGCATACAAACACAACACGCACCCGACGATCGAAGACATCTCCGCACAGGAATCCAAC
ATCCTGGGCGCATTCTGCGACATGAACGACGTAGAAGTACCGCTGCACCTGCTGCGTTACGTATGCCT
GTTCTGCGGCAAAAACGGCCTGTCCTAAAAGCTT

A.1.4 USP37 Insert Sequence

Insert length: 732 bp

Sequencing primers used to confirm insertion: T7 Promoter / T7 Terminator

Restriction Sites Used: NdeI / XhoI

Antibiotic Selection: Kanamycin

Insert Sequence: CATATGGCACTGCACTCCCTGCACGGCCCGATCCGTATCAACTGCCTGAAAGTAG
GCACGTCCAAATGGAAAGAAGGCTGCTGCGAAGTAATCGAAAAAGACAACAAATACTCCCTGGTAG
TAAACTACAACGCAGGCGGCGGCCCGACGAAATTCCAGCTGACGCAGAACATCAAAACGATCGTACT
GAAACCGTCCGGCTGCACGCAGTCCCGTCTGATGCTGACGCTGAAAGACGCATCCTCCCTGACGATC
GACAAAGTACCGCTGAACAAAGCAGAAAACCTGAAACACTTCCTGGAAGGCCTGGACAAAGCATCC

ACGGTAAAATCCACGCAGGGCTCCGGCTCCTTCTCCGGCGTACTGGGCAACCGTTCCACGCAGATCG

AAGCAAACCGTTCCCTGCTGAACAAAACGCAGACGCCGTCCAAACGTGTATCCTTCGACAACAAAGA

CGAAACGCCGGTAAAAAAATCCCTGTCCAACACGGGCCGTGTATCCATCAAAACGTCCCCGGGCAAC

ACGGTATCCGCAGGCCGTTCCGCAATCAACACGACGCCGTCCACGCCGCAGCGTACGTCCCTGATGG

AATCCCGTTCCGAAAAACGTAAACGTATCCAGACGCCGTCCCCGGAAATCGTAGAAGACTACCCGAA

AGAAAACGACTCCTCCACGACGAACAAAGCACTGTCCGACGCAGGCCGTCGTTTCCTGTCCTCCTCCT

AACTCGAG

A.1.5 RFWD3 Insert Sequence

Insert length: 1061 bp

Sequencing primers used to confirm insertion: T7 Promoter / T7 Terminator

Restriction Sites Used: NdeI / XhoI

Antibiotic Selection: Kanamycin

Insert Sequence: CATatggcacaagaagaaatggaggtggatcttcctaacttattgtatcccatggattcaaacagagaag

tgagcgcatcacatcagccccttggtagtaggcaagttctttttttgcaacccccacttacatattcagatgactcagaggagcttttctt

agggccagaagagccaaatgatgttatcgttttggattctggggaggaggcccctgcacaggttgtggcaccaactaatgctctaca

gatgctccacggcgctctagaacagctacggcaagctgctgagcaacgctcctctgtacgtcgtgcaagggttcaaagaaggagtgc

caggcggcagcaaagaggagggtcacaacgcacagctggaactaactctcgtgcttcattgaatagcttcttccaaataaacagaa

cccaaggcttggctcctacatcagaaagagttgagcgaaatgctctcttgaggacagaagctacaagaacctcaccaggggcagt

tctgatgaaactgtggaactaagtgaggaagaggaggggatagaaagctccacagatgttgatgaagtagagattaatgcaggcg

ctgcaccacctgcagagccagcccctgaggagcttcagattaatgtcgtagaggttcaagcagaggcccctgcagtgtctaacttagt

aactgttcctgaaagtgtcaccctaccccttcaaacacaaacaaaacagaaaacaccagtgaaacagttgtcaccagtgaaaactct

gccacctgaagaagacgaaggggacacatgtgcaattgctttgagccatggacaaatgctggacagcaccgtctttcagccctgcgc

tgtggtcatttatttggcttcacctgcatcgaacgttggctgaaggggggtgctgccaagtgcccacagtgcaataagaaggcaaaac

gcgctgatattgttgtgctatatgcaagatcactgaaagccctggacacaagtgagcaggaaagaatgaaaagctccctggaaaag

gagcagagtatgcgcaggaaggcataaCTCGAG

A.1.6 TRAIP Insert Sequence

Insert length: 1454 bp

Sequencing primers used to confirm insertion: T7 Promoter / T7 Terminator

Restriction Sites Used: NcoI / EcoRI

Antibiotic Selection: Kanamycin

Insert Sequence: CCatgggcCAtCACCAtCACCAtCACGAACAAAAACTCATCTCAGAAGAGGATCTGcc

catacgcgcctactgtacgatttgctcggacttcttcgacaatacgcgggatgtggccgcgattacctgtgggcacacgttccatcagg

agtgtttgttacagtggtttcactcggctccacatcgtacctgcccacagtgtcgaatccaggttagctccaggcaaatcatcaacaag

ctcttctttgatattggcggagaggaggagaccgtacttgatgcagagtccttgaagaatgaagttgacagaataaaagccagtctcc

tcgtgaaagagaaggagaaaagagaatgccagggtcttgtggactctttacgagagatgctagatgtcagaaatgtcactatacaat

cccaacagaaggagttgggtgatatggaaatgctgtgttcaacactgaagaaacaaataaagttcttggataaacagcagtcagag

accaaagctgccaaggatgaagctcgaaaactgagaaacaagctgaaaactatggaaagcattgaagtcttgttgcagtctcagcg

atcagaagtggaggagatgatcagagatatgggatcaggacaggctgctgtagaacaacttgcaatatactgtgtatcattaaaaa

aagaatatgagaatttaaaagaagtccgaaaatcttctgcagagatgaccgagaagctaagaaaggaattattttcttctaaccaca

aggcacaaaaggctgagctggagttaactaaagtacgggaagagctcagtgccagtcagaaggagcttcacagtgcagataagga

aatcatgagtttaaagaaaaaggttgagtttttgcagaagacccttaccacaccaacggcatctaatgaagcaattagtcgtttgatc

tttgagagtcctgcacccatcggtttggaaagaccgaagctccgaccaccaatgatggggaatgatatcaaccttgatgtcaccttcg

acattgatacacctgaacacaacacacaaaaatctgttgttgctccattcaagaagatgaaatttgataataaagagcatcctttatc

cagcccaacgaaaaaccctctgcaggagagcaaaggtttaatgagttgggcaggaggcaggacaggagctgatgaagatgatgac

cttaccttgccatctttcattaagaactcgctgcttcacaagaaacctgtagggagtctacttggccttcggcaaaacacaggagctgt
acggactggatttgatggattgggtggaagaacaaaattcatccagcctagtaacctaacagaaatccgacctttgcatcaaaagat
gaaaaggaaaaaagtttccaggcccacagcttgtacttcctcacttgccaaccagcccaggctcgaagacttcttgaaataaGAAT
TC

A.1.7 TRIP12 Insert Sequence

Insert length: 1227 bp

Sequencing primers used to confirm insertion: T7 Promoter / T7 Terminator

Restriction Sites Used: NdeI / XhoI

Antibiotic Selection: Kanamycin

Insert Sequence: CATATGAAAAAACGTACGGTAAACCGTGAAGACCTGCTGAAACAGGCAGAATCC
GTAATGCAGGACCTGGGCTCCTCCCGTGCAATGCTGGAAATCCAGTACGAAAACGAAGTAGGCACG
GGCCTGGGCCCGACGCTGGAATTCTACGCACTGGTATCCCAGGAACTGCAGCGTGCAGACCTGGGCC
TGTGGCGTGGCGAAGAAGTAACGCTGCCGAACCCGAAAGGCTCCCAGGAAGGCACGAAATACATCC
ACAACCTGCAGGGCCTGTTCGCACTGCCGTTCGGCCGTACGGCAAAACCGGCACACATCGCAAAAGT
AAAAATGAAATTCCGTTTCCTGGGCAAACTGATGGCAAAAGCAATCATGGACTTCCGTCTGGTAGAC
ATCCCGCTGGGCCTGCCGTTCTACAAATGGATGCTGCGTCAGGAATCCTCCCTGGCAACGCACGACCT
GGTAAACATCGACCCGGTAGTAGCAAAATCCGTATACCACCTGGAAGACATCGTACGTCAGAAAAAA
CGTCTGGAACAGGACAAAGCACAGACGAAAGAATCCCTGCAGTTCGCACTGGAATCCCTGAACATGA
ACGGCTGCTCCGTAGAAGACCTGGGCCTGGACTTCACGCTGCCGGGCTTCCCGAACATCGAACTGAA
AAAAGGCGGCAAAGACGTACCGGTAACGATCCACAACCTGGAAGACTACGTACGTCTGGTAATCTAC
TGGGCACTGAACGAAGGCGTATCCCGTCAGCTGGACTCCTTCCGTGACGGCTTCGAATCCGTATTCCC
GCTGAACCACCTGCAGTACTTCTACCCGGAAGAACTGGACCAGCTGCTGTGCGGCTCCCGTGCAGAC

CCGTGGGACGTAAAAACGCTGATGGAATGCTGCCGTCCGGACCACGGCTACACGCACGACTCCCGTG

CAGTAAAATCCCTGTTCGAAATCCTGTCCTCCTTCGACAAAGAACAGCAGCGTCTGTTCCTGCAGTTC

GTAACGGGCTCCCCGCGTCTGCCGGTAGGCGGCTTCCGTTCCCTGAACCCGCCGCTGACGATCGTAC

GTAAAACGTTCGAAGCAACGGAAAACCCGGACGACTTCCTGCCGTCCGTAATGACGTGCGTAAACTA

CCTGAAACTGCCGGACTACTCCTCCATCGACATCATGCGTGAAAAACTGCTGATGGCAGCACGTGAA

GGCCAGCAGTCCTTCCACCTGTCCTGACTCGAG

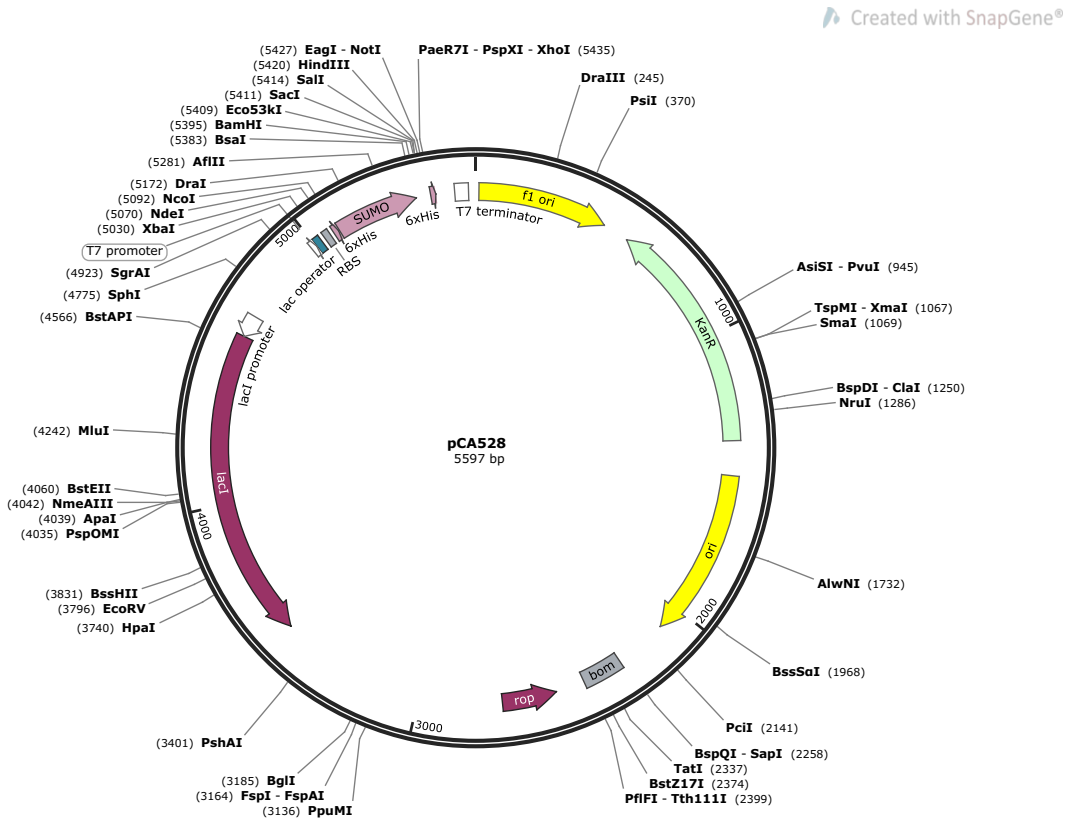


Figure A.2: **pCA528 Plasmid Map**. Shown is the pCA528 plasmid backbone used to clone the TRAIP sequence from the pET28 into a SUMO-expressing vector; facilitating TRAIP expression from a T7 promoter and the inclusion of both 6X His-tag and SUMO tags. Plasmid backbone sequence was acquired from the LabGenius public resource database (available at beta.labgenius.us). Figure generated using SnapGene (Insightful Science; available at snapgene.com).

A.2 Plasmid constructs and sequences used in mammalian cell lines

Detailed below are the plasmid maps and full homology arm sequences used to generate conditional Auxin-Inducible degron cell lines. Generation of plasmids for creating degron cells in this project was carried out as part of a JSPS summer fellowship, with the assistance of Prof. M. Kanemaki (National Institute of Genetics, Japan) as detailed in Natsume et al. (2016). Briefly, CRISPR plasmids were generated using the pX330-U6-Chimeric_BB-CBh-hSpCas9 plasmid backbone (addgene: 42230). CRISPR-targetting sites were identified close to either the first Methionine, or stop codon, dependent on the terminus being tagged (IDT CRISPR-site tool; available at idtdna.com). Complimentary synthesised gRNA for these purposes was provided by the Kanemaki lab and cloned into the pX330 plasmids using BbsiI restriction enzyme sites. For DONOR plasmid creation, targetting homology arms were selected approximately 500 bp upstream and downstream of the targetting CRISPR site. The selected region of interest was amplified from HCT116 genomic DNA by PCR and cloned into pBluescript backbones using standard cloning techniques (carried out by the Kanemaki lab). Inverse PCR was then used to insert restriction enzyme sites required for tagging cassette placement. Finally, the homology targetting arms were cloned into the appropriate DONOR plasmid backbone (Natsume et al., 2016). This appendix section includes all DONOR and CRISPR plasmids used.

A.2.1 LRR1

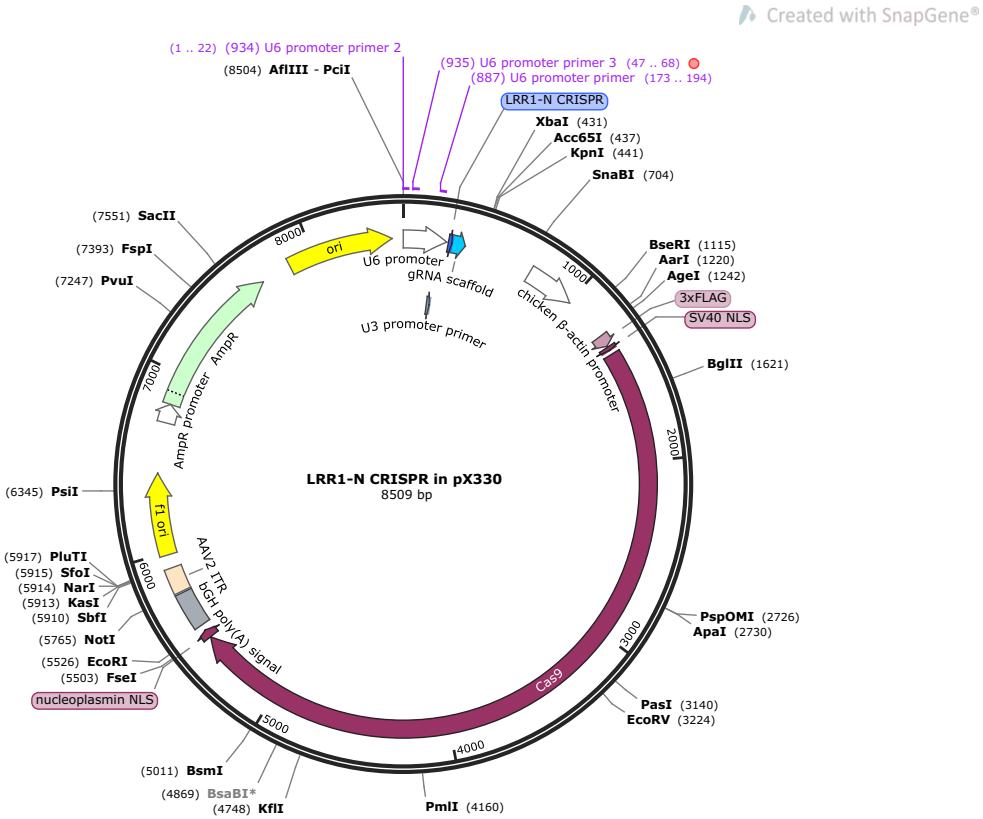


Figure A.3: **CRISPR plasmid used to generate LRR1 degron cells**. Shown is the generated plasmid using pX330 plasmid backbones. The targetting gRNA sequence inserted was as follows: 5' TGTAGCTTCATCTCGCCCAA 3'. Figure generated using SnapGene (Insightful Science; available at snapgene.com).

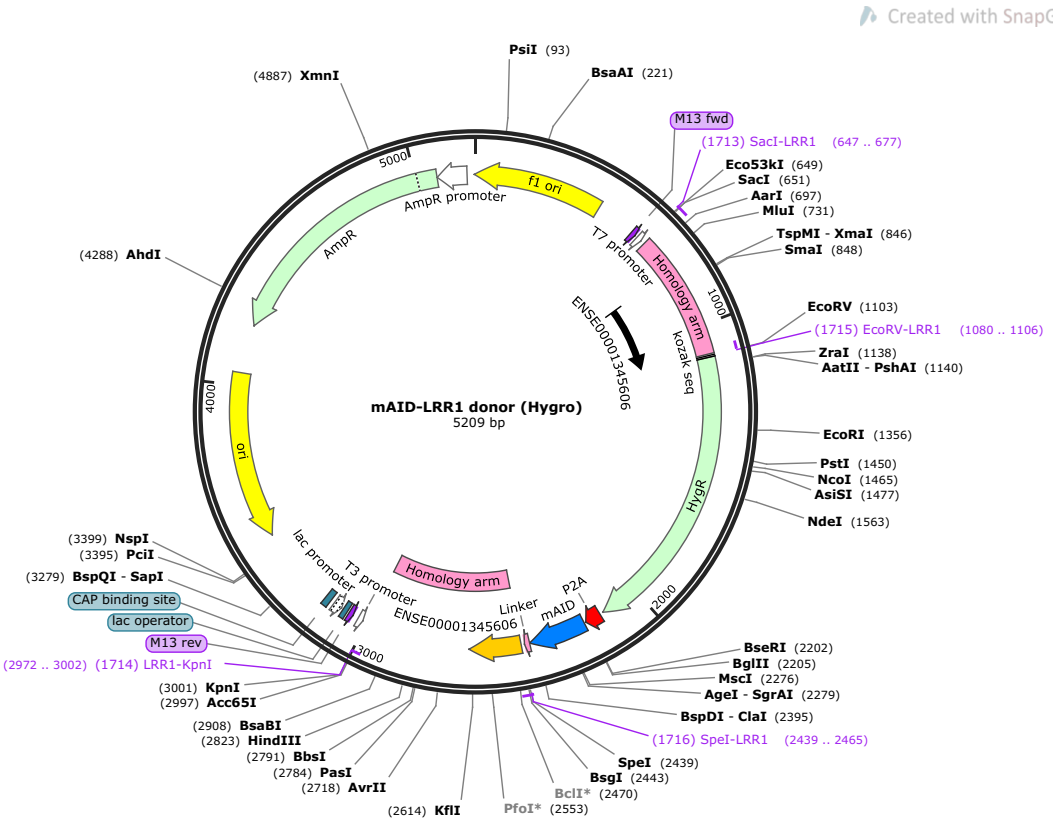


Figure A.4: **DONOR plasmid used to generate mAID-LRR1 cell lines**. Shown is the generated DONOR plasmid. The homology arm sequences used are as follows: targetting upstream homology arm: GRCh38:14:49,598,567-49,599,117:1 in refseq CM000676. Downstream homology arm: GRCh38:14:49,599,021-49,599,563:1 in refseq CM000676. Figure generated using SnapGene (Insightful Science; available at snapgene.com).

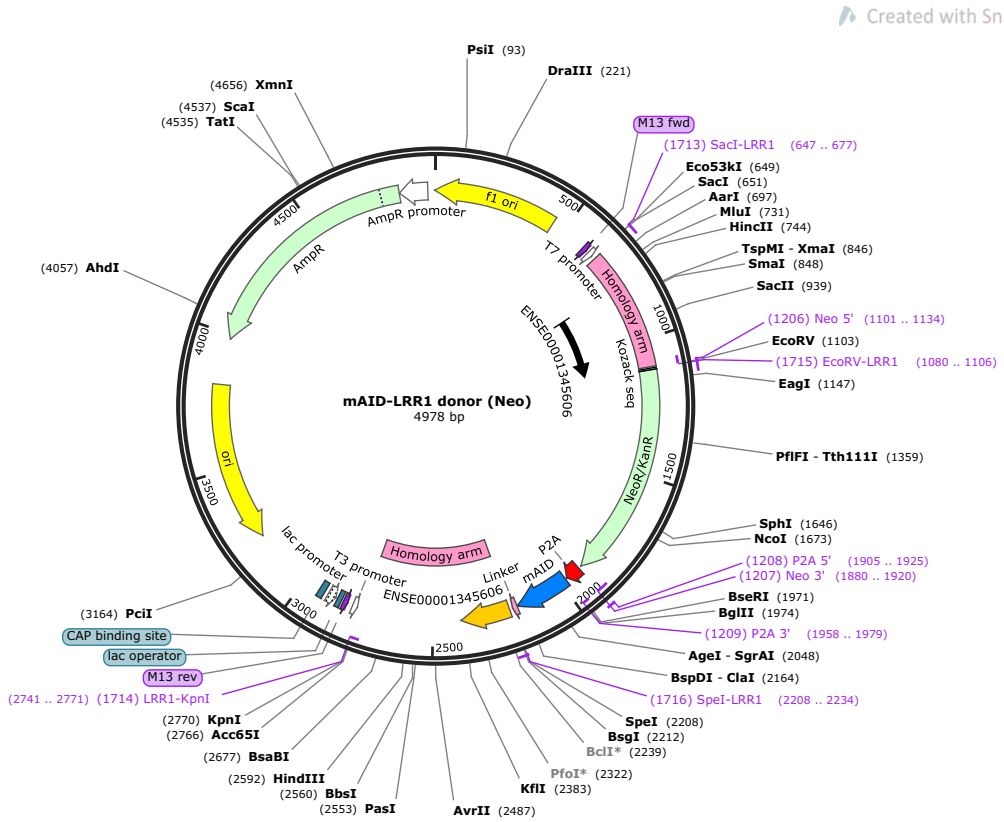


Figure A.5: **DONOR plasmid used to generate mAID-LRR1 cell lines II**. Shown is the generated DONOR plasmid for use in hTERT-RPE1 cell lines. The resistance cassette was exchanged using standard molecular cloning techniques; from Hygromycin to Neomycin. The homology arm sequences used are as follows: targetting upstream homology arm: GRCh38:14:49,598,567-49,599,117:1 in refseq CM000676. Downstream homology arm: GRCh38:14:49,599,021-49,599,563:1 in refseq CM000676. Figure generated using SnapGene (Insightful Science; available at snapgene.com).

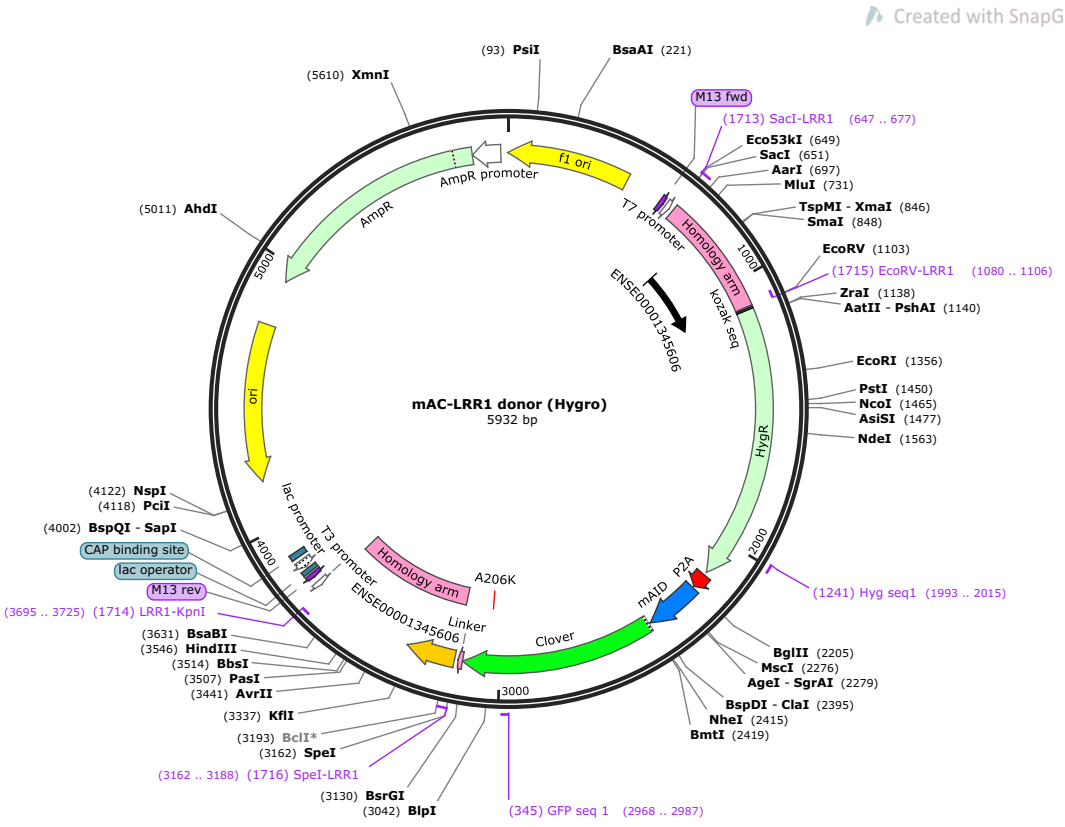


Figure A.6: **DONOR plasmid used to generate mAC-LRR1 cell lines**. Shown is the generated DONOR plasmid. The homology arm sequences used are as follows: targetting upstream homology arm: GRCh38:14:49,598,567-49,599,117:1 in refseq CM000676. Downstream homology arm: GRCh38:14:49,599,021-49,599,563:1 in refseq CM000676. Figure generated using SnapGene (Insightful Science; available at snapgene.com).

A.2.2 TRAIP

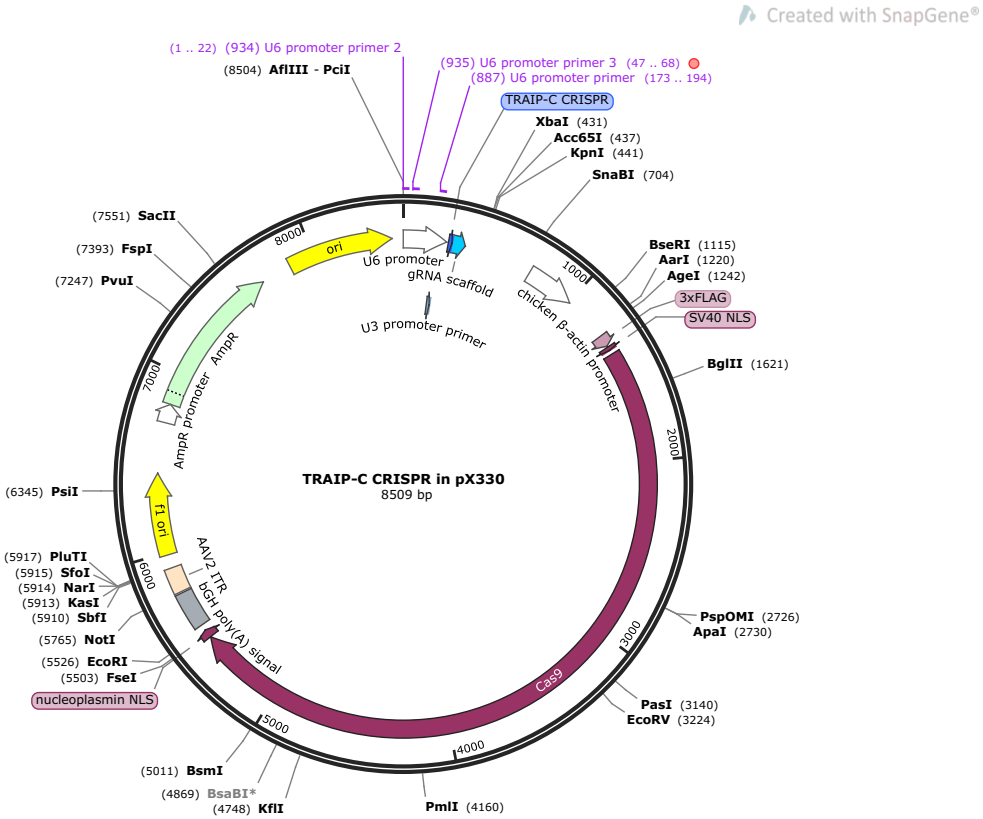


Figure A.7: **CRISPR plasmid used to generate TRAIP degron cells**. Shown is the generated plasmid using pX330 plasmid backbones. The targetting gRNA sequence inserted was as follows: 5'-CTCACTGTTCTCACGACCAC-3'. Figure generated using SnapGene (Insightful Science; available at snapgene.com).

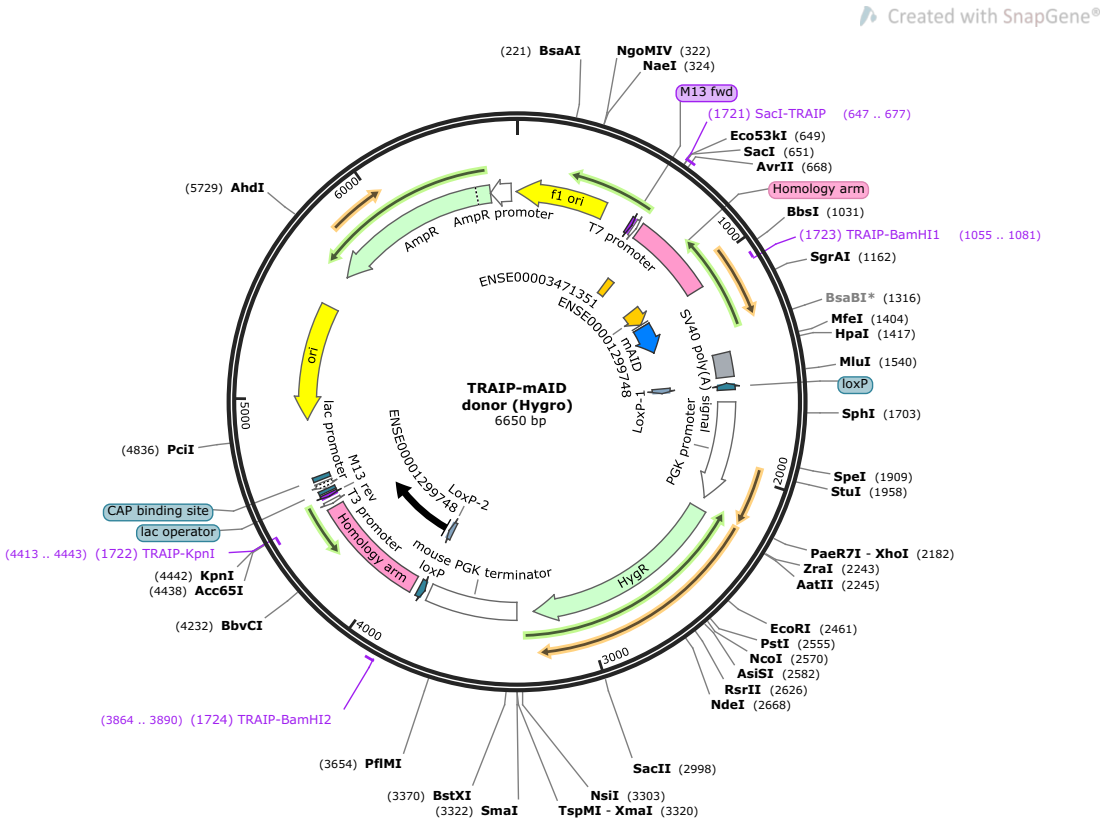


Figure A.8: **DONOR plasmid used to generate TRAIP-mAID cell lines**. Shown is the generated DONOR plasmid. The homology arm sequences used are as follows: upstream homology arm: GRCh38:3:49,828,700-49,828,123:2 in refseq CM000665. Downstream homology arm GRCh38:3:49,828,133-49,828,697:2 in refseq CM000665. Figure generated using SnapGene (Insightful Science; available at snapgene.com).

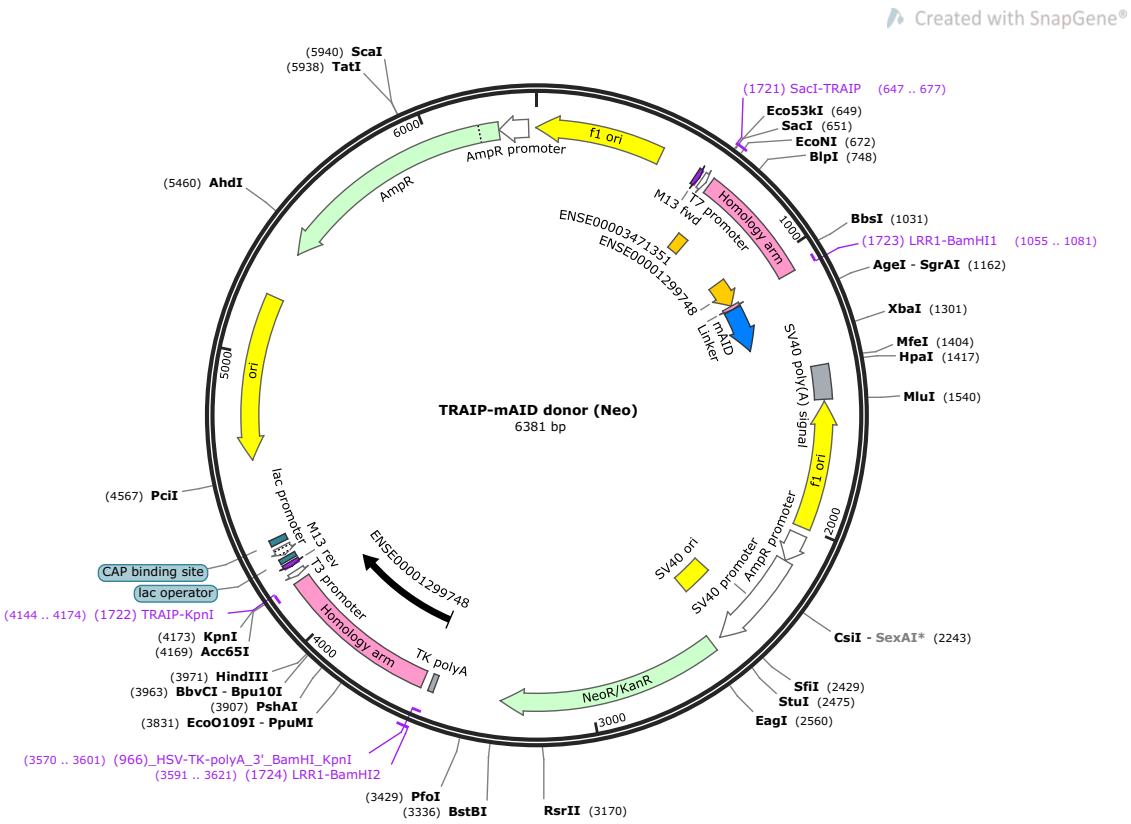


Figure A.9: **DONOR plasmid used to generate TRAIP-mAID cell lines II**. Shown is the generated DONOR plasmid for use in hTERT-RPE1 cell lines. The resistance cassette was exchanged using standard molecular cloning techniques; from Hygromycin to Neomycin. The homology arm sequences used are as follows: upstream homology arm: GRCh38:3:49,828,700-49,828,123:2 in refseq CM000665. Downstream homology arm GRCh38:3:49,828,133-49,828,697:2 in refseq CM000665. Figure generated using SnapGene (Insightful Science; available at snapgene.com).

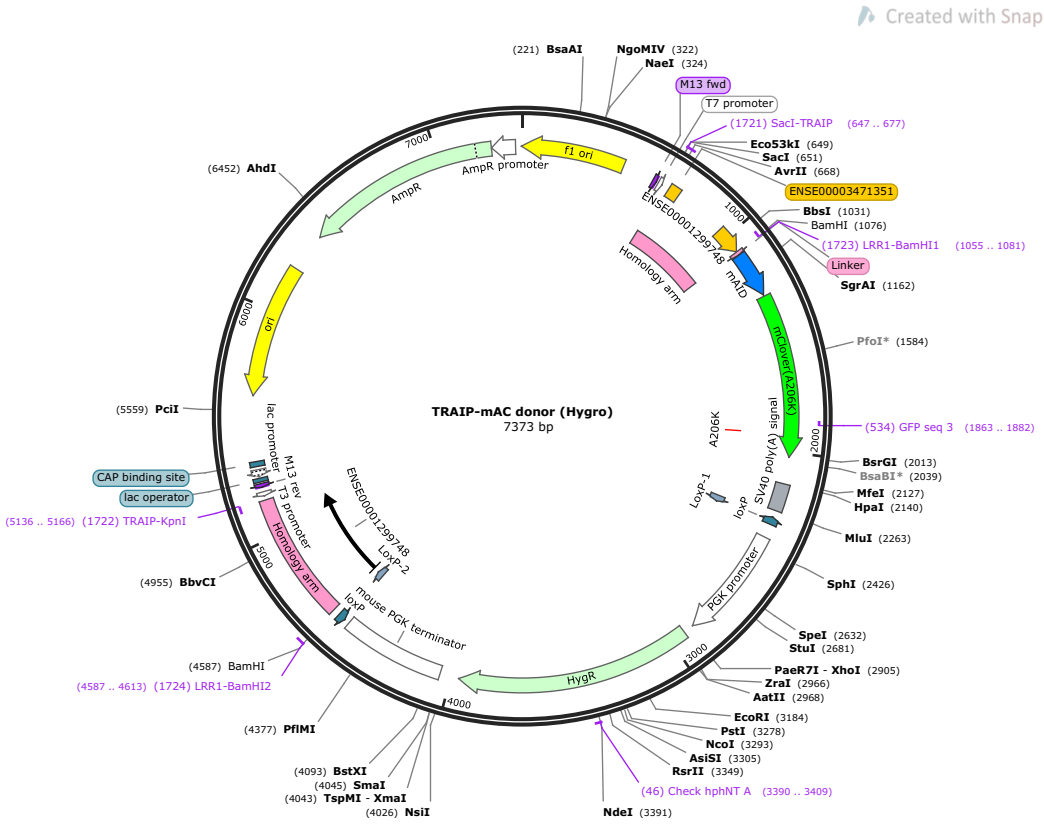


Figure A.10: **DONOR plasmid used to generate TRAIP-mAC cell lines**. Shown is the generated DONOR plasmid. The homology arm sequences used are as follows: upstream homology arm: GRCh38:3:49,828,700-49,828,123:2 in refseq CM000665. Downstream homology arm GRCh38:3:49,828,133-49,828,697:2 in refseq CM000665. Figure generated using SnapGene (Insightful Science; available at snapgene.com).

Bibliography

Akutsu, M., Dikic, I., and Bremm, A. (2016). Ubiquitin chain diversity at a glance. *J Cell Sci*, 129(5):875–880.

Alabert, C., Bukowski-Wills, J. C., Lee, S. B., Kustatscher, G., Nakamura, K., de Lima Alves, F., Menard, P., Mejlvang, J., Rappsilber, J., and Groth, A. (2014). Nascent chromatin capture proteomics determines chromatin dynamics during DNA replication and identifies unknown fork components. *Nat Cell Biol*, 16(3):281–293.

Almeida, S., Ryser, S., Obarzanek-Fojt, M., Hohl, D., and Huber, M. (2011). The TRAF-Interacting Protein (TRIP) Is a Regulator of Keratinocyte Proliferation. *Journal of Investigative Dermatology*, 131(2):349–357.

Alver, R. C., Chadha, G. S., and Blow, J. J. (2014). The contribution of dormant origins to genome stability: from cell biology to human genetics. *DNA repair*, 19(100):182–189.

Amunugama, R., Willcox, S., Wu, R. A., Abdullah, U. B., El-Sagheer, A. H., Brown, T., McHugh, P. J., Griffith, J. D., and Walter, J. C. (2018). Replication Fork Reversal during DNA Interstrand Crosslink Repair Requires CMG Unloading. *Cell reports*, 23(12):3419–3428.

Andrysik, Z., Bender, H., Galbraith, M. D., and Espinosa, J. M. (2021). Multi-omics analysis

reveals contextual tumor suppressive and oncogenic gene modules within the acute hypoxic response. *Nature Communications 2021 12:1*, 12(1):1–18.

Anindya, R., Aygün, O., and Svejstrup, J. Q. (2007). Damage-Induced Ubiquitylation of Human RNA Polymerase II by the Ubiquitin Ligase Nedd4, but Not Cockayne Syndrome Proteins or BRCA1. *Molecular Cell*, 28(3):386–397.

Aparicio, T., Megías, D., and Méndez, J. (2012). Visualization of the MCM DNA helicase at replication factories before the onset of DNA synthesis. *Chromosoma*, 121(5):499–507.

Aparicio, T. S., Guillou, E., Coloma, J., Montoya, G., and Mé Ndez, J. (2009). The human GINS complex associates with Cdc45 and MCM and is essential for DNA replication. *Nucleic Acids Research*, 37(7):2087–2095.

Aranda, S., Rutishauser, D., and Ernfors, P. (2014). Identification of a large protein network involved in epigenetic transmission in replicating DNA of embryonic stem cells. *Nucleic acids research*, 42(11):6972–6986.

Arias, E. E. and Walter, J. C. (2006). PCNA functions as a molecular platform to trigger Cdt1 destruction and prevent re-replication. *Nature Cell Biology*, 8(1):84–90.

Ashwell, S. (2012). Checkpoint Kinase and Wee1 Inhibitors as Anticancer Therapeutics. *DNA Repair in Cancer Therapy*, pages 211–234.

Atanassov, B. S. and Dent, S. Y. (2011). USP22 regulates cell proliferation by deubiquitinating the transcriptional regulator FBP1. *EMBO Rep*, 12(9):924–930.

Auton, M., Rösgen, J., Sinev, M., Holthauzen, L. M. F., and Bolen, D. W. (2011). Osmolyte

effects on protein stability and solubility: a balancing act between backbone and side-chains. *Biophysical chemistry*, 159(1):90–99.

Banaszynski, L. A., chun Chen, L., Maynard-Smith, L. A., Ooi, A. G., and Wandless, T. J. (2006). A Rapid, Reversible, and Tunable Method to Regulate Protein Function in Living Cells Using Synthetic Small Molecules. *Cell*, 126(5):995–1004.

Barnieh, F. M., Loadman, P. M., and Falconer, R. A. (2021). Progress towards a clinically-successful ATR inhibitor for cancer therapy. *Current Research in Pharmacology and Drug Discovery*, 2:100017.

Bartek, J. and Lukas, J. (2001). Mammalian G1- and S-phase checkpoints in response to DNA damage. *Current opinion in cell biology*, 13(6):738–747.

Bartkova, J., Rezaei, N., Liontos, M., Karakaidos, P., Kletsas, D., Issaeva, N., Vassiliou, L. V. F., Kolettas, E., Niforou, K., Zoumpourlis, V. C., Takaoka, M., Nakagawa, H., Tort, F., Fugger, K., Johansson, F., Sehested, M., Andersen, C. L., Dyrskjot, L., Ørntoft, T., Lukas, J., Kittas, C., Helleday, T., Halazonetis, T. D., Bartek, J., and Gorgoulis, V. G. (2006). Oncogene-induced senescence is part of the tumorigenesis barrier imposed by DNA damage checkpoints. *Nature 2006 444:7119*, 444(7119):633–637.

Baus, F., Gire, V., Fisher, D., Piette, J., and Dulić, V. (2003). Permanent cell cycle exit in G2 phase after DNA damage in normal human fibroblasts. *The EMBO journal*, 22(15):3992–4002.

Bell, S. P. and Labib, K. (2016). Chromosome duplication in Saccharomyces cerevisiae. *Genetics*, 203(3):1027–1067.

Belov, A. M., Kozole, J., Bean, M. F., MacHutta, C. A., Zhang, G., Gao, E. N., Ghislain, L., Datwani,

S. S., Leveridge, M., and Annan, R. S. (2020). Acoustic Mist Ionization-Mass Spectrometry: A Comparison to Conventional High-Throughput Screening and Compound Profiling Platforms. *Analytical chemistry*, 92(20):13847–13854.

Bermejo, R., Lai, M. S., and Foiani, M. (2012). Preventing Replication Stress to Maintain Genome Stability: Resolving Conflicts between Replication and Transcription. *Molecular Cell*, 45(6):710–718.

Berti, M. and Vindigni, A. (2016). Replication stress: getting back on track. *Nature structural & molecular biology*, 23(2):103–109.

Bertoli, C., Skotheim, J. M., and De Bruin, R. A. (2013). Control of cell cycle transcription during G1 and S phases. *Nature reviews. Molecular cell biology*, 14(8):518–528.

Bertolin, A. P., Hoffmann, J. S., and Gottifredi, V. (2020). Under-Replicated DNA: The Byproduct of Large Genomes? *Cancers*, 12(10):1–20.

Besse, A., Campos, A. D., Webster, W. K., and Darnay, B. G. (2007). TRAF-interacting protein (TRIP) is a RING-dependent ubiquitin ligase. *Biochem Biophys Res Commun*, 359(3):660–664.

Bicknell, L. S., Bongers, E. M., Leitch, A., Brown, S., Schoots, J., Harley, M. E., Aftimos, S., Al-Aama, J. Y., Bober, M., Brown, P. A., Van Bokhoven, H., Dean, J., Edrees, A. Y., Feingold, M., Fryer, A., Hoefsloot, L. H., Kau, N., Knoers, N. V., MacKenzie, J., Opitz, J. M., Sarda, P., Ross, A., Temple, I. K., Toutain, A., Wise, C. A., Wright, M., and Jackson, A. P. (2011a). Mutations in the pre-replication complex cause Meier-Gorlin syndrome. *Nature Genetics 2011 43:4*, 43(4):356–359.

Bicknell, L. S., Walker, S., Klingseisen, A., Stiff, T., Leitch, A., Kerzendorfer, C., Martin, C. A.,

Yeyati, P., Al Sanna, N., Bober, M., Johnson, D., Wise, C., Jackson, A. P., O'Driscoll, M., and Jeggo, P. A. (2011b). Mutations in ORC1, encoding the largest subunit of the origin recognition complex, cause microcephalic primordial dwarfism resembling Meier-Gorlin syndrome. *Nature Genetics 2011 43:4*, 43(4):350–355.

Blakemore, D., Vilaplana-Lopera, N., Almaghrabi, R., Gonzalez, E., Moya, M., Ward, C., Murphy, G., Gambus, A., Petermann, E., Stewart, G. S., and García, P. (2021). MYBL2 and ATM suppress replication stress in pluripotent stem cells. *EMBO Reports*, 22(5):e51120.

Boehm, E. M., Gildenberg, M. S., and Washington, M. T. (2016). The Many Roles of PCNA in Eukaryotic DNA Replication. In *Enzymes*, volume 39, pages 231–254. Academic Press.

Bowers, J. L., Randell, J. C., Chen, S., and Bell, S. P. (2004). ATP hydrolysis by ORC catalyzes reiterative Mcm2-7 assembly at a defined origin of replication. *Molecular Cell*, 16(6):967–978.

Bowry, A., Kelly, R. D., and Petermann, E. (2021). Hypertranscription and replication stress in cancer. *Trends in Cancer*, 7(9):863–877.

Bregman, D. B., Halaban, R., Van Gool, A. J., Henning, K. A., Friedberg, E. C., and Warren, S. L. (1996). UV-induced ubiquitination of RNA polymerase II: a novel modification deficient in Cockayne syndrome cells. *Proceedings of the National Academy of Sciences of the United States of America*, 93(21):11586–11590.

Brownell, J. E., Sintchak, M. D., Gavin, J. M., Liao, H., Bruzzese, F. J., Bump, N. J., Soucy, T. A., Milhollen, M. A., Yang, X., Burkhardt, A. L., Ma, J., Loke, H. K., Lingaraj, T., Wu, D., Hamman, K. B., Spelman, J. J., Cullis, C. A., Langston, S. P., Vyskocil, S., Sells, T. B., Mallender, W. D., Visiers, I., Li, P., Claiborne, C. F., Rolfe, M., Bolen, J. B., and Dick, L. R. (2010). Substrate-assisted

inhibition of ubiquitin-like protein-activating enzymes: the NEDD8 E1 inhibitor MLN4924 forms a NEDD8-AMP mimetic in situ. *Molecular cell*, 37(1):102–111.

Brüning, J. G. and Marians, K. J. (2020). Replisome bypass of transcription complexes and R-loops. *Nucleic Acids Research*, 48(18):10353–10367.

Buckley, D. L., Raina, K., Darricarrere, N., Hines, J., Gustafson, J. L., Smith, I. E., Miah, A. H., Harling, J. D., and Crews, C. M. (2015). HaloPROTACS: Use of Small Molecule PROTACs to Induce Degradation of HaloTag Fusion Proteins. *ACS chemical biology*, 10(8):1831.

Bunz, F., Dutriaux, A., Lengauer, C., Waldman, T., Zhou, S., Brown, J. P., Sedivy, J. M., Kinzler, K. W., and Vogelstein, B. (1998). Requirement for p53 and p21 to sustain G2 arrest after DNA damage. *Science (New York, N.Y.)*, 282(5393):1497–1501.

Burgers, P. M. (2009). Polymerase dynamics at the eukaryotic DNA replication fork. *Journal of Biological Chemistry*, 284(7):4041–4045.

Burrows, A. C., Prokop, J., and Summers, M. K. (2012). Skp1-Cul1-F-box ubiquitin ligase (SCF(betaTrCP))-mediated destruction of the ubiquitin-specific protease USP37 during G2-phase promotes mitotic entry. *J Biol Chem*, 287(46):39021–39029.

Byun, T. S., Pacek, M., Yee, M. C., Walter, J. C., and Cimprich, K. A. (2005). Functional uncoupling of MCM helicase and DNA polymerase activities activates the ATR-dependent checkpoint. *Genes & Development*, 19(9):1040–1052.

Carpenter, A. E., Jones, T. R., Lamprecht, M. R., Clarke, C., Kang, I. H., Friman, O., Guertin, D. A., Chang, J. H., Lindquist, R. A., Moffat, J., Golland, P., and Sabatini, D. M. (2006). CellProfiler:

Image analysis software for identifying and quantifying cell phenotypes. *Genome Biology*, 7(10):1–11.

Carthew, R. W. and Sontheimer, E. J. (2009). Origins and Mechanisms of miRNAs and siRNAs. *Cell*, 136(4):642–655.

Cayrou, C., Ballester, B., Peiffer, I., Fenouil, R., Coulombe, P., Andrau, J. C., Van Helden, J., and Méchali, M. (2015). The chromatin environment shapes DNA replication origin organization and defines origin classes. *Genome Research*, 25(12):1873–1885.

Cerami, E., Gao, J., Dogrusoz, U., Gross, B. E., Sumer, S. O., Aksoy, B. A., Jacobsen, A., Byrne, C. J., Heuer, M. L., Larsson, E., Antipin, Y., Reva, B., Goldberg, A. P., Sander, C., and Schultz, N. (2012). The cBio Cancer Genomics Portal: An Open Platform for Exploring Multidimensional Cancer Genomics DataThe cBio Cancer Genomics Portal: An Open Platform for Exploring Multidimensional Cancer Genomics Data. *Cancer Discovery*, 2(5):401–404.

Champoux, J. J. (2001). DNA topoisomerases: structure, function, and mechanism. *Annu. Rev. Biochem.*, 70(1):369–413.

Chandra, T., Kirschner, K., Thuret, J. Y., Pope, B. D., Ryba, T., Newman, S., Ahmed, K., Samarajiwa, S. A., Salama, R., Carroll, T., Stark, R., Janky, R. S., Narita, M., Xue, L., Chicas, A., Nũnez, S., Janknecht, R., Hayashi-Takanaka, Y., Wilson, M. D., Marshall, A., Odom, D. T., Babu, M. M., Bazett-Jones, D. P., Tavaré, S., Edwards, P. A., Lowe, S. W., Kimura, H., Gilbert, D. M., and Narita, M. (2012). Independence of Repressive Histone Marks and Chromatin Compaction during Senescent Heterochromatic Layer Formation. *Molecular Cell*, 47(2):203–214.

Chang, H. H., Pannunzio, N. R., Adachi, N., and Lieber, M. R. (2017). Non-homologous DNA end

joining and alternative pathways to double-strand break repair. *Nature Reviews Molecular Cell Biology 2017 18:8*, 18(8):495–506.

Chapard, C., Hohl, D., and Huber, M. (2015). The TRAF-interacting protein (TRAIP) is a novel E2F target with peak expression in mitosis. *Oncotarget*, 6(25):20933–20945.

Chapard, C., Meraldi, P., Gleich, T., Bachmann, D., Hohl, D., and Huber, M. (2014a). TRAIP is a regulator of the spindle assembly checkpoint. *J Cell Sci*, 127(Pt 24):5149–5156.

Chapard, C., Meraldi, P., Gleich, T., Bachmann, D., Hohl, D., and Huber, M. (2014b). TRAIP is a regulator of the spindle assembly checkpoint. *Journal of Cell Science*, 127(24):5149–5156.

Chédin, F., Hartono, S. R., Sanz, L. A., and Vanoosthuyse, V. (2021). Best practices for the visualization, mapping, and manipulation of R-loops. *The EMBO Journal*, 40(4):e106394.

Chen, L., Chen, J. Y., Zhang, X., Gu, Y., Xiao, R., Shao, C., Tang, P., Qian, H., Luo, D., Li, H., Zhou, Y., Zhang, D. E., and Fu, X. D. (2017). R-ChIP Using Inactive RNase H Reveals Dynamic Coupling of R-loops with Transcriptional Pausing at Gene Promoters. *Molecular cell*, 68(4):745–757.e5.

Chen, Y. H., Keegan, S., Kahli, M., Tonzi, P., Fenyö, D., Huang, T. T., and Smith, D. J. (2019). Transcription shapes DNA replication initiation and termination in human cells. *Nature structural & molecular biology*, 26(1):67.

Chisnall, B., Johnson, C., Kulaberoglu, Y., and Chen, Y. W. (2014). Insoluble protein purification with sarkosyl: facts and precautions. *Methods in molecular biology (Clifton, N.J.)*, 1091:179–186.

Christensen, D. E., Brzovic, P. S., and Klevit, R. E. (2007). E2–BRCA1 RING interactions dictate

synthesis of mono- or specific polyubiquitin chain linkages. *Nature Structural & Molecular Biology 2007 14:10*, 14(10):941–948.

Chung, H. K., Jacobs, C. L., Huo, Y., Yang, J., Krumm, S. A., Plemper, R. K., Tsien, R. Y., and Lin, M. Z. (2015). Tunable and reversible drug control of protein production via a self-excising degron. *Nature Chemical Biology*, 11(9):713–720.

Clague, M. J., Urbé, S., and Komander, D. (2019). Breaking the chains: deubiquitylating enzyme specificity begets function. *Nature Reviews Molecular Cell Biology 2019 20:6*, 20(6):338–352.

Clyne, R. K. and Kelly, T. J. (1995). Genetic analysis of an ARS element from the fission yeast Schizosaccharomyces pombe. *The EMBO Journal*, 14(24):6348–6357.

Cong, L., Ran, F. A., Cox, D., Lin, S., Barretto, R., Habib, N., Hsu, P. D., Wu, X., Jiang, W., Marraffini, L. A., and Zhang, F. (2013). Multiplex genome engineering using CRISPR/Cas systems. *Science*, 339(6121):819–823.

Conlon, I. and Raff, M. (1999). Size control in animal development. *Cell*, 96(2):235–244.

Coster, G., Frigola, J., Beuron, F., Morris, E. P., and Diffley, J. F. (2014). Origin Licensing Requires ATP Binding and Hydrolysis by the MCM Replicative Helicase. *Molecular Cell*, 55(5):666–677.

Cvetic, C. and Walter, J. C. (2005). Eukaryotic origins of DNA replication: Could you please be more specific? *Seminars in Cell and Developmental Biology*, 16(3):343–353.

Das, M., Singh, S., Pradhan, S., and Narayan, G. (2014). MCM Paradox: Abundance of Eukaryotic Replicative Helicases and Genomic Integrity. *Molecular biology international*, 2014:1–11.

Datta, A. and Jinks-Robertson, S. (1995). Association of increased spontaneous mutation rates with high levels of transcription in yeast. *Science (New York, N.Y.)*, 268(5217):1616–1619.

Davis, A. J. and Chen, D. J. (2013). DNA double strand break repair via non-homologous end-joining. *Translational cancer research*, 2(3):130–143.

Deegan, T. D., Baxter, J., Ortiz Bazán, M. Á., Yeeles, J. T., and Labib, K. P. (2019). Pif1-Family Helicases Support Fork Convergence during DNA Replication Termination in Eukaryotes. *Molecular Cell*, 74(2):231–244.e9.

Deegan, T. D., Mukherjee, P. P., Fujisawa, R., Rivera, C. P., and Labib, K. (2020). CMG helicase disassembly is controlled by replication fork DNA, replisome components and a ubiquitin threshold. *eLife*, 9:1–33.

Degorce, F., Card, A., Soh, S., Trinquet, E., Knapik, G. P., and Xie, B. (2009). HTRF: A technology tailored for drug discovery - a review of theoretical aspects and recent applications. *Current chemical genomics*, 3(1):22–32.

Demchenko, A. P. (2013). Beyond annexin V: fluorescence response of cellular membranes to apoptosis. *Cytotechnology*, 65(2):157–172.

Deng, L., Wu, R. A., Sonneville, R., Kochenova, O. V., Labib, K., Pellman, D., and Walter, J. C. (2019). Mitotic CDK Promotes Replisome Disassembly, Fork Breakage, and Complex DNA Rearrangements. *Molecular Cell*, 73(5):915–929.e6.

Dewar, J. M., Budzowska, M., and Walter, J. C. (2015). The mechanism of DNA replication termination in vertebrates. *Nature*, 525(7569):345–350.

Douglas, M. E., Ali, F. A., Costa, A., and Diffley, J. F. (2018). The mechanism of eukaryotic CMG helicase activation. *Nature*, 555(7695):265–268.

Duan, H., Mansour, S., Reed, R., Gillis, M. K., Parent, B., Liu, B., Sztupinszki, Z., Birkbak, N., Szallasi, Z., Elia, A. E., Garber, J. E., and Pathania, S. (2020). E3 ligase RFWD3 is a novel modulator of stalled fork stability in BRCA2-deficient cells. *The Journal of Cell Biology*, 219(6):e201908192.

Dulić, V., Stein, G. H., Far, D. F., and Reed, S. I. (1998). Nuclear accumulation of p21Cip1 at the onset of mitosis: a role at the G2/M-phase transition. *Molecular and cellular biology*, 18(1):546–557.

Dungrawala, H., Rose, K. L., Bhat, K. P., Mohni, K. N., Glick, G. G., Couch, F. B., and Cortez, D. (2015). The Replication Checkpoint Prevents Two Types of Fork Collapse without Regulating Replisome Stability. *Molecular Cell*, 59(6):998–1010.

Duxin, J. P., Dewar, J. M., Yardimci, H., and Walter, J. C. (2014). Repair of a DNA-protein crosslink by replication-coupled proteolysis. *Cell*, 159(2):346–357.

Edwards, M. C., Tutter, A. V., Cvetic, C., Gilbert, C. H., Prokhorova, T. A., and Walter, J. C. (2002). MCM2-7 complexes bind chromatin in a distributed pattern surrounding the origin recognition complex in Xenopus egg extracts. *The Journal of biological chemistry*, 277(36):33049–33057.

Elia, A. E., Wang, D. C., Willis, N. A., Boardman, A. P., Hajdu, I., Adeyemi, R. O., Lowry, E., Gygi, S. P., Scully, R., and Elledge, S. J. (2015). RFWD3-Dependent Ubiquitination of RPA Regulates Repair at Stalled Replication Forks. *Mol Cell*, 60(2):280–293.

Emanuele, M. J., Elia, A. E., Xu, Q., Thoma, C. R., Izhar, L., Leng, Y., Guo, A., Chen, Y. N., Rush, J., Hsu, P. W., Yen, H. C., and Elledge, S. J. (2011). Global identification of modular cullin-RING ligase substrates. *Cell*, 147(2):459–474.

Engeland, K. (2017). Cell cycle arrest through indirect transcriptional repression by p53: I have a DREAM. *Cell Death & Differentiation 2018 25:1*, 25(1):114–132.

Erickson, B., Sheridan, R. M., Cortazar, M., and Bentley, D. L. (2018). Dynamic turnover of paused pol II complexes at human promoters. *Genes and Development*, 32(17-18):1215–1225.

Evrin, C., Clarke, P., Zech, J., Lurz, R., Sun, J., Uhle, S., Li, H., Stillman, B., and Speck, C. (2009). A double-hexameric MCM2-7 complex is loaded onto origin DNA during licensing of eukaryotic DNA replication. *Proceedings of the National Academy of Sciences of the United States of America*, 106(48):20240–20245.

Falck, J., Mailand, N., Syljuåsen, R. G., Bartek, J., and Lukas, J. (2001). The ATM-Chk2-Cdc25A checkpoint pathway guards against radioresistant DNA synthesis. *Nature*, 410(6830):842–847.

Fan, Y., Köberlin, M. S., Ratnayeke, N., Liu, C., Deshpande, M., Gerhardt, J., and Meyer, T. (2021). Lrr1-mediated replisome disassembly promotes dna replication by recycling replisome components. *Journal of Cell Biology*, 220(8):e202009147.

Fanning, E., Klimovich, V., and Nager, A. R. (2006). A dynamic model for replication protein A (RPA) function in DNA processing pathways. *SURVEY AND SUMMARY*, 34(15):4126 – 4137.

Feeney, L., Muñoz, I. M., Lachaud, C., Toth, R., Appleton, P. L., Schindler, D., and Rouse, J. (2017). RPA-Mediated Recruitment of the E3 Ligase RFWD3 Is Vital for Interstrand Crosslink Repair and Human Health. *Molecular Cell*, 66(5):610.

Fenech, M., Kirsch-Volders, M., Natarajan, A. T., Surralles, J., Crott, J. W., Parry, J., Norppa, H., Eastmond, D. A., Tucker, J. D., and Thomas, P. (2011). Molecular mechanisms of

micronucleus, nucleoplasmic bridge and nuclear bud formation in mammalian and human cells. *Mutagenesis*, 26(1):125–132.

Feng, W., Guo, Y., Huang, J., Deng, Y., Zang, J., and Huen, M. S. (2016). TRAIP regulates replication fork recovery and progression via PCNA. *Cell Discov*, 2:16016.

Fenwick, A. L., Kliszczak, M., Cooper, F., Murray, J., Sanchez-Pulido, L., Twigg, S. R., Goriely, A., McGowan, S. J., Miller, K. A., Taylor, I. B., Logan, C., Bozdogan, S., Danda, S., Dixon, J., Elsayed, S. M., Elsobky, E., Gardham, A., Hoffer, M. J., Koopmans, M., McDonald-McGinn, D. M., Santen, G. W., Savarirayan, R., de Silva, D., Vanakker, O., Wall, S. A., Wilson, L. C., Yuregir, O. O., Zackai, E. H., Ponting, C. P., Jackson, A. P., Wilkie, A. O., Niedzwiedz, W., and Bicknell, L. S. (2016). Mutations in CDC45, Encoding an Essential Component of the Pre-initiation Complex, Cause Meier-Gorlin Syndrome and Craniosynostosis. *American journal of human genetics*, 99(1):125–138.

Fernández-Cid, A., Riera, A., Tognetti, S., Herrera, M. C., Samel, S., Evrin, C., Winkler, C., Gardenal, E., Uhle, S., and Speck, C. (2013). An ORC/Cdc6/MCM2-7 Complex Is Formed in a Multistep Reaction to Serve as a Platform for MCM Double-Hexamer Assembly. *Molecular Cell*, 50(4):577–588.

Flatt, P. M., Tang, L. J., Scatena, C. D., Szak, S. T., and Pietenpol, J. A. (2000). p53 Regulation of G2 Checkpoint Is Retinoblastoma Protein Dependent. *Molecular and Cellular Biology*, 20(12):4210.

Forment, J. V. and Jackson, S. P. (2015). A flow-cytometry-based method to simplify the analysis and quantification of protein association to chromatin in mammalian cells. *Nature protocols*, 10(9):1297–1307.

Frankel, S., Sohn, R., and Leinwand, L. (1991). The use of sarkosyl in generating soluble protein after bacterial expression. *Proceedings of the National Academy of Sciences of the United States of America*, 88(4):1192–1196.

Franz, A., Ackermann, L., and Hoppe, T. (2016a). Ring of Change: CDC48/p97 Drives Protein Dynamics at Chromatin. *Frontiers in Genetics*, 7(MAY):10.3389/fgene.2016.00073.

Franz, A., Orth, M., Pirson, P. A., Sonneville, R., Blow, J. J., Gartner, A., Stemmann, O., and Hoppe, T. (2011). CDC-48/p97 coordinates CDT-1 degradation with GINS chromatin dissociation to ensure faithful DNA replication. *Molecular cell*, 44(1):85–96.

Franz, A., Pirson, P. A., Pilger, D., Halder, S., Achuthankutty, D., Kashkar, H., Ramadan, K., and Hoppe, T. (2016b). Chromatin-associated degradation is defined by UBXN-3/FAF1 to safeguard DNA replication fork progression. *Nature communications*, 7.

French, M. E., Koehler, C. F., and Hunter, T. (2021). Emerging functions of branched ubiquitin chains. *Cell Discovery 2021 7:1*, 7(1):1–10.

Fu, X., Yucer, N., Liu, S., Li, M., Yi, P., Mu, J. J., Yang, T., Chu, J., Jung, S. Y., O'Malley, B. W., Gu, W., Qin, J., and Wang, Y. (2010). RFWD3-Mdm2 ubiquitin ligase complex positively regulates p53 stability in response to DNA damage. *Proc Natl Acad Sci U S A*, 107(10):4579–4584.

Fujisawa, R. and Labib, K. P. (2022). Multiple UBX proteins reduce the ubiquitin threshold of the mammalian p97-UFD1-NPL4 unfoldase. *bioRxiv*, page 2022.01.13.476277.

Fungtammasan, A., Walsh, E., Chiaromonte, F., Eckert, K. A., and Makova, K. D. (2012). A genome-wide analysis of common fragile sites: What features determine chromosomal instability in the human genome? *Genome Research*, 22(6):993.

Gaillard, H., García-Muse, T., and Aguilera, A. (2015). Replication stress and cancer. *Nature Reviews Cancer*, 15(5):276–280.

Galderisi, U., Jori, F. P., and Giordano, A. (2003). Cell cycle regulation and neural differentiation. *Oncogene*, 22:5208–5219.

Gallina, I., Hendriks, I. A., Hoffmann, S., Larsen, N. B., Johansen, J., Colding-Christensen, C. S., Schubert, L., Sellés-Baiget, S., Fábián, Z., Kühbacher, U., Gao, A. O., Räschle, M., Rasmussen, S., Nielsen, M. L., Mailand, N., and Duxin, J. P. (2021). The ubiquitin ligase RFWD3 is required for translesion DNA synthesis. *Molecular Cell*, 81(3):442.

Gambus, A., Jones, R. C., Sanchez-Diaz, A., Kanemaki, M., van Deursen, F., Edmondson, R. D., and Labib, K. (2006). GINS maintains association of Cdc45 with MCM in replisome progression complexes at eukaryotic DNA replication forks. *Nat Cell Biol*, 8(4):358–366.

Gambus, A., Khoudoli, G. A., Jones, R. C., and Blow, J. J. (2011). MCM2-7 form double hexamers at licensed origins in Xenopus egg extract. *Journal of Biological Chemistry*, 286(13):11855–11864.

Gan, H., Serra-Cardona, A., Hua, X., Zhou, H., Labib, K., Yu, C., and Zhang, Z. (2018). The Mcm2-Ctf4-Polα Axis Facilitates Parental Histone H3-H4 Transfer to Lagging Strands. *Molecular cell*, 72(1):140–151.e3.

Gao, J., Aksoy, B. A., Dogrusoz, U., Dresdner, G., Gross, B., Sumer, S. O., Sun, Y., Jacobsen, A., Sinha, R., Larsson, E., Cerami, E., Sander, C., and Schultz, N. (2013). Integrative analysis of complex cancer genomics and clinical profiles using the cBioPortal. *Science signaling*, 6(269):10.1126/scisignal.2004088.

Garribba, L. and Santaguida, S. (2022). The Dynamic Instability of the Aneuploid Genome. *Frontiers in Cell and Developmental Biology*, 10:327.

Gatti, M., Imhof, R., Huang, Q., Baudis, M., and Altmeyer, M. (2020). The Ubiquitin Ligase TRIP12 Limits PARP1 Trapping and Constrains PARP Inhibitor Efficiency. *Cell reports*, 32(5):107985.

Gelot, C., Magdalou, I., and Lopez, B. S. (2015). Replication Stress in Mammalian Cells and Its Consequences for Mitosis. *Genes*, 6(2):267.

George, A., YC, H., AJ, C., Y, Z., and AM, M. (2018). A Comprehensive Atlas of E3 Ubiquitin Ligase Mutations in Neurological Disorders. *Frontiers in genetics*, 9(FEB):10.3389/fgene.2018.00029.

Georgescu, R., Yuan, Z., Bai, L., De Luna Almeida Santos, R., Sun, J., Zhang, D., Yurieva, O., Li, H., and O'Donnell, M. E. (2017). Structure of eukaryotic CMG helicase at a replication fork and implications to replisome architecture and origin initiation. *Proceedings of the National Academy of Sciences of the United States of America*, 114(5):E697–E706.

Germain, C. P. S., Zhao, H., Sinha, V., Sanz, L. A., Chédin, F., and Barlow, J. H. (2021). Genomic patterns of transcription-replication interactions in mouse primary B cells. *bioRxiv*, page 2021.04.13.439211.

Gillespie, P. J., Gambus, A., and Blow, J. J. (2012a). Preparation and use of Xenopus egg extracts to study DNA replication and chromatin associated proteins. *Methods*, 57(2):203–213.

Gillespie, P. J., Gambus, A., and Blow, J. J. (2012b). Preparation and use of Xenopus egg extracts to study DNA replication and chromatin associated proteins. *Methods*, 57(2):203–213.

Gire, V. and Dulic, V. (2015). Senescence from G2 arrest, revisited. *Cell cycle (Georgetown, Tex.)*, 14(3):297–304.

Gleich, T., Quadroni, M., Yigit, G., Wollnik, B., Huber, M., Pich, C., and Hohl, D. (2021). Traip regulates dna double-strand break-induced atm activation. *bioRxiv*, page 10.1101/2021.10.11.462297.

Goldstein, G., Scheid, M., Hammerling, U., Schlesinger, D. H., Niall, H. D., and Boyse, E. A. (1975). Isolation of a polypeptide that has lymphocyte-differentiating properties and is probably represented universally in living cells. *Proceedings of the National Academy of Sciences of the United States of America*, 72(1):11.

Gong, Z. and Chen, J. (2011). E3 Ligase RFWD3 Participates in Replication Checkpoint Control. *The Journal of Biological Chemistry*, 286(25):22308.

Gottipati, P., Cassel, T. N., Savolainen, L., and Helleday, T. (2008). Transcription-associated recombination is dependent on replication in Mammalian cells. *Molecular and cellular biology*, 28(1):154–164.

Grou, C. P., Pinto, M. P., Mendes, A. V., Domingues, P., and Azevedo, J. E. (2015). The de novo synthesis of ubiquitin: identification of deubiquitinases acting on ubiquitin precursors. *Sci Rep*, 5:12836.

Gudjonsson, T., Altmeyer, M., Savic, V., Toledo, L., Dinant, C., Grofte, M., Bartkova, J., Poulsen, M., Oka, Y., Bekker-Jensen, S., Mailand, N., Neumann, B., Heriche, J. K., Shearer, R., Saunders, D., Bartek, J., Lukas, J., and Lukas, C. (2012). TRIP12 and UBR5 suppress spreading of chromatin ubiquitylation at damaged chromosomes. *Cell*, 150(4):697–709.

Guernsey, D. L., Matsuoka, M., Jiang, H., Evans, S., MacGillivray, C., Nightingale, M., Perry, S., Ferguson, M., Leblanc, M., Paquette, J., Patry, L., Rideout, A. L., Thomas, A., Orr, A., McMaster, C. R., Michaud, J. L., Deal, C., Langlois, S., Superneau, D. W., Parkash, S., Ludman, M., Skidmore, D. L., and Samuels, M. E. (2011). Mutations in origin recognition complex gene ORC4 cause Meier-Gorlin syndrome. *Nature Genetics 2011 43:4*, 43(4):360–364.

Guillou, E., Ibarra, A., Coulon, V., Casado-Vela, J., Rico, D., Casal, I., Schwob, E., Losada, A., and Méndez, J. (2010). Cohesin organizes chromatin loops at DNA replication factories. *Genes & Development*, 24(24):2812–2822.

Guo, Z., Zeng, Y., Chen, Y., Liu, M., Chen, S., Yao, M., Zhang, P., Zhong, F., Jiang, K., He, S., and Yuan, G. (2020). TRAIP promotes malignant behaviors and correlates with poor prognosis in liver cancer. *Biomedicine & pharmacotherapy = Biomedecine & pharmacotherapie*, 124:109857.

Guturi, K. K. N., Bohgaki, M., Bohgaki, T., Srikumar, T., Ng, D., Kumareswaran, R., El Ghamrasni, S., Jeon, J., Patel, P., Eldin, M. S., Bristow, R., Cheung, P., Stewart, G. S., Raught, B., Hakem, A., and Hakem, R. (2016). RNF168 and USP10 regulate topoisomerase IIalpha function via opposing effects on its ubiquitylation. *Nat Commun*, 7:12638.

Hann, Z. S., Ji, C., Olsen, S. K., Lu, X., Lux, M. C., Tan, D. S., and Lima, C. D. (2019). Structural basis for adenylation and thioester bond formation in the ubiquitin E1. *Proceedings of the National Academy of Sciences*, 116(31):15475–15484.

Harley, M. E., Murina, O., Leitch, A., Higgs, M. R., Bicknell, L. S., Yigit, G., Blackford, A. N., Zlatanou, A., Mackenzie, K. J., Reddy, K., Halachev, M., McGlasson, S., Reijns, M. A. M., Fluteau, A., Martin, C. A., Sabbioneda, S., Elcioglu, N. H., Altmuller, J., Thiele, H., Greenhalgh,

L., Chessa, L., Maghnie, M., Salim, M., Bober, M. B., Nurnberg, P., Jackson, S. P., Hurles, M. E., Wollnik, B., Stewart, G. S., and Jackson, A. P. (2016). TRAIP promotes DNA damage response during genome replication and is mutated in primordial dwarfism. *Nat Genet*, 48(1):36–43.

Hart, T., Chandrashekhar, M., Aregger, M., Steinhart, Z., Brown, K. R., MacLeod, G., Mis, M., Zimmermann, M., Fradet-Turcotte, A., Sun, S., Mero, P., Dirks, P., Sidhu, S., Roth, F. P., Rissland, O. S., Durocher, D., Angers, S., and Moffat, J. (2015). High-Resolution CRISPR Screens Reveal Fitness Genes and Genotype-Specific Cancer Liabilities. *Cell*, 163(6):1515–1526.

He, J., Zhu, Q., Wani, G., and Wani, A. A. (2017). UV-induced proteolysis of RNA polymerase II is mediated by VCP/p97 segregase and timely orchestration by Cockayne syndrome B protein. *Oncotarget*, 8(7):11004.

Hedglin, M., Kumar, R., and Benkovic, S. J. (2013). Replication clamps and clamp loaders. *Cold Spring Harbor Perspectives in Biology*, 5(4):1–19.

Heller, R. C., Kang, S., Lam, W. M., Chen, S., Chan, C. S., and Bell, S. P. (2011). Eukaryotic origin-dependent DNA replication in vitro reveals sequential action of DDK and S-CDK kinases. *Cell*, 146(1):80–91.

Henrikus, S. S. and Costa, A. (2021). Towards a Structural Mechanism for Sister Chromatid Cohesion Establishment at the Eukaryotic Replication Fork. *Biology*, 10(6):466.

Herman, R. K. and Dworkin, N. B. (1971). Effect of gene induction on the rate of mutagenesis by ICR-191 in Escherichia coli. *Journal of bacteriology*, 106(2):543–550.

Hernández-Pérez, S., Cabrera, E., Amoedo, H., Rodríguez-Acebes, S., Koundrioukoff, S.,

Debatisse, M., Méndez, J., and Freire, R. (2016). USP37 deubiquitinates Cdt1 and contributes to regulate DNA replication. *Molecular oncology*, 10(8):1196–1206.

Hershko, A. and Ciechanover, A. (1998). The ubiquitin system. *Annu Rev Biochem*, 67:425–479.

Hill, J., Eickhoff, P., Drury, L. S., Costa, A., and Diffley, J. F. (2020). The eukaryotic replisome requires an additional helicase to disarm dormant replication origins. *bioRxiv*, page 2020.09.17.301366.

Hochstrasser, M. (2009). Origin and function of ubiquitin-like proteins. *Nature 2009 458:7237*, 458(7237):422–429.

Hoffmann, S., Smedegaard, S., Nakamura, K., Mortuza, G. B., Raschle, M., Ibanez de Opakua, A., Oka, Y., Feng, Y., Blanco, F. J., Mann, M., Montoya, G., Groth, A., Bekker-Jensen, S., and Mailand, N. (2016). TRAIP is a PCNA-binding ubiquitin ligase that protects genome stability after replication stress. *J Cell Biol*, 212(1):63–75.

Hoppe-Seyler, F. and Butz, K. (1993). Repression of endogenous p53 transactivation function in HeLa cervical carcinoma cells by human papillomavirus type 16 E6, human mdm-2, and mutant p53. *Journal of Virology*, 67(6):3111.

Hospenthal, M. K., Freund, S. M., and Komander, D. (2013). Assembly, analysis and architecture of atypical ubiquitin chains. *Nat Struct Mol Biol*, 20(5):555–565.

Hsu, R. Y., Giri, S., Wang, Y., Lin, Y. C., Liu, D., Wopat, S., Chakraborty, A., Prasanth, K. V., and Prasanth, S. G. (2020). The E3 ligase RFWD3 stabilizes ORC in a p53-dependent manner. *Cell Cycle*, 19(21):2927.

Huang, D. T., Hunt, H. W., Zhuang, M., Ohi, M. D., Holton, J. M., and Schulman, B. A. (2007). Basis for a ubiquitin-like protein thioester switch toggling E1-E2 affinity. *Nature*, 445(7126):394–398.

Huang, J., Liu, S., Bellani, M. A., Thazhathveetil, A. K., Ling, C., DeWinter, J. P., Wang, Y., Wang, W., and Seidman, M. M. (2013). The DNA Translocase FANCM/MHF Promotes Replication Traverse of DNA Interstrand Crosslinks. *Molecular cell*, 52(3):434–446.

Huibregtse, J., M, S., S, B., and PM, H. (1995). A family of proteins structurally and functionally related to the E6-AP ubiquitin-protein ligase. *Proceedings of the National Academy of Sciences of the United States of America*, 92(7):2563–2567.

Hungria, V. T. d. M., Crusoé, E. d. Q., Bittencourt, R. I., Maiolino, A., Magalhães, R. J. P., Sobrinho, J. d. N., Pinto, J. V., Fortes, R. C., Moreira, E. d. S., and Tanaka, P. Y. (2019). New proteasome inhibitors in the treatment of multiple myeloma. *Hematology, Transfusion and Cell Therapy*, 41(1):76.

Ilves, I., Petojevic, T., Pesavento, J. J., and Botchan, M. R. (2010). Activation of the MCM2-7 Helicase by Association with Cdc45 and GINS Proteins. *Molecular Cell*, 37(2):247–258.

Inano, S., Sato, K., Katsuki, Y., Kobayashi, W., Tanaka, H., Nakajima, K., Nakada, S., Miyoshi, H., Knies, K., Takaori-Kondo, A., Schindler, D., Ishiai, M., Kurumizaka, H., and Takata, M. (2017). RFWD3-Mediated Ubiquitination Promotes Timely Removal of Both RPA and RAD51 from DNA Damage Sites to Facilitate Homologous Recombination. *Mol Cell*, 66(5):622–634.e8.

Ingham, R. J., Gish, G., and Pawson, T. (2004). The Nedd4 family of E3 ubiquitin ligases: functional diversity within a common modular architecture. *Oncogene 2004 23:11*, 23(11):1972–1984.

Jackson, A. P., Laskey, R. A., and Coleman, N. (2014). Replication Proteins and Human Disease. In *Cold Spring Harb Perspect Biol*, volume 6.

Jackson, S. P. and Bartek, J. (2009). The DNA-damage response in human biology and disease. *Nature*, 461(7267):1071.

Jain, N. K. and Roy, I. (2009). Effect of trehalose on protein structure. *Protein Science : A Publication of the Protein Society*, 18(1):24.

Jenkyn-Bedford, M., Jones, M. L., Baris, Y., Labib, K. P. M., Cannone, G., Yeeles, J. T. P., and Deegan, T. D. (2021). A Conserved Mechanism for Regulating Replisome Disassembly in Eukaryotes. *Nature 2021*, pages 1–25.

Jiang, F. and Doudna, J. A. (2017). CRISPR-Cas9 Structures and Mechanisms. *Annual review of biophysics*, 46:505–529.

Jullien, L., Mestre, M., Roux, P., and Gire, V. (2013). Eroded human telomeres are more prone to remain uncapped and to trigger a G2 checkpoint response. *Nucleic acids research*, 41(2):900–911.

Kajiro, M., Tsuchiya, M., ichi Kawabe, Y., Furumai, R., Iwasaki, N., Hayashi, Y., Katano, M., Nakajima, Y., Goto, N., Watanabe, T., Murayama, A., Oishi, H., Ema, M., Takahashi, S., Kishimoto, H., and Yanagisawa, J. (2011). The E3 Ubiquitin Ligase Activity of Trip12 Is Essential for Mouse Embryogenesis. *PLoS ONE*, 6(10):25871.

Kamentsky, L., Jones, T. R., Fraser, A., Bray, M. A., Logan, D. J., Madden, K. L., Ljosa, V., Rueden, C., Eliceiri, K. W., and Carpenter, A. E. (2011). Improved structure, function and compatibility

for CellProfiler: modular high-throughput image analysis software. *Bioinformatics (Oxford, England)*, 27(8):1179–1180.

Kanke, M., Kodama, Y., Takahashi, T. S., Nakagawa, T., and Masukata, H. (2012). Mcm10 plays an essential role in origin DNA unwinding after loading of the CMG components. *The EMBO Journal*, 31(9):2182.

Kermi, C., Furno, E. L., and Maiorano, D. (2017). Regulation of DNA Replication in Early Embryonic Cleavages. *Genes*, 8(1):42.

Keszthelyi, A., Minchell, N. E., and Baxter, J. (2016). The causes and consequences of topological stress during DNA replication.

Klingseisen, A. and Jackson, A. P. (2011). Mechanisms and pathways of growth failure in primordial dwarfism. *Genes & development*, 25(19):2011–2024.

Knapp, K. M., Jenkins, D. E., Sullivan, R., Harms, F. L., von Elsner, L., Ockeloen, C. W., de Munnik, S., Bongers, E. M., Murray, J., Pachter, N., Denecke, J., Kutsche, K., and Bicknell, L. S. (2021). MCM complex members MCM3 and MCM7 are associated with a phenotypic spectrum from Meier-Gorlin syndrome to lipodystrophy and adrenal insufficiency. *European journal of human genetics : EJHG*, 29(7):1110–1120.

Kneissig, M., Keuper, K., De Pagter, M. S., Van Roosmalen, M. J., Martin, J., Otto, H., Passerini, V., Sparr, A. C., Renkens, I., Kropveld, F., Vasudevan, A., Sheltzer, J., Kloosterman, W. P., and Storchová, Z. (2019). Micronuclei-based model system reveals functional consequences of chromothripsis in human cells. *eLife*, 8:e50292.

Knies, K., Inano, S., Ramirez, M. J., Ishiai, M., Surralles, J., Takata, M., and Schindler, D.

(2017). Biallelic mutations in the ubiquitin ligase RFWD3 cause Fanconi anemia. *J Clin Invest*, 127(8):3013–3027.

Köhler, C., Koalick, D., Fabricius, A., Parplys, A. C., Borgmann, K., Pospiech, H., and Grosse, F. (2016). Cdc45 is limiting for replication initiation in humans. *Cell cycle (Georgetown, Tex.)*, 15(7):974–985.

Komander, D. and Rape, M. (2012). The ubiquitin code. *Annu Rev Biochem*, 81:203–229.

Koresawa, M. and Okabe, T. (2004). High-throughput screening with quantitation of ATP consumption: a universal non-radioisotope, homogeneous assay for protein kinase. *Assay and drug development technologies*, 2(2):153–160.

Kotsantis, P., Silva, L. M., Irmscher, S., Jones, R. M., Folkes, L., Gromak, N., and Petermann, E. (2016). Increased global transcription activity as a mechanism of replication stress in cancer. *Nature Communications 2016 7:1*, 7(1):1–13.

Koyanagi, E., Kakimoto, Y., Yoshifuji, F., Natsume, T., Higashitani, A., Ogi, T., Carr, A. M., Kanemaki, M. T., and Daigaku, Y. (2021). Global landscape of replicative DNA polymerase usage in the human genome. *bioRxiv*, page 2021.11.14.468503.

Krenning, L., Feringa, F. M., Shaltiel, I. A., VandenBerg, J., and Medema, R. H. (2014). Transient activation of p53 in G2 phase is sufficient to induce senescence. *Molecular cell*, 55(1):59–72.

Kunkel, T. A. and Burgers, P. M. (2008). Dividing the workload at a eukaryotic replication fork. 18(11):521–527.

Kuo, L. J. and Yang, L. X. (2008). γ-H2AX - A Novel Biomarker for DNA Double-strand Breaks. *In Vivo*, 22(3):305–309.

Kuznetsova, A. V., Meller, J., Schnell, P. O., Nash, J. A., Ignacak, M. L., Sanchez, Y., Conaway, J. W., Conaway, R. C., and Czyzyk-Krzeska, M. F. (2003). von Hippel-Lindau protein binds hyperphosphorylated large subunit of RNA polymerase II through a proline hydroxylation motif and targets it for ubiquitination. *Proceedings of the National Academy of Sciences of the United States of America*, 100(5):2706–2711.

Lambert, S. and Carr, A. M. (2013). Impediments to replication fork movement: stabilisation, reactivation and genome instability. *Chromosoma 2013 122:1*, 122(1):33–45.

Lara-Gonzalez, P., Westhorpe, F. G., and Taylor, S. S. (2012). The Spindle Assembly Checkpoint. *Current Biology*, 22(22):R966–R980.

Larrieu, D., Brunet, M., Vargas, C., Hanoun, N., Ligat, L., Dagnon, L., Lulka, H., Pommier, R. M., Selves, J., Jády, B. E., Bartholin, L., Cordelier, P., Dufresne, M., and Torrisani, J. (2020). The E3 ubiquitin ligase TRIP12 participates in cell cycle progression and chromosome stability. *Scientific reports*, 10(1):789.

Larsen, N. B., Gao, A. O., Sparks, J. L., Gallina, I., Wu, R. A., Mann, M., Räschle, M., Walter, J. C., and Duxin, J. P. (2019). Replication-Coupled DNA-Protein Crosslink Repair by SPRTN and the Proteasome in Xenopus Egg Extracts. *Molecular Cell*, 73(3):574–588.e7.

Lecona, E., Rodriguez-Acebes, S., Specks, J., Lopez-Contreras, A. J., Ruppen, I., Murga, M., Muñoz, J., Mendez, J., and Fernandez-Capetillo, O. (2016). USP7 is a SUMO deubiquitinase essential for DNA replication. *Nature structural & molecular biology*, 23(4):270–277.

Lee, I. and Schindelin, H. (2008). Structural insights into E1-catalyzed ubiquitin activation and transfer to conjugating enzymes. *Cell*, 134(2):268–278.

Lee, S. Y., Lee, S. Y., and Choi, Y. (1997). TRAF-interacting protein (TRIP): a novel component of the tumor necrosis factor receptor (TNFR)- and CD30-TRAF signaling complexes that inhibits TRAF2-mediated NF-kappaB activation. *J Exp Med*, 185(7):1275–1285.

Leibly, D. J., Nguyen, T. N., Kao, L. T., Hewitt, S. N., Barrett, L. K., and Van Voorhis, W. C. (2012). Stabilizing Additives Added during Cell Lysis Aid in the Solubilization of Recombinant Proteins. *PLoS ONE*, 7(12):e52482.

Leonard, A. C. and Mechali, M. (2013). DNA replication origins. *Cold Spring Harbor Perspectives in Medicine*, 3(10):a010116.

Lerner, L. K. and Sale, J. E. (2019). Replication of G Quadruplex DNA. *Genes*, 10(2):95.

Li, C., Irrazabal, T., So, C. C., Berru, M., Du, L., Lam, E., Ling, A. K., Gommerman, J. L., Pan-Hammarström, Q., and Martin, A. (2018). The H2B deubiquitinase Usp22 promotes antibody class switch recombination by facilitating non-homologous end joining. *Nature communications*, *9*(1):1006.

Li, M., Wu, W., Deng, S., Shao, Z., and Jin, X. (2021). TRAIP modulates the IGFBP3/AKT pathway to enhance the invasion and proliferation of osteosarcoma by promoting KANK1 degradation. *Cell Death & Disease 2021 12:8*, 12(8):1–13.

Li, X. and Heyer, W. D. (2008). Homologous recombination in DNA repair and DNA damage tolerance. *Cell research*, 18(1):99–113.

Liang, K., Woodfin, A. R., Slaughter, B. D., Unruh, J. R., Box, A. C., Rickels, R. A., Gao, X., Haug, J. S., Jaspersen, S. L., and Shilatifard, A. (2015). Mitotic Transcriptional Activation: Clearance

of Actively Engaged Pol II via Transcriptional Elongation Control in Mitosis. *Molecular cell*, 60(3):435–445.

Lin, J. J., Milhollen, M. A., Smith, P. G., Narayanan, U., and Dutta, A. (2010). NEDD8 targeting drug MLN4924 elicits DNA re-replication by stabilizing Cdt1 in S Phase, triggering checkpoint activation, apoptosis and senescence in cancer cells. *Cancer research*, 70(24):10310.

Lin, Y. C., Wang, Y., Hsu, R., Giri, S., Wopat, S., Arif, M. K., Chakraborty, A., Prasanth, K. V., and Prasanth, S. G. (2018). PCNA-mediated stabilization of E3 ligase RFWD3 at the replication fork is essential for DNA replication. *Proc Natl Acad Sci U S A*, 115(52):13282–13287.

Liu, W., Morito, D., Takashima, S., Mineharu, Y., Kobayashi, H., Hitomi, T., Hashikata, H., Matsuura, N., Yamazaki, S., Toyoda, A., Kikuta, K., Takagi, Y., Harada, K. H., Fujiyama, A., Herzig, R., Krischek, B., Zou, L., Kim, J. E., Kitakaze, M., Miyamoto, S., Nagata, K., Hashimoto, N., and Koizumi, A. (2011). Identification of RNF213 as a susceptibility gene for moyamoya disease and its possible role in vascular development. *PLoS One*, 6(7):e22542.

Liu, X., Yang, X., Li, Y., Zhao, S., Li, C., Ma, P., and Mao, B. (2016). Trip12 is an E3 ubiquitin ligase for USP7/HAUSP involved in the DNA damage response. *FEBS Lett*, 590(23):4213–4222.

Liu, Y., Chen, S., Wang, S., Soares, F., Fischer, M., Meng, F., Du, Z., Lin, C., Meyer, C., DeCaprio, J. A., Brown, M., Liu, X. S., and He, H. H. (2017). Transcriptional landscape of the human cell cycle. *Proceedings of the National Academy of Sciences of the United States of America*, 114(13):3473–3478.

Liu, Y., Kao, H.-I., and Bambara, R. A. (2004). Flap Endonuclease 1: A Central Component of DNA Metabolism. *Annual Review of Biochemistry*, 73(1):589–615.

Lobato-Gil, S., Heidelberger, J. B., Maghames, C., Bailly, A., Brunello, L., Rodriguez, M. S., Beli, P., and Xirodimas, D. P. (2021). Proteome-wide identification of NEDD8 modification sites reveals distinct proteomes for canonical and atypical NEDDylation. *Cell reports*, 34(3):108635.

Logan, C. V., Murray, J. E., Parry, D. A., Robertson, A., Bellelli, R., Tarnauskaitė, Ž., Challis, R., Cleal, L., Borel, V., Fluteau, A., Santoyo-Lopez, J., Aitman, T. J., Biankin, A. V., Cooke, S. L., Humphrey, W. I., Martin, S., Mennie, L., Meynert, A., Miedzybrodzka, Z., Murphy, F., Nourse, C., Semple, C. A., Williams, N., Aitman, T., Barroso, I., Basel, D., Bicknell, L. S., Goel, H., Hu, H., Huff, C., Hutchison, M., Joyce, C., Knox, R., Lacroix, A. E., Langlois, S., McCandless, S., McCarrier, J., Metcalfe, K. A., Morrissey, R., Murphy, N., Netchine, I., O'Connell, S. M., Olney, A. H., Paria, N., Rosenfeld, J. A., Sherlock, M., Syverson, E., White, P. C., Wise, C., Yu, Y., Zacharin, M., Banerjee, I., Reijns, M., Bober, M. B., Semple, R. K., Boulton, S. J., Rios, J. J., and Jackson, A. P. (2018). DNA Polymerase Epsilon Deficiency Causes IMAGe Syndrome with Variable Immunodeficiency. *American journal of human genetics*, 103(6):1038–1044.

Lopez-Contreras, A. J., Ruppen, I., Nieto-Soler, M., Murga, M., Rodriguez-Acebes, S., Remeseiro, S., Rodrigo-Perez, S., Rojas, A. M., Mendez, J., Munoz, J., and Fernandez-Capetillo, O. (2013). A proteomic characterization of factors enriched at nascent DNA molecules. *Cell reports*, 3(4):1105–1116.

Lorenz, S. (2018). Structural mechanisms of HECT-type ubiquitin ligases. *Biological Chemistry*, 399(2):127–145.

Lossaint, G., Larroque, M., Ribeyre, C., Bec, N., Larroque, C., Décaillet, C., Gari, K., and Constantinou, A. (2013). FANCD2 binds MCM proteins and controls replisome function upon activation of s phase checkpoint signaling. *Molecular cell*, 51(5):678–690.

Low, E., Chistol, G., Zaher, M. S., Kochenova, O. V., and Walter, J. C. (2020). The DNA replication fork suppresses CMG unloading from chromatin before termination. *Genes and Development*, 34(21):1534–1545.

Luger, K., Mader, A. W., Richmond, R. K., Sargent, D. F., and Richmond, T. J. (1997). Crystal structure of the nucleosome core particle at 2.8 Angstrom resolution. *Nature 1997 389:6648*, 389(6648):251–260.

Ma, K., Qiu, L., Mrasek, K., Zhang, J., Liehr, T., Quintana, L. G., and Li, Z. (2012). Common Fragile Sites: Genomic Hotspots of DNA Damage and Carcinogenesis. *International Journal of Molecular Sciences*, 13(9):11974.

MacAlpine, D. M. and Almouzni, G. (2013). Chromatin and DNA replication. *Cold Spring Harbor perspectives in biology*, 5(8):a010207.

Madsen, L., Molbæk, K., Larsen, I. B., Nielsen, S. V., Poulsen, E. G., Walmod, P. S., Hofmann, K., Seeger, M., Chien, C. Y., Chen, R. H., Kriegenburg, F., and Hartmann-Petersen, R. (2014). Human ASPL/TUG interacts with p97 and complements the proteasome mislocalization of a yeast ubx4 mutant, but not the ER-associated degradation defect. *BMC Cell Biology*, 15(1):1–10.

Madsen, P. and Celis, J. E. (1985). S-phase patterns of cyclin (PCNA) antigen staining resemble topographical patterns of DNA synthesis. A role for cyclin in DNA replication? *FEBS letters*, 193(1):5–11.

Mailand, N., Falck, J., Lukas, C., Syljuåsen, R. G., Welcker, M., Bartek, J., and Lukas, J. (2000). Rapid destruction of human Cdc25A in response to DNA damage. *Science (New York, N.Y.)*, 288(5470):1425–1429.

Mao, Z., Ke, Z., Gorbunova, V., and Seluanov, A. (2012). Replicatively senescent cells are arrested in G1 and G2 phases. *Aging*, 4(6):431–435.

Marblestone, J. G., Edavettal, S. C., Lim, Y., Lim, P., Zuo, X., and Butt, T. R. (2006). Comparison of SUMO fusion technology with traditional gene fusion systems: Enhanced expression and solubility with SUMO. *Protein Science : A Publication of the Protein Society*, 15(1):182.

Maréchal, A. and Zou, L. (2013). DNA Damage Sensing by the ATM and ATR Kinases. *Cold Spring Harbor Perspectives in Biology*, 5(9):a012716.

Marheineke, K. and Hyrien, O. (2004). Control of replication origin density and firing time in Xenopus egg extracts: role of a caffeine-sensitive, ATR-dependent checkpoint. *The Journal of biological chemistry*, 279(27):28071–28081.

Maric, M., Maculins, T., De Piccoli, G., and Labib, K. (2014). Cdc48 and a ubiquitin ligase drive disassembly of the CMG helicase at the end of DNA replication. *Science*, 346(6208):1253596.

Martínez-Alonso, M., González-Montalbán, N., García-Fruitós, E., and Villaverde, A. (2009). Learning about protein solubility from bacterial inclusion bodies. *Microbial Cell Factories*, 8(1):4.

Masumoto, H., Muramatsu, S., Kamimura, Y., and Araki, H. (2002). S-Cdk-dependent phosphorylation of Sld2 essential for chromosomal DNA replication in budding yeast. *Nature*, 415:651–655.

Matheson, C. J., Backos, D. S., and Reigan, P. (2016). Targeting WEE1 Kinase in Cancer. *Trends in Pharmacological Sciences*, 37(10):872–881.

Matsuoka, S., Ballif, B. A., Smogorzewska, A., McDonald, E. R., Hurov, K. E., Luo, J., Bakalarski, C. E., Zhao, Z., Solimini, N., Lerenthal, Y., Shiloh, Y., Gygi, S. P., and Elledge, S. J. (2007). ATM and ATR substrate analysis reveals extensive protein networks responsive to DNA damage. *Science*, 316(5828):1160–1166.

McCann, J. J., Vasilevskaya, I. A., Neupane, N. P., Shafi, A. A., McNair, C., Dylgjeri, E., Mandigo, A. C., Schiewer, M. J., Schrecengost, R. S., Gallagher, P., Stanek, T. J., McMahon, S. B., Berman-Booty, L. D., Ostrander, W. F., and Knudsen, K. E. (2020). USP22 Functions as an Oncogenic Driver in Prostate Cancer by Regulating Cell Proliferation and DNA Repair. *Cancer research*, 80(3):430–443.

McQuin, C., Goodman, A., Chernyshev, V., Kamentsky, L., Cimini, B. A., Karhohs, K. W., Doan, M., Ding, L., Rafelski, S. M., Thirstrup, D., Wiegraebe, W., Singh, S., Becker, T., Caicedo, J. C., and Carpenter, A. E. (2018). CellProfiler 3.0: Next-generation image processing for biology. *PLOS Biology*, 16(7):e2005970.

Melo-Cardenas, J., Zhang, Y., Zhang, D. D., and Fang, D. (2016). Ubiquitin-specific peptidase 22 functions and its involvement in disease. *Oncotarget*, 7(28):44848.

Merkle, J. A., Rickmyre, J. L., Garg, A., Loggins, E. B., Jodoin, J. N., Lee, E., Wu, L. P., and Lee, L. A. (2009). no poles encodes a predicted E3 ubiquitin ligase required for early embryonic development of Drosophila. *Development (Cambridge, England)*, 136(3):449.

Mevissen, T. and Komander, D. (2017). Mechanisms of Deubiquitinase Specificity and Regulation. *Annual review of biochemistry*, 86:159–192.

Michaloglou, C., Vredeveld, L. C., Soengas, M. S., Denoyelle, C., Kuilman, T., Van Der Horst,

C. M., Majoor, D. M., Shay, J. W., Mooi, W. J., and Peeper, D. S. (2005). BRAFE600-associated senescence-like cell cycle arrest of human naevi. *Nature*, 436(7051):720–724.

Miller, T. C. R., Locke, J., Greiwe, J. F., Diffley, J. F. X., and Costa, A. (2019). Mechanism of head-to-head MCM double-hexamer formation revealed by cryo-EM. *Nature 2019 575:7784*, 575(7784):704–710.

Moiseeva, T. N., Qian, C., Sugitani, N., Osmanbeyoglu, H. U., and Bakkenist, C. J. (2019a). WEE1 kinase inhibitor AZD1775 induces CDK1 kinase-dependent origin firing in unperturbed G1-And S-phase cells. *Proceedings of the National Academy of Sciences of the United States of America*, 116(48):23891–23893.

Moiseeva, T. N., Qian, C., Sugitani, N., Osmanbeyoglu, H. U., and Bakkenist, C. J. (2019b). WEE1 kinase inhibitor AZD1775 induces CDK1 kinase-dependent origin firing in unperturbed G1- and S-phase cells. *Proceedings of the National Academy of Sciences of the United States of America*, 116(48):23891–23893.

Moreno, A., Carrington, J. T., Albergante, L., Mamun, M. A., Haagensen, E. J., Komseli, E. S., Gorgoulis, V. G., Newman, T. J., and Blow, J. J. (2016). Unreplicated DNA remaining from unperturbed S phases passes through mitosis for resolution in daughter cells. *Proceedings of the National Academy of Sciences of the United States of America*, 113(39):E5757–E5764.

Moreno, O. M., Paredes, A. C., Suarez-Obando, F., and Rojas, A. (2021). An update on Fanconi anemia: Clinical, cytogenetic and molecular approaches (Review). *Biomedical Reports*, 15(3):74.

Moreno, S. P., Bailey, R., Campion, N., Herron, S., and Gambus, A. (2014). Polyubiquitylation

drives replisome disassembly at the termination of DNA replication. *Science*, 346(6208):477–481.

Moreno, S. P. and Gambus, A. (2015). Regulation of Unperturbed DNA Replication by Ubiquitylation. *Genes*, 6:451–468.

Moreno, S. P. and Gambus, A. (2020). Mechanisms of eukaryotic replisome disassembly. *Biochemical Society Transactions*, 48(3):823–836.

Moreno, S. P., Jones, R. M., Poovathumkadavil, D., Scaramuzza, S., and Gambus, A. (2019). Mitotic replisome disassembly depends on TRAIP ubiquitin ligase activity. *Life Science Alliance*, 2(2):e201900390.

Moser, J., Miller, I., Carter, D., and Spencer, S. L. (2018). Control of the restriction point by rb and p21. *Proceedings of the National Academy of Sciences of the United States of America*, 115(35):E8219–E8227.

Mourón, S., Rodriguez-Acebes, S., Martínez-Jiménez, M. I., García-Gómez, S., Chocrón, S., Blanco, L., and Méndez, J. (2013). Repriming of DNA synthesis at stalled replication forks by human PrimPol. *Nature Structural & Molecular Biology 2013 20:12*, 20(12):1383–1389.

Moyer, S. E., Lewis, P. W., and Botchan, M. R. (2006). Isolation of the Cdc45/Mcm2-7/GINS (CMG) complex, a candidate for the eukaryotic DNA replication fork helicase. *Proceedings of the National Academy of Sciences of the United States of America*, 103(27):10236–10241.

Mu, J. J., Wang, Y., Luo, H., Leng, M., Zhang, J., Yang, T., Besusso, D., Sung, Y. J., and Qin, J. (2007). A proteomic analysis of ataxia telangiectasia-mutated (ATM)/ATM-Rad3- related

(ATR) substrates identifies the ubiquitin-proteasome system as a regulator for DNA damage checkpoints. *Journal of Biological Chemistry*, 282(24):17330–17334.

Nakagawa, T. and Nakayama, K. (2015). Protein monoubiquitylation: targets and diverse functions. *Genes to Cells*, 20(7):543.

Nam, E. A. and Cortez, D. (2011). ATR signalling: more than meeting at the fork. *The Biochemical journal*, 436(3):527–536.

Nardi, I. K., Stark, J. M., Larsen, A., Salgia, R., and Raz, D. J. (2020). USP22 Interacts with PALB2 and Promotes Chemotherapy Resistance via Homologous Recombination of DNA Double-Strand Breaks. *Molecular cancer research : MCR*, 18(3):424–435.

Natsume, T., Kiyomitsu, T., Saga, Y., and Kanemaki, M. T. (2016). Rapid Protein Depletion in Human Cells by Auxin-Inducible Degron Tagging with Short Homology Donors. *Cell Reports*, 15(1):210–218.

Navarro, R., Chen, L. C., Rakhit, R., and Wandless, T. J. (2016). A Novel Destabilizing Domain Based on a Small-Molecule Dependent Fluorophore. *ACS Chemical Biology*, 11(8):2101–2104.

Nejad, M., Housh, K., Rodriguez, A. A., Haldar, T., Kathe, S., Wallace, S. S., Eichman, B. F., and Gates, K. S. (2020). Unhooking of an interstrand cross-link at DNA fork structures by the DNA glycosylase NEIL3. *DNA repair*, 86:102752.

Nguyen, H. C. and Wang, W. (2017). Cullin-RING E3 Ubiquitin Ligases: Bridges to Destruction. *Subcellular Biochemistry*, 83:323–347.

Ning, Z., Wang, A., Liang, J., Xie, Y., Liu, J., Feng, L., Yan, Q., and Wang, Z. (2014). USP22 promotes the G1/S phase transition by upregulating FoxM1 expression via beta-catenin

nuclear localization and is associated with poor prognosis in stage II pancreatic ductal adenocarcinoma. *Int J Oncol*, 45(4):1594–1608.

Noton, E. and Diffley, J. F. (2000). CDK inactivation is the only essential function of the APC/C and the mitotic exit network proteins for origin resetting during mitosis. *Molecular cell*, 5(1):85–95.

Olsen, S. K. and Lima, C. D. (2013). Structure of a ubiquitin E1-E2 complex: insights to E1-E2 thioester transfer. *Mol Cell*, 49(5):884–896.

Paiva, S. L. and Crews, C. M. (2019). Targeted Protein Degradation: Elements of PROTAC Design. *Current opinion in chemical biology*, 50:111.

Palmer, I. and Wingfield, P. T. (2012). Preparation and Extraction of Insoluble (Inclusion-Body) Proteins from Escherichia coli. *Current protocols in protein science / editorial board, John E. Coligan ... [et al.]*, 0 6(SUPPL.70):10.1002/0471140864.ps0603s38.

Pan, Y., An, N., Deng, X., Zhang, Q., and Du, X. (2021). RNF220 promotes the proliferation of leukaemic cells and reduces the degradation of the Cyclin D1 protein through USP22. *Blood cells, molecules & diseases*, 86:102490.

Panier, S. and Boulton, S. J. (2013). Double-strand break repair: 53BP1 comes into focus. *Nature Reviews Molecular Cell Biology 2013 15:1*, 15(1):7–18.

Park, E. S., Choi, S., Kim, J. M., Jeong, Y., Choe, J., Park, C. S., Choi, Y., and Rho, J. (2007). Early embryonic lethality caused by targeted disruption of the TRAF-interacting protein (TRIP) gene. *Biochemical and Biophysical Research Communications*, 363(4):971–977.

Park, I. S., Han, Y., Chung, H. J., Jung, Y. W., Kim, Y., and Kim, H. (2016). SUMOylation regulates nuclear localization and stability of TRAIP/RNF206. *Biochem Biophys Res Commun*, 470(4):881–887.

Park, I. S., Jo, K. S., Won, H. S., and Kim, H. (2015). Dimerization of TRAF-interacting protein (TRAIP) regulates the mitotic progression. *Biochem Biophys Res Commun*, 463(4):864–869.

Park, J. M., Yang, S. W., Yu, K. R., Ka, S. H., Lee, S. W., Seol, J. H., Jeon, Y. J., and Chung, C. H. (2014). Modification of PCNA by ISG15 plays a crucial role in termination of error-prone translesion DNA synthesis. *Mol Cell*, 54(4):626–638.

Parry, D. A., Tamayo-Orrego, L., Carroll, P., Marsh, J. A., Greene, P., Murina, O., Uggenti, C., Leitch, A., Kaposzta, R., Mero, G., Nagy, A., Orlik, B., Kovacs-Paszthy, B., Quigley, A. J., Riszter, M., Rankin, J., Reijns, M. A., Szakszon, K., and Jackson, A. P. (2020). PRIM1 deficiency causes a distinctive primordial dwarfism syndrome. *Genes and Development*, 34(21):1520–1533.

Patil, M., Pabla, N., and Dong, Z. (2013). Checkpoint kinase 1 in DNA damage response and cell cycle regulation. *Cellular and molecular life sciences : CMLS*, 70(21):4009–4021.

Pellegrini, L. and Costa, A. (2016). New Insights into the Mechanism of DNA Duplication by the Eukaryotic Replisome. 41(10):859–871.

Pennycook, B. R., Vesela, E., Peripolli, S., Singh, T., Barr, A. R., Bertoli, C., and de Bruin, R. A. (2020). E2F-dependent transcription determines replication capacity and S phase length. *Nature Communications 2020 11:1*, 11(1):1–10.

Petermann, E. and Helleday, T. (2010). Pathways of mammalian replication fork restart. *Nature reviews. Molecular cell biology*, 11(10):683–687.

Petermann, E., Lan, L., and Zou, L. (2022). Sources, resolution and physiological relevance of r-loops and RNA–DNA hybrids. *Nature Reviews Molecular Cell Biology*, pages 10.1038/s41580–022–00474–x.

Peters, J. M. and Nishiyama, T. (2012). Sister Chromatid Cohesion. *Cold Spring Harbor Perspectives in Biology*, 4(11):a011130.

Petroski, M. D. and Deshaies, R. J. (2005). Function and regulation of cullin-RING ubiquitin ligases. *Nature reviews. Molecular cell biology*, 6(1):9–20.

Picard, F., Cadoret, J. C., Audit, B., Arneodo, A., Alberti, A., Battail, C., Duret, L., and Prioleau, M. N. (2014). The Spatiotemporal Program of DNA Replication Is Associated with Specific Combinations of Chromatin Marks in Human Cells. *PLoS Genetics*, 10(5):e1004282.

Plechanovova, A., Jaffray, E. G., Tatham, M. H., Naismith, J. H., and Hay, R. T. (2012). Structure of a RING E3 ligase and ubiquitin-loaded E2 primed for catalysis. *Nature*, 489(7414):115–120.

Pommier, Y., Sun, Y., Huang, S. Y. N., and Nitiss, J. L. (2016). Roles of eukaryotic topoisomerases in transcription, replication and genomic stability. *Nature Reviews Molecular Cell Biology*, 17(11):703–721.

Poot, S., G, T., and D, F. (2017). Meddling with Fate: The Proteasomal Deubiquitinating Enzymes. *Journal of molecular biology*, 429(22):3525–3545.

Postow, L., Crisona, N. J., Peter, B. J., Hardy, C. D., and Cozzarelli, N. R. (2001). Topological challenges to DNA replication: Conformations at the fork. *Proceedings of the National Academy of Sciences of the United States of America*, 98(15):8219–8226.

Prigent, C. and Dimitrov, S. (2003). Phosphorylation of serine 10 in histone H3, what for? *Journal of cell science*, 116(Pt 18):3677–3685.

Prioleau, M. and MacAlpine, D. (2016). DNA replication origins-where do we begin? *Genes & development*, 30(15):1683–1697.

Qiu, S., Jiang, G., Cao, L., and Huang, J. (2021). Replication Fork Reversal and Protection. *Frontiers in Cell and Developmental Biology*, 9:670392.

Ran, F. A., Hsu, P. D., Wright, J., Agarwala, V., Scott, D. A., and Zhang, F. (2013). Genome engineering using the CRISPR-Cas9 system. *Nature protocols*, 8(11):2281.

Randell, J. C., Bowers, J. L., Rodríguez, H. K., and Bell, S. P. (2006). Sequential ATP hydrolysis by Cdc6 and ORC directs loading of the Mcm2-7 helicase. *Molecular Cell*, 21(1):29–39.

Raschle, M., Smeenk, G., Hansen, R. K., Temu, T., Oka, Y., Hein, M. Y., Nagaraj, N., Long, D. T., Walter, J. C., Hofmann, K., Storchova, Z., Cox, J., Bekker-Jensen, S., Mailand, N., and Mann, M. (2015). Proteomics reveals dynamic assembly of repair complexes during bypass of DNA cross-links. *Science*, 348(6234):1253671–1253671.

Ratner, J. N., Balasubramanian, B., Corden, J., Warren, S. L., and Bregman, D. B. (1998). Ultraviolet radiation-induced ubiquitination and proteasomal degradation of the large subunit of RNA polymerase II. Implications for transcription-coupled DNA repair. *The Journal of biological chemistry*, 273(9):5184–5189.

Rattner, J. B., Rao, A., Fritzler, M. J., Valencia, D. W., and Yen, T. J. (1993). CENP-F is a ca 400 kDa kinetochore protein that exhibits a cell-cycle dependent localization. *Cell Motility and the Cytoskeleton*, 26(3):214–226.

Regamey, A., Hohl, D., Liu, J. W., Roger, T., Kogerman, P., Toftgård, R., and Huber, M. (2003). The tumor suppressor CYLD interacts with TRIP and regulates negatively nuclear factor kappaB activation by tumor necrosis factor. *The Journal of experimental medicine*, 198(12):1959–1964.

Remus, D., Beuron, F., Tolun, G., Griffith, J. D., Morris, E. P., and Diffley, J. F. (2009). Concerted Loading of Mcm2-7 Double Hexamers around DNA during DNA Replication Origin Licensing. *Cell*, 139(4):719–730.

Reynolds, J. J., Bicknell, L. S., Carroll, P., Higgs, M. R., Shaheen, R., Murray, J. E., Papadopoulos, D. K., Leitch, A., Murina, O., Tarnauskaite, Z., Wessel, S. R., Zlatanou, A., Vernet, A., Von Kriegsheim, A., Mottram, R. M., Logan, C. V., Bye, H., Li, Y., Brean, A., Maddirevula, S., Challis, R. C., Skouloudaki, K., Almoisheer, A., Alsaif, H. S., Amar, A., Prescott, N. J., Bober, M. B., Duker, A., Faqeih, E., Seidahmed, M. Z., Al Tala, S., Alswaid, A., Ahmed, S., Al-Aama, J. Y., Altmüller, J., Al Balwi, M., Brady, A. F., Chessa, L., Cox, H., Fischetto, R., Heller, R., Henderson, B. D., Hobson, E., Nürnberg, P., Percin, E. F., Peron, A., Spaccini, L., Quigley, A. J., Thakur, S., Wise, C. A., Yoon, G., Alnemer, M., Tomancak, P., Yigit, G., Taylor, A. M. R., Reijns, M. A., Simpson, M. A., Cortez, D., Alkuraya, F. S., Mathew, C. G., Jackson, A. P., and Stewart, G. S. (2017). Mutations in DONSON disrupt replication fork stability and cause microcephalic dwarfism. *Nature Genetics 2017 49:4*, 49(4):537–549.

Rieder, D., Trajanoski, Z., and McNally, J. G. (2012). Transcription factories. *Frontiers in Genetics*, 3(OCT):221.

Roth, S., Fulcher, L. J., and Sapkota, G. P. (2019). Advances in targeted degradation of endogenous proteins. *Cell Mol Life Sci*, 76(14):2761–2777.

Rudolph, M. J., Wuebbens, M. M., Rajagopalan, K. V., and Schindelin, H. (2001). Crystal

structure of molybdopterin synthase and its evolutionary relationship to ubiquitin activation. *Nat Struct Biol*, 8(1):42–46.

Ryba, T., Hiratani, I., Lu, J., Itoh, M., Kulik, M., Zhang, J., Schulz, T. C., Robins, A. J., Dalton, S., and Gilbert, D. M. (2010). Evolutionarily conserved replication timing profiles predict long-range chromatin interactions and distinguish closely related cell types. *Genome Research*, 20(6):761–770.

Sale, J. E. (2013). Translesion DNA Synthesis and Mutagenesis in Eukaryotes. *Cold Spring Harbor Perspectives in Biology*, 5(3):a012708.

Saponaro, M. (2022). Transcription–Replication Coordination. *Life 2022, Vol. 12, Page 108*, 12(1):108.

Saponaro, M., Kantidakis, T., Mitter, R., Kelly, G. P., Heron, M., Williams, H., Söding, J., Stewart, A., and Svejstrup, J. Q. (2014). RECQL5 Controls Transcript Elongation and Suppresses Genome Instability Associated with Transcription Stress. *Cell*, 157(5):1037.

Savić, D. J. and Kanazir, D. T. (1972). The effect of a histidine operator-constitutive mutation on UV-induced mutability within the histidine operon ofSalmonella typhimurium. *Molecular and General Genetics MGG 1972 118:1*, 118(1):45–50.

Sawyer, S. L., Cheng, I. H., Chai, W., and Tye, B. K. (2004). Mcm10 and Cdc45 cooperate in origin activation in Saccharomyces cerevisiae. *Journal of Molecular Biology*, 340(2):195–202.

Schafer, K. A. (1998). The cell cycle: a review. *Veterinary pathology*, 35(6):461–478.

Schauer, G. D., Spenkelink, L. M., Lewis, J. S., Yurieva, O., Mueller, S. H., van Oijen, A. M., and O'Donnell, M. E. (2020). Replisome bypass of a protein-based R-loop block by

Pif1. *Proceedings of the National Academy of Sciences of the United States of America*, 117(48):30354–30361.

Scheffner, M. and Kumar, S. (2014). Mammalian HECT ubiquitin-protein ligases: Biological and pathophysiological aspects. *Biochimica et Biophysica Acta (BBA) - Molecular Cell Research*, 1843(1):61–74.

Schindelin, J., Arganda-Carreras, I., Frise, E., Kaynig, V., Longair, M., Pietzsch, T., Preibisch, S., Rueden, C., Saalfeld, S., Schmid, B., Tinevez, J. Y., White, D. J., Hartenstein, V., Eliceiri, K., Tomancak, P., and Cardona, A. (2012). Fiji: an open-source platform for biological-image analysis. *Nature Methods 2012 9:7*, 9(7):676–682.

Schlager, B., Straessle, A., and Hafen, E. (2012). Use of anionic denaturing detergents to purify insoluble proteins after overexpression. *BMC biotechnology*, 12:95.

Schulman, B. A. and Harper, J. W. (2009). Ubiquitin-like protein activation by E1 enzymes: the apex for downstream signalling pathways. *Nat Rev Mol Cell Biol*, 10(5):319–331.

Segurado, M. and Tercero, J. A. (2009). The S-phase checkpoint: targeting the replication fork. *Biology of the cell*, 101(11):617–627.

Seki, T. and Diffley, J. F. (2000). Stepwise assembly of initiation proteins at budding yeast replication origins in vitro. *Proceedings of the National Academy of Sciences of the United States of America*, 97(26):14115–14120.

Sengupta, S., Van Deursen, F., De Piccoli, G., and Labib, K. (2013). Dpb2 Integrates the Leading-Strand DNA Polymerase into the Eukaryotic Replisome. *Current Biology*, 23(7):543–552.

Shachar, S., Ziv, O., Avkin, S., Adar, S., Wittschieben, J., Reißner, T., Chaney, S., Friedberg, E. C., Wang, Z., Carell, T., Geacintov, N., and Livneh, Z. (2009). Two-polymerase mechanisms dictate error-free and error-prone translesion DNA synthesis in mammals. *The EMBO Journal*, 28(4):383.

Shen, M., Schmitt, S., Buac, D., and Dou, Q. P. (2013). Targeting the ubiquitin–proteasome system for cancer therapy. *Expert opinion on therapeutic targets*, 17(9):1091.

Sherwood, R., Takahashi, T. S., and Jallepalli, P. V. (2010). Sister acts: coordinating DNA replication and cohesion establishment. *Genes & Development*, 24(24):2723–2731.

Shi, P., Su, Y., Li, R., Zhang, L., Chen, C., Zhang, L., Faaberg, K., and Huang, J. (2018). Dual Regulation of Host TRAIP Post-translation and Nuclear/Plasma Distribution by Porcine Reproductive and Respiratory Syndrome Virus Non-structural Protein 1α Promotes Viral Proliferation. *Frontiers in Immunology*, 9:3023.

Siddiqui, K., On, K. F., and Diffley, J. F. (2013). Regulating DNA replication in Eukarya. *Cold Spring Harbor Perspectives in Biology*, 5(9):a012930.

Simon, A. C., Zhou, J. C., Perera, R. L., Van Deursen, F., Evrin, C., Ivanova, M. E., Kilkenny, M. L., Renault, L., Kjaer, S., Matak-Vinkovi, D., Labib, K., Costa, A., and Pellegrini, L. (2014). A Ctf4 trimer couples the CMG helicase to DNA polymerase Î± in the eukaryotic replisome. *Nature*, 510(7504):293–297.

Sirbu, B. M., McDonald, W. H., Dungrawala, H., Badu-Nkansah, A., Kavanaugh, G. M., Chen, Y., Tabb, D. L., and Cortez, D. (2013). Identification of proteins at active, stalled, and collapsed replication forks using isolation of proteins on nascent DNA (iPOND) coupled with mass spectrometry. *The Journal of biological chemistry*, 288(44):31458–31467.

Skourti-Stathaki, K. and Proudfoot, N. J. (2014). A double-edged sword: R loops as threats to genome integrity and powerful regulators of gene expression. *Genes & Development*, 28(13):1384–1396.

Sloper-Mould, K. E., Jemc, J. C., Pickart, C. M., and Hicke, L. (2001). Distinct functional surface regions on ubiquitin. *J Biol Chem*, 276(32):30483–30489.

Smolka, J. A., Sanz, L. A., Hartono, S. R., and Chédin, F. (2021). Recognition of RNA by the S9.6 antibody creates pervasive artifacts when imaging RNA:DNA hybrids. *The Journal of Cell Biology*, 220(6):e202004079.

Somesh, B. P., Reid, J., Liu, W. F., Søgaard, T. M. M., Erdjument-Bromage, H., Tempst, P., and Svejstrup, J. Q. (2005). Multiple mechanisms confining RNA polymerase II ubiquitylation to polymerases undergoing transcriptional arrest. *Cell*, 121(6):913–923.

Somesh, B. P., Sigurdsson, S., Saeki, H., Erdjument-Bromage, H., Tempst, P., and Svejstrup, J. Q. (2007). Communication between Distant Sites in RNA Polymerase II through Ubiquitylation Factors and the Polymerase CTD. *Cell*, 129(1):57–68.

Sonneville, R., Bhowmick, R., Hoffmann, S., Mailand, N., Hickson, I. D., and Labib, K. (2019). TRAIP drives replisome disassembly and mitotic DNA repair synthesis at sites of incomplete DNA replication. *eLife*, 8:e48686.

Sonneville, R., Moreno, S. P., Knebel, A., Johnson, C., Hastie, C. J., Gartner, A., Gambus, A., and Labib, K. (2017). CUL2-LRR1 and UBXN-3 drive replisome disassembly during DNA replication termination and mitosis. *Nat Cell Biol*, 5(19):468–479.

Soo Lee, N., Jin Chung, H., Kim, H. J., Yun Lee, S., Ji, J. H., Seo, Y., Hun Han, S., Choi, M., Yun, M.,

Lee, S. G., Myung, K., Kim, Y., Chul Kang, H., and Kim, H. (2016). TRAIP/RNF206 is required for recruitment of RAP80 to sites of DNA damage. *Nat Commun*, 7:10463.

Soucy, T. A., Smith, P. G., Milhollen, M. A., Berger, A. J., Gavin, J. M., Adhikari, S., Brownell, J. E., Burke, K. E., Cardin, D. P., Critchley, S., Cullis, C. A., Doucette, A., Garnsey, J. J., Gaulin, J. L., Gershman, R. E., Lublinsky, A. R., Mcdonald, A., Mizutani, H., Narayanan, U., Olhava, E. J., Peluso, S., Rezaei, M., Sintchak, M. D., Talreja, T., Thomas, M. P., Traore, T., Vyskocil, S., Weatherhead, G. S., Yu, J., Zhang, J., Dick, L. R., Claiborne, C. F., Rolfe, M., Bolen, J. B., and Langston, S. P. (2009). An inhibitor of NEDD8-activating enzyme as a new approach to treat cancer. *Nature*, 458:732–736.

Sparks, J. L., Chistol, G., Gao, A. O., Raschle, M., Larsen, N. B., Mann, M., Duxin, J. P., and Walter, J. C. (2019). The CMG Helicase Bypasses DNA-Protein Cross-Links to Facilitate Their Repair. *Cell*, 176(1-2):167–181 e21.

Speck, C., Chen, Z., Li, H., and Stillman, B. (2005). ATPase-dependent cooperative binding of ORC and Cdc6 to origin DNA. *Nature Structural and Molecular Biology*, 12(11):965–971.

Srivatsan, A., Tehranchi, A., MacAlpine, D. M., and Wang, J. D. (2010). Co-Orientation of Replication and Transcription Preserves Genome Integrity. *PLOS Genetics*, 6(1):e1000810.

Starita, L. M., Horwitz, A. A., Keogh, M. C., Ishioka, C., Parvin, J. D., and Chiba, N. (2005). BRCA1/BARD1 ubiquitinate phosphorylated RNA polymerase II. *The Journal of biological chemistry*, 280(26):24498–24505.

Starostina, N. G., Simpliciano, J. M., McGuirk, M. A., and Kipreos, E. T. (2010). CRL2(LRR-1) targets a CDK inhibitor for cell cycle control in C. elegans and actin-based motility regulation in human cells. *Developmental cell*, 19(5):753–764.

Stinchcomb, D. T., Struhl, K., and Davis, R. W. (1979). Isolation and characterisation of a yeast chromosomal replicator. *Nature*, 282(5734):39–43.

Stoimenov, I., Gottipati, P., Schultz, N., and Helleday, T. (2011). Transcription inhibition by 5,6-dichloro-1-beta-D-ribofuranosylbenzimidazole (DRB) causes DNA damage and triggers homologous recombination repair in mammalian cells. *Mutation research*, 706(1-2):1–6.

Stoll, K. E., Brzovic, P. S., Davis, T. N., and Klevit, R. E. (2011). The Essential Ubc4/Ubc5 Function in Yeast Is HECT E3-dependent, and RING E3-dependent Pathways Require Only Monoubiquitin Transfer by Ubc4. *The Journal of Biological Chemistry*, 286(17):15165.

Stromberg, B. R., Singh, M., Torres, A. E., Burrows, A. C., Pal, D., Insinna, C., Rhee, Y., Dickson, A. S., Westlake, C. J., and Summers, M. K. (2021). The deubiquitinating enzyme USP37 enhances CHK1 activity to promote the cellular response to replication stress. *The Journal of biological chemistry*, 297(4):101184.

Sun, L. and Chen, Z. J. (2004). The novel functions of ubiquitination in signaling. *Curr Opin Cell Biol*, 16(2):119–126.

Suvorova, I. I., Grigorash, B. B., Chuykin, I. A., Pospelova, T. V., and Pospelov, V. A. (2016). G1 checkpoint is compromised in mouse ESCs due to functional uncoupling of p53-p21Waf1 signaling. *Cell cycle (Georgetown, Tex.)*, 15(1):52–63.

Swatek, K. N. and Komander, D. (2016). Ubiquitin modifications. *Cell Res*, 26(4):399–422.

Sy, S. M., Jiang, J., O, W. S., Deng, Y., and Huen, M. S. (2013). The ubiquitin specific protease USP34 promotes ubiquitin signaling at DNA double-strand breaks. *Nucleic Acids Res*, 41(18):8572–8580.

Tada, S., Li, A., Maiorano, D., Mechali, M., and Blow, J. J. (2001). Repression of origin assembly in metaphase depends on inhibition of RLF-B/Cdt1 by geminin. *Nature cell biology*, 3(2):107–113.

Taherbhoy, A., Schulman, B., and Kaiser, S. (2012). Ubiquitin-like modifiers. *Essays in biochemistry*, 52(1):51–63.

Tanaka, S. and Araki, H. (2013). Helicase activation and establishment of replication forks at chromosomal origins of replication. *Cold Spring Harbor Perspectives in Biology*, 5(12):a010371.

Tao, H., Liu, W., Simmons, B. N., Harris, H. K., Cox, T. C., and Massiah, M. A. (2010). Purifying natively folded proteins from inclusion bodies using sarkosyl, Triton X-100, and CHAPS. *BioTechniques*, 48(1):61–64.

Tarcan, Z., Poovathumkadavil, D., Skagia, A., and Gambus, A. (2021). The p97 cofactor Ubxn7 facilitates replisome disassembly during S-phase. *bioRxiv*, page 2021.12.16.472925.

Tarnauskaitė, Ž., Bicknell, L. S., Marsh, J. A., Murray, J. E., Parry, D. A., Logan, C. V., Bober, M. B., de Silva, D. C., Duker, A. L., Sillence, D., Wise, C., Jackson, A. P., Murina, O., and Reijns, M. A. (2019). Biallelic variants in DNA2 cause microcephalic primordial dwarfism. *Human Mutation*, 40(8):1063–1070.

Tate, J. G., Bamford, S., Jubb, H. C., Sondka, Z., Beare, D. M., Bindal, N., Boutselakis, H., Cole, C. G., Creatore, C., Dawson, E., Fish, P., Harsha, B., Hathaway, C., Jupe, S. C., Kok, C. Y., Noble, K., Ponting, L., Ramshaw, C. C., Rye, C. E., Speedy, H. E., Stefancsik, R., Thompson, S. L., Wang, S., Ward, S., Campbell, P. J., and Forbes, S. A. (2019). COSMIC: the Catalogue Of Somatic Mutations In Cancer. *Nucleic Acids Research*, 47(D1):D941–D947.

Terzi, M. Y., Izmirli, M., and Gogebakan, B. (2016). The cell fate: senescence or quiescence. *Molecular Biology Reports*, 43(11):1213–1220.

Thurman, R. E., Day, N., Noble, W. S., and Stamatoyannopoulos, J. A. (2007). Identification of higher-order functional domains in the human ENCODE regions. *Genome Research*, 17(6):917–927.

Trempe, J.-F., Sauvé, V., Grenier, K., Seirafi, M., Tang, M. Y., Ménade, M., Al-Abdul-Wahid, S., Krett, J., Wong, K., Kozlov, G., Nagar, B., Fon, E. A., and Gehring, K. (2013). Structure of Parkin Reveals Mechanisms for Ubiquitin Ligase Activation. *Science*, 340(6139):1451–1455.

Truong, L. N. and Wu, X. (2011). Prevention of DNA re-replication in eukaryotic cells. *Journal of Molecular Cell Biology*, 3(1):13.

Tu, Y., Chen, C., Pan, J., Xu, J., Zhou, Z. G., and Wang, C. Y. (2012). The Ubiquitin Proteasome Pathway (UPP) in the regulation of cell cycle control and DNA damage repair and its implication in tumorigenesis. *Int J Clin Exp Pathol*, 5(8):726–738.

Tufegdzic Vidakovic, A., Harreman, M., Dirac-Svejstrup, A. B., Boeing, S., Roy, A., Encheva, V., Neumann, M., Wilson, M., Snijders, A. P., and Svejstrup, J. Q. (2019). Analysis of RNA polymerase II ubiquitylation and proteasomal degradation. *Methods (San Diego, Calif.)*, 159-160:146.

Typas, D., Luijsterburg, M. S., Wiegant, W. W., Diakatou, M., Helfricht, A., Thijssen, P. E., van den Broek, B., Mullenders, L. H., and van Attikum, H. (2015). The de-ubiquitylating enzymes USP26 and USP37 regulate homologous recombination by counteracting RAP80. *Nucleic Acids Res*, 43(14):6919–6933.

van der Meijden, C. M. J., Lapointe, D. S., Luong, M. X., Peric-Hupkes, D., Cho, B., Stein, J. L., van Wijnen, A. J., and Stein, G. S. (2002). Gene Profiling of Cell Cycle Progression through S-Phase Reveals Sequential Expression of Genes Required for DNA Replication and Nucleosome Assembly1. *Cancer Research*, 62(11):3233–3243.

Van Esch, H., Colnaghi, R., Freson, K., Starokadomskyy, P., Zankl, A., Backx, L., Abramowicz, I., Outwin, E., Rohena, L., Faulkner, C., Leong, G. M., Newbury-Ecob, R. A., Challis, R. C., Õunap, K., Jaeken, J., Seuntjens, E., Devriendt, K., Burstein, E., Low, K. J., and O'Driscoll, M. (2019). Defective DNA Polymerase alpha-Primase Leads to X-Linked Intellectual Disability Associated with Severe Growth Retardation, Microcephaly, and Hypogonadism. *The American Journal of Human Genetics*, 104(5):957–967.

Varshavsky, A. (2001). Ubiquitin. In *Encyclopedia of Genetics*, pages 2091 – 2093. Academic Press N.Y, 4 edition.

Vaz, B., Halder, S., and Ramadan, K. (2013). Role of p97/VCP (Cdc48) in genome stability. *Front Genet*, 4:60.

Vélez-Cruz, R. and Johnson, D. G. (2017). The Retinoblastoma (RB) Tumor Suppressor: Pushing Back against Genome Instability on Multiple Fronts. *International Journal of Molecular Sciences*, 18(8):1776.

Verma, R., Oania, R., Fang, R., Smith, G. T., and Deshaies, R. J. (2011). Cdc48/p97 Mediates UV-Dependent Turnover of RNA Pol II. *Molecular Cell*, 41(1):82–92.

Vicencio, J. M., Galluzzi, L., Tajeddine, N., Ortiz, C., Criollo, A., Tasdemir, E., Morselli, E., Ben Younes, A., Maiuri, M. C., Lavandero, S., and Kroemer, G. (2008). Senescence, apoptosis

or autophagy? When a damaged cell must decide its path–a mini-review. *Gerontology*, 54(2):92–99.

Villa, F., Fujisawa, R., Ainsworth, J., Nishimura, K., Lie-A-Ling, M., Lacaud, G., Karim, &., and Labib, P. M. (2021). CUL2LRR1, TRAIP and p97 control CMG helicase disassembly in the mammalian cell cycle. *EMBO reports*, 22(3):e52164.

Walczak, H., Iwai, K., and Dikic, I. (2012). Generation and physiological roles of linear ubiquitin chains. *BMC Biology*, 10:23.

Walden, H. and Rittinger, K. (2018). RBR ligase–mediated ubiquitin transfer: a tale with many twists and turns. *Nature Structural & Molecular Biology 2018 25:6*, 25(6):440–445.

Wang, C., Xi, J., Begley, T. P., and Nicholson, L. K. (2001). Solution structure of ThiS and implications for the evolutionary roots of ubiquitin. *Nat Struct Biol*, 8(1):47–51.

Wang, J., Rojas, P., Mao, J., Mustè Sadurnì, M., Garnier, O., Xiao, S., Higgs, M. R., Garcia, P., and Saponaro, M. (2021). Persistence of RNA transcription during DNA replication delays duplication of transcription start sites until G2/M. *Cell Reports*, 34(7):108759.

Wang, Y., jian Lu, J., He, L., and Yu, Q. (2011). Triptolide (TPL) inhibits global transcription by inducing proteasome-dependent degradation of RNA polymerase II (Pol II). *PLoS ONE*, 6(9):23993.

Weber, A. M. and Ryan, A. J. (2015). ATM and ATR as therapeutic targets in cancer. *Pharmacology & therapeutics*, 149:124–138.

Wessel, S. R., Mohni, K. N., Luzwick, J. W., Dungrawala, H., and Cortez, D. (2019). Functional

Analysis of the Replication Fork Proteome Identifies BET Proteins as PCNA Regulators. *Cell Reports*, 28(13):3497–3509.e4.

Wickliffe, K. E., Lorenz, S., Wemmer, D. E., Kuriyan, J., and Rape, M. (2011). The mechanism of linkage-specific ubiquitin chain elongation by a single-subunit E2. *Cell*, 144(5):769–781.

Willis, N. A., Chandramouly, G., Huang, B., Kwok, A., Follonier, C., Deng, C., and Scully, R. (2014). BRCA1 controls homologous recombination at Tus/Ter-stalled mammalian replication forks. *Nature*, 510(7506):556.

Wilson, M. D., Harreman, M., and Svejstrup, J. Q. (2013). Ubiquitylation and degradation of elongating RNA polymerase II: the last resort. *Biochimica et biophysica acta*, 1829(1):151–157.

Wohlschlegel, J. A., Dhar, S. K., Prokhorova, T. A., Dutta, A., and Walter, J. C. (2002). Xenopus Mcm10 binds to origins of DNA replication after Mcm2-7 and stimulates origin binding of Cdc45. *Molecular Cell*, 9(2):233–240.

Wohlschlegel, J. A., Dwyer, B. T., Dhar, S. K., Cvetic, C., Walter, J. C., and Dutta, A. (2000). Inhibition of eukaryotic DNA replication by geminin binding to Cdt1. *Science*, 290(5500):2309–2312.

Wu, R. A., Pellman, D. S., and Walter, J. C. (2021). The ubiquitin ligase TRAIP: double-edged sword at the replisome. *Trends in cell biology*, 31(2):75.

Wu, R. A., Semlow, D. R., Kamimae-Lanning, A. N., Kochenova, O. V., Chistol, G., Hodskinson, M. R., Amunugama, R., Sparks, J. L., Wang, M., Deng, L., Mimoso, C. A., Low, E., Patel, K. J., and Walter, J. C. (2019). TRAIP is a master regulator of DNA interstrand crosslink repair. *Nature*, 567(7747):267–272.

Yang, C., Trent, S., Ionescu-Tiba, V., Lan, L., Shioda, T., Sgroi, D., and Schmidt, E. V. (2006). Identification of cyclin D1- and estrogen-regulated genes contributing to breast carcinogenesis and progression. *Cancer research*, 66(24):11649–11658.

Yao, N. Y. and O'donnell, M. (2010). SnapShot: The Replisome. *Cell*, 141(6):1088–1088.

Ye, Y. and Rape, M. (2009). Building ubiquitin chains: E2 enzymes at work. *Nature Reviews Molecular Cell Biology 2009 10:11*, 10(11):755–764.

Yeeles, J. T., Deegan, T. D., Janska, A., Early, A., and Diffley, J. F. (2015). Regulated eukaryotic DNA replication origin firing with purified proteins. *Nature*, 519(7544):431–435.

Yeeles, J. T. P., Janska, A., Early, A., and Diffley Correspondence, J. F. X. (2017). How the Eukaryotic Replisome Achieves Rapid and Efficient DNA Replication. *Molecular Cell*, 65:105–116.

Yesbolatova, A., Natsume, T., ichiro Hayashi, K., and Kanemaki, M. T. (2019). Generation of conditional auxin-inducible degron (AID) cells and tight control of degron-fused proteins using the degradation inhibitor auxinole. *Methods*, 164-165:73–80.

Yesbolatova, A., Saito, Y., Kitamoto, N., Makino-Itou, H., Ajima, R., Nakano, R., Nakaoka, H., Fukui, K., Gamo, K., Tominari, Y., Takeuchi, H., Saga, Y., ichiro Hayashi, K., and Kanemaki, M. T. (2020). The auxin-inducible degron 2 technology provides sharp degradation control in yeast, mammalian cells, and mice. *Nature Communications*, 11(1):5701.

Yuan, J., Luo, K., Zhang, L., Cheville, J. C., and Lou, Z. (2010). USP10 Regulates p53 Localization and Stability by Deubiquitinating p53. *Cell*, 140(3):384.

Yuan, Y. F., Ren, Y. X., Yuan, P., Yan, L. Y., and Qiao, J. (2016). TRAIP is involved in chromosome alignment and SAC regulation in mouse oocyte meiosis. *Scientific Reports 2016 6:1*, 6(1):1–9.

Zeman, M. K. and Cimprich, K. A. (2014). Causes and consequences of replication stress. *Nat Cell Biol*, 16(1):2–9.

Zhang, J., Dewar, J. M., Budzowska, M., Motnenko, A., Cohn, M. A., and Walter, J. C. (2015). DNA interstrand cross-link repair requires replication-fork convergence. *Nature Structural & Molecular Biology 2015 22:3*, 22(3):242–247.

Zhang, M., Hu, C., Tong, D., Xiang, S., Williams, K., Bai, W., Li, G. M., Bepler, G., and Zhang, X. (2016). Ubiquitin-specific Peptidase 10 (USP10) Deubiquitinates and Stabilizes MutS Homolog 2 (MSH2) to Regulate Cellular Sensitivity to DNA Damage. *The Journal of biological chemistry*, 291(20):10783–10791.

Zhang, W., Feng, J., and Li, Q. (2020). The replisome guides nucleosome assembly during DNA replication. *Cell & Bioscience 2020 10:1*, 10(1):1–14.

Zhang, X. Y., Varthi, M., Sykes, S. M., Phillips, C., Warzecha, C., Zhu, W., Wyce, A., Thorne, A. W., Berger, S. L., and McMahon, S. B. (2008). The putative cancer stem cell marker USP22 is a subunit of the human SAGA complex required for activated transcription and cell-cycle progression. *Mol Cell*, 29(1):102–111.

Zhao, Z., Wu, M., Zhang, X., Jin, Q., Wang, Y., Zou, C., Huang, G., Yin, J., Xie, X., and Shen, J. (2020). CB-5083, an inhibitor of P97, suppresses osteosarcoma growth and stem cell properties by altering protein homeostasis. *American Journal of Translational Research*, 12(6):2956.

Zheng, L. and Shen, B. (2011). Okazaki fragment maturation: nucleases take centre stage. *Journal of Molecular Cell Biology*, 3(1):23.

Zhou, H., Zaher, M. S., Walter, J. C., and Brown, A. (2021). Structure of CRL2Lrr1, the E3 ubiquitin ligase that promotes DNA replication termination in vertebrates. *Nucleic acids research*, 49(22):13194–13206.

Zhou, H. J., Wang, J., Yao, B., Wong, S., Djakovic, S., Kumar, B., Rice, J., Valle, E., Soriano, F., Menon, M. K., Madriaga, A., Kiss Von Soly, S., Kumar, A., Parlati, F., Yakes, F. M., Shawver, L., Le Moigne, R., Anderson, D. J., Rolfe, M., and Wustrow, D. (2015). Discovery of a First-in-Class, Potent, Selective, and Orally Bioavailable Inhibitor of the p97 AAA ATPase (CB-5083). *Journal of Medicinal Chemistry*, 58(24):9480–9497.

Zhou, Q. and Geahlen, R. L. (2009). The protein-tyrosine kinase Syk interacts with TRAF-interacting protein TRIP in breast epithelial cells. *Oncogene 2009 28:10*, 28(10):1348–1356.

Zimmerman, E. S., Schulman, B. A., and Zheng, N. (2010). Structural assembly of cullin-RING ubiquitin ligase complexes. *Current opinion in structural biology*, 20(6):714–721.